

2006

Evaluation of GaN and InGaN semiconductors as potentiometric anion selective electrodes

Dimitrova, Rozalina Stefanova

<http://knowledgecommons.lakeheadu.ca/handle/2453/4078>

Downloaded from Lakehead University, Knowledge Commons

**EVALUATION OF GaN AND InGaN SEMICONDUCTORS AS
POTENTIOMETRIC ANION SELECTIVE ELECTRODES**

by

Rozalina Dimitrova

**A thesis
presented to Lakehead University
in fulfilment of the
thesis requirement for the degree of
Masters of Science
in
Environmental Engineering**

Thunder Bay, Ontario, Canada, 2006

© Rozalina Dimitrova 2006



Library and
Archives Canada

Bibliothèque et
Archives Canada

Published Heritage
Branch

Direction du
Patrimoine de l'édition

395 Wellington Street
Ottawa ON K1A 0N4
Canada

395, rue Wellington
Ottawa ON K1A 0N4
Canada

Your file *Votre référence*
ISBN: 978-0-494-31852-2
Our file *Notre référence*
ISBN: 978-0-494-31852-2

NOTICE:

The author has granted a non-exclusive license allowing Library and Archives Canada to reproduce, publish, archive, preserve, conserve, communicate to the public by telecommunication or on the Internet, loan, distribute and sell theses worldwide, for commercial or non-commercial purposes, in microform, paper, electronic and/or any other formats.

The author retains copyright ownership and moral rights in this thesis. Neither the thesis nor substantial extracts from it may be printed or otherwise reproduced without the author's permission.

AVIS:

L'auteur a accordé une licence non exclusive permettant à la Bibliothèque et Archives Canada de reproduire, publier, archiver, sauvegarder, conserver, transmettre au public par télécommunication ou par l'Internet, prêter, distribuer et vendre des thèses partout dans le monde, à des fins commerciales ou autres, sur support microforme, papier, électronique et/ou autres formats.

L'auteur conserve la propriété du droit d'auteur et des droits moraux qui protègent cette thèse. Ni la thèse ni des extraits substantiels de celle-ci ne doivent être imprimés ou autrement reproduits sans son autorisation.

In compliance with the Canadian Privacy Act some supporting forms may have been removed from this thesis.

Conformément à la loi canadienne sur la protection de la vie privée, quelques formulaires secondaires ont été enlevés de cette thèse.

While these forms may be included in the document page count, their removal does not represent any loss of content from the thesis.

Bien que ces formulaires aient inclus dans la pagination, il n'y aura aucun contenu manquant.


Canada

ABSTRACT

Ion selective electrodes (ISEs) are chemical sensors primarily used for in situ analysis and monitoring of air, water, and land. Despite their easy fabrication, low cost, and simple usage, ISEs still suffer from the sensitivity of their response to temperature variations, solution turbidity, interferences from other ions in solution, drift of the electrode potential, membrane fouling, and short lifetime. As a result, investigating new materials to develop ISEs that can address some of these limitations is a worthwhile and challenging topic of research.

The excellent mechanical, thermal and chemical stability of gallium nitride (GaN) and indium gallium nitride (InGaN) semiconductors, coupled with their resistance to corrosion and low toxicity if dissolved, are some of the properties that make these materials prime candidates for a variety of sensor applications, particularly at high temperatures and in harsh environments. This thesis evaluates the potential of these two semiconductor materials for replacing conventional ISE membranes with a solid-state semiconductor surface/solution interface.

The benefits gained from this novel design of the ISE sensing element are assessed. These include:

- Easy fabrication and simple use;
- Well defined semiconductor/electrolyte interface;
- Mechanical and chemical stability;
- Durability.

Wafers composed of undoped GaN crystal films (50-nm thick) grown on Al₂O₃ (sapphire) were scribed to pieces measuring approximately 5 mm by 10 mm for the construction of two GaN electrodes - Sample 1 and Sample 2. The GaN thin films had mixed surface polarity, exposing both the Ga-face (0001) and the N-face (0001) of the crystal, although Ga-face regions were dominant. The InGaN (In_{0.2}Ga_{0.8}N) samples were fabricated by mixing GaN and InN in an 80:20 ratio. A 50-nm In_{0.2}Ga_{0.8}N layer was grown on a GaN buffer on a sapphire wafer. All InGaN samples had their InGa-face (0001) exposed. One electrode – Sample 3 – was constructed with InGaN. The semiconductor electrodes were employed as working electrodes in a conventional three-electrode electrochemical cell assembly to detect anions in various potassium and sodium salt solutions. The sensitivity of the electrodes to individual anions was determined by measuring

the open circuit potential (OCP) in each solution versus a reference electrode (Saturated Calomel Electrode). The charge transfer reactions occurring at the semiconductor/electrolyte interface were investigated through cyclic voltammetry (CV), while electrochemical impedance experiments provided information about the structure of the interface.

GaN and InGaN electrodes have relatively fast response times (between 50 and 700s) that compare favourably with the response times of commercial ISEs. The response time depends on the electrode material and on the type of electrolyte: as the strength of adsorption of the anion increases, the response time decreases.

OCP measurements revealed good sensitivity of GaN and InGaN electrodes to changes in anion concentration and to pH variations. Calibration curves (OCP versus activity of anions) generally contain a linear region having a slope close the theoretical value of 58.3mV/decade of activity change, which is consistent with previous results reported in the literature for GaN electrodes. The linearity regions for the GaN and InGaN electrodes are relatively narrow and only encompass one or two decades of activity change in some solutions. This behaviour may be caused by the mixed polarity of the electrode surface and/or by contamination of the electrode sensing element. The average potential drift of 1.7mV/day for GaN and the InGaN electrodes is similar to that of other ISEs.

The potential charge transfer reactions occurring at the semiconductor/electrolyte interface were identified through cyclic voltammetry experiments and by comparing the positions of the valence and conduction band edges of the semiconductor with the standard potentials of the redox couples in the electrolyte solutions. The anodic current recorded under anodic polarization may be associated with the oxidation of anionic species of the conducting salt in the electrolyte and with the oxidation of water to oxygen gas. In most of the tested solutions, the cathodic current observed during the cathodic scan is believed to result from the hydrogen evolution reaction.

It is suggested that the response of the semiconductor electrodes is based on the potential, generated at the semiconductor/electrolyte interface as a result of specific and non-specific adsorption of the anions from the solutions on the positively charged Ga-face or InGa-face electrode surface. The adsorption processes result in the formation of a double layer on the electrolyte side of the semiconductor/electrolyte interface and a space charge layer on the

semiconductor side. At high concentrations of a conducting salt in the electrolyte solution, all electric charges on the solution side are concentrated within the Helmholtz layer, and the double layer on the solution side can therefore be approximated by a single parallel-plate capacitor. Similarly to the Helmholtz layer, the space charge layer on the semiconductor side can also be approximated by a parallel plate capacitor. In practice, the main part of the potential drop across the semiconductor/ electrolyte interface occurs across the space charge layer of the semiconductor and, as a result, the main contribution to the total interfacial capacitance comes from the capacitance of the space charge layer of the semiconductor. Thus, in the simplest model, the semiconductor/ electrolyte interface can be represented by a charge transfer resistance $R_{1_{ct}}$ and a space charge layer capacity C_{sc} connected in parallel. The validity of the suggested model of the semiconductor electrode/ electrolyte interface was investigated with Electrochemical Impedance Spectroscopy (EIS). EIS experiments demonstrated that at high frequencies the impedance of the electrochemical system is indeed dominated by the space charge layer of the semiconductor. At low frequencies, however, the impedance is controlled by the slow diffusion of electroactive species across the layer of adsorbed ions present at the surface of the semiconductor. The equivalent circuit model proposed to fit the experimental data contains elements that represent the series-connected resistances of bulk of the semiconductor and the electrolyte, the capacitance of the space-charge layer connected in parallel with the charge transfer resistance across the space charge layer, and the Warburg impedance modeling the diffusion-controlled processes at the interface. Calculated parameters of the circuit elements are in conformity with the results reported in the literature for semiconductor electrodes. The developed circuit models can effectively fit the EIS experimental data for GaN and InGaN electrodes.

Scanning electron microscopy and energy dispersive spectroscopy confirmed that the surface of the GaN and InGaN films used in this study have a mixed polarity that exposes both the N-face and the Ga-face (or InGa-face) of the crystal.

The effect of the strong polarization on the GaN semiconductor electrode was investigated by cyclic voltammetry and by EDS. Etching of the GaN surface was observed under anodic polarization conditions.

This study has demonstrated that both GaN and InGaN semiconductors possess some potential as novel materials for construction of potentiometric anion selective electrodes. The fabricated GaN and InGaN sample electrodes showed good response to all tested organic and inorganic anions and pH sensitivity. They also demonstrated good chemical and mechanical stability and hence, GaN and InGaN semiconductors could be employed to construct ion selective electrodes that are both durable and easy to use. The study also showed that some of the electrode characteristics and specifically, their region of linearity and the reproducibility of OCP results leave space for improvement and necessitate further research. One direction in which future efforts could be targeted is to clarify the effect of surface polarity on the electrode response and to determine the actual electrochemical reactions occurring in the electrochemical system.

ACKNOWLEDGEMENTS

There are many people who deserve my gratitude for having provided contributions and support in the development of this thesis. First and foremost, I would like to thank my research supervisors, Dr. Dimiter Alexandrov, Dr. Lionel Catalan and Dr. Aicheng Chen for their valuable input, time, edits, idea and advice. Without their support this thesis would not have been possible.

I would also like to offer thanks to the fellow students working in the Electrochemical and in the Industrial Waste Management Laboratories for their help with using the laboratory equipment.

Last, but certainly not least, I would like to thank my family and in particular, my husband, Emil, and my daughter, Monica, for their continued support and encouragement. It is them this Thesis is dedicated to. Thanks and I love you!

TABLE OF CONTENTS

ABSTRACT	ii
ACKNOWLEDGEMENTS	vi
TABLE OF CONTENTS	vii
LIST OF TABLES	x
LIST OF FIGURES	xi
NOMENCLATURE	xiii
I. LITERATURE REVIEW	I-1
I.1. Applications of ISEs in Environmental Analysis	I-1
I.2. Classification of Ion Selective Electrodes	I-5
I.2.1. Primary Ion-Selective Electrodes	I-5
I.2.1.1. Crystalline Electrodes	I-5
I.2.1.2. Non-Crystalline Electrodes	I-5
I.2.2. Compound or Multiple Membrane (Multiple Layer) ISEs	I-8
I.2.2.1. Gas Sensing Electrodes	I-8
I.2.2.2. Enzyme Substrate Electrodes	I-9
I.2.3. Metal Contact or All-Solid-State ISEs	I-9
I.3. Assessment of ISEs	I-10
I.4. Characterization of GaN and InGaN Semiconductor Crystals	I-13
I.5. Response Mechanisms of GaN and InGaN Semiconductor Electrodes to Ions in Solution	I-15
I.5.1. Band Structure and Electrical Conductivity of GaN and InGaN	I-15
I.5.2. The Semiconductor/Electrolyte Interface	I-19
I.6. Previous Electrochemical Studies of GaN	I-28
I.7. Operation of ISEs	I-31
I.7.1. Calibration of ISEs	I-31
I.7.1.1. Direct Calibration	I-31
I.7.1.1.1. Method Description	I-31
I.7.1.1.2. Linear Range	I-33
I.7.1.1.3. Total Measuring Range	I-33
I.7.1.1.4. Limit of Detection	I-34
I.7.1.2. Incremental Methods	I-34
I.7.1.2.1. Standard Additions	I-34
I.7.1.2.2. Sample Additions	I-35
I.7.1.2.3. Sample Subtractions	I-35
I.7.1.3. Titration Methods	I-35

I.7.2.	Sources of Error	I-36
I.7.2.1.	Diffusion	I-36
I.7.2.2.	Sample Ionic Strength	I-37
I.7.2.3.	Interferences	I-39
I.7.2.4.	Selectivity Coefficient.....	I-40
I.7.2.5.	Accuracy of Measurements	I-41
I.7.2.6.	Temperature	I-41
I.7.2.7.	pH	I-42
I.7.2.8.	Response Time.....	I-42
I.7.2.9.	Potential Drift	I-43
I.8.	Rationale and Objectives for the Thesis	I-44
I.8.1.	Gaps in Knowledge for GaN- and InGaN-Based Ion Selective Potentiometric Sensors Prior to the Thesis.....	I-44
I.8.2.	Thesis Objectives	I-45
II.	MATERIALS AND METHODS	II-1
II.1.	GaN and InGaN Electrode Fabrication.....	II-1
II.2.	Electrochemical Measurements	II-3
II.2.1.	Solutions	II-3
II.2.2.	Electrochemical Cell Assembly	II-3
II.2.3.	Open Circuit (OC) Potential Measurements.....	II-5
II.2.4.	Cyclic Voltammetry.....	II-6
II.2.5.	Electrochemical Impedance Spectroscopy	II-8
II.3.	Surface Analytical Techniques	II-13
II.3.1.	Scanning Electron Microscopy	II-14
II.3.2.	Energy Dispersive Spectroscopy	II-14
III.	RESULTS & DISCUSSION.....	III-1
III.1.	Performed Experiments	III-1
III.2.	Response Time.....	III-7
III.2.1.	Response Time Measurements	III-7
III.2.2.	Reproducibility of the Response Time Results.....	III-20
III.3.	Total Potentiometric Response	III-28
III.3.1.	Baseline Measurements, i.e. Measuring the Sample Electrodes Response in NPW	III-28
III.3.2.	Comparison Between the GaN and InGaN Sample Electrodes.....	III-30
III.3.3.	Total Potentiometric Response	III-33
III.4.	Construction of Calibration Curves.....	III-33
III.5.	Reproducibility of Results	III-53
III.6.	Investigation of pH Response of the Sample Electrodes	III-62

III.7.	Cyclic Voltammetry	III-64
III.8.	Electrochemical Impedance Spectroscopy.....	III-75
III.9.	Potentiostatic Experiments	III-93
III.10.	Range Tests	III-97
III.11.	Surface Study of GaN and InGaN Sample Electrodes.....	III-99
IV.	SUMMARY AND CONCLUSIONS	IV-1
IV.1.	Summary of Research Results and Conclusions	IV-1
IV.1.1.	Response Time	IV-1
IV.1.2.	Total Potentiometric Response	IV-2
IV.1.3.	Calibration Curves (Response Range and Slope)	IV-2
IV.1.4.	Reproducibility	IV-3
IV.1.5.	pH Response	IV-3
IV.1.6.	CV Results.....	IV-3
IV.1.7.	EIS study	IV-3
IV.1.8.	Potentiostatic Experiments	IV-4
IV.1.9.	Range Tests	IV-4
IV.1.10.	Surface Studies and Elemental Analysis.....	IV-4
IV.2.	Overall Conclusions.....	IV-4
IV.3.	Recommendations for Further Research	IV-5
V.	APPENDIX A	V-1
VI.	REFERENCES.....	VI-1

LIST OF TABLES

Table III.1 Performed Experiments by measurement types and sample electrodes	III-2
Table III.2 OC potentials measured with GaN/S1 and InGaN/S3 in KNO ₃ solutions before and after cleaning	III-28
Table III.3 Variation of OCPs with solution for GaN sample electrodes S1 and S2	III-30
Table III.4 Variation of OCPs with activity of anions and type of electrolyte for GaN/S1 and InGaN/S3 electrodes	III-32
Table III.5 Total Potentiometric Response of GaN (S1) and InGaN (S3) sample electrodes for several potassium and sodium salts	III-33
Table III.6 Summary of the Calibration Curves evaluation	III-46
Table III.7 Variation of OC potential with concentration.....	III-48
Table III.8 Equivalent Circuit Parameters for S1 (GaN) in 0.1M electrolyte solutions	III-90
Table III.9 Equivalent Circuit Parameters for S3 (InGaN) in 0.1M electrolyte solutions	III-90

LIST OF FIGURES

Fig. I.1 Basic ISE setup.....	I-2
Fig. I.2 Environmental Applications of Ion-Selective Electrodes.....	I-4
Fig. I.3 Use and operation of the glass electrode	I-6
Fig. I.4 Wurtzite crystal structure of GaN	I-13
Fig. I.5 Crystal structure of a Ga-face GaN crystal	I-15
Fig. I.6 Crystal structure of InGaN showing the directions of the dipole moments along In–N and Ga–N bonds	I-15
Fig. I.7 Band diagram of a semiconductor	I-16
Fig. I.8 Electrical conduction in intrinsic semiconductor.....	I-16
Fig. I.9 Electron band structures in solids at 0°K	I-18
Fig. I.10 Energy levels in an electrolyte and in an intrinsic semiconductor.....	I-19
Fig. I.11 Positions of the Fermi level in a semiconductor and the redox level in an electrolyte.....	I-20
Fig. I.12 Energy level model of the semiconductor/electrolyte interface.....	I-22
Fig. I.13 Structure of the semiconductor/electrolyte interface.....	I-25
Fig. I.14 Calibration curves of the GaN-based sensor to four different potassium salts.....	I-29
Fig. I.15 pH sensitivity of the GaN sensor in 2 M KOH before (circles) and after (squares) oxidative treatment	I-30
Fig. I.16 Typical ISE Calibration Graph.....	I-33
Fig. I.17 Definition and determination of response time.....	I-43
Fig. II.1 Construction of the GaN and InGaN sample electrodes.....	II-2
Fig. II.2 Prepared Test Electrodes	II-2
Fig. II.3 Electrochemical Experiments setup.....	II-4
Fig. II.4 Cyclic Voltammetry Experiment	II-7
Fig. II.5 Sinusoidal response in a linear system.....	II-8
Fig. II.6 Nyquist plot.....	II-9
Fig. II.7 Simple equivalent circuit	II-12
Fig. III.1 Variation of measured open circuit potential with time in various electrolyte solutions	III-7
Fig. III.2 Variation of the GaN sample electrode S1 response time with activity of anions in three electrolyte solutions.....	III-10
Fig. III.3 Variation of the GaN sample electrode S1 response time with activity of anions in three electrolyte solutions.....	III-12
Fig. III.4 Effect of electrode material on the response time in KNO ₃ , KBr and KI solutions during two series of measurements.....	III-14
Fig. III.5 Reproducibility of response time results for GaN sample electrode S1 in KNO ₃ , KBr and KI solutions	III-21
Fig. III.6 Reproducibility of response time results for InGaN sample electrode S3 in KNO ₃ , KBr and KI solutions	III-24

Fig. III.7 Response of GaN sample electrode S1 and InGaN sample electrode S3 in NPW.....	III-29
Fig. III.8 Calibration curves of the GaN sample electrode, S1, and the InGaN sample electrode, S3, in nine test electrolytes	III-34
Fig. III.9 Comparison between measured OCPs for GaN sample electrode S1 and adjusted OCPs reported by Chaniotakis et al. (2004)	III-49
Fig. III.10 Reproducibility of OCP measurements in various salt solutions	III-54
Fig. III.11 Variation of OC potential with pH for GaN sample electrode S1, InGaN sample electrode S3 and GaN electrodes, utilized by Alifragis et al. (2005)	III-63
Fig. III.12 Cyclic Voltammograms for GaN sample electrodes in 0.1M salt solutions	III-64
Fig. III.13 Comparison of GaN band edge energies with energy levels of redox couples in tested solutions	III-71
Fig. III.14 Nyquist Plots for GaN sample electrode S1 in 0.1M electrolyte solutions.....	III-77
Fig. III.15 Nyquist Plots for InGaN sample electrode, S3 in 0.1M electrolyte solutions.....	III-81
Fig. III.16 Equivalent Circuit Model for GaN sample electrode S1.....	III-86
Fig. III.17 Equivalent Circuit Model for InGaN sample electrode S3.....	III-86
Fig. III.18 Representation of the capacitance of the semiconductor/electrolyte interface	III-86
Fig. III.19 Variation of current density with time for GaN sample electrode S1 in 0.1M KCl solution at cathodic polarization	III-95
Fig. III.20 Current oscillations for GaN sample electrode S2 at cathodic polarization in 0.1M KCl solution....	III-96
Fig. III.21 Variation of current with time for GaN sample electrode S2 in 0.1M KCl solution at cathodic polarization after deposition of additional layer of epoxy glue	III-97
Fig. III.22 Cyclic voltammograms for GaN sample electrode S2 for two scans with increasing end potentials	III-98
Fig. III.23 SEM images of GaN and InGaN unused sample materials.....	III-100
Fig. III.24 SEM images of GaN sample electrode, S2 after experiments	III-100
Fig. III.25 EDS results for GaN and InGaN unused sample materials.....	III-101
Fig. III.26 EDS results for different regions of GaN sample electrode, S2 after experiments.....	III-102

NOMENCLATURE

Symbol	Meaning	Unit
A	Surface area of the electrode	m ²
a _i	Activity of species <i>i</i> in solution	
C	Total interfacial capacitance	F cm ⁻²
C _D	Capacitance of the diffuse or Gouy layer	F cm ⁻²
C _H	Capacitance of the Helmholtz layer	F cm ⁻²
ϕ	Concentration of species <i>i</i> in solution	mol L ⁻¹
C _O [*]	Concentration of the oxidized species in the bulk of the solution	mol m ⁻³
C _R [*]	Concentration of the reduced species in the bulk of the solution	mol m ⁻³
C _{SC}	Capacitance of the space charge layer of the semiconductor	F cm ⁻²
D	Effective diffusion coefficient of the redox species	m ² s ⁻¹
D _O	Diffusion coefficient of the oxidized species	m ² s ⁻¹
D _R	Diffusion coefficient of the reduced species	m ² s ⁻¹
e	Elementary charge	A s
ℰ	Electric field strength	V cm ⁻¹
E	Electron energy	eV
E ⁰ _{redox}	Redox level corresponding to the standard electrode potential of the redox couple	eV
E _c	Energy of the lower edge of the conduction band	eV
E _{cs}	Energy of the lower edge of the conduction band at the surface of the semiconductor	eV
E _f	Fermi level energy	eV
E _g	Band gap energy	eV
E _{ox}	Most probable energy level for the oxidizing agent of the redox couple	eV
E _{red}	Most probable energy level for the reducing agent of the redox couple	eV
E _v	Energy of the upper edge of the valence band	eV
E _{vs}	Energy of the upper edge of the valence band at the surface of the semiconductor	eV
F	The Faraday constant (9.6485309 x 10 ⁴)	C mol ⁻¹
f	Phase shift angle	rad
f(E)	Fermi distribution	
I	Ionic strength	
i ₀	Amplitude of the output current signal	A

Symbol	Meaning	Unit
i_t	Output current at time t	A
j	Imaginary number	
k	Boltzmann constant (1.38×10^{-23})	$J K^{-1}$
K_{ij}^{pot}	Potentiometric selectivity coefficient of species j with respect to the principal species i	
L	Inductance	H
L_D	Debye length	cm
n	number of electrons exchanged in the redox reaction	
Q_i	Charge density stored in a capacitor	$F V cm^{-2}$
R	Gas constant (8.314510)	$J K^{-1} mol^{-1}$
$R1_{ct}, R2_{ct}$	Charge transfer resistance	Ω
R_s	Solution resistance	Ω
R_{sc}	Resistance of the semiconductor	Ω
t	Time	
T	The absolute temperature (294)	K
U	Electrical potential	V
U_0	Amplitude of the input voltage signal	V
U_{fb}	Flatband potential	V
U_m	Electrode potential	V
U_t	Input voltage at time t	V
x_1	Length of the Helmholtz plane	cm
Z'	Real component of the complex impedance	Ωcm^2
Z''	Imaginary component of the complex impedance	Ωcm^2
Z_0	Amplitude of the impedance	Ωcm^2
Z_{CPE}	Impedance of constant phase element	Ωcm^2
Z_i	Charge of the ion i	
Z_t	Impedance at time t	Ωcm^2
Z_w	Warburg impedance	Ωcm^2

Symbol	Meaning	Unit
Greek Symbols		
γ_i	Activity coefficient of species i in solution	
δ	Effective thickness of the diffusion layer	m
ϵ	Dielectric constant of the electrolyte	
ϵ_0	Permittivity of free space (8.85×10^{-14})	F cm ⁻¹
η	Overpotential	V
μ	Mobility of carriers corresponding to the energy difference between bulk conduction band edge and Fermi energy	cm ² V ⁻¹ s ⁻¹
$\overline{\Delta\mu_e}$	Difference in electrochemical potential of the electrons in the reference and the working electrode	eV
σ	Polarization charge	A s cm ⁻²
σ_w	Warburg coefficient	
$\Delta\phi_{sc}$	Potential change across the space charge layer	V
ω	Radial frequency	rad

I. LITERATURE REVIEW

The following literature review of ion selective electrodes begins by an overview of the advantages of ISEs that have determined the broad range of their applications in environmental analysis (Section I.1). Next, the classification of ion selective electrodes places the electrodes utilized in the current research project in the context of commercially available electrodes (Section I.2). The potential advantages of solid-state ion selective electrodes based on semiconductor sensing elements over the conventional ISEs are given special attention. Section I.3 lists the main criteria against which the performance of an ion selective electrode is assessed when determining its usefulness for a particular application. Section I.4 focuses on the characterization of the GaN and InGaN semiconductor crystals, including their main physical properties, crystal structure, and surface polarity. Section I.5 deals with the response mechanism of the GaN and InGaN semiconductor electrodes to ions in solution. An overview of the previous studies of GaN as a potentiometric anion selective electrode is provided in Section I.6. Section I.7 addresses the practical operation of ISEs, including calibration methods, and provides insights into the most important parameters affecting the performance of ISEs, with an emphasis on problems pertaining to the construction of the electrodes, the methods of their application, and environmental factors such as temperature, interfering ions, and ionic strength. Section I.8 outlines the rationale and lists the objectives for the thesis.

I.1. Applications of ISEs in Environmental Analysis

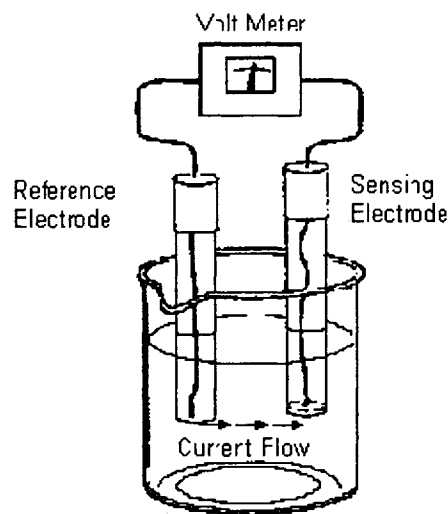
Continuous in situ monitoring of air, water, and land quality is essential in many environmental applications. New emerging technologies such as the ion selective electrodes (ISEs) can, in principle, meet environmental requirements and provide a suitable solution to a wide range of environmental issues (Bourgeois et al, 2003).

Ion-selective electrodes (ISEs) are the most widely used chemical sensors and have proved especially useful as tools in the analysis and monitoring of ions of biological and environmental importance (Toth, 1999). The use of ISEs in environmental analysis offers several advantages over other methods of analysis (Lynde, 2005). First, the cost of initial setup is relatively low. The basic ISE setup (Fig. I.1) includes a meter (capable of reading millivolts), a probe (selective for each analyte of interest), and various consumables used for pH or ionic strength adjustments.

Literature Review

ISE determinations are not subject to interferences such as colour in the sample, and there are few matrix modifications needed to conduct the analyses. This makes ISEs ideal for clinical use (blood gas analysis) where they are most popular; however, they have found practical applications in the analysis of environmental samples, often where in-situ determinations are needed and not practical with other method (Lynde, 2005).

Fig. I.1 Basic ISE setup
(Lynde, 2005)



Other advantages of the Ion-Selective Electrodes include (NICO 2000 Ltd.):

- When compared to many other analytical techniques, ISEs are relatively inexpensive, simple to use, and can be applied over a wide concentration range.
- The most recent plastic-bodied all solid-state or gel-filled models are very robust, durable, and ideal for use in either field or laboratory environments.
- Under the most favourable conditions, i.e. when measuring ions in relatively dilute aqueous solutions where interfering ions are not a problem, they can be used very rapidly and easily (e.g. simply dipping in lakes or rivers, dangling from a bridge or dragging behind a boat).

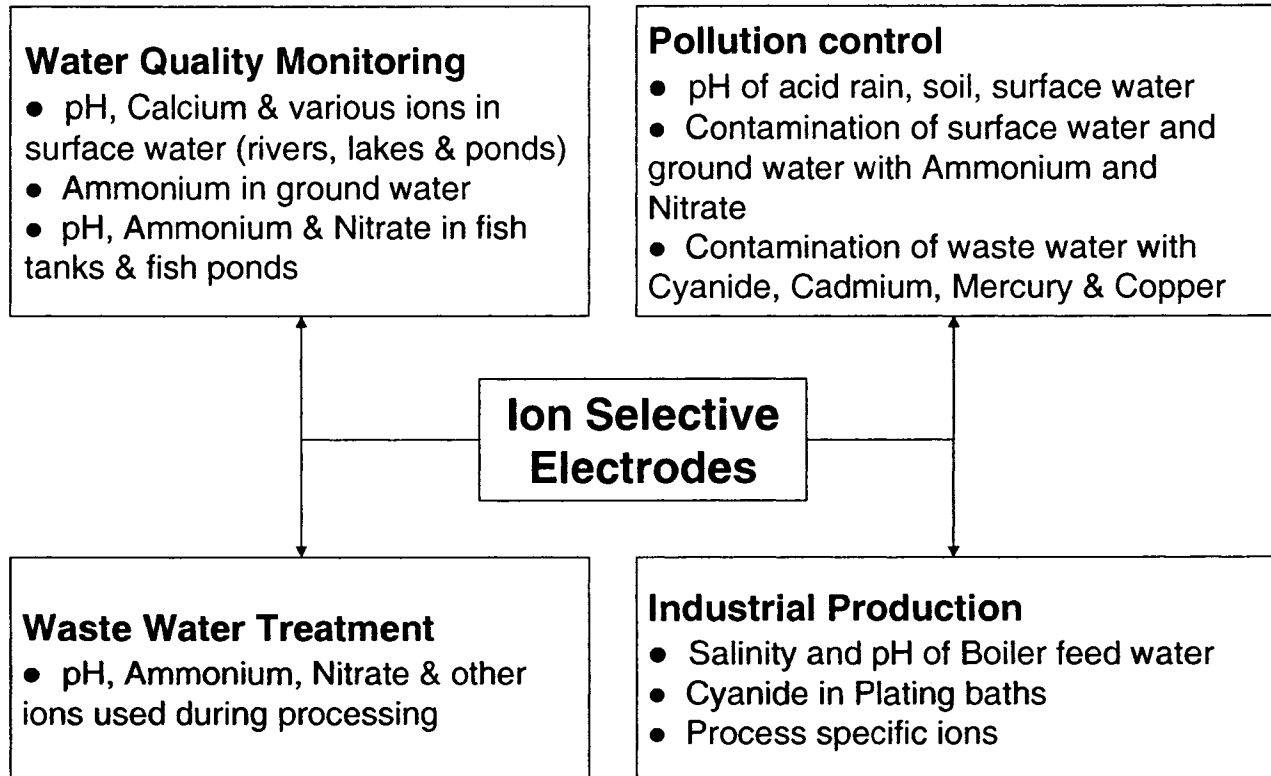
Literature Review

- They are particularly useful in applications where only an order of magnitude concentration estimate is required, or when it is only necessary to know that a particular ion is below a certain concentration level.
- They are invaluable for the continuous monitoring of changes in concentration: e.g. for potentiometric titrations or for monitoring the uptake of nutrients or the consumption of reagents.
- They are particularly useful in biological/environmental applications because they measure the activity of the ion directly, rather than the concentration.
- For applications where interfering ions, pH levels, or high concentrations are a problem, many manufacturers can supply a library of specialized experimental methods and special reagents to overcome many of these difficulties.
- With careful use, frequent calibration, and an awareness of the limitations, they can achieve accuracy and precision levels of ± 2 or 3% for some ions and thus compare favourably with analytical techniques, which require far more complex and expensive instrumentation.
- ISEs are one of the few techniques that can measure both positive and negative ions.
- They are unaffected by sample colour or turbidity.
- ISEs can be used in aqueous solutions over a wide temperature range. Crystal membranes can operate in the range 0°C to 80°C and plastic membranes from 0°C to 50°C.

In many frequently performed analyzes, such as the determination of nitrate in drinking water, ISEs are already replacing some of the conventional techniques; in other cases, such as on-line monitoring of fluoride in drinking water, the use of ISEs have made feasible measurements which are otherwise almost impossible (NICO 2000 Ltd.). The growth of these applications has been fast in relation to the growth of other techniques, partly because the sensors themselves became widely available commercially soon after their development and are, in some cases, also quite

easy to make in the laboratory (NICO 2000 Ltd.). Another contributory factor is that the associated apparatus, such as pH meters and magnetic stirrers, is already part of the standard equipment of most analytical laboratories. The above advantages have made the ISE especially popular and resulted in the broad range of their application. Some of the most common environmental applications of ISEs are presented in Figure I.2.

Fig. I.2 Environmental Applications of Ion-Selective Electrodes
(NICO 2000 Ltd., 2005)



The low cost of fabrication and the non-invasive methods of application alongside with simplicity, rapidity, robustness, and size are some of the essential qualities that have made the ISEs especially attractive, despite a number of limitations that are associated with both the technology itself and its application in ever changing environment conditions (Bourgeois et al, 2003). Despite the increasing range and diversity of ISEs currently available, their utilization for continuous in situ measurements of ion concentration remains largely limited by environmental factors such as temperature, turbidity of measured samples, interferences from other ions in solution, fouling problems with the membranes, short lifetime, and the need for frequent calibration (Bourgeois et al, 2003).

I.2. Classification of Ion Selective Electrodes

Several types of sensing electrodes are commercially available. They are classified by the nature of the membrane material used to construct the electrode. It is this difference in membrane construction that makes an electrode selective for a particular ion.

I.2.1. Primary Ion-Selective Electrodes

I.2.1.1. Crystalline Electrodes

Crystalline electrodes may be homogeneous or heterogeneous (IUPAC, 1994). They contain mobile ions of one sign and fixed sites of opposite sign. Homogeneous membrane electrodes are ISEs in which the membrane is a crystalline material prepared from either a single compound or a homogeneous mixture of compounds (i.e., Ag_2S , $\text{AgI}/\text{Ag}_2\text{S}$). Heterogeneous membrane electrodes are formed when an active substance, or mixture of active substances, is mixed with an inert matrix, such as silicone rubber or PVC, or placed on hydrophobized graphite or conducting epoxy, to form the heterogeneous sensing membrane (IUPAC, 1994). In both homogeneous and heterogeneous types, potentials are developed at the membrane surface due to the ion-exchange process (Covington, 1979).

Examples of crystalline electrodes applications include the analysis of silver/sulphide, lead, copper (II), cyanide, thiocyanate, chloride, and fluoride. The fluoride electrode is a typical example of a semiconductor crystalline electrode (NICO 2000 Ltd.). Here, the membrane consists of a single lanthanum fluoride crystal, which has been doped with europium fluoride to reduce the bulk resistivity of the crystal. It is 100% selective for F^- ions and is only interfered with by OH^- , which reacts with the lanthanum to form lanthanum hydroxide, with the consequent release of extra F^- ions. This interference can be eliminated by adding a pH buffer to the samples to keep the pH in the range 4 to 8 and hence ensure a low OH^- concentration in the solutions (NICO 2000 Ltd.).

I.2.1.2. Non-Crystalline Electrodes

In these electrodes, a support matrix containing an ion exchanger (either cationic or anionic), a plasticizer solvent, and possibly an uncharged, selectivity-enhancing species, forms the ion-

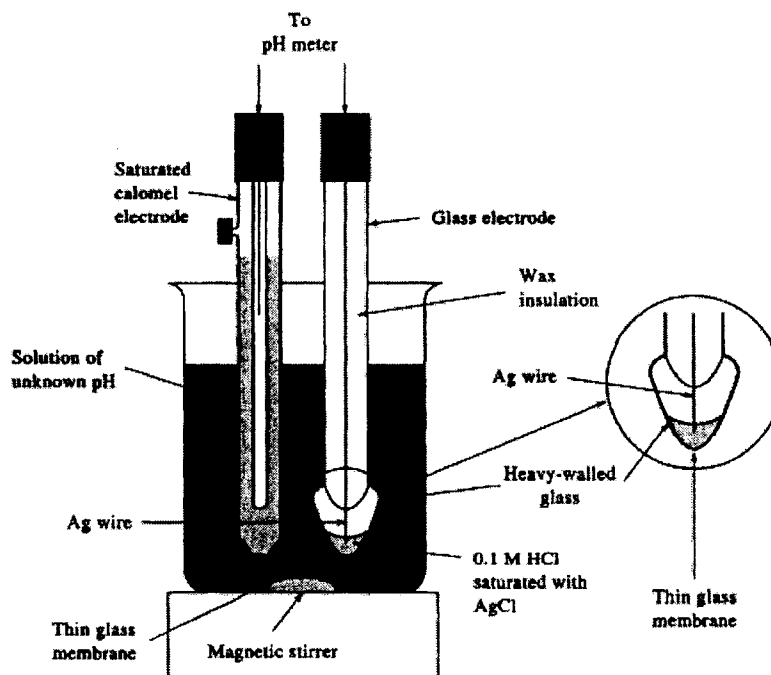
selective membrane, which is usually interposed between two aqueous solutions (IUPAC, 1994). The support can be either macro porous (e.g., poly(propylene carbonate) filter, glass fit, etc.) or micro porous (e.g. "thirsty" glass or inert polymeric material such as PVC) and yields a "solidified" homogeneous mixture when combined with the ion-exchanger and the solvent. These electrodes exhibit a response due to the presence of the ion-exchange material in the membrane.

Glass membrane electrodes are an example of non-crystalline electrodes (Covington, 1979). The oldest glass membrane electrode has been used to measure pH (Rieger, 1994). The electrode, shown on Fig. I.3a, consists of a glass tube, the end of which is a glass membrane about 0.1mm thick (and therefore very fragile). Inside the tube is an Ag/AgCl electrode (Ag wire coated with AgCl) and 0.1M HCL solution.

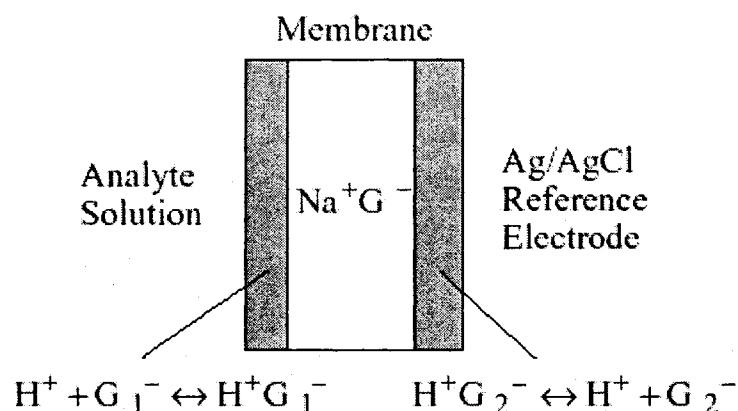
The glass electrode is used by dipping it into a test solution and completing the electrochemical cell with a reference electrode (Fig. I.3a).

Fig. I.3 Use and operation of the glass electrode

a) Electrochemical cell consisting of a glass membrane electrode and a Reference electrode



b) construction of the glass membrane, where G^- denote the glass anionic sites



The glass used in the membrane is a mixture of sodium and calcium silicates – Na_2SiO_3 and $CaSiO_3$ – and silicon dioxide, SiO_2 (Rieger, 1994) and is called “dry glass”. The silicon atoms tend to be four-coordinate, so that the glass is an extensively cross-linked polymer of SiO_4 units with electrostatically bound Na^+ and Ca^{2+} ions. The dry glass is weakly conductive, with the charge carried primarily by the Na^+ ions. The Ca^{2+} ions are much less mobile than Na^+ and contribute little to the conductance. The dry glass is also quite hygroscopic and takes up a significant amount of water in a surface layer perhaps as much as $0.1\mu m$ deep. In the hydrated layers (one on either side of the membrane) there is equilibrium between H^+ and Na^+ electrostatically bound to anionic sites in the glass (the SiO_4 units mentioned before) and in solution (Rieger, 1994). In aqueous solutions, the ion exchange reaction that is taking place at the surface on both sides of the glass membrane is given by:



If the concentration of $H^+(aq)$ in the measured solution is low, this equilibrium shifts to the left; i.e., Na^+ from the interior of the glass membrane (dry glass) tends to migrate into the hydrated region to maintain electrical neutrality (Rieger, 1994) and H^+ ions from the internal 0.1M HCl solution penetrate a little deeper into the glass membrane to replace the Na^+ ions that have migrated to the external hydrated layer. This combination of ion migration gives sufficient electric current that the potential is measurable with a high-impedance voltmeter. Since the H^+ ions are intrinsically smaller and faster moving than Na^+ , most of the current in the hydrated region is carried by H^+ . As a result, the glass electrode behaves as if it was permeable to H^+ and thus acts as an indicator electrode sensitive to pH (Rieger, 1994).

Literature Review

Glass electrodes respond with virtually perfect selectivity to hydrogen ions over the pH range 0-11. Above pH 11, response to alkali ions becomes important with some glasses, and such electrodes become unusable above pH 12. Glass membrane electrodes are also available for the measurement of sodium ions.

The solvent-polymeric-membrane electrode is another example of non-crystalline electrode (IUPAC, 1994). It consists of various ion-exchange materials incorporated into an inert matrix such as PVC, polyethylene, or silicone rubber (Covington, 1979). After the membrane is formed, it is sealed to the end of a PVC tube. The potential developed at the membrane surface is related to the concentration of the species of interest. Electrodes of this type are used to measure potassium, calcium, chloride, fluoroborate, nitrate, perchlorate, potassium, and water hardness.

By replacing the glass or solvent-polymeric membrane with a thin layer of a water immiscible liquid ion exchanger, another type of non-crystalline ion-selective electrode may be constructed (Rieger, 1994). This type of electrodes are called liquid membrane electrodes. For example, by using the calcium salt of an organophosphoric acid in an organic solvent as the liquid ion exchanger and contacting the ion-exchange solution with aqueous test solution through a thin porous membrane, a membrane system permeable to Ca^{2+} ions (and to some degree to other divalent ions) is obtained. On the inner side of the membrane is an Ag/AgCl electrode with CaCl_2 electrolyte. Thus a membrane potential proportional to $\ln([\text{Ca}^{2+}]_{\text{out}}/[\text{Ca}^{2+}]_{\text{in}})$ is developed. Liquid membrane electrodes are commercially available for Ca^{2+} , K^+ , Cl^- , NO_3^- , ClO_4^- and BF_4^- (Rieger, 1994).

1.2.2. Compound or Multiple Membrane (Multiple Layer) ISEs

1.2.2.1. Gas Sensing Electrodes

Gas sensing electrodes are available for the measurement of dissolved gas species such as ammonia, carbon dioxide, nitrogen oxide, and sulphur dioxide (Orion Research Inc., 1997). These electrodes have a gas permeable membrane and an internal buffer solution. Gas molecules diffuse across the membrane and react with the buffer solution, changing the pH of the buffer (Orion Research Inc., 1997). The pH of the buffer solution changes as the gas reacts with it. This change is then sensed by the ion-selective electrode and is related to the partial pressure of the

gaseous species in the sample (IUPAC, 1994). Gas sensing electrodes do not require an external reference electrode because they are constructed with a build-in reference electrode.

1.2.2.2. Enzyme Substrate Electrodes

Enzyme substrate electrodes are sensors in which an ISE is covered with a coating containing an enzyme, which causes the reaction of an organic or inorganic substance (substrate) to produce a species to which the electrode responds (IUPAC, 1994). Alternatively, the sensor could be covered with a layer of substrate, which reacts with the enzyme, co-factor, or inhibitor to be assayed.

1.2.3. Metal Contact or All-Solid-State ISEs

The GaN and InGaN electrodes, studied in the current research project, fall within this category. These electrodes depend on both ionic and electronic conductivities (mixed conductors), unlike the conventional ISEs that depend only on ionic conductivities (IUPAC, 1994). In solid state ISEs, the conventional membrane is replaced by a semiconductor sensing element, e.g. GaN or InGaN. They do not have an inner electrolyte solution or an inner reference electrode (IUPAC, 1994). Instead, the inner side of the sensing element is contacted by a solid. This configuration contrasts with normal membrane usage in which electrolyte solutions contact both sides of the membranes.

Solid-state chemical sensors owe their popularity to their small size, simple operation, high sensitivity, and relatively simple associated electronics (Alifragis et al., 2005). However, most of them still suffer from low selectivity (Alifragis et al., 2005). They also have poor shelf life and are relatively less stable at higher temperatures. For example, the Si substrate-based gas sensor can only operate below 200°C (Kim et al., 1999), and the lanthanum fluoride-based fluoride selective sensor can only operate between 0 and 50°C (Analytical Technology, Inc, 2006). The construction of ISE sensing elements made of semiconductor materials is expected to widen the temperature range of measurements due to the greater thermal stability of the semiconductor membranes in comparison with other solid-state membranes (e.g., crystalline membranes, which can operate in the range 0°C to 80°C or plastic membranes, which can operate from 0°C to 50°C (NICO 2000 Ltd.). The replacement of conventional membranes with a solid-state semiconductor surface/solution interface also provides an improved ISE stability and durability

and ensures better ISE sensitivity, because the sensing element does not become contaminated by organic contaminants (Alifragis et al., 2005).

I.3. Assessment of ISEs

There are many points against which the performance and utility of a particular electrode may be assessed for comparative purposes or to judge its usefulness in a particular application (Bailey, 1980). The most important are as follows:

- Response range and slope
- Selectivity
- Stability and reproducibility
- Response time
- Sensitivity to temperature, pressure, light, etc
- Frequency and ease of maintenance
- Mechanical design
- Availability
- Cost and lifetime

The response range of ISEs is very large compared with that of most analytical devices (Bailey, 1980). Nearly all electrodes respond over at least four decades of concentration in a virtually theoretical manner and some, such as the sodium electrode, respond over eight decades of concentration. It is best to choose an electrode and to fix the experimental conditions so that measurements are made at concentrations higher than the Nernstian limit of response (Bailey, 1980). The response of the electrode is referred to as Nernstian whenever the electrode potential is proportional to the logarithm of the activity of the measured ions (Bailey, 1980). Hence, the lower limit of Nernstian response, or the Nernstian limit, may be defined as the lowest activity of the tested ion at which the plot of the electrode potential versus the logarithm of activity of the measured ion begins to depart from linearity. Below this limit, the electrode response becomes progressively more and more irreproducible, which results in increasing measurement errors.

Literature Review

The selectivity of ion selective electrodes is central to their design and is one of the most important criteria in their assessment for a particular application (Bailey, 1980). No ion selective electrode responds exclusively to the ion which it is designed to measure, although it is often more responsive to this primary ion than to others. If another, interfering, ion is present at a concentration which is large compared to the primary ion, the electrode response will have contributions from both the primary and interfering ions. The degree of selectivity of the electrode for the primary ion, A, with respect to an interfering ion, B, is expressed by the potentiometric selectivity coefficient, $K_{A,B}^{pot}$, which is defined by the Nikolsky-Eisenman equation (IUPAC, 1994):

$$U = \text{constant} + \frac{2.303RT}{Z_A F} \lg \left[a_A + K_{A,B}^{pot} a_B^{Z_A/Z_B} + K_{A,C}^{pot} a_C^{Z_A/Z_C} + \dots \right] \quad (1.2)$$

where:

U is the experimentally measured voltage of a cell (in V) when the only variables are activities in the test solution;

R is the gas constant and is equal to 8.314510 J K⁻¹ mol⁻¹;

T is the absolute temperature (in K);

F is the Faraday constant and is equal to 9.6485309 x 10⁴ C mol⁻¹;

a_A is the activity of the ion A;

a_B & a_C are the activities of the interfering ions B and C respectively;

$K_{A,B}^{pot}$ is the potentiometric selectivity coefficient for ion B with respect to the principal ion A;

Z_A is the charge number - an integer with sign and magnitude corresponding to the charge of the principal ion A;

Z_B & Z_C are charge numbers corresponding to the charge of interfering ions, B and C, respectively. Sign of these charge numbers is the same as that of the principal ion.

When an electrode is very selective for A in comparison with B, $K_{A,B}^{pot}$ will be much less than unity. Conversely, if the electrode responds preferentially to B rather than A, $K_{A,B}^{pot}$ will be greater than unity (Bailey, 1980).

The stability and reproducibility of the electrode response are primarily controlled by the environment, in particular by temperature; the response always tends to be more stable and reproducible in solutions of high ionic strength containing large activities of the sensed ions

Literature Review

(Bailey, 1980). Instability may also be caused by excessive susceptibility of the electrode to static electricity, which may result from poor electrode design, faulty connections inside the electrode, or a poor quality cable. A good electrode used under the right conditions should show negligible drift of potential between successive calibrations (with calibration ideally carried out once a day) and should be able to reproduce the potential to ± 0.1 mV.

The response times of most electrodes are sufficiently short for most analytical purposes (Bailey, 1980). Typically electrodes take just one or two minutes to reach equilibrium; thus the measurement time compares very favourably with most other analytical techniques. Factors affecting the response time have been discussed by Ryan and Fleet (1975); they conclude that three main factors determine the magnitude of the response time: (1) the type of membrane. The response speed of the different types is generally in the order: solid-state membranes > PVC membranes > liquid membranes. (2) The rate of change of solution activity. Rapid solution movement on the electrode surface helps to reduce response times. (3) The presence of interferents. Interferents generally slow the response (Bailey, 1980).

The temperature coefficient (dU/dT) of most electrodes (where U is the measured electrode potential and T is the absolute temperature) is appreciable. Therefore, knowledge of its magnitude is important so that the degree of temperature control required to maintain adequate electrode stability may be calculated. In some cases, it is possible to match the temperature coefficient of the ion selective electrode to that of the reference electrode so that the cell is approximately temperature-insensitive with respect to shift in potential (Bailey, 1980).

The frequency at which an electrode requires maintenance and the time taken to complete the maintenance are important, since their product gives the time the electrode is out of service. This is particularly important for electrodes used in continuous analyzers (Bailey, 1980).

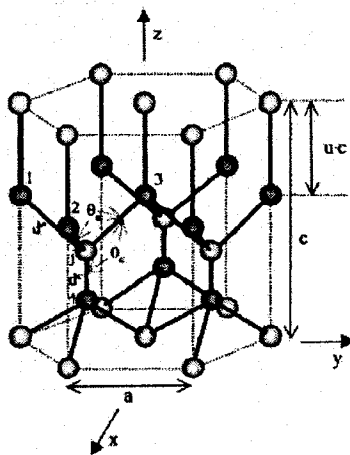
Good mechanical design plays an important role in ensuring that an electrode produces a stable and reproducible response, has a long life, and is easily serviced.

I.4. Characterization of GaN and InGaN Semiconductor Crystals

Gallium nitride (GaN) is a semiconductor material with a wide bandgap (3.4 eV). GaN is a very hard, mechanically stable material with a large heat capacity. In its pure form, it resists cracking and can be deposited in thin film on sapphire, despite the mismatch in their lattice constants. GaN crystals are also rich in defects: 100 million to 10 billion per cm^2 (Ponce, 1997).

Unlike most other III-V semiconductor compounds that crystallize in diamond or zincblende lattice structure, the GaN native crystal has a wurtzite structure. The wurtzite lattice can be considered as two interpenetrating hexagonal close-packed (HCP) lattices (Memming, 2001). In the case of GaN, the sub lattices are composed of gallium and nitrogen atoms. The wurtzite structure has a tetrahedral arrangement of four equidistant nearest neighbours, similar to a zincblende structure (Fig. I.4).

Fig. I.4 Wurtzite crystal structure of GaN
(Takayama et al., 2001)



Mixing GaN with InN yields InGaN, which is a ternary group III/group V direct band gap semiconductor material with high heat capacity and a high tolerance to lattice defects. Its band gap can be tuned by varying the amount of indium in the alloy. The band gap of $\text{In}_{0.2}\text{Ga}_{0.8}\text{N}$ (1.0 eV) is quite narrow in comparison with GaN (Alexandrov et al, 2006). InGaN is often grown on a GaN buffer on a transparent substrate, e.g. sapphire or silicon carbide.

Literature Review

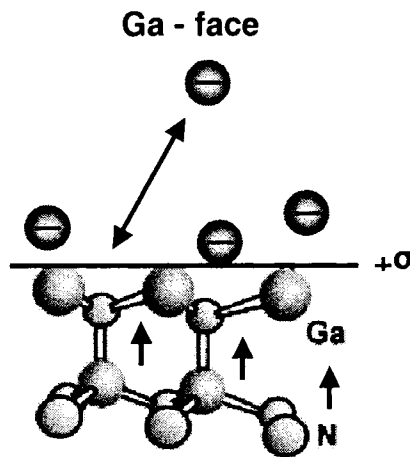
The $\text{In}_{0.2}\text{Ga}_{0.8}\text{N}$ crystal also has a wurtzite crystal structure similar to the structure of its constituent binary alloys – GaN and InN. In InGaN, crystal mixing occurs in the group-III element sublattices of the wurtzite structure (Ga and In). Although the ratio of In/Ga in the InGaN semiconductor can be anywhere between 0.02/0.98 and 0.3/0.7, this particular composition of the InGaN samples has been chosen because in $\text{In}_{0.2}\text{Ga}_{0.8}\text{N}$ the In-contents (20% on molar basis) is sufficient to ensure that:

- the InGaN electrode will have pronouncedly higher conductivity than the GaN electrode (due to its narrow band gap); and
- GaN and InGaN semiconductor electrons will keep enough similarities to allow comparison between the two electrodes and evaluation of the effect of semiconductor bandgap width on the electrode performance.

The polarity of the GaN and InGaN surface and thus, the ability of the electrode to selectively coordinate cations or anions in solution, depends on the orientation of the crystal, and surface properties vary from one crystal plane to the other (Memming, 2001). Therefore, it is very important to properly characterize the surface in the studies of surface and interface effects.

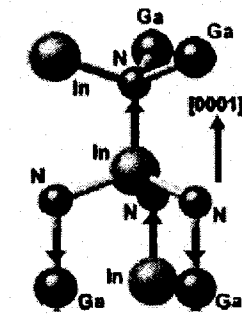
The termination of the GaN crystal at the Ga-face causes a positive polarization charge, $+\sigma$, which can interact with compensating ions in the solution (Fig. I.5). The surface of the GaN wurtzite crystal is characterized by the fact that each gallium atom has 2 bonds to the underlying nitrogen atomic plane and one uncompensated bond on the outer face. Recent studies have shown that the surface gallium atoms are relatively electron deficient, because of the higher electronegativity of N atoms in comparison with Ga atoms in the GaN wurtzite lattice (Chaniotakis et al., 2004). These electron deficient atoms can attract anions from the solution to form a layer of specifically adsorbed ions on the surface of the electrode.

Fig. I.5 Crystal structure of a Ga-face GaN crystal



Similarly to GaN, the surface of an InGaN alloy terminated at the InGa-face also has a positive polarization charge. Microscopic dipoles are caused by a separation of charge between In or Ga atoms and N atoms aligned along the [0001] direction, as shown in Fig. I.6. These dipoles interact with anions from the solution to result in the formation of an adsorbed surface layer.

Fig. I.6 Crystal structure of InGaN showing the directions of the dipole moments along In–N and Ga–N bonds
(Adapted from Miller and Yu, 2001)



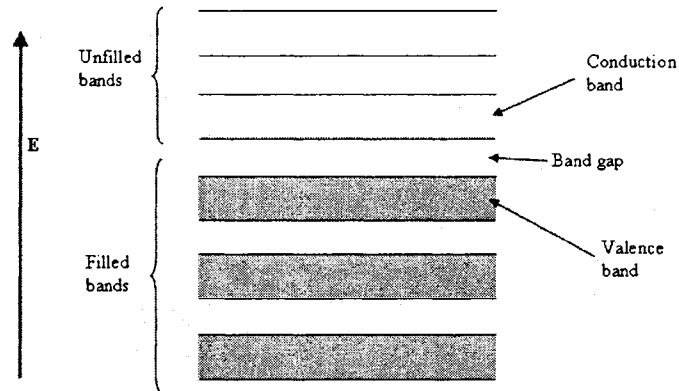
I.5. Response Mechanisms of GaN and InGaN Semiconductor Electrodes to Ions in Solution

I.5.1. Band Structure and Electrical Conductivity of GaN and InGaN

GaN and InGaN are intrinsic semiconductors. Intrinsic semiconductors are those in which the electrical behaviour is based on the electronic structure inherent to the pure material, rather than on impurities. The band structure of intrinsic semiconductors at 0K is characterized by a valence

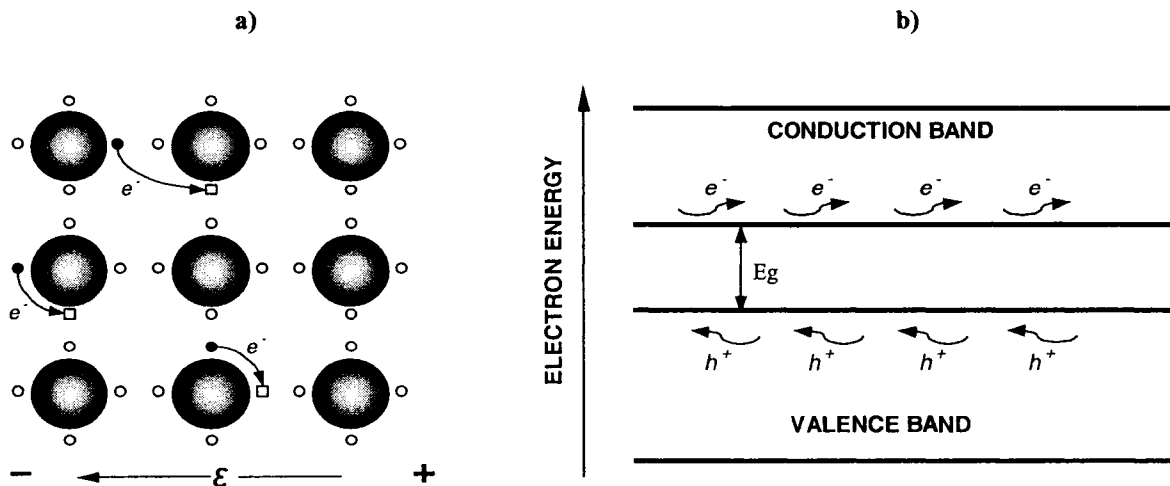
band that is completely filled with electrons and an empty conduction band (Fig 1.7). There is no overlap between the valence and the conduction bands, and the two are separated by an energy band gap, E_g .

Fig. I.7 Band diagram of a semiconductor



In an intrinsic semiconductor, there are two types of charge carriers – free electrons and holes. For every electron excited into the conduction band, there is a vacant electron state in the valence band. Under the influence of an electric field, the position of the missing electron within the crystal lattice changes because valence electrons can move to fill the vacant state (Fig. I.8a). Thus, the missing electron from the valence band can be treated as a positively charged particle called a hole. A hole is considered to have a charge that is of the same magnitude as that of an electron, but of opposite sign. In the presence of an electric field, excited electrons and holes move in opposite directions (Fig. I.8b).

Fig. I.8 Electrical conduction in intrinsic semiconductor



Literature Review

The band gap of GaN (3.4eV) is considered quite wide. InN has a narrower band gap (1.9eV), and the band gap of InGaN (1.0eV) is narrower than that of both of its constituent alloys (Alexandrov et al, 2006). Although, this may seem illogical, the band gap of the InGaN is controlled by the inhomogeneous mixing between GaN and InN binary alloys, resulting in defects in the crystal structure of the InGaN alloy. These defects are characterized by the occurrence of non-stoichiometric substitution of In atoms with N atoms in the crystal lattice, which gives rise to n-type conductivity (electron carriers) in the intrinsic InGaN and shifts the band gap to a smaller value (Alexandrov et al, 2005). Despite its n-type conductivity InGaN is still considered an intrinsic semiconductor as the conductivity of the InGaN is determined by the unique electronic structure of the material rather than by doping. Unlike InGaN, where majority carriers are electrons, the number of free electrons equals the number of holes in GaN.

In solids, the energy corresponding to the highest filled state at 0°K is called the Fermi energy, E_f , and in most semiconductors it lies within the band gap. Exceptions make the so called degenerated semiconductors, which are characterized with extremely high impurity concentrations and the Fermi level in these semiconductors may pass the conduction or the valence band edges. The discussion, presented below is only applicable to the non-degenerated semiconductors as the GaN and InGaN utilized in the project follow within this category.

The Fermi function $f(E)$ is defined as the probability that a given available electron energy state will be occupied at a given temperature and has the form:

$$f(E) = \frac{1}{e^{(E-E_f)/kT} + 1} \quad (1.3)$$

where:

E is the available energy state at which the value of the Fermi function is sought;

E_f is the Fermi energy level (eV);

T is the absolute temperature (in K);

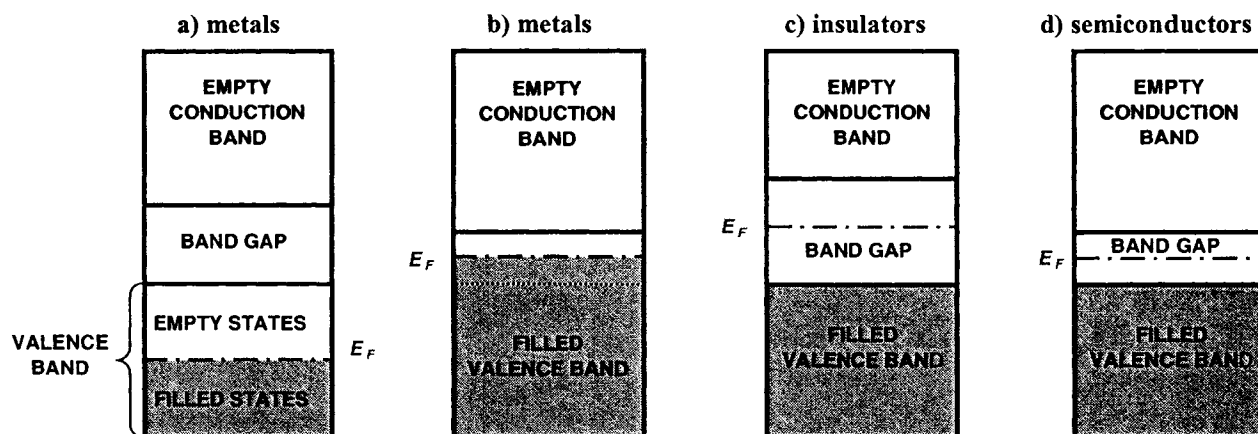
k is the Boltzmann constant (1.38×10^{-23} JK⁻¹)

Only those electrons with energies greater than E_f can participate in charge transfer reactions or be accelerated in the presence of an electric field. Holes have energies less than E_f and also

participate in the electric conduction process. Thus, the electrical conductivity of a solid is a direct function of the numbers of free electrons and holes. Additionally, the difference between conductive and non conductive materials lies in the number of these electron and hole charge carriers (Callister, 1997).

For an electron to become free, it must be excited into one of the empty and available energy states above E_f . In metals, there are vacant energy states adjacent to the highest filled state at E_f . A half-filled valence band is shown in Figure I.9a. This situation occurs in materials consisting of atoms that contain only one valence electron per atom. Most highly conducting metals including copper, gold, and silver satisfy this condition. Materials consisting of atoms that contain two valence electrons (e.g., magnesium) can still be highly conductive if the resulting filled valence band overlaps with an empty conduction band, as shown of Figure I.9b. For the above two scenarios (Fig. I.9a and b), very little energy is required to promote electrons into the low-lying empty states. However, no conduction is expected for the scenario shown on Fig. I.9c where a completely filled band is separated from the next higher empty state by a large energy gap. Such materials behave as insulators. Finally, Fig. I.9d shows the situation in semiconductors: for an electron within the valence band to become free, it must be promoted across the energy band gap and into the empty states at the bottom of the conduction band. This is possible only by supplying to the electron the difference in energy between these two states, which is approximately equal to the band gap energy, E_g .

Fig. I.9 Electron band structures in solids at 0°K



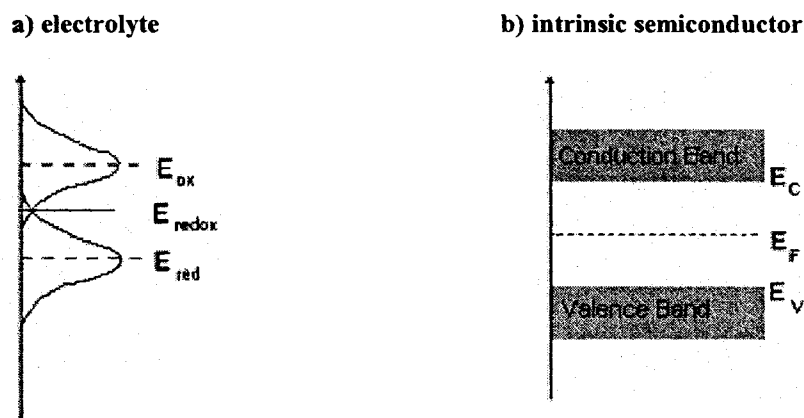
Although in semiconductors the Fermi energy lies above the top end of the valence band, there are no electrons at the Fermi energy level. This is because whether the electrons will be available at a particular energy level is determined not only by the position of the Fermi level but also on the electron density of states. Moreover, the electron population at a given energy level depends on the product of the Fermi function and the electron density of states. In semiconductors, although the Fermi function has a finite value in the band gap, there are no available energy states in the band gap. Hence, no electrons are present above the valence band at 0K.

Given the width of the band gaps in GaN and InGaN, less energy is required to excite electrons across the band gap of InGaN than GaN. As a result, under the same excitation, InGaN is more conductive than GaN.

1.5.2. The Semiconductor/Electrolyte Interface

Fig. I.10 shows the energy levels in a) the electrolyte and b) an intrinsic semiconductor electrode (such as GaN). The energy is plotted on the ordinate, and the probability of finding the energy level of an ion at that energy is plotted on the abscissa.

Fig. I.10 Energy levels in an electrolyte and in an intrinsic semiconductor
(Adapted from Ottow, 2006)



In the electrolyte (Fig. I.10a), three energy levels exist:

- E_{redox}^0 is the redox level corresponding to the standard electrode potential of the redox couple,
- E_{ox} is the most probable energy level of the oxidant in the redox couple, and

Literature Review

- E_{red} is the most probable energy level of the reductant in the redox couple.

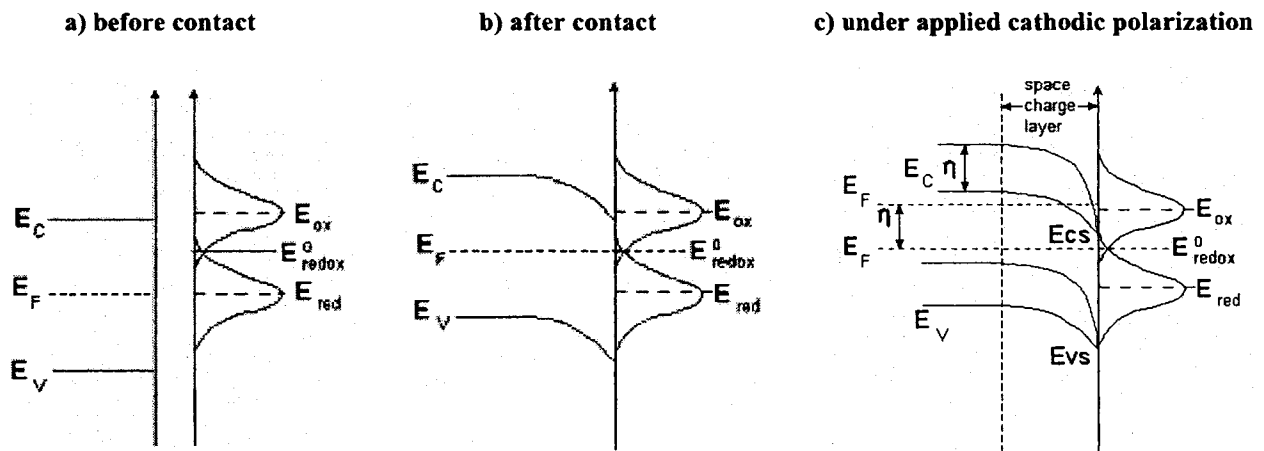
$E_{ox} \neq E_{red}$ because the energy level of the oxidized ion is different from the energy level of the reduced ion, due to differences in the solvation shell between the oxidized and reduced ions.

In Fig. I.10b, the semiconductor energy levels are shown with the level of the valance band, the conduction band, and the Fermi energy.

When the semiconductor is brought into contact with an electrolyte containing a redox couple, the Fermi level and the redox level align (Fig. I.11b). Because these two energy levels were different before the contact (Fig. I.11a), this process is accompanied by a charge transfer from the semiconductor to the electrolyte or from the electrolyte to the semiconductor, depending on the relative positions of the semiconductor Fermi level and the redox level. The direction of charge transfer is always from higher to lower energy level. As a result of this process a charge separation occurs at the semiconductor/electrolyte interface and gives rise to a potential difference. For example, for the situation shown in Fig. I.11a, the charge transfer would occur from the electrolyte to the semiconductor, as the redox level E_{redox}^0 before the contact is higher than the semiconductor Fermi level E_f .

Fig. I.11 Positions of the Fermi level in a semiconductor and the redox level in an electrolyte

(Adapted from Ottow, 2006)



If an external potential is imposed on the semiconductor electrode (Fig. I.11c), the Fermi level of the semiconductor electrode moves upward when the potential is made more cathodic and downward when the potential becomes more anodic. It has been shown that the positions of the

Literature Review

energy band edges at the semiconductor surface in contact with aqueous electrolyte (E_{cs} and E_{vs}) are pinned and independent of any redox system added to the solution or potential imposed on the electrode (Memming, 2001). Assuming that the energy band edges at the surface, E_{cs} and E_{vs} , remain at the same position and that the energy bands within the bulk semiconductor, E_c and E_v , move upward or downward when the position of the Fermi energy level moves, then the overall energy bands within the semiconductor electrode are bent under polarization. The region across which this bending occurs is called the space charge layer.

When the working semiconductor electrode and the reference electrode are brought in contact with an electrolyte solution, equilibrium is established and the electrochemical potential over all contacting phases is constant. However, if the reference electrode and the working (semiconductor) electrode are different and are placed in a two-compartment cell, then equilibrium throughout the whole cell does not exist because exchange of ions between the two compartments has been made impossible. On the other hand, equilibrium still exists in two half cells. In this scenario, the electrochemical potential of the electrons in the two electrodes is different. This difference in electrochemical potential can be measured as a voltage U_m between the reference electrode and the working (semiconductor) electrode and is related to the electrochemical potential by:

$$U_m = \Delta \overline{\mu}_e F \quad (1.4)$$

where:

U_m is the measured potential (V)

$\Delta \overline{\mu}_e$ is the difference in electrochemical potential of the electrons in the reference and the working electrode (eV)

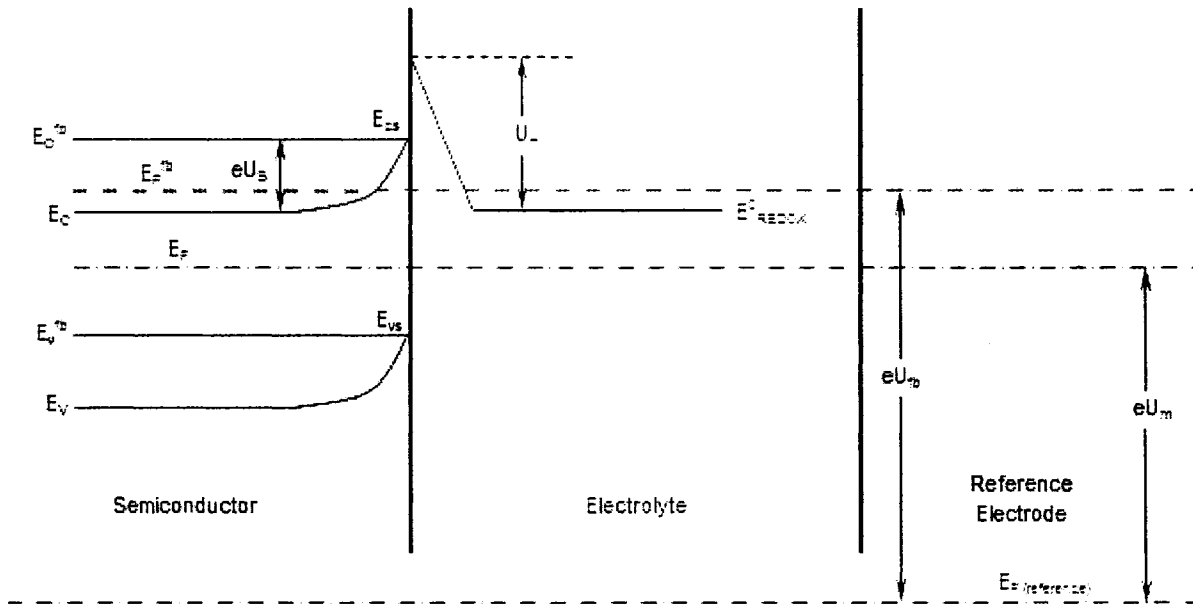
F is the Faraday constant and is equal to $9.6485309 \times 10^4 \text{ C mol}^{-1}$

Since the electrochemical potential of electrons in a metal or a semiconductor is also the Fermi level E_f , the measured electrode potential U_m can be directly related to the energy difference between the Fermi level of the semiconductor electrode and the Fermi level of the reference electrode. If U_m is the measured electrode potential (V) and e is the elementary charge of the electron ($1.6 \times 10^{-19} \text{ As}$), then the product eU_m (eV) is the energy difference between the Fermi

Literature Review

level of the semiconductor electrode and the Fermi level of the reference electrode (Fig. I.12). Similarly, if eU_s (eV) is the energy difference between the energy levels of the bottom of the conduction band at the surface and within the bulk semiconductor, then a very important characteristic of the semiconductor is the value of U_m when U_s is 0.

Fig. I.12 Energy level model of the semiconductor/electrolyte interface



This value of U_m is called the “flat band potential”, U_{fb} . In practice, an appropriate voltage can be applied at the semiconductor electrode to make U_s zero and then, the value of $U_{fb}=U_m$ can be measured directly. If the value of U_{fb} is known for a particular semiconductor, then the positions of E_{cs} and E_{vs} can be determined from:

$$eU_{fb} = E_{cs} - \mu \quad (1.5)$$

$$E_{vs} = E_{cs} - E_g \quad (1.6)$$

where:

e is the elementary charge of the electron (1.6×10^{-19} As)

μ is the mobility of carriers corresponding to the energy difference between bulk conduction band edge and Fermi energy, ($\text{cm}^2\text{V}^{-1}\text{s}^{-1}$)

E_g is the semiconductor band gap energy, (eV)

Literature Review

Although U_{fb} and the position of the energy band edges (E_{cs} and E_{vs}) at the semiconductor surface are independent of the redox system, they depend on the pH of the electrolyte. Hence, it is important to determine these semiconductor characteristics at a given pH value.

In the ideal case, the flat band potential and band edge potentials at the semiconductor surface for a given semiconductor should be the same regardless of material doping (Memming, 2001). In practice, however, it is known that slow charge transfer kinetics at the semiconductor/electrolyte interface can cause a shift in the band edge potentials because of charge accumulation (Bansal and Turner, 2000). Accumulation of electrons at the interface shifts the potentials to more negative values, and accumulation of holes at the interface shifts the potentials toward more positive values. Beach et al. (2003) determined the flat band potentials U_{fb} for n-type and p-type GaN as a function of pH. On the basis of the determined U_{fb} , they calculated the band edge potentials at the semiconductor surface for both types of GaN doping and found that the band edge potentials at the semiconductor surface for p-type GaN are 0.7V to 1V more negative than for n-type GaN (Beach et al., 2003). On the basis of their results, the value of the band edge potentials at the semiconductor surface for the undoped GaN sample electrodes used in the current research project were taken as the average of n-type and p-type GaN band edge potentials values, i.e:

- $E_{cs} = -1.30\text{eV}$ versus the standard Calomel electrode (SCE) or $E_{cs} = -1.058\text{eV}$ versus the standard hydrogen electrode (SHE) at pH = 5.5 (this was the measured pH for the test electrolyte solutions).
- $E_{vs} = +2.1\text{eV}$ versus SCE or $E_{vs} = +2.342\text{eV}$ versus SHE at pH = 5.5.

The InGaN band edge potentials at the semiconductor surface were determined on the basis of the study by Fujii et al (2005), who investigated the InGaN band edge potentials at the semiconductor surface as a function of In composition in the alloy. For 20% In content in the InGaN alloy on molar basis, the band edge potentials at the semiconductor surface obtained through interpolation of their results are:

- $E_{cs} = -0.40\text{eV}$ versus the Ag/AgCl reference electrode or $E_{cs} = -0.188\text{eV}$ versus SHE at pH = 5.5.

Literature Review

- $E_{vs} = +2.5\text{eV}$ versus the Ag/AgCl reference electrode or $E_{vs} = +2.712\text{eV}$ versus SHE at pH = 5.5.

The charge transfer across the semiconductor/electrolyte interface occurs via the energy bands. The positions of the energy band edges at the semiconductor surface are pinned and do not change after the addition of a redox system to an aqueous electrolyte or under polarization of the electrode. Therefore, the positions of the energy levels of the redox system, E_{ox} , E_{red} and E_{redox}^0 , remain unchanged with respect to the energy band edges E_{cs} and E_{vs} at the semiconductor surface. Consequently, if we place E_{redox}^0 , E_{cs} , and E_{vs} on the same energy scale, we can compare the energy levels of the bands in the semiconductor at the surface with the energy levels of the ions in solutions and predict the direction of the charge transfer processes at the semiconductor/electrolyte interface. A detailed description of the approach that is followed when determining the interfacial processes is provided in Section III.7 of Chapter III: Results and Discussion.

In addition to the charge transfer processes at the semiconductor/electrolyte interface, adsorption/desorption reactions also occur.

Once the semiconductor electrode (GaN or InGaN) is immersed in solution, its surface is easily attacked by water molecules and anions because of the positive charge of the electron deficient Ga-atoms in the case of the GaN electrode, and Ga and In atoms in the case of the InGaN electrode. The following types of interactions are possible:

- Electrostatic interaction between the positively charged Ga-surface (or InGa-surface) and the water dipoles and anions in solution, i.e., non-specific adsorption processes.
- Chemical reactions between water molecules and the positively charged outer Ga-atoms (Ga and In atoms in the case of the InGaN electrode) resulting in formation of N-Ga-OH chemical bonds and the generation of H^+ ions, i.e., specific adsorption processes:



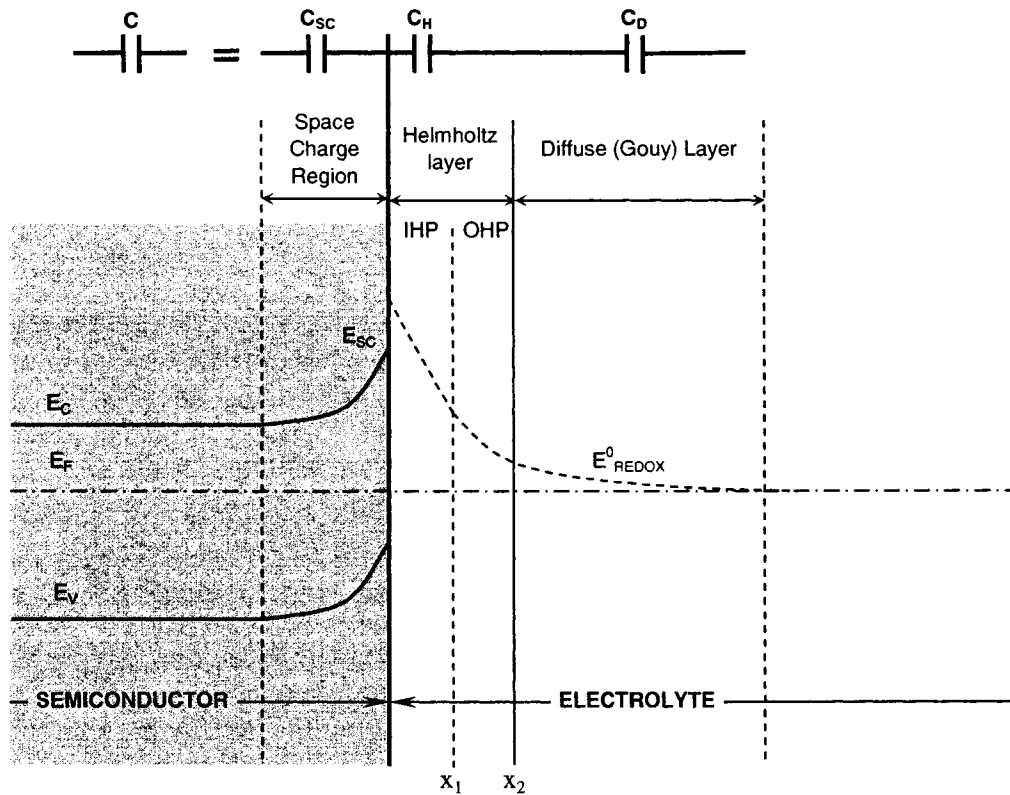
- Because of the mixed polarity of the GaN crystal, the surface of the electrode also contains some N-face regions, where the negatively charged, electron excessive N-atoms will attract

hydrogen cations from the solution to form GaN-H chemical bonds according to the following reactions:



All of the above processes result in the formation of a double layer on the electrolyte side of the semiconductor/electrolyte interface and a space charge region on the semiconductor side (Fig. I.13). The red dashed line through the liquid represents the variation of potential over the interfacial region.

Fig. I.13 Structure of the semiconductor/electrolyte interface



The solution side of the double layer itself consists of several layers. As the Ga-face regions (respectively InGa-face) are dominant at the semiconductor electrode surface the following discussion will focus on them. The first layer is formed of OH^- ions specifically adsorbed on the electrode surface and is called the Inner Helmholtz Plane (IHP). The center of electrical charge in the IHP is located at distance x_1 from the semiconductor/ electrolyte interface. The second layer is formed of non-specifically adsorbed water dipoles and anions that have kept their

Literature Review

solvation shells. They can only approach the electrode surface at a distance x_2 . This second layer is called the Outer Helmholtz Plane (OHP). Furthermore, because the interaction between solvated anions and the positively charged surface involves only long-range electrostatic forces, the excess anions are distributed over a relatively large region extending from the OHP to the bulk solution. This three dimensional region is called the diffuse layer or the Gouy layer.

The formation of the double layer on the electrolyte side creates a charge imbalance at the semiconductor/electrolyte interface, which is compensated by the accumulation of counter charges on the semiconductor side. These counter charges are holes that move within the valence band of the semiconductor and towards the interface. Unlike in metal electrodes where the charge carrier density is high and counter charges are located just below the interface, the carrier density in the semiconductor is smaller and the excess counter charges are distributed over a larger region extending from the interface into the bulk semiconductor called the Space Charge Region (SCR).

At high concentrations of a conducting salt in the electrolyte solution, the excess electric charges on the solution side are concentrated within the IHP and the OHP; while at low concentration they are distributed over the much thicker diffuse or Gouy layer. In the former case, the double layer on the solution side can be approximated by a single parallel-plate capacitor. The charge density Q_i stored in such a capacitor is related to the voltage drop U across the capacitor by:

$$Q_i = \frac{\epsilon\epsilon_0}{x_1} U \quad (1.11)$$

where:

ϵ is the dielectric constant of the electrolyte

ϵ_0 is the permittivity of vacuum ($8.85 \times 10^{-14} \text{ Fcm}^{-1}$)

x_1 is the length of the Helmholtz plane (cm)

The differential capacity is then given by:

$$C_H = \frac{dQ_i}{dU} = \frac{\epsilon\epsilon_0}{x_1} \quad (1.12)$$

Literature Review

If we use $\epsilon = 20$ and $x_1 = 5 \times 10^{-8} \text{ cm}$, we obtain $C_H \approx 3 \times 10^{-5} \text{ Fcm}^{-2}$. For solutions with high salt concentration ($\geq 10^{-2} \text{ M}$), it is safe to neglect the potential drop across the diffuse double layer and to only take into account the potential drop across the Helmholtz layer (Memming, 2001).

With semiconductor electrodes, either adsorption/desorption or electron transfer processes can control the potential of the Helmholtz layer formed at the semiconductor/electrolyte interface. However, similarly to insulators, the potential of the Helmholtz layer is most often dominated by adsorption/desorption processes rather than by the charge transfer process (Morrison, 1980). The exception is heavily doped semiconductors, in which the density of charge carriers is so high that their behaviour approximates that of metals, where the potential of the Helmholtz layer is controlled by charge transfer processes. As for metals, there can be redox reactions at the surface of semiconductor electrodes, with electron transfer occurring from the semiconductor to the electrolyte or in the opposite direction. However, the amount of charge accumulated at the interface as a result of these charge transfer processes is negligible in comparison with the amount of charge stored as a result of adsorption/desorption processes.

Similarly to the Helmholtz layer, the space charge region can also be approximated by a parallel plate capacitor, with a charge density given by:

$$Q_{sc} = \epsilon \epsilon_0 E_s \quad (1.13)$$

where:

ϵ is the dielectric constant of the semiconductor

ϵ_0 is the permittivity of vacuum (Fcm^{-1})

E_s is the electric field strength (Vcm^{-1})

The differential capacity of the space charge layer is given by:

$$C_{sc} = \frac{\epsilon \epsilon_0}{L_D} \cosh\left(\frac{e \Delta \phi_{sc}}{kT}\right) \quad (1.14)$$

where:

k is the Boltzmann constant ($1.38 \times 10^{-23} \text{ JK}^{-1}$)

T is the absolute temperature (K)

Literature Review

L_D is the Debye length, i.e. the distance over which significant charge separation can occur (cm)

$\Delta\phi_{SC}$ is the potential change across the space charge layer (V)

e is the elementary charge

The total differential capacity of the semiconductor/electrolyte interface, C , can then be approximated by two capacitors, C_{SC} and C_H , connected in series:

$$\frac{1}{C} = \frac{1}{C_{SC}} + \frac{1}{C_H} \quad (1.15)$$

I.6. Previous Electrochemical Studies of GaN

The properties of GaN and InGaN semiconductors have been previously investigated in several electrochemical studies (Kobayashi et al, 2005; Fujii and Ohkawa, 2006; Fujii et al, 2005) but the main emphasis of these studies has been on GaN and InGaN potential applications as photo electrodes in photo electrochemical cells for solar powered production of hydrogen. While the development of other semiconductor-based sensors has been extensive, the investigation of GaN and InGaN sensors is at an early stage.

Chaniotakis et al. (2004) studied the potential application of GaN as a potentiometric anion sensor and reported that the sensor responds selectively to the tested anions in aqueous solutions. For their experiments, they utilized sensing element consisting of 0.5 μm Ga-face GaN (0001) films grown on sapphire (Al_2O_3). The GaN samples were undoped. The sensor contact was made by bonding a 0.1mm-diameter platinum wire with indium to the edge of the GaN sensing element. The entire electrode assembly was covered with epoxy glue leaving only the GaN surface exposed to the solution. The response of these potentiometric sensors was investigated with electrochemical techniques such as open circuit potential (OCP) measurements and electrochemical impedance spectroscopy (EIS). The selectivity of the sensor was tested for various salts dissolved in water (KF, KNO_3 , KCl, $\text{HOC}_6\text{H}_4\text{COONa}$, KSCN, CH_3COOK , KClO_4 , KBr and KI). Fig. I.14 shows OPC values versus anion concentration for four different salts.

Fig. I.14 Calibration curves of the GaN-based sensor to four different potassium salts
 (○) KF, (□) KCl, (Δ) KNO₃ and (*) KSCN (Chaniotakis et al., 2004)

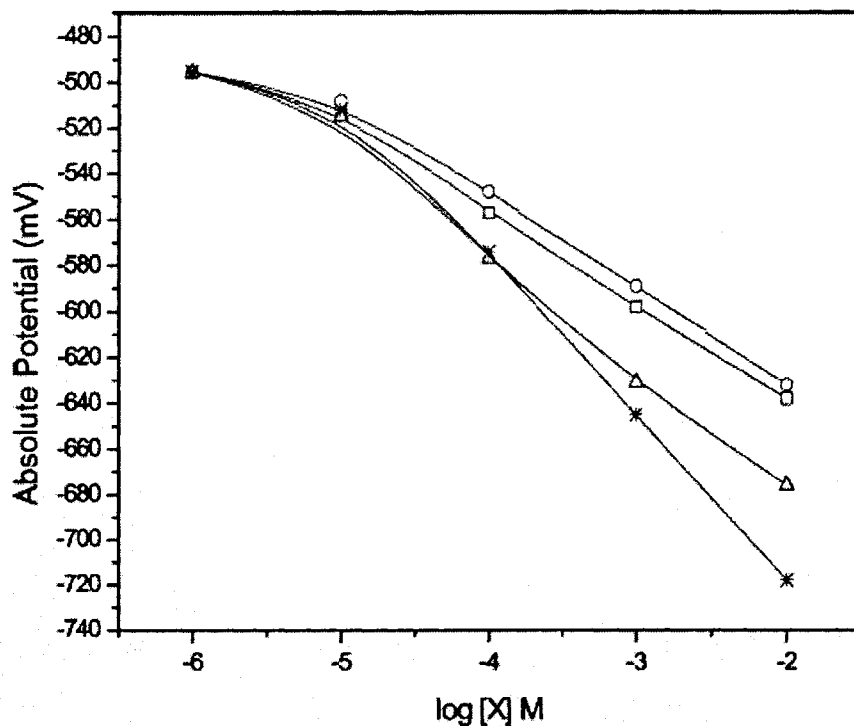


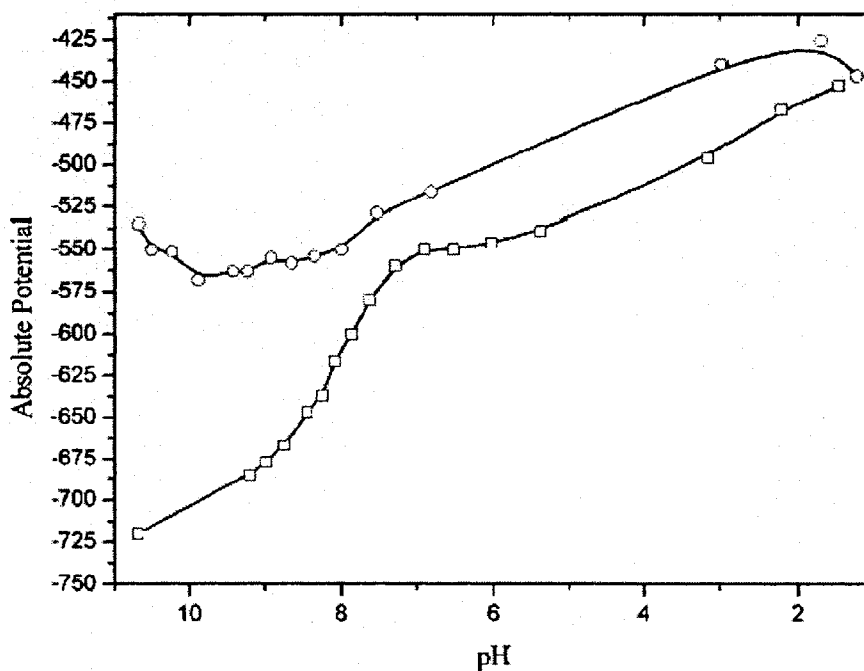
Fig. I.14 shows that the sensitivity of the GaN depends on the type of anion. Chaniotakis et al. explained that the potentiometric response of the GaN-based electrode is due to the fact that the Ga-face GaN (0001) surface has two complete bonds to the nitrogen atoms of the underlying atomic plane and one remaining bond “unbound”. This makes the Ga-atoms electron defective with respect to the nitrogen atoms and thus susceptible to coordination with negatively charged species such as anions. Chaniotakis et al. suggested that if the surface of the GaN crystal can selectively interact with charged species, the observed potentiometric response is due to the preferential adsorption of the specific ions in the Helmholtz layer. Electrochemical impedance studies were carried out to demonstrate that the generated electrode potential is based purely on the Helmholtz layer. EIS results showed that the complex impedance of GaN electrode system is inversely proportional to the activity of the anions, i.e. the complex impedance increases as the anion activity decreases. However, Chaniotakis et al. did not attempt to model the obtained impedance spectra with an analogous equivalent circuit model and, consequently, did not calculate the parameters required to characterize the interfacial features such as double layer capacitance, semiconductor resistance, solution resistance, etc. Investigations of electrode stability reported by Chaniotakis et al showed that the GaN sensor exhibits extremely high

Literature Review

mechanical and chemical stability and can not be etched or destroyed under any wet chemical conditions. They elaborated that the etching of the GaN surface can be performed to a limited degree only under photoelectrochemical activation and in very corrosive environments. Their experiments showed that the potential of the GaN sensor is very stable over time and exhibits no significant potential drift if the sensor remains immersed in electrolyte solution for up to 5 days. The response time of the sensor in the investigated electrolyte solutions was found to be very fast and within 50s. Based on their experimental results and observations, Chaniotakis et al. concluded that the response of the GaN sensor to anions is purely a surface phenomenon involving anion coordination and resulting in the generation of an interfacial potential related to the activity of the anions.

In another study of a GaN anion selective potentiometric sensor, Alifragis et al (2005) showed that the GaN sensor also responds to pH changes. The construction of their Ga-polarity GaN (0001) electrodes was similar to the construction of the GaN sensors utilized by Chaniotakis et al. The results showed that the electrode potential becomes more positive when the pH decreases (Fig. I.15).

Fig. I.15 pH sensitivity of the GaN sensor in 2 M KOH before (circles) and after (squares) oxidative treatment (Alifragis et al., 2004)



Literature Review

Alifragis et al concluded that the observed response of the GaN semiconductor electrode to pH changes is due to the selective interaction of the positively charged Ga-face GaN surface with the hydroxide anions in solution. Further investigation of the GaN sensor pH response showed that if the surface of the electrode is oxidized, i.e. etched (exposing both Ga-face sites and N-face sites), then the response to pH changes becomes mixed and is due to coordination of hydroxide ions by the Ga-face sites and hydrogen ions by the N-face sites.

Alifragis et al. also studied the response of the GaN sensor to three different anions: HPO_4^{2-} , Cl^- and ClO_4^- through open circuit potential measurements and electrochemical impedance spectroscopy. Their results corroborated the theory of Chaniotakis et al. (2004) that the GaN semiconductor electrode response is based on the outer face interaction between anion in solution with gallium atoms on the GaN surface. Alifragis et al found that the response time and the reversibility of the GaN electrode response to the above mentioned anions is very fast and reproducible.

1.7. Operation of ISEs

In this section, some of the essential procedures and features of the operation of ISEs will be introduced.

1.7.1. Calibration of ISEs

There are a number of calibration methods based on measurements of electrochemical cell potentials (Rieger, 1994). For convenience these can be divided into two groups: those which determine concentration (or activity) directly from the measured potential of an electrochemical cell; and those in which the potential of a cell is used to determine the equivalence (end) point in a titration (Rieger, 1994). The first group of calibration methods is subdivided to direct calibration and incremental methods.

1.7.1.1. Direct Calibration

1.7.1.1.1 Method Description

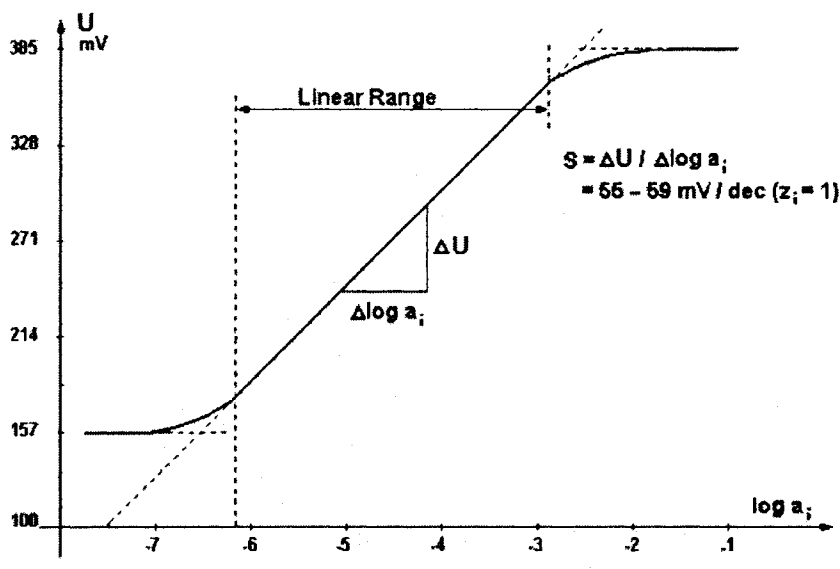
Direct calibration is the simplest and most widely used method for ISEs (NICO 2000 Ltd.). Calibration is carried out by immersing the electrode in a series of standard solutions of known concentration and plotting a graph of the potential reading (mV) versus the log of the activity (or

Literature Review

the actual activity on a logarithmic X-axis) (See Fig. I.16). This should give a straight line over the whole linear concentration range. When this method is used, it is important that the test solution have the same ionic strength as that of the standards so that the activity coefficients remain constant (Rieger, 1994). However, activity is difficult to determine in complex solutions and it is generally more useful to plot concentration units (NICO 2000 Ltd.). In this case the effect of variable activity coefficients in solutions with high ionic strength can be minimized by adding a solution of high ionic strength called ionic strength adjustment buffer (ISAB) to all standards and samples in order to ensure that all measured solutions have the same ionic strength and avoid errors due to differences between the measured activity and the actual concentration. The idea is that the ISAB is added in sufficient quantity to completely swamp the ionic effects of the host solutions and hence give a uniform ionic strength in all samples and standards. In this case, the straight-line calibration curve can be constructed using concentration units, and the unknown concentrations can be read directly from the calibration graph (NICO 2000 Ltd.). Often, a fixed pH solution or buffer controls the hydrogen ion activity (pH) as well as ionic strength. Nevertheless, it must be noted that if the samples to be measured are likely to have a total ionic strength less than about 0.01M for monovalent ions (0.001M for divalent ions), then the activity effect should be insignificant and it may not be necessary to add ISAB (NICO 2000 Ltd.).

The slope of the calibration graph is the change in potential response per decade of concentration change. This is typically around 59 mV/decade for monovalent ions and 29 mV for divalent ions. The slope will have a negative value for negative ions, i.e., a higher concentration means more negative ions in solution and therefore a lower potential (NICO 2000 Ltd.).

Fig. I.16 Typical ISE Calibration Graph
(NICO 2000, Ltd., 2005)



A significant advantage of this calibration method is that it can be used to measure large batches of samples covering a wide range of concentrations very rapidly without having to change the range, recalibrate, or make any complicated calculations (NICO 2000 Ltd.). Moreover, if an ISAB is not used, it is not necessary to measure the volume of the samples or standards. Quite acceptable results can be obtained for some elements by simply dangling the electrodes in a river or pond or effluent outflow without the need to take samples in small beakers (NICO 2000 Ltd.).

1.7.1.1.2 Linear Range

The linear range of the electrode is defined as that part of the calibration curve through which a linear regression would demonstrate that the data points do not deviate from linearity by more than 18 mV. For many electrodes this range can extend from 1 M down to 10^{-6} or even 10^{-7} M (NICO 2000 Ltd.).

1.7.1.1.3 Total Measuring Range

The total measuring range includes the linear part of the graph as shown below, together with a lower curved portion where the response to varying concentration becomes progressively less as the concentration reduces. Samples can be measured in this lower range but it must be noted that more closely spaced calibration points are required in order to define the curve accurately, and the percentage error per mV on the calculated concentration will become progressively higher as the slope reduces (NICO 2000 Ltd.).

Literature Review

1.7.1.1.4 Limit of Detection

For monovalent ions, the International Union of Pure and Applied Chemistry (IUPAC) defines the detection limit as the concentration at which the measured potential differs from that predicted by the linear regression by more than 18 mV. The practical limit of detection can be calculated by plotting a calibration graph using several standards at the lower end of the concentration range and below it. At least two standards are required to define the slope in the linear range, and two other standards are required to show the position of the horizontal section below the limit of detection, where the electrode is unresponsive to concentration change. The limit of detection is then defined as the crossing point of the two straight lines drawn through these points (NICO 2000 Ltd.).

1.7.1.2. Incremental Methods

There are three main types of incremental methods in general use:

- Standard (or Known) Additions,
- Sample Additions,
- Sample Subtractions.

1.7.1.2.1 Standard Additions

By first measuring the potential of an unknown solution and then adding a known amount of the substance detected, the incremental response of the voltmeter in effect calibrates the scale (Rieger, 1994). The advantages of this procedure are that the concentration is determined without the tedium of a calibration curve, and, more importantly, calibration is obtained on the same solution under the same measurement conditions, possibly avoiding some systematic errors. On the other hand, if the calibration curve is not linear, the know addition method would introduce a large uncorrectable error (Rieger, 1994).

As a rule, the calibration curve method is preferable if many analyzes are to be done (Rieger, 1994). If only a few analyzes are to be performed, the standard addition method is usually faster. In either case, the method should have been carefully investigated to remove systematic errors (Rieger, 1994).

Literature Review

1.7.1.2.2 Sample Additions

This is a procedure that uses sequential addition of the unknown-concentration sample to a standard while recording the changes in the cell potential (IUPAC, 1994).

1.7.1.2.3 Sample Subtractions

This is a variation of the Standard Addition Method (IUPAC, 1994). This procedure involves adding a small amount of sample solution to a standard solution of an ion with which it will react stoichiometrically to form a complex or precipitate, thus reducing the concentration of both ions (NICO 2000 Ltd.). The ISE used is sensitive to the reactive ion in the standard, not to the sample.

The main advantage of this method is that it can extend the range of ions measurable by ISEs to other ions for which no ion-sensitive membranes are available. For example, there is currently no ISE capable of detecting the sulphate ion (NICO 2000 Ltd.). However, sulphate can be removed from solution by precipitating as barium sulphate, and there is an ISE that is sensitive to barium. Therefore, sulphate can be measured by first measuring the potential of a pure barium chloride standard, then adding a known volume of a sample containing sulphate and waiting for precipitation to be completed, and finally measuring the potential of the barium electrode again. The amount of precipitated barium can then be calculated using a similar equation to that used for the Sample Addition method. The sulphate content in the sample is the same as the precipitated barium, since each sulphate ion combines with one barium ion (NICO 2000 Ltd.).

1.7.1.3. Titration Methods

ISEs have also been used as detectors of the end point of a titration. Titration methods use a titrant (such as EDTA) that complexes or reacts with the ion to be analyzed (Orion Research Inc., 1997). If either the titrant or the titrated substance is detected by an ISE, a plot of the cell potential versus the volume of the titrant shows a sharp increase or decrease in potential at the endpoint (Rieger, 1994). These end point determinations can often be more precise than other ISE methods because they depend on the accuracy of the volumetric measurements rather than the measurement of the electrode potential (NICO 2000 Ltd.). For example, when a calcium solution is titrated against the complexing reagent EDTA, there is a gradual decrease in the Ca concentration as more EDTA is added until the end point when all the Ca disappears from

solution. The progress of this titration can be monitored using a calcium electrode (NICO 2000 Ltd.).

This method can also be used to extend the range of ions measurable by ISEs (NICO 2000 Ltd.). For example, aluminium cannot be measured by direct potentiometry but it can be titrated by reacting with sodium fluoride and monitoring the reaction using a fluoride electrode. Titration methods can also be used for elements for which it is difficult to maintain stable standard solutions or and are toxic undesirable to handle as concentrated standard solutions. For example, cyanide solutions can be titrated against a hypochlorite solution, which forms a complex with the cyanide ions and effectively removes them from solution. The amount of cyanide in the original solution is proportional to the amount of hypochlorite used from the start of the titration until the end-point when there is no further change in the cyanide electrode potential (NICO 2000 Ltd.).

1.7.2. Sources of Error

There are several factors that can cause difficulties when ISE technology is applied to the measurement of ions (NICO 2000 Ltd.). These are reviewed below.

1.7.2.1. Diffusion

The standard voltage given by a reference electrode is only correct if there is no additional voltage produced by a liquid junction potential formed at the porous plug between the filling (internal) solution and the external test solution. At the junction between these two electrolytes, ions from one solution diffuse into the other. Orion Research points out that differences in the rates of diffusion of ions based on size can lead to some error (Orion Research Inc., 1997). In the example of sodium iodide, sodium diffuses across the junction at a given rate. Iodide moves much slower due to its larger size. A charge separation occurs related to the differences in mobilities of the ions in the two solutions. This charge separation produces a potential difference across the junction called the liquid junction potential (Bailey, 1980). When an analysis with an ion selective electrode is carried out, it is assumed that the liquid junction potential in the standard solutions used to calibrate the electrode remains constant in all subsequent measurements. Any change in the liquid junction potential when the standards are replaced with the sample solutions is termed the residual junction potential and constitutes an error in the analytical measurement (Bailey, 1980). To compensate for this type of error, it is important that

Literature Review

a positive flow of filling solution move through the junction, thus minimizing the effect of different diffusion rates of the ions, and that the junction not become clogged or fouled (Orion Research Inc., 1997).

1.7.2.2. Sample Ionic Strength

ISEs measure the concentration of ions in equilibrium at the membrane surface (NICO 2000 Ltd.). In dilute solutions, this concentration is directly related to the total number of ions in solution but at higher concentrations, inter-ionic interactions between all ions in the solution (both positive and negative) tend to reduce the mobility, and thus there are relatively fewer of the measured ions in the vicinity of the membrane than in the bulk solution. Thus, the measured potential is less than it would be if it reflected the total number of ions in the solution, and this causes an erroneously low estimate of the concentration in samples with a high concentration and/or a complex matrix.

Ionic strength is a measure of the total effect of all the ions in a solution. The ionic strength of the sample is defined as the sum of the molar concentrations multiplied by the square of the charge of all the ions:

$$I = \frac{1}{2} \sum c_i Z_i^2 \quad (1.16)$$

where:

I is the ionic strength;

c_i is the amount concentration of the ion i (usually in moles per litre);

Z_i is the charge of the ion i.

The effective concentration measured at the electrode head is known as the activity of the ion (NICO 2000 Ltd.). In general chemical terms, it is the number of ions taking place in any chemical reaction – measured in concentration units. The activity coefficient is the ratio of the activity divided by the concentration. This is a variable factor that depends on the charge and ionic radius of the measured ion as well as the total ionic strength of the solution. For solutions with ionic strength $I < 10^{-2.3}$, the activity coefficient is given by the Debye-Huckel equation:

$$\text{Log} \gamma_i = -AZ_i^2 (I^{1/2}) \quad (1.17)$$

Literature Review

For solutions with ionic strength $I < 0.5$, the activity coefficient is given by the Davies equation:

$$\text{Log } \gamma_i = -AZ_i^2 \left[I^{1/2} / (1 + I^{1/2}) - 0.3I \right] \quad (1.18)$$

where $A = 0.512$ for water at 25°C .

The activity coefficient is always less than one and becomes smaller as the ionic strength increases. Hence, the difference between measured activity and actual concentration becomes higher at higher concentrations. This effect causes two main problems in ISE measurements. Firstly, when constructing a calibration graph using concentration units, the line is seen to curve away from linearity as the concentration increases (it remains straight up to higher concentrations if activity units are used). Thus, if concentration units are used, it is necessary to measure many more calibration points in order to define the curve more precisely and permit accurate interpolation of sample results. Secondly, it is most likely that the sample solutions will contain other ions in addition to the ion being measured. Hence, the ionic strength of the samples may be significantly higher than that of the standards. Thus, there will be an incompatibility between the calibration line and the measured samples leading to errors in the interpolated results. Using equations (1.16), (1.17) and (1.18) it is possible to calculate the activity coefficient and the concentration of the measured ion in a solution where the concentrations of all the other ions are known. However, in most practical applications, this is not possible or very difficult and time-consuming.

For ion concentration measurements, steps must be taken to minimize the effect of the ionic strength of the sample. This is because ISEs directly measure the activity of the ion that can differ significantly from concentration in samples with complex matrices and high ionic strength. For samples with high ionic strength, there are five possible methods that can be used to avoid the error introduced by the difference between activity and concentration (NICO 2000 Ltd.):

- Bring the ionic strength to the same level in both the calibrating standard solutions and the samples by adding a suitable ionic strength adjustment buffer (ISAB) to both. This adjustment is large compared to the ionic strength of the sample.

Literature Review

- Dilute the samples to a level where the ionic strength effect is insignificant, while making sure that the detected ion is still within the linear range of the electrode.
- For samples with complex but known matrix, make up the standards in a similar matrix, which does not contain ions that would interfere with the measurement.
- Use the activity coefficient to calculate the concentration. As noted above, the activity coefficient can be calculated for simple solutions with known concentrations of all the ions, but this is not possible in many practical applications where the samples may have a complex or unknown matrix.
- Use the standard addition (or sample addition) method where the potential is measured before and after a known small volume of standard (or sample) is added to a larger volume of sample (or standard) and the ionic strength is not altered significantly (NICO 2000 Ltd.).

1.7.2.3. Interferences

The background matrix can affect the accuracy of measurements taken using ISEs. Most ion-selective membranes are not entirely ion-specific and can permit the passage of ions different from the target ion that may be present in the test solution, thus causing the problem of ionic interference (NICO 2000 Ltd.). According to the IUPAC definition, the interfering substance may be any substance, other than the ion being measured, whose presence in the sample solution affects the measured potential of a cell (IUPAC, 1994). Interfering substances fall into two classes: "electrode/electrochemical" interferences and "chemical" interferences. Examples of the first class include (IUPAC, 1994):

- those substances which give a similar response to the ion being measured and whose presence generally results in an apparent increase in the activity (or concentration) of the ion to be determined (e.g., Na^+ for the Ca^{2+} electrode).
- electrolytes present at a high concentration that give rise to appreciable liquid junction potential differences or result in a significant activity coefficient decrease.

The second class of substances that should be recognized as chemical interferences includes (IUPAC, 1994):

- species that interact with the ion being measured so as to decrease its activity or apparent concentration. The electrode continues to report the true activity (e.g., CN^- present in the measurement of Ag^+), but a considerable gap will occur between the activity and concentration of the ions even in very dilute solutions. Under these circumstances, the determination of ionic concentration may be problematic.
- substances interacting with the membrane itself by blocking the surface or changing its chemical composition (i.e., organic solvents for the liquid or polyvinyl chloride (PVC) membrane electrodes) are grouped as interferences or electrode poisons.

1.7.2.4. Selectivity Coefficient

The ability of an ion-selective electrode to distinguish between different ions in the same solution is expressed as the selectivity coefficient (NICO 2000 Ltd.). If the primary ion for which the electrode is sensitive is A and the interfering ion is B, then a selectivity coefficient of 0.1 would mean that the electrode is ten times more sensitive to A than to B. If the coefficient is 1 then the electrode is equally sensitive to both. Unfortunately, the selectivity coefficient is not constant and depends on several factors including the concentration of both elements, the total ionic strength of the solution, and the temperature. Thus, the selectivity coefficient cannot be used to make accurate corrections for the interfering ion in any simple manner (NICO 2000 Ltd.).

A common example of interference is that of the chloride ion on the nitrate electrode (NICO 2000 Ltd.). In this case, the selectivity coefficient is only about 0.003. This means that an equal concentration of chloride would only add about 0.3 % to the nitrate signal. Nevertheless, in many natural waters the Cl/NO_3 ratio can be as high as 50:1 or even more, thus causing a possible 15 or 20% increase in the apparent NO_3 signal. In this case, however, the chloride ion can be removed from solution by precipitating as the sparingly soluble silver chloride. So, by adding measured quantities of the appropriate reagents to samples and standards, the analyst can overcome this problem in the laboratory (NICO 2000 Ltd.). However, this is not possible for in situ measurements.

1.7.2.5. Accuracy of Measurements

The measured potential differences (ISE versus outer reference electrode potentials) are linearly dependent on the logarithm of the activity of a given ion in solution according to the Nikolsky-Eisenman equation (See Equation 1.2). The calculation of ionic concentration is dependent on a precise measurement of the potential difference (NICO 2000 Ltd.). For example, only a 1 mV error will cause at least a 4% error in the calculated concentration of a monovalent ion and more than 8% for a divalent ion. This is because the theoretical value for the slope at 25°C is 59.2 mV/decade for monovalent ions and 29.6 mV/decade for divalent ions (NICO 2000 Ltd.). In practical application, however, these slopes can vary considerably because of variations in temperature, deviations from "ideal" behaviour, minor impurities or contamination of the ion-selective membrane, or measurements near the detection limit of the electrode in the non-linear range. The critical factor is not so much the actual value of the slope but that this should be as high as possible and remain constant over the range of concentrations and the time period required for the analyzes. Thus, when measuring ion concentrations, it is essential to take extra precautions to minimize any errors in the measurement of the electrode potential.

1.7.2.6. Temperature

It is important that temperature be controlled as variations in this parameter can lead to significant measurement errors. A single degree (°C) change in sample temperature can lead to measurement errors greater than 4% (Orion Research Inc., 1997). In some cases, it is possible to match the temperature coefficient of the ion-selective electrode to that of the reference electrode so that the cell is approximately temperature-insensitive with respect to shift in the measured potential (Bailey, 1980). Correction must still, however, be made for the change in response slope of the ion-selective electrode with temperature. The isopotential concept may also be used to determine ways of minimizing temperature effects. According to the IUPAC definition, for an ion-selective electrode cell, there is often a particular activity of the measured ion for which the potential of the cell is independent of temperature (IUPAC, 1994). That activity, and the corresponding potential difference, define the isopotential point and if they are known, then the calibration is usually done at this activity. If the subsequent measurements are to be done at different temperatures, using the isopotential point and knowing the value of the electrode slope

Literature Review

enables to compensate (correct) the measured activity at any temperature to a reference temperature (usually 25°C).

1.7.2.7. pH

Some samples may require conversion of the analyte to one form by adjusting the pH of the solution (e.g. ammonia) (Lynde, 2005). Failure to adjust the pH in these instances can lead to significant measurement errors. In many cases, pH control is necessary for accurate and repeatable measurements. Certain ions exhibit a different activity when different concentrations of hydrogen ions are present in solution. This occurrence will not only alter the potential due to the specific ion that is measured, it may also allow other ions in solution to become active that otherwise were not (Lynde, 2005). This increased activity from the other ions will interfere with the ability to evaluate the ion of interest. Some ISEs will only work effectively over a narrow pH range (NICO 2000 Ltd.).

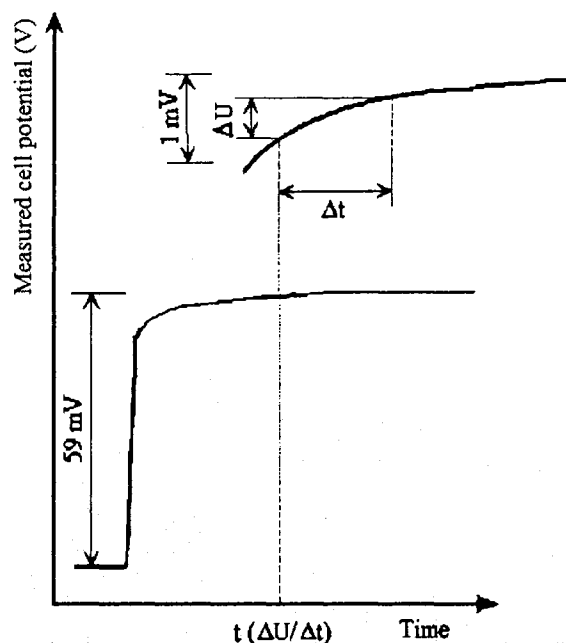
1.7.2.8. Response Time

One of the most attractive features of ion-selective electrodes is the speed with which they permit a sample to be analyzed, and the ease with which the methods may be made semi-automatic or fully-automatic (Bailey, 1980). If samples are measured by a direct calibration method, all that needs to be done is to pretreat the sample by addition of aliquot or a pretreatment agent (ionic strength adjustment buffer or pH buffer), stir the sample, and put the ion-selective electrode and reference electrode into it. The equilibrium cell potential may be read usually within about a minute and the answer obtained. Rapid solution movement on the electrode surface by stirring helps to reduce the response times of the ion selective electrodes even further. Thus about 20-30 samples per hour may be analyzed manually. If the sensor is incorporated in a flow system, discrete samples may be analyzed at rates up to about 60 per hour or a sample stream may be analyzed continuously (Bailey, 1980).

Response time (Fig. I.17) is the time which elapses between the instant when an ion-selective electrode and a reference electrode (ISE cell) are brought into contact with a sample solution (or at which the activity of the ion of interest in a solution is changed) and the first instant at which

the potential/time slope ($\Delta U/\Delta t$) becomes equal to a limiting value selected on the basis of the experimental conditions and/or requirements concerning the accuracy (IUPAC, 1994).

Fig. I.17 Definition and determination of response time
(IUPAC, 1994)



1.7.2.9. Potential Drift

The stability of ion-selective electrodes is affected by both chemical and physical factors. Ideally, the components of the electrodes should be stable within the electrochemical cell and should not react with the species in the test solution. In practice, however, samples often contain species that oxidize, complex or otherwise react with the components of the electrode, and thus produce a drift or shift in the measured potential of the electrochemical cell. According to the IUPAC definition, potential drift is “the slow non-random change with time in the potential of an ion-selective electrode cell assembly maintained in a solution of constant composition and temperature” (IUPAC, 1994). The determination of the drift is carried out by a linear curve fitting on the data set collected in a given period of time in a solution of constant composition and temperature. The slope of the potential versus time line is called drift. The random potential deviations around the line define the standard deviation of the measured potential data (IUPAC, 1994).

The effect of potential drift can easily be seen if a series of standard solutions are repeatedly measured over a period of time (NICO 2000 Ltd.). The results show that the relationship between the potentials measured in the different solutions (i.e., the electrode slope) remains essentially the same but the actual value of the potentials generally drifts downwards. This is somewhat surprising in view of the fact that many ISE specifications quote a potential drift of less than 1 mV per day. However, it must be noted that this figure is an attempt to define the drift which is attributable to the ISE alone, which is impossible to measure directly due to other potential differences in other parts of the measuring system. Thus, the ISE drift factor only applies to the unlikely and impractical situation when the ion-selective electrode is constantly immersed in a 1000-mg/L solution but the reference electrode is removed between each measurement. Constantly removing and replacing an ISE in different solutions will produce hysteresis (or memory) effects, the extent of which depends on the relative concentrations of the new and old solutions. Thus, if the same solution is re-measured after measuring a different one, it cannot be expected to give exactly the same potential reading the second time (NICO 2000 Ltd.).

Furthermore, reference electrodes have stable voltages over short periods of time but tend to suffer from slow drift in the liquid junction potential when immersed for long periods (NICO 2000 Ltd.). Moreover, as discussed previously, it is unlikely that the liquid junction potential will always settle to exactly the same value whenever a reference electrode is immersed in a new solution, or even re-immersed in the same one. Indeed, for some electrode combinations in samples with a complex matrix, this re-equilibration can cause differences of several millivolts (NICO 2000 Ltd.).

I.8. Rationale and Objectives for the Thesis

I.8.1. Gaps in Knowledge for GaN- and InGaN-Based Ion Selective Potentiometric Sensors Prior to the Thesis

Previous studies by Chaniotakis et al. (2004) and Alifragis et al (2005) (previously reviewed in Section I.6) provide no comprehensive model of the electrode response mechanism or analysis of the structure of the semiconductor/electrolyte interface. They also lack an investigation of the electrochemical processes occurring at the interface. The electrochemical impedance spectroscopy (EIS) experiments reported by Chaniotakis et al. (2004) and Alifragis et al. (2005)

show the impedance spectra obtained for the GaN electrodes but do not calculate and evaluate the parameters of the equivalent circuit model they applied to fit the EIS experimental results. Moreover, there is no reported study of InGaN within the context of a potentiometric anion sensor. Hence, any information about the behaviour of the InGaN as an ion selective electrode represents a contribution to the current state of knowledge.

1.8.2. Thesis Objectives

This thesis is designed to achieve two main objectives:

- i) to bridge some of the gaps in the existing knowledge with respect to the study of GaN and InGaN semiconductors as potentiometric anion selective electrodes and
- ii) to determine if these materials could potentially solve some problems associated with conventional ISEs.

The specific objectives of the thesis are the following:

- i) To evaluate the performance of constructed GaN and InGaN sample electrodes against the following criteria:
 - response time;
 - sensitivity to inorganic and organic anions in a wide range of electrolyte solutions (KF, KNO₃, KCl, HOC₆H₄COONa, KSCN, CH₃COOK, KClO₄, KBr and KI with concentrations of 10⁻¹M, 10⁻² M, 10⁻³ M, 10⁻⁴ M, 10⁻⁵ M and 10⁻⁶ M);
 - linear range and slope of calibration curves;
 - pH response;
 - drift of electrode potential;
 - reproducibility of electrode response results.
- ii) To develop a comprehensive theoretical model of the response mechanism of the GaN and InGaN semiconductor electrodes.
- iii) To investigate the ability of the GaN and InGaN semiconductor electrodes to respond to anions in electrolyte solutions with different concentrations.
- iv) To study the structure and the properties of the semiconductor/electrolyte interface and the charge transfer processes occurring at the interface.

II. MATERIALS AND METHODS

II.1. GaN and InGaN Electrode Fabrication

Undoped gallium nitride (GaN) samples were received ready-made from an external laboratory. Ga-face GaN (0001) wurtzite crystal films (50 nm thick) were grown on Al₂O₃ (sapphire) wafers with a diameter of 40 mm by molecular beam epitaxy (MBE). MBE is a technique for deposition of one or more pure materials onto a single crystalline substrate (wafer) one layer of atoms at a time under ultra-high vacuum (UHV) to form a single crystal (Rinaldy, 2002). The two wafers were then shipped to Lakehead University, where they were scribed to rectangular pieces measuring approximately 5 mm by 10 mm. Two of the pieces were used for the construction of two GaN test electrodes - Sample 1 and Sample 2. As the first step of the electrode construction, each wafer piece was attached with epoxy glue on a rectangular pad of insulating circuit board material measuring 10 x 20 mm (Fig. II.1). Copper plates were soldered on two ends of the GaN pieces with low temperature solder (Cerrotru Alloy 5800-2 [138.3°C]). A 1.8-mm diameter copper wire was bonded with the same solder to one of the copper plates, and a 0.5-mm diameter insulated copper wire was bonded to the other copper plate (Fig. II.1). The bottom of the circuit board pad, the top of the copper plates and approximately 70 mm of the copper wires were covered with epoxy glue to ensure that only the semiconductor film was exposed when the electrode was immersed in liquid.

Fig. II.1 Construction of the GaN and InGaN sample electrodes

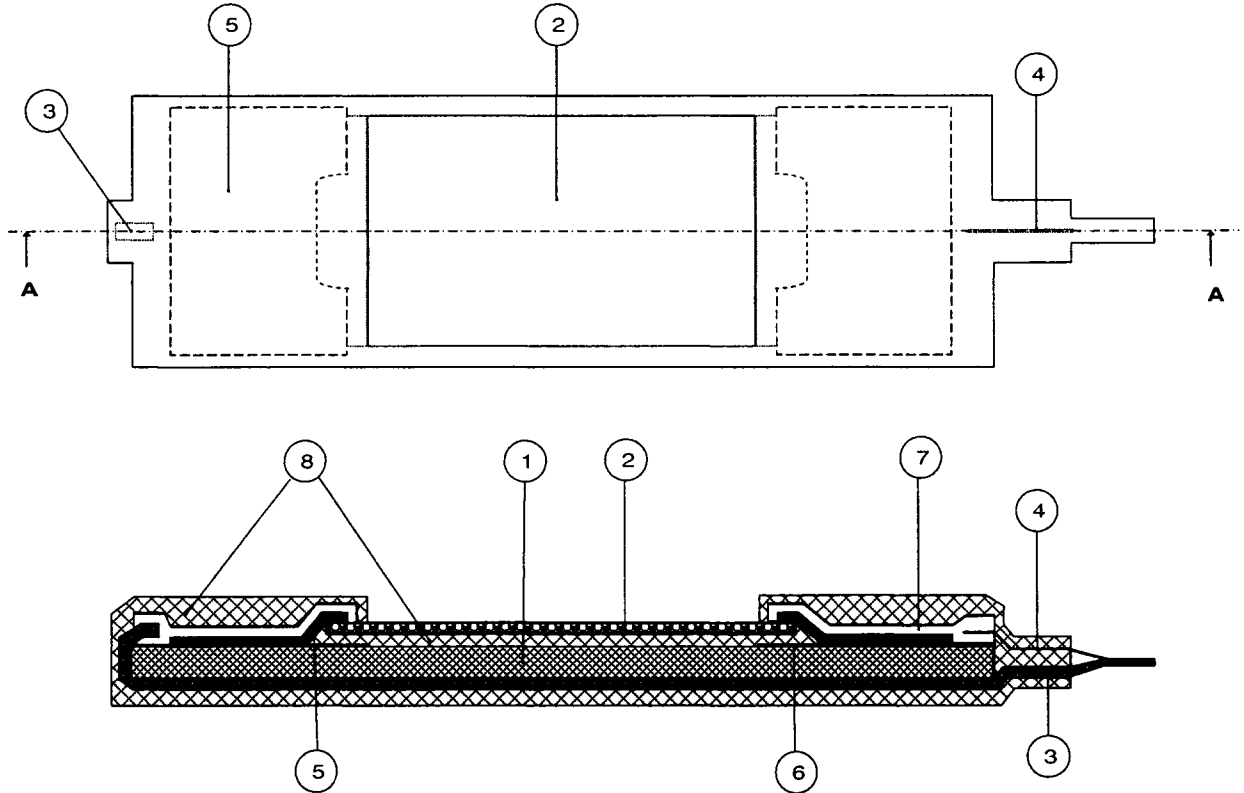
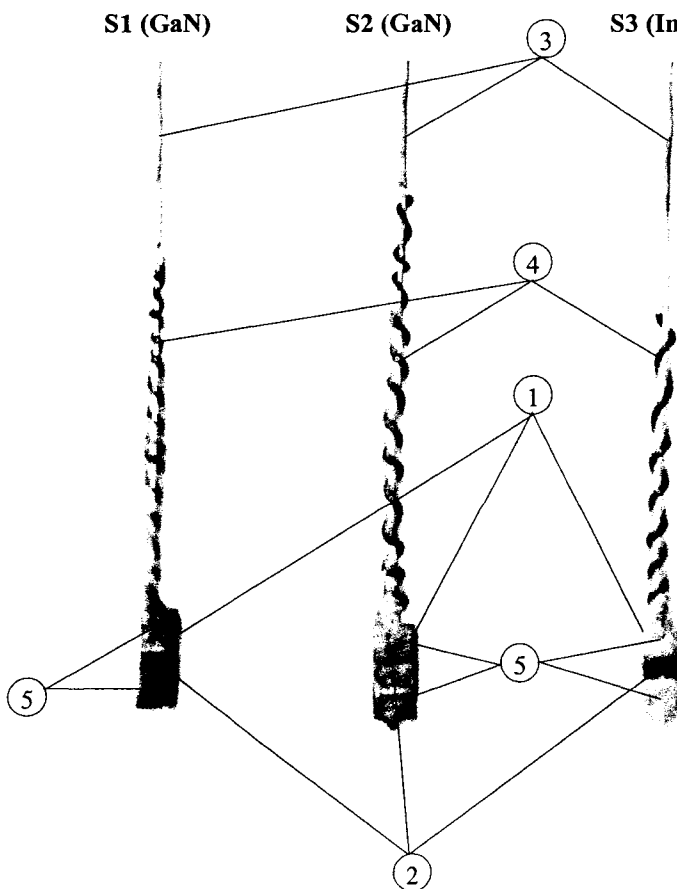


Fig. II.2 Prepared Test Electrodes



Legend:

- 1 – Insulating circuit board material
- 2 – Wafer piece (GaN/InGaN)
- 3 – 1.8-mm diameter copper wire
- 4 – 0.5-mm diameter insulated copper wire
- 5 – Copper plates
- 6 – Copper trace
- 7 – Low temperature solder
- 8 – Epoxy glue

Materials and Methods

The completed electrodes are shown on Fig. II.2. There was no pre-treatment (etching the surface) of the electrodes prior testing.

The indium gallium nitride ($\text{In}_{0.2}\text{Ga}_{0.8}\text{N}$) samples were also fabricated externally by mixing gallium nitride (GaN) and indium nitride (InN) in an 80:20 ratio. The 50 nm-thick $\text{In}_{0.2}\text{Ga}_{0.8}\text{N}$ layer was grown on a GaN buffer on a sapphire wafer having a diameter of 25.6 mm. All InGaN samples had their InGa-face (0001) exposed. One electrode – Sample 3 – was constructed following the same procedure as previously described for the GaN electrodes.

II.2. Electrochemical Measurements

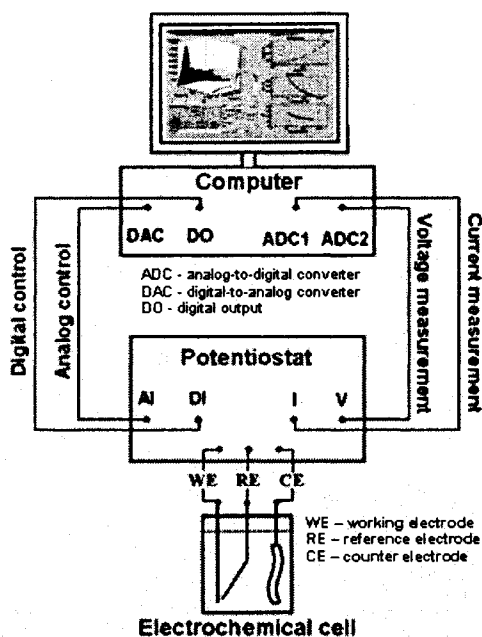
II.2.1. Solutions

All electrolyte solutions were prepared with reagent-grade salts and nanopure water (NPW, 18.2M Ω , Barnstead D11911 Nanopure Diamond) in the laboratory. Stock solutions (0.1M) of (KF, KNO₃, KCl, HOC₆H₄COONa, KSCN, CH₃COOK, KClO₄, KBr and KI) salts were made initially and sequentially diluted to produce concentrations of 10⁻² M, 10⁻³ M, 10⁻⁴ M, 10⁻⁵ M and 10⁻⁶ M for the construction of complete calibration curves for each type of electrode.

II.2.2. Electrochemical Cell Assembly

Electrochemical experiments were performed in a conventional three-electrode electrochemical cell consisting of a reference electrode, a working electrode (semiconductor), and a counter electrode (also called an auxiliary electrode). The potential measurements were done versus a saturated calomel electrode (SCE) connected to the electrolyte by means of a salt bridge made of a glass capillary tube filled with a saturated KCl solution. The standard potential of the SCE reference electrode is $E^0(\text{SCE}) = 0.242 \text{ V}$ versus the normal hydrogen electrode (NHE). The experimental set-up for the electrochemical experiments is presented on Fig. II.3.

Fig. II.3 Electrochemical Experiments setup
(Ragoisha, 2004)



In electrochemical terms, the half-cell can be represented by:



The electrode reaction is:



A platinum wire electrode was used as the counter electrode. This electrode had a sufficiently large surface (more than 10 times larger than the surface of the working electrode) to ensure that its interface with the electrolyte did not influence the current-potential curves. When not in use, the sample electrodes were kept submerged in NPW, and they were thoroughly rinsed with NPW before each experiment. To remove dissolved oxygen from the solution and to keep the cell oxygen-free throughout the experiments, the electrolytes were purged with argon gas prior to the measurements, and argon was blown over the solutions during the measurements. Before each series of measurements with a new electrolyte, the following procedures were carried out to ensure cleanliness of the equipment: 1) the platinum counter electrode was thermally treated with a gas burner to remove species that could have been adsorbed on the electrode surface from the previous electrolyte, 2) the electrochemical cell was cleaned by submerging it into a hot bath (90°C) of concentrated hydrochloric and sulphuric acids for one hour and 3) the cell was rinsed

with double distilled water and NPW in that sequence. All experiments were carried out at room temperature, which was almost constant at $21 \pm 1^\circ\text{C}$.

II.2.3. Open Circuit (OC) Potential Measurements

OCP measurements were performed in solutions of each salt (KF, KNO₃, KCl, HOC₆H₄COONa, KSCN, CH₃COOK, KClO₄, KBr and KI) with concentrations of 10^{-1}M , 10^{-2}M , 10^{-3}M , 10^{-4}M , 10^{-5}M and 10^{-6}M . These measurements were used to construct complete calibration curves and to provide information about the response time of the semiconductor electrodes in solutions of varying composition and concentration. The values of OC potentials were reported with respect to the SCE reference electrode.

The calibration curves for each sample electrode were obtained using the direct calibration method. This method was preferred over all other methods of calibration because of its simplicity and wide application for calibration of ISEs. To build the calibration curves for all salts, each sample electrode was consecutively immersed in a series of standard salt solutions with known concentrations, starting from the solution with the lowest concentration and moving in the direction of concentration increase. In each solution, a reading of the OC electrode potential was taken. To avoid any errors due to the ionic strength effect, the measured OCPs were plotted as a function of the activity of anions present in the calibrating solution, instead of their concentration. All anionic activities were calculated with the VMINTEQ chemical speciation modeling software. The region of linearity was determined from the constructed calibration curves for each sample electrode and each salt. The linear range and the slope of the calibration curves were evaluated and compared to the theoretical slope values and to the results reported in the literature for GaN potentiometric anion selective electrodes. The total potentiometric response of the GaN and InGaN sample electrodes was calculated, as it provided an indication of the overall sensitivity of the electrodes to the measured ions.

The reproducibility of the OCP measurements and the magnitude of the electrode drift were investigated by repeating the OCP measurements over the entire concentration range in three of the nine electrolytes. The value of the electrode drift was compared with drift values reported in the literature for other ion selective electrodes.

Materials and Methods

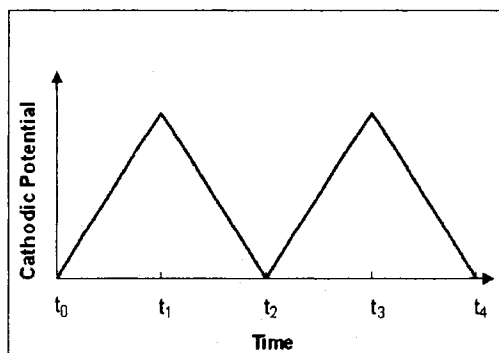
OCP measurements were also performed in solutions with varying pH values to determine if the GaN and InGaN semiconductor electrodes showed a pH response. The pH response experiments in the acidic pH range (pH = 5.45 - 1.34) were performed in 0.1M KCl solution to which small amounts of 0.1M HCl were added to decrease the pH to the desired value (aiming to decrease the pH by approximately one unit after each incremental addition of HCl). The pH experiments in the intermediate to basic range (pH=5.40 - 12.80) were performed in 0.1M KCl solution to which small amounts of 0.1M KOH were added to increase the pH in increments of approximately one unit. The pH of the solutions was measured with a calibrated pH glass electrode (Brinkman 713 pH Meter).

II.2.4. Cyclic Voltammetry

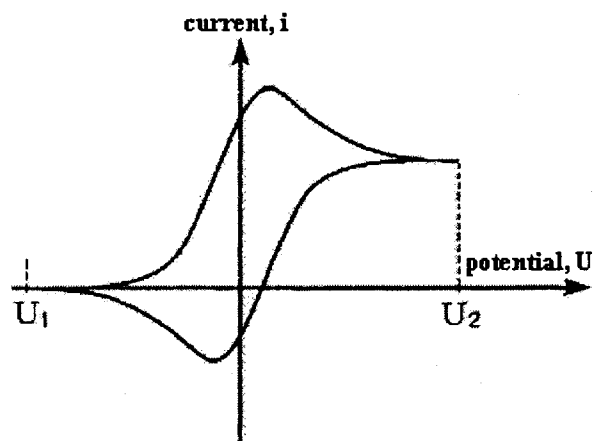
Cyclic voltammetry is a potentiodynamic electrochemical technique for studying the properties of the semiconductor/electrolyte interface. It can provide information about reversibility of electrode reactions occurring in the interfacial region, reaction rates and rate constants as a function of applied voltage on the electrode, reactivity of the species in solution, electrode material, the nature of the electrode surface, the structure of the interfacial region over which the electron transfer occurs, etc. In cyclic voltammetry, the working electrode potential follows a linearly ramping potential versus time as shown on Fig. II.4a. The potential that is cycled is actually the potential difference between the working electrode and the reference electrode. The direction of the potential is reversed at the end of the first scan. Thus the perturbation waveform is usually of the form of an isosceles triangle.

Fig. II.4 Cyclic Voltammetry Experiment

a) Cyclic Voltammetry Potential Waveform



b) Cyclic Voltammogram for a reversible system



The potential is measured between the reference electrode and the working electrode, and the current is measured between the working electrode and the counter electrode. The results are then plotted as current (i) versus potential (U) (Fig. II.4b). These plots are termed “polarization curves” or “cyclic voltammograms”, and they can be used for determining the formal redox potentials of the electroactive species present in the solution, detecting chemical reactions, e.g. adsorption that precede or follow the electrochemical reaction, and evaluating electron transfer kinetics.

The results of the CV studies were analyzed to obtain information about the electrochemical reactions taking place at the semiconductor/electrolyte interface. To gain a full understanding of the processes that occur at different potential values, the GaN electrodes were scanned repeatedly in the cathodic and anodic regions, and the current flowing through the electrochemical cell was recorded. The electrochemical reactions responsible for the observed current were then determined.

The etching processes at the GaN semiconductor, which can be directly related to the stability of the electrode in the studied test solutions, were investigated by performing a series of range tests during which the potential of the electrode was scanned to highly negative and highly positive values (with respect to the electrode's OCP in the solution). The resulting cyclic voltammograms were compared with the ones reported in the literature and recorded also for GaN electrodes.

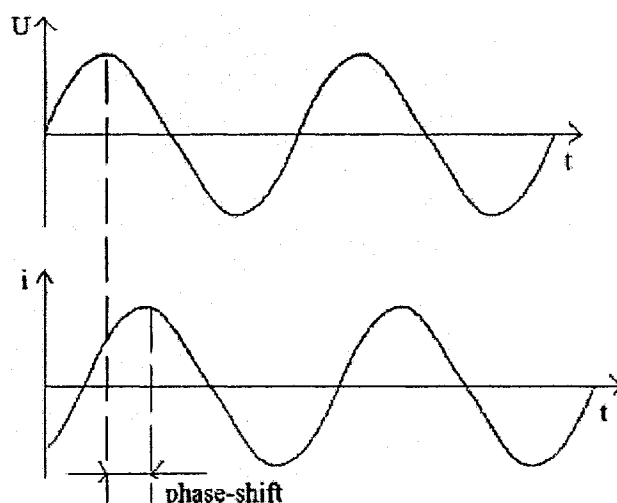
Materials and Methods

They were also analyzed to determine the reactions that contribute to the observed cathodic and anodic currents. Because cyclic voltammetry is a technique that can supply information about the type of electrochemical reactions (oxidation or reduction) occurring at the semiconductor/ electrolyte interface but cannot identify specific reactions, surface studies were also performed to gain additional insights about the charge transfer processes that actually took place in the electrochemical system during the range tests.

II.2.5. Electrochemical Impedance Spectroscopy

Electrochemical impedance spectroscopy (EIS) is an electrochemical technique in which a low amplitude alternating potential (AC) wave is imposed on top of a DC potential, and the resulting current through the electrochemical cell is measured. The relationship between the voltage and current is termed “impedance”, and it is used for characterizing the electrochemical response of interfacial processes and structures. Electrochemical impedance is normally measured using a small sinusoidal excitation signal. This is done so that the cell's response is pseudo-linear, in which case the output signal is of the same frequency as the input signal but is shifted in time, as shown on Fig. II.5.

Fig. II.5 Sinusoidal response in a linear system



The impedance of an electrochemical system can be calculated from:

$$Z = \frac{U_t}{i_t} = \frac{U_0 \sin(\omega t)}{i_0 \sin(\omega t - \phi)} = Z_0 \frac{\sin(\omega t)}{\sin(\omega t + \phi)} \quad (2.3)$$

Materials and Methods

where:

U_0 is the amplitude of the input voltage signal (V)

U_t is the input voltage at time t (V)

ω is the radial frequency (rad)

i_0 is the amplitude of the output current signal (A)

i_t is the output current at time t (A)

ϕ is the phase shift angle (rad)

Z_0 is the amplitude of the impedance (Ω)

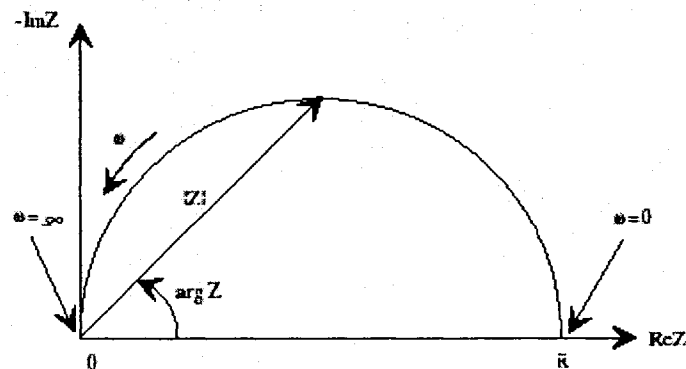
Z_t is the impedance at time t (Ω)

The impedance can also be represented as a complex function:

$$Z(\omega) = \frac{U}{i} = Z_0 \exp(j\phi) = Z_0 (\cos \phi + j \sin \phi) \quad (2.4)$$

The impedance from expression (2.4) is composed of a real and an imaginary part. The real part is plotted on the x-axis and the imaginary part on the y-axis of a diagram termed a “Nyquist plot” (Fig. II.6). In this plot, the y-axis is negative and each point corresponds to the total impedance of the system at one frequency. The low frequency data are on the right side of the plot and higher frequencies are on the left, i.e., the radial frequency ω is increasing from right to left. On the Nyquist plot, the impedance can be represented as a vector of length $|Z|$. The angle between this vector and the x-axis is ϕ .

Fig. II.6 Nyquist plot



Materials and Methods

The most common approach for analyzing impedance data is by fitting it to an analogous equivalent circuit model. The procedure employed is to build a circuit and curve fit the impedance of that circuit to the measured impedance spectra. Circuit elements most commonly used to model electrochemical impedance spectra are combinations of resistances, capacitances, and inductors. The impedance equations for the elements are:

$$\text{Resistor: } Z = R \quad (2.5)$$

$$\text{Capacitor: } Z = \frac{1}{j\omega C} \quad (2.6)$$

$$\text{Inductor: } Z = j\omega L \quad (2.7)$$

where

R is the resistance (Ω)

j is the imaginary number

C is the capacitance of the capacitor (F)

L is the inductance of the inductor (H)

The capacitors in real electrochemical systems, however, often do not behave ideally. Instead, they act as a constant phase element (CPE), which is characterized by a phase shift between the perturbation signal and the resulting current different from $\pi/2$ (unlike the ideal capacitor which has a phase shift exactly equal to $\pi/2$). The capacitance of the CPE is given by:

$$Z = \frac{1}{C} (j\omega)^{-\alpha}, \quad (2.8)$$

where

α is an exponent, which equals 1 for a capacitor.

The rate of an electrochemical reaction can be strongly influenced by diffusion of a reactant towards or a product away from the electrode surface. This is often the case when a solution species must diffuse through a film on the electrode surface. This situation can exist when the electrode is covered with reaction products or adsorbed solution components. Whenever diffusion effects completely dominate the electrochemical reaction mechanism, the impedance is called the Warburg impedance.

Materials and Methods

The Warburg impedance depends on the frequency of potential perturbation. At high frequencies, the Warburg impedance is small since the diffusing reactants don't have to move very far. At low frequencies, the reactants have to diffuse farther, increasing the Warburg impedance. For diffusion-controlled electrochemical reactions, the current is 45 degrees out of phase with the imposed potential. With this phase relationship, the real and imaginary components of the impedance vector are equal at all frequencies. In terms of simple equivalent circuits, the behaviour of a Warburg impedance (a 45 degree phase shift) is midway between that of a resistor (0 degree phase shift) and a capacitor (90 degree phase shift). The Warburg impedance has two forms: infinite length and finite length Warburg impedance.

The infinite length Warburg impedance assumes an infinite thickness of the diffusion layer across which the charged particles diffuse. It is given by the following equation:

$$Z_w = \sigma_w (\omega)^{-1/2} (1 - j) \quad (2.9)$$

where:

ω is the radial frequency (rad)

j is the imaginary number

σ_w is the Warburg coefficient

In this equation, the Warburg coefficient is defined as:

$$\sigma_w = \frac{RT}{n^2 F^2 A \sqrt{2}} \left(\frac{1}{C_o^* \sqrt{D_o}} + \frac{1}{C_R^* \sqrt{D_R}} \right) \quad (2.10)$$

where:

n is the number of electrons exchanged in the redox reaction

R is the gas constant equal to $8.314510 \text{ J K}^{-1} \text{ mol}^{-1}$

T is the absolute temperature (K)

F is the Faraday constant equal to $9.6485309 \times 10^4 \text{ C mol}^{-1}$

C_o^* is the concentration of the oxidized species in the bulk of the solution (mol m^{-3})

C_R^* is the concentration of the reduced species in the bulk of the solution (mol m^{-3})

D_o is the diffusion coefficient of the oxidized species ($\text{m}^2 \text{ s}^{-1}$)

D_R is the diffusion coefficient of the reduced species ($\text{m}^2 \text{ s}^{-1}$)

Materials and Methods

A is the surface area of the electrode (m^2)

The finite length Warburg Impedance assumes that the diffusion layer is bounded, which is the common case in real electrochemical systems. If the electroactive species diffuse across a thin film at the electrode surface in open circuit conditions, i.e., in the absence of a DC current flow, then the Warburg impedance is given by the following equation:

$$Z_W = \sigma_w \omega^{-1/2} (1-j) \coth \left(\delta \left(\frac{j\omega}{D} \right)^{1/2} \right) \quad (2.11)$$

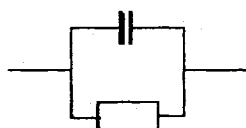
where:

D is an average value of the diffusion coefficient of the redox species ($\text{m}^2 \text{s}^{-1}$)

δ is the effective thickness of the diffusion layer (m).

These circuit elements are joined in a variety of ways to model the circuit. For example, the equivalent circuit modelling the impedance spectra shown in Fig. II.6 consists of a resistor and a capacitor in parallel, as represented on Fig. II.7.

Fig. II.7 Simple equivalent circuit



In chemical terms, R_{ct} is the charge transfer resistance across the double layer and C is a double layer capacitance. Often, an equivalent circuit model that fits the data will suggest some chemical model, process, or mechanism, which can be proposed and tested. Thus, analogous circuit elements bridge gaps in knowledge and allow the electrochemist to use the EIS to estimate chemical reaction rates and reaction mechanisms in poorly characterized systems. EIS can be also utilized to characterize different interrelated processes (interfacial charge transfer, diffusion, adsorption, etc.) and interfacial objects (double electric layer, space charge layers, etc.) at the non-stationary electrochemical interface.

OC potential, Cyclic voltammetry and EIS measurements were performed with a Solartron SI 1287 Electrochemical Interface System combined with a Frequency Response Analyzer

Materials and Methods

(Solartron 1252A). The electrode response signal was recorded on a personal computer using the CorrWare, CorrView 2, ZPlot and ZView2 softwares included in the Solartron Analyzer equipment. A sinusoidal perturbation signal with potential amplitude of 10mV at a base potential of 0.00V versus OC potential was applied to obtain impedance spectra. Since the results from the EIS showed pronounced scattering of data in the low frequency range (0-100Hz), the EIS diagrams (Nyquist plots) were recorded in the restricted frequency range of 100Hz - 300KHz.

EIS was the main tool for the analysis of the structure of the semiconductor/electrolyte interface and was also applied to verify the developed theoretical model of the interface (See Chapter I/ Section I.5). Analogous equivalent circuit models were designed to fit the recorded impedance spectra, and the parameters of the equivalent circuits were calculated and compared with the values reported in the literature for other semiconductor electrodes. The elements of the equivalent circuit model correspond to the physical and electrochemical phenomena occurring at the interface such as the formation of the solution double layer, the space charge layer in the semiconductor, the layer of adsorbed ions on the surface of the electrode, and the charge transfer process. The information needed to characterize these elements was obtained from the values of the parameters defining the circuit elements of the equivalent circuit models. In this way, the capacitance of the double layer in the different electrolyte solutions, the capacitance of the space charge layer in the semiconductor electrode, the charge transfer resistance of the layer of adsorbed ions on the electrode surface and other important components of the semiconductor/electrolyte interface were evaluated.

II.3. Surface Analytical Techniques

The surface studies allowed investigating the morphology of the GaN and InGaN samples, with the main emphasis placed on the polarity of the surface of the GaN and InGaN thin films. These studies provided additional information about the electrochemical reactions that took place in the system during the range tests. Scanning Electron Microscopy (SEM) and Energy Dispersive Spectroscopy (EDS) were the two techniques selected for the surface studies because the related equipment was readily available and because the quality of images and of elemental distribution diagrams provided by these techniques was sufficient for the purposes of the qualitative analysis.

II.3.1. Scanning Electron Microscopy

SEM is an imaging technique that uses secondary electrons that are ejected from a sample to image a surface. When the electrons penetrate the sample, they are diffracted to form a diffraction pattern. A detector above the sample detects the secondary electrons to produce an intensity map as a function of the electron beam position, which is displayed on a computer screen. The electron beams are produced by applying a high voltage to a hot tungsten filament, and accelerating the emitted electrons through a high electric field, typically 10-100keV. The electron beam is then focused with magnetic field lenses to a typical spot diameter of 1-100nm on the sample.

The use of electron beams requires that the sample be placed in a vacuum chamber for analysis (typically from 10^{-5} to 10^{-7} Torr). For SEM imaging (secondary electrons mode), samples must be electrically conductive. If the sample conductivity is relatively low (which is the case with both GaN and InGaN semiconducting materials), the applied electron beam gradually charges the sample and, as a result, the quality of the produced image becomes very poor. A possible solution to this problem is to deposit a thin film of conductive material (i.e. gold) on the surface of the studied sample and thus increase its conductivity without significantly affecting the observed surface morphology. Therefore, to improve the quality of the SEM images, the surface of the GaN and InGaN samples was coated with an atomic layer of gold.

II.3.2. Energy Dispersive Spectroscopy

The elemental analysis of the GaN and InGaN sample electrodes was performed using energy dispersive X-Ray spectroscopy (EDS) before and after electrochemical experiments to identify possible changes in the surface composition of the sample electrodes. EDS is a chemical microanalysis technique used in conjunction with SEM to characterize the elemental composition of the analyzed sample (Materials Evaluation and Engineering, Inc., 2001). Features or phases as small as 1 μm or less can be analyzed. When the sample is bombarded by the SEM's electron beam, electrons are ejected from the atoms comprising the sample's surface. The resulting electron vacancies are filled by electrons from a higher state, and an x-ray is emitted to balance the energy difference between the two electrons' states. The x-ray energy is characteristic of the element from which it was emitted. The EDS x-ray detector measures the relative abundance of

Materials and Methods

emitted x-rays versus their energy. The spectrum of x-ray energy versus counts is evaluated to determine the elemental composition of the investigated sample.

In the Thesis the SEM images were taken with a JEOL JSM 5900 SEM. The elemental composition of the GaN and InGaN samples at different locations was measured by EDS using an Oxford Link ISIS system calibrated using a series of standards. Garnet was used for Mg, Al, and Si; orthoclase for K and Na; wollastonite for Ca; barite for S; and the respective pure metals for Cu, Fe, Pb, and Zn.

III. RESULTS & DISCUSSION

This chapter presents and discusses the results derived from the previously outlined experimental methods. Presented results are grouped by types of performed experiments in several sections:

III.1. Performed Experiments

Performed experiments can be classified into ten groups:

- Response Time of GaN sample electrodes S1 and S2 and InGaN sample electrode S3.
- Total Potentiometric Response.
- Construction of calibration curves, i.e. investigation of variations in electrodes response with activity of anions in the solution.
- Experiments to assess the reproducibility of results.
- Investigation of pH response of the sample electrodes.
- Cyclic Voltammetry Experiments
- Electrochemical Impedance Spectroscopy Measurements
- Potentiostatic experiments.
- Range Tests
- Surface study of GaN and InGaN sample electrodes.

A detailed breakdown of the performed experiments is provided in Table III.1.

Table III.1 Performed Experiments by measurement types and sample electrodes

Experiment Description	Material: GaN/Sample 1			Material: GaN/Sample 2			Material: InGaN/Sample 3		
	Measurement types:			Measurement types:			Measurement types:		
	OCP	EIS	CV	OCP	EIS	CV	OCP	EIS	CV
1. Response time of GaN sample electrode S1 and InGaN sample electrode S3									
10 ⁻⁶ – 10 ⁻¹ M KF solutions	X						X		
10 ⁻⁶ – 10 ⁻¹ M KNO ₃ solutions	X						X		
10 ⁻⁶ – 10 ⁻¹ M KCl solutions	X						X		
10 ⁻⁶ – 10 ⁻¹ M HOC ₆ H ₄ COONa solutions	X						X		
10 ⁻⁶ – 10 ⁻¹ M KSCN solutions	X						X		
10 ⁻⁶ – 10 ⁻¹ M CH ₃ COOK solutions	X						X		
10 ⁻⁶ – 10 ⁻¹ M KClO ₄ solutions	X						X		
10 ⁻⁶ – 10 ⁻¹ M KBr solutions	X						X		
10 ⁻⁶ – 10 ⁻¹ M KI solutions	X						X		
2. Construction of Calibration Curves: Investigation of variations in electrodes response with activity of anions in the solution.									
2.1 KF solutions									
10 ⁻⁶ M	X	X					X	X	
10 ⁻⁵ M	X	X					X	X	
10 ⁻⁴ M	X	X					X	X	
10 ⁻³ M	X	X					X	X	
10 ⁻² M	X	X					X	X	
10 ⁻¹ M	X	X	X			X	X	X	
2.2 KNO ₃ solutions (immediately after cleaning with 1M HCl solution and 24 hours after cleaning)									
10 ⁻⁶ M	X	X					X	X	
10 ⁻⁵ M	X	X					X	X	
10 ⁻⁴ M	X	X					X	X	

Results & Discussion

Experiment Description	Material: GaN/Sample 1			Material: GaN/Sample 2			Material: InGaN/Sample 3		
	Measurement types:			Measurement types:			Measurement types:		
	OCP	EIS	CV	OCP	EIS	CV	OCP	EIS	CV
10 ⁻³ M	X	X					X	X	
10 ⁻² M	X	X					X	X	
10 ⁻¹ M	X	X		X	X	X	X	X	
2.3 KCl solutions									
10 ⁻⁶ M	X	X		X	X		X	X	
10 ⁻⁵ M	X	X		X	X		X	X	
10 ⁻⁴ M	X	X		X	X		X	X	
10 ⁻³ M	X	X		X	X		X	X	
10 ⁻² M	X	X		X	X		X	X	
10 ⁻¹ M	X	X	X	X	X		X	X	
2.4 HOC ₆ H ₄ COONa solutions									
10 ⁻⁶ M	X	X					X	X	
10 ⁻⁵ M	X	X					X	X	
10 ⁻⁴ M	X	X					X	X	
10 ⁻³ M	X	X					X	X	
10 ⁻² M	X	X					X	X	
10 ⁻¹ M	X	X	X				X	X	
2.5 KSCN solutions									
10 ⁻⁶ M	X	X					X	X	
10 ⁻⁵ M	X	X					X	X	
10 ⁻⁴ M	X	X					X	X	
10 ⁻³ M	X	X					X	X	
10 ⁻² M	X	X					X	X	
10 ⁻¹ M	X	X	X				X	X	
2.6 CH ₃ COOK solutions									
10 ⁻⁶ M	X	X					X	X	
10 ⁻⁵ M	X	X					X	X	
10 ⁻⁴ M	X	X					X	X	
10 ⁻³ M	X	X					X	X	

Reproduced with permission of the copyright owner. Further reproduction prohibited without permission.

Results & Discussion

Experiment Description	Material: GaN/Sample 1			Material: GaN/Sample 2			Material: InGaN/Sample 3		
	Measurement types:			Measurement types:			Measurement types:		
	OCP	EIS	CV	OCP	EIS	CV	OCP	EIS	CV
10 ⁻² M	X	X					X	X	
10 ⁻¹ M	X	X				X	X	X	
2.7 KClO ₄ solutions									
10 ⁻⁶ M	X	X					X	X	
10 ⁻⁵ M	X	X					X	X	
10 ⁻⁴ M	X	X					X	X	
10 ⁻³ M	X	X					X	X	
10 ⁻² M	X	X					X	X	
10 ⁻¹ M	X	X					X	X	
2.8 KBr solutions									
10 ⁻⁶ M	X	X		X	X		X	X	
10 ⁻⁵ M	X	X		X	X		X	X	
10 ⁻⁴ M	X	X		X	X		X	X	
10 ⁻³ M	X	X		X	X		X	X	
10 ⁻² M	X	X		X	X		X	X	
10 ⁻¹ M	X	X		X		X	X	X	
2.9 KI solutions									
10 ⁻⁶ M	X	X					X	X	
10 ⁻⁵ M	X	X					X	X	
10 ⁻⁴ M	X	X					X	X	
10 ⁻³ M	X	X					X	X	
10 ⁻² M	X	X					X	X	
10 ⁻¹ M	X	X				X	X	X	
3. Baseline Measurements: Investigating the sample electrodes response in NPW.	X			X			X		
4. Experiments to assess the reproducibility of results									
10 ⁻⁶ – 10 ⁻¹ M KNO ₃ solutions	X						X		
10 ⁻⁶ – 10 ⁻¹ M KBr solutions	X						X		

Reproduced with permission of the copyright owner. Further reproduction prohibited without permission.

Results & Discussion

Experiment Description	Material: GaN/Sample 1			Material: GaN/Sample 2			Material: InGaN/Sample 3		
	Measurement types:			Measurement types:			Measurement types:		
	OCP	EIS	CV	OCP	EIS	CV	OCP	EIS	CV
10 ⁻⁶ – 10 ⁻¹ M KI solutions	X						X		
4. Investigation of pH response of the sample electrodes									
4.1 Acidic solutions (0.1M KCl + 0.1M HCl)									
pH=3.13	X						X		
pH=2.15	X						X		
pH=1.37	X						X		
4.2 Basic solutions (0.1M KCl + 0.1M KOH)									
pH=6.94	X						X		
pH=7.80	X						X		
pH=8.75	X						X		
pH=9.84	X						X		
pH=10.84	X						X		
pH=11.84	X						X		
pH=12.56	X						X		
5. Potentiostatic experiments, solution 0.1M KCl + 0.1M HCl, pH=1.37									
5.1 Measurements performed before potential step with U= -1.1V				X					
5.2 Measurements performed after potential step with U= -1.1V				X	X				
5.1 Measurements performed before potential step with U= -1.2V	X			X					
5.2 Measurements performed after potential step with U= -1.2V.	X	X		X	X				
6. Surface study of GaN and InGaN sample electrodes: Scanning Electron Microscopy		X			X			X	

Results & Discussion

Experiment Description	Material: GaN/Sample 1			Material: GaN/Sample 2			Material: InGaN/Sample 3		
	Measurement types:			Measurement types:			Measurement types:		
	OCP	EIS	CV	OCP	EIS	CV	OCP	EIS	CV
7. Elemental Analysis of the GaN and InGaN sample electrodes sensing element: Energy Dispersive Spectroscopy	X			X			X		

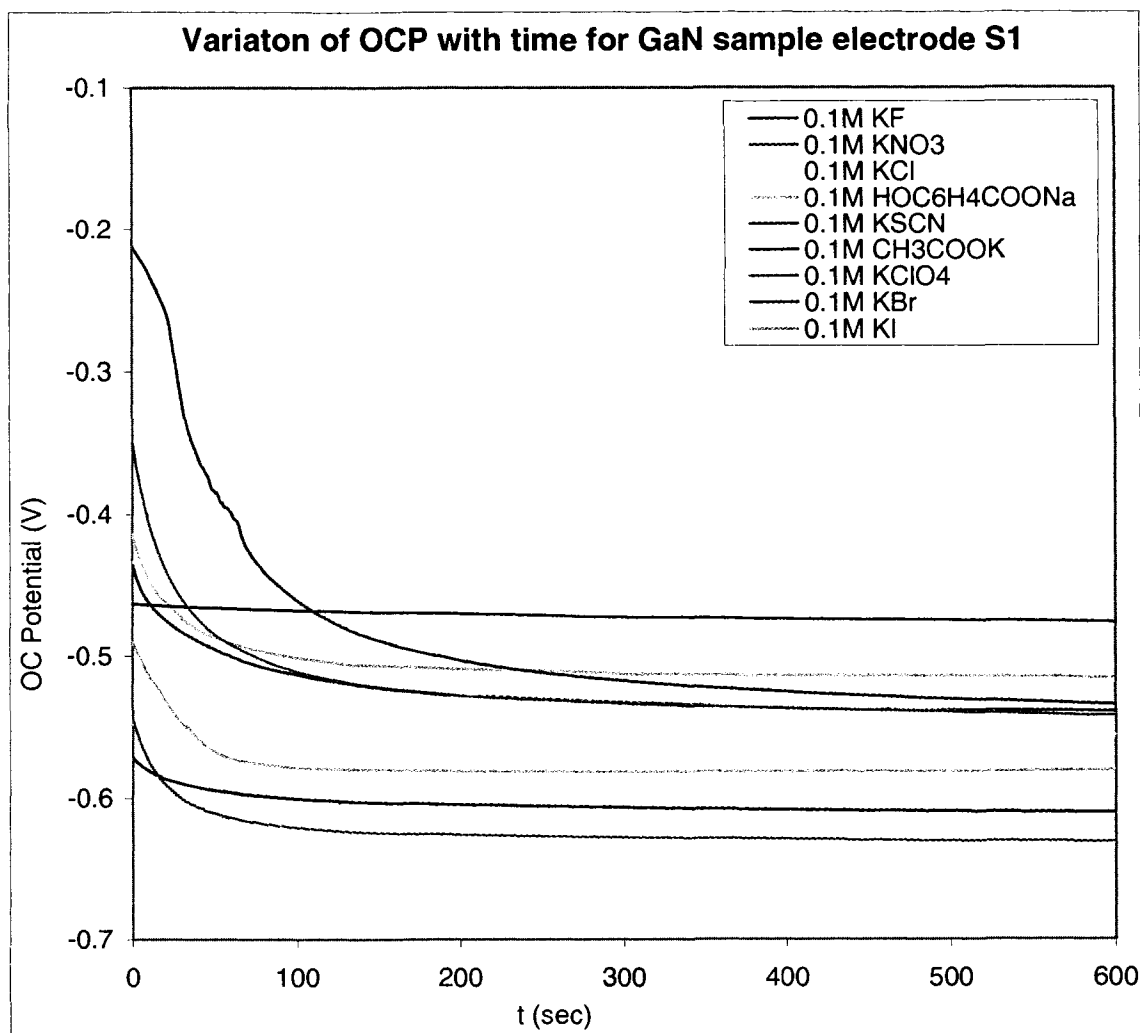
III.2. Response Time

III.2.1. Response Time Measurements

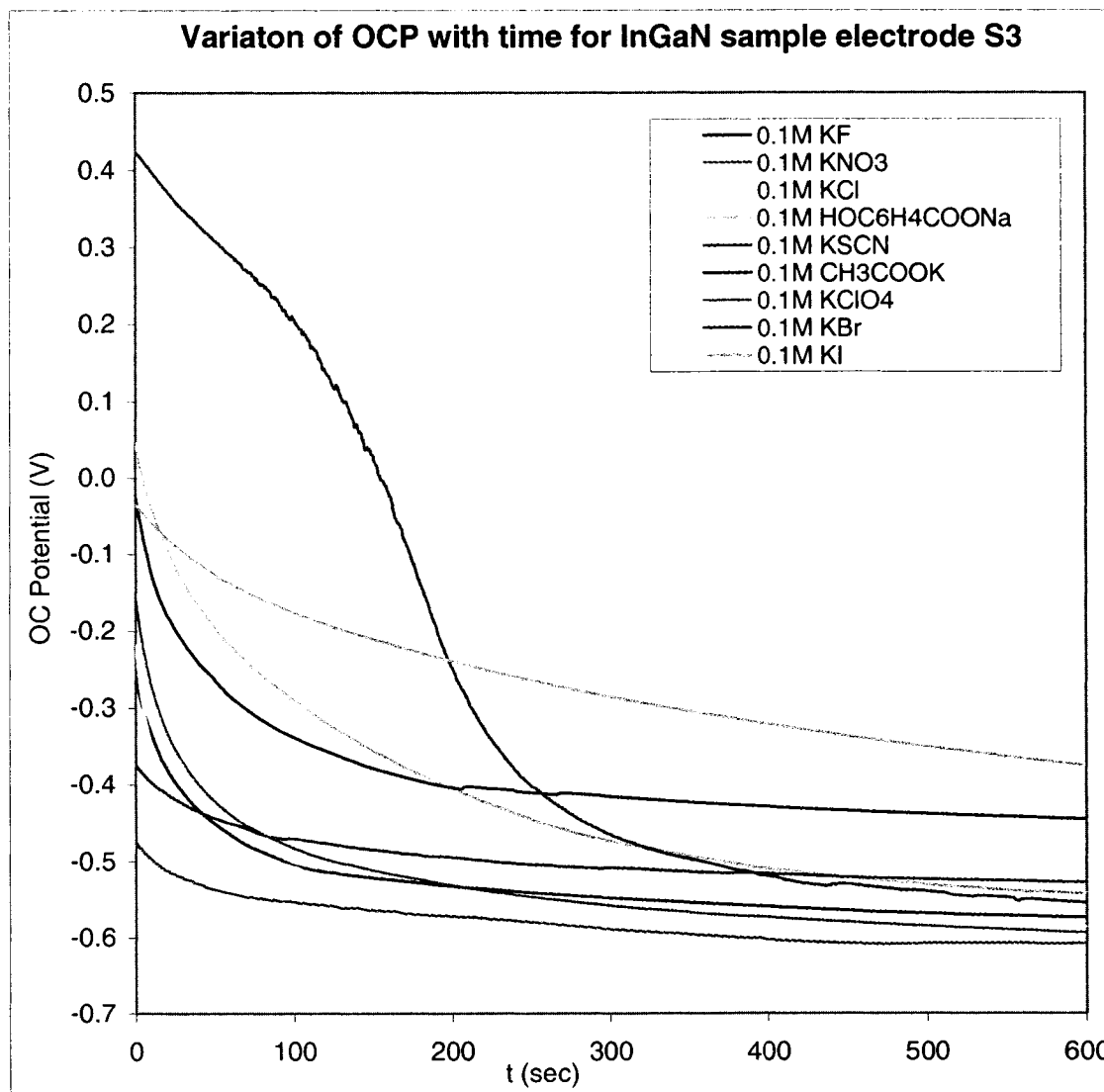
The results of the initial investigation of the GaN sample electrodes S1 and InGaN sample electrode S3 show that the measured open circuit potential (OCP) becomes more negative with time for all 0.1M potassium and sodium salts solutions until the potential stabilizes around a steady state value (Fig. III.1a and b).

Fig. III.1 Variation of measured open circuit potential with time in various electrolyte solutions

a) GaN sample electrode S1



b) InGaN sample electrode S3



The time, which elapses between the instant when the working semiconductor electrode and the reference electrode are brought into contact with the measured standard solution and the first instant at which, the open circuit potential/time slope ($\Delta U/\Delta t$) becomes 5mV/min or less is considered to represent the electrode response time. For the investigated semiconductor electrodes the response time varies between 50 sec and 700 sec, depending on:

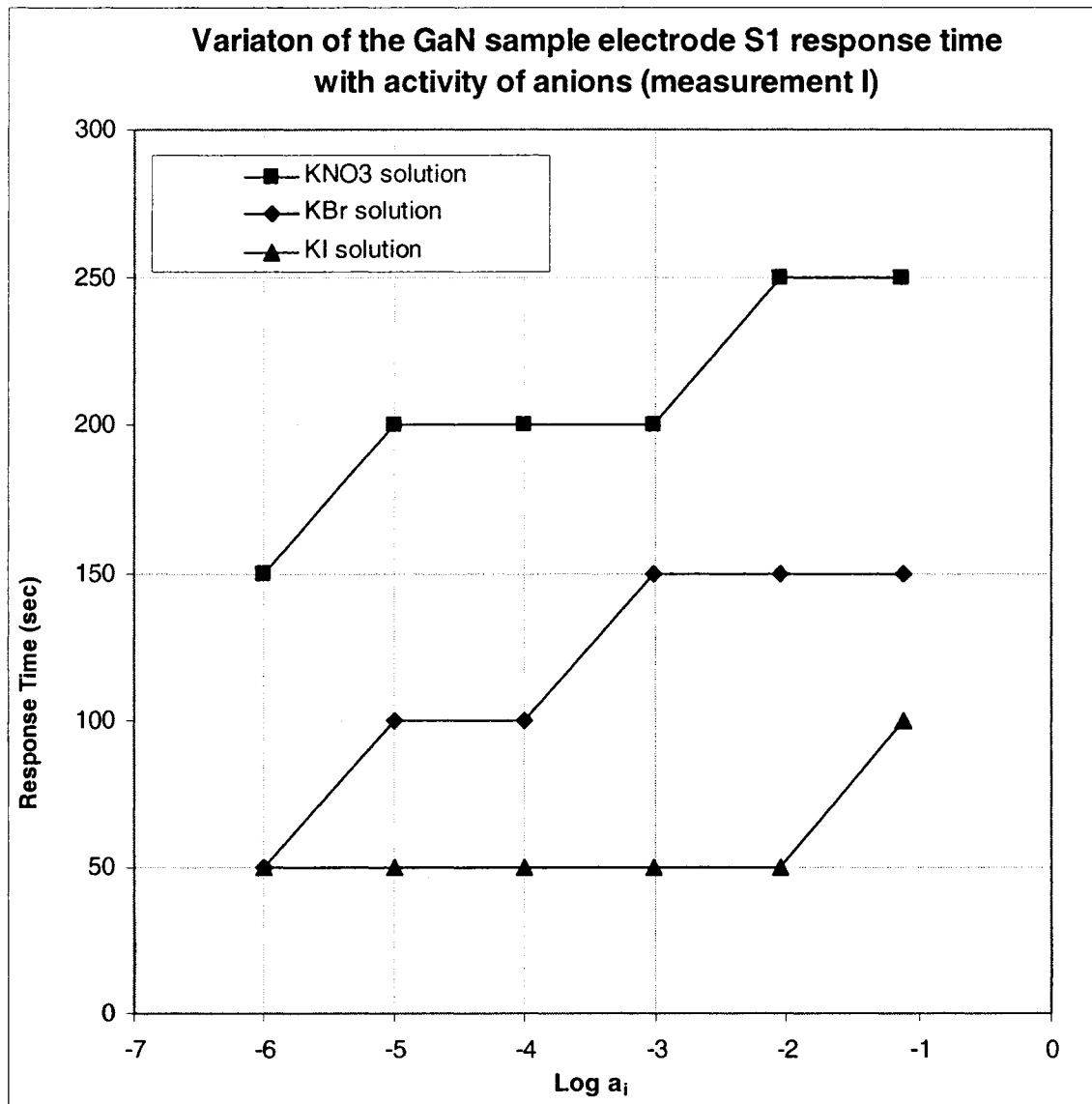
- type of the electrolyte.
- electrode material; and
- activity of anions in tested solutions.

Results & Discussion

A more detailed study of the electrodes response time as a function of activity of anions, electrode material, and type of electrolyte was performed in three electrolyte solutions (KNO_3 , KBr , and KI). These solutions were selected because there is sufficient information about the adsorption capacity of the anions ($\text{NO}_3^- < \text{Br}^- < \text{I}^-$), and also their adsorption capacities are quite different from each other. In contrast, the adsorption capacities of the investigated organic anions are not well known and some of the anions have very similar adsorption capacities (for example NO_3^- and Cl^-). For these anions it is difficult to determine if the variations in the response time are caused by the slightly different adsorption capacity of the anions or by some other factors such as temperature variations or errors in the measurement system. To ensure that the obtained results are reproducible, the experiments in these three solutions with both GaN sample electrode S1 and InGaN sample electrode S3 were repeated. The time between the two series of measurements was 3 months. Fig. III.2 shows the variation of the response time for GaN sample electrode S1 with activity of anions in three electrolyte solutions (KNO_3 , KBr and KI) during the two series of measurements. Fig. III.3 shows the same variation but for the InGaN sample electrode S3.

Fig. III.2 Variation of the GaN sample electrode S1 response time with activity of anions in three electrolyte solutions

a) Measurement I



b) Measurement II

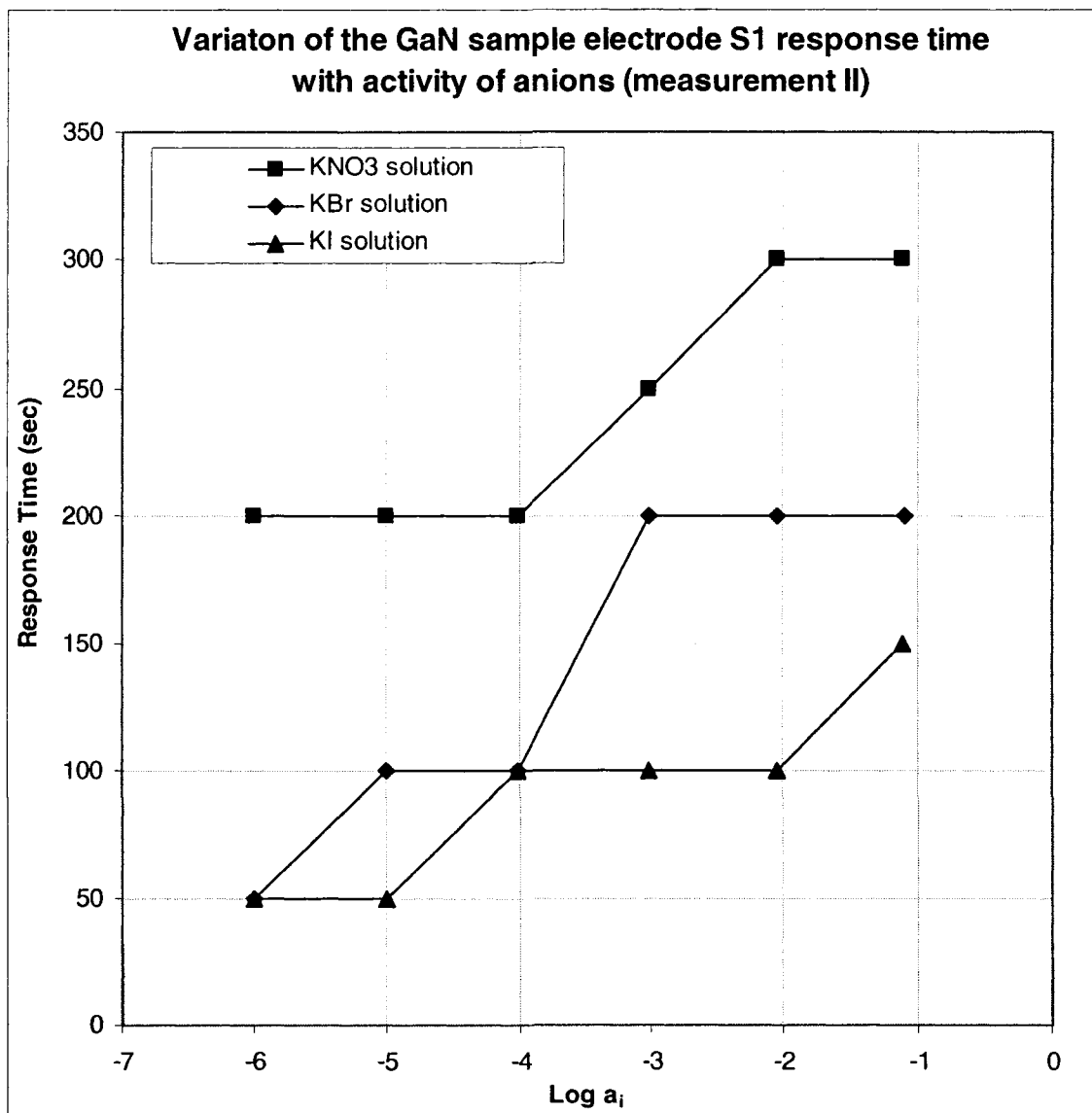
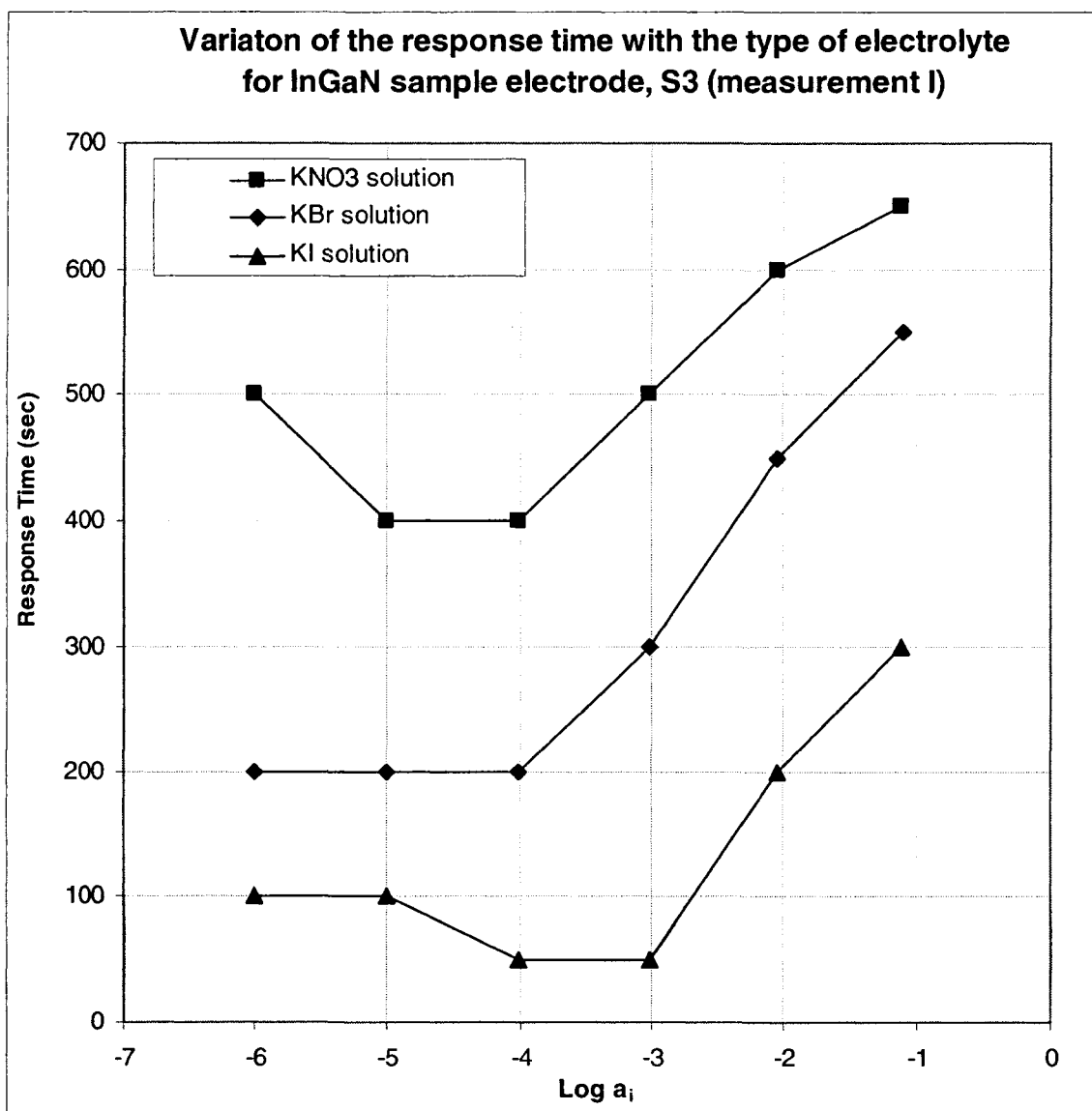
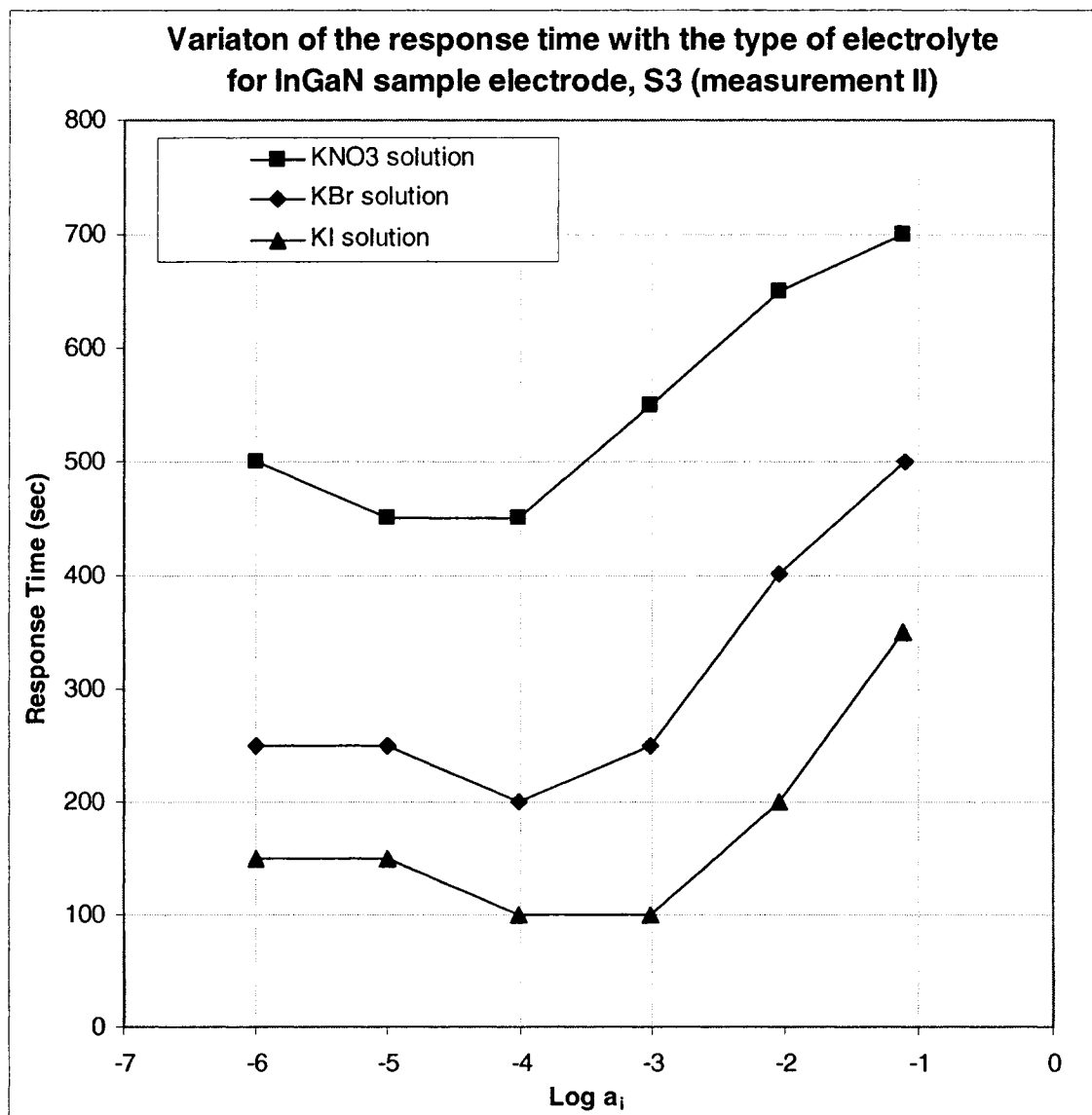


Fig. III.3 Variation of the GaN sample electrode S1 response time with activity of anions in three electrolyte solutions

a) Measurement I



b) Measurement II



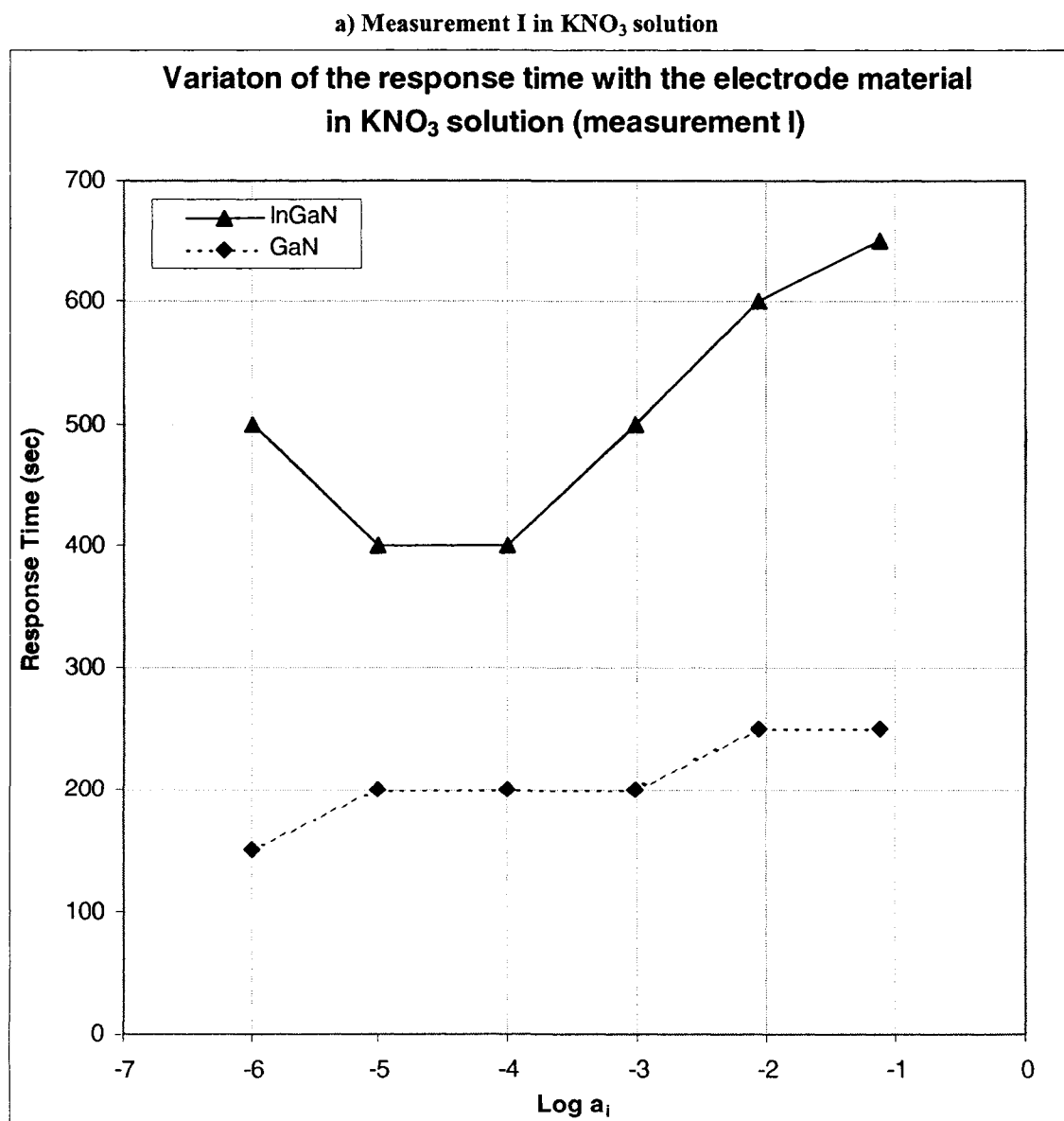
Since the detailed analysis of the variation of the response time with activity of anions and type of electrolyte was only performed for three solutions (KNO₃, KBr, and KI), the conclusions below are limited to these solutions. Fig. III.2 and Fig. III.3 show that the response time of both GaN sample electrode S1 and InGaN sample electrode S3 increases in the following order: KI < KBr < KNO₃. Although the response times recorded during the first series of measurements are slightly different (by 50 seconds or less) from those recorded during the second series of measurements, the order of response time variation with type of electrolyte remains unchanged. This order can be attributed to the adsorption capacity of the measured anions, which increases in

Results & Discussion

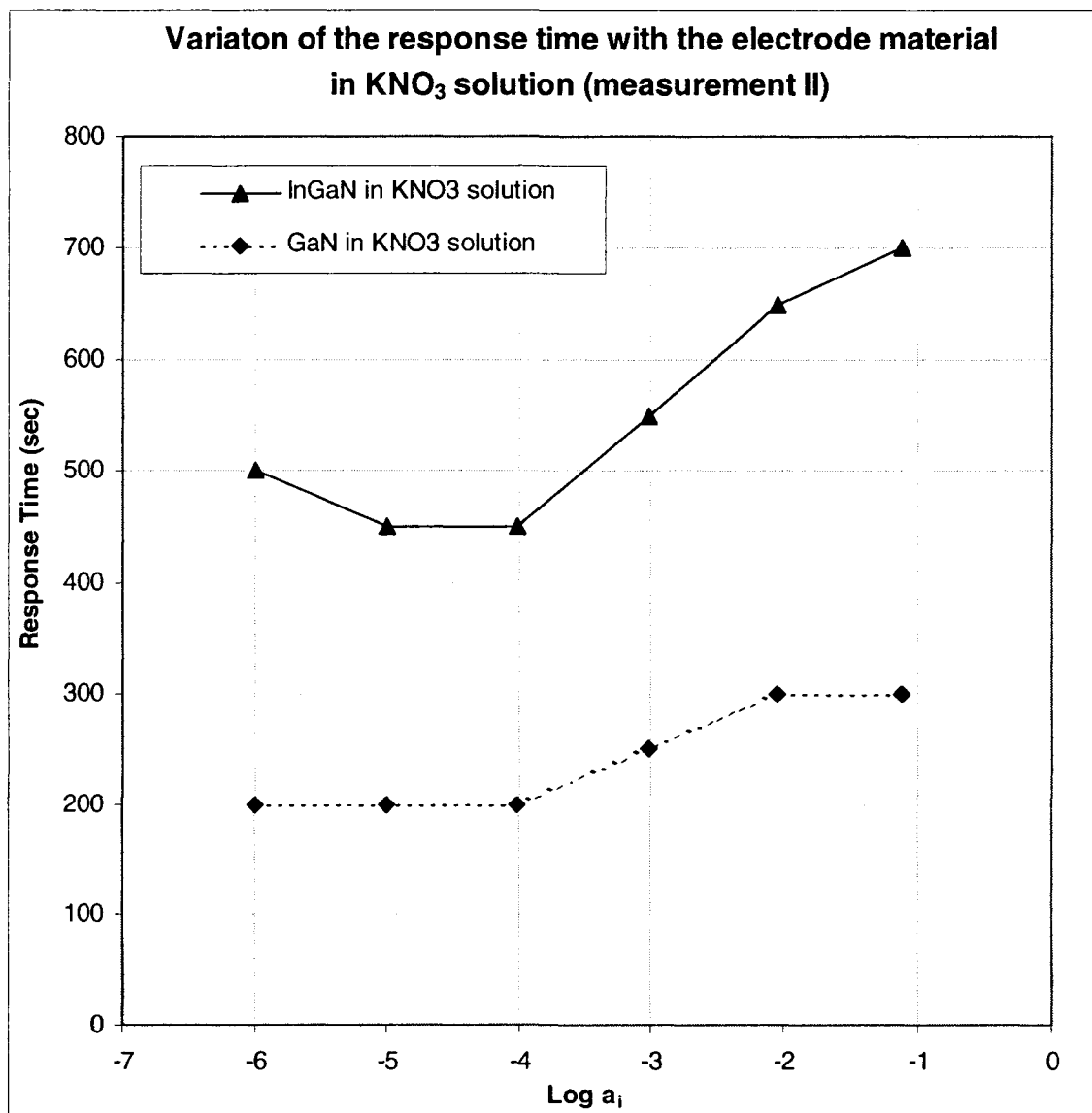
the following order: $\text{NO}_3^- < \text{Br}^- < \text{I}^-$. The I^- anions, which have the strongest adsorption capacity, are adsorbed faster than the Br^- and NO_3^- anions at the electrode surface, and the measured response time is therefore faster. In contrast, the NO_3^- anions have the weakest adsorption capacity, and the response time of the electrodes in NO_3^- solutions is slower than in Br^- or I^- solutions.

Fig. III.4 illustrates the effect of the electrode material on the observed response time in the three electrolyte solutions selected for a detailed investigation of the response time results during two series of measurements.

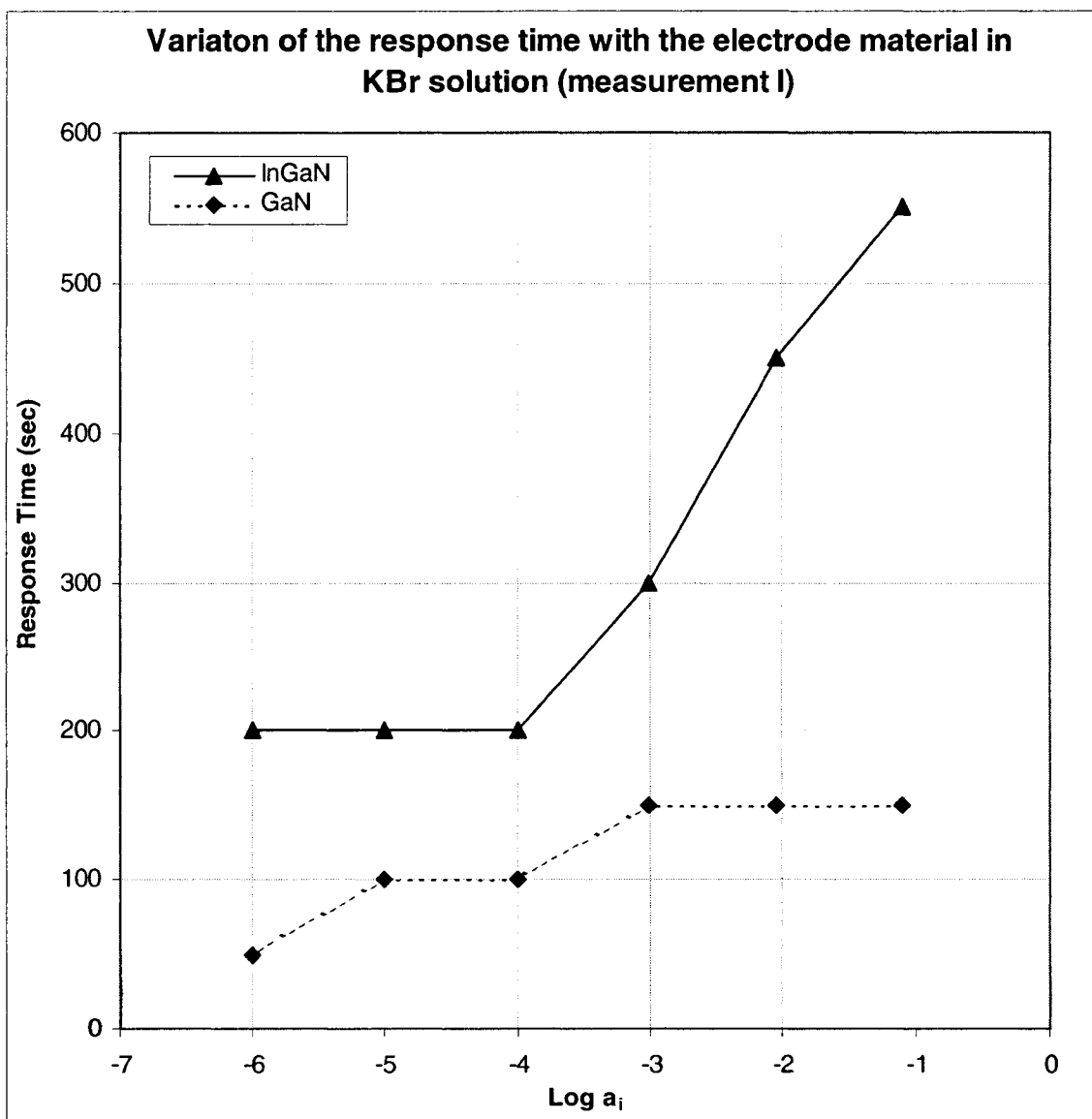
Fig. III.4 Effect of electrode material on the response time in KNO_3 , KBr and KI solutions during two series of measurements



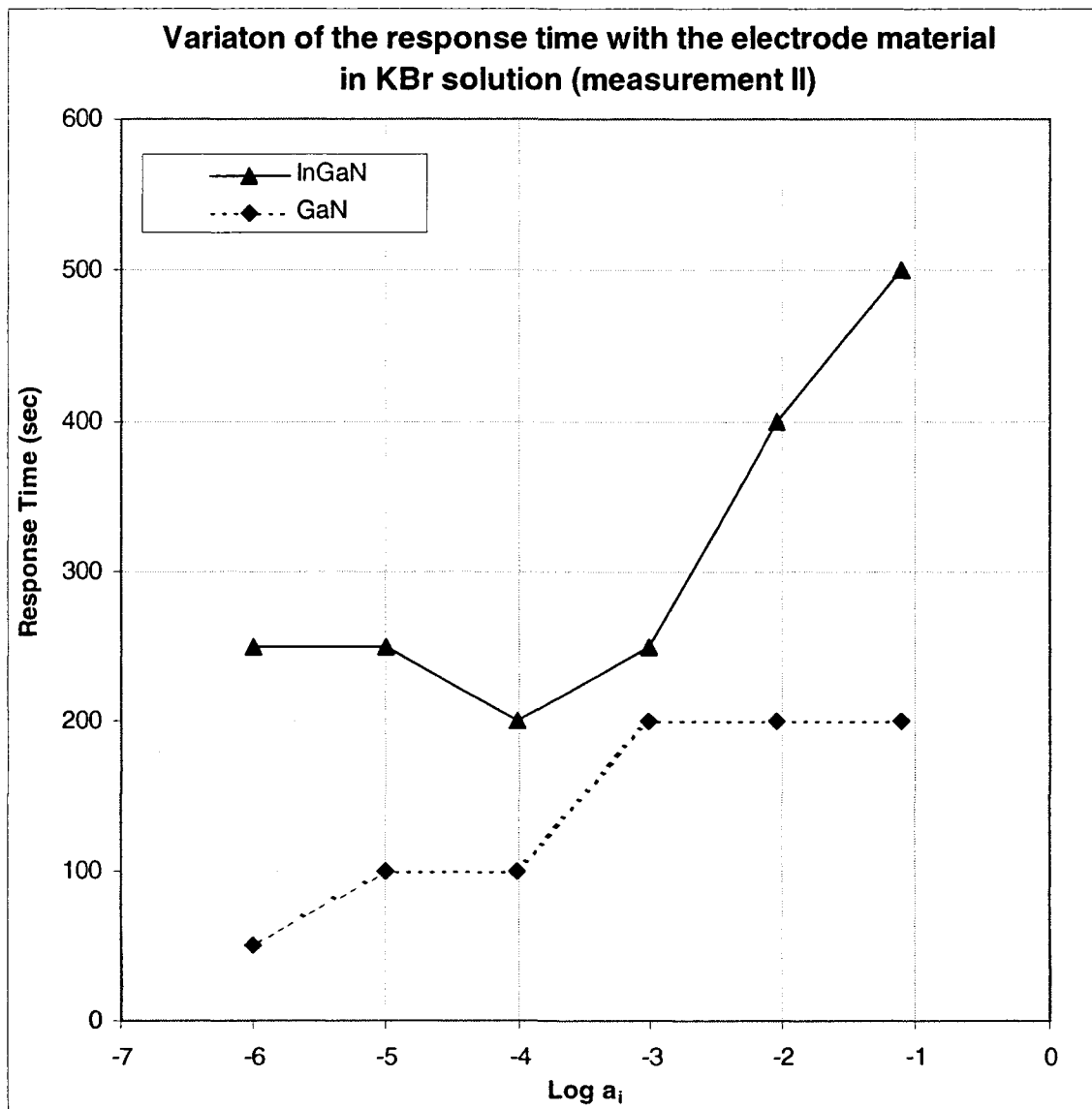
b) Measurement II in KNO₃ solution



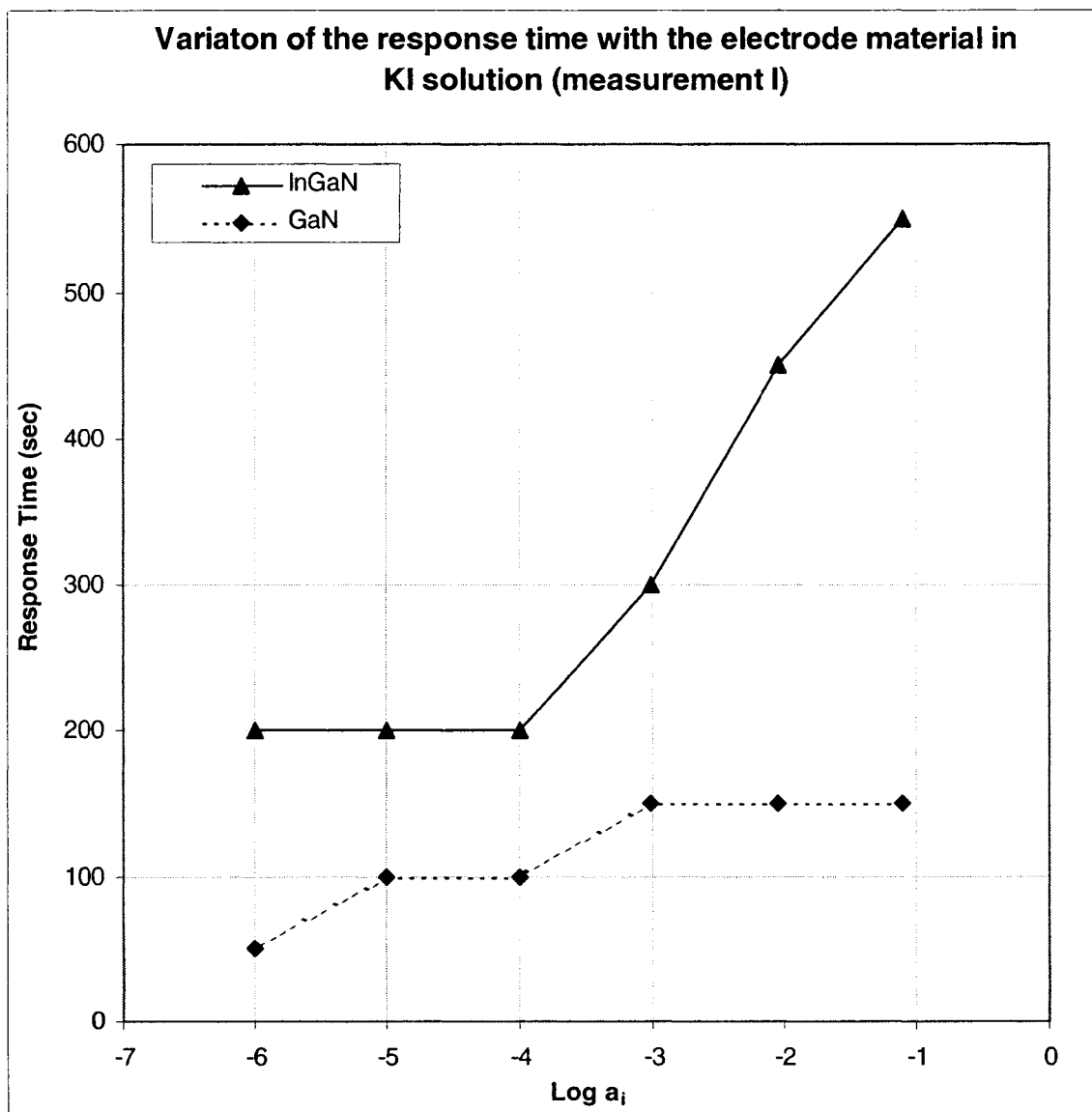
c) Measurement I in KBr solution



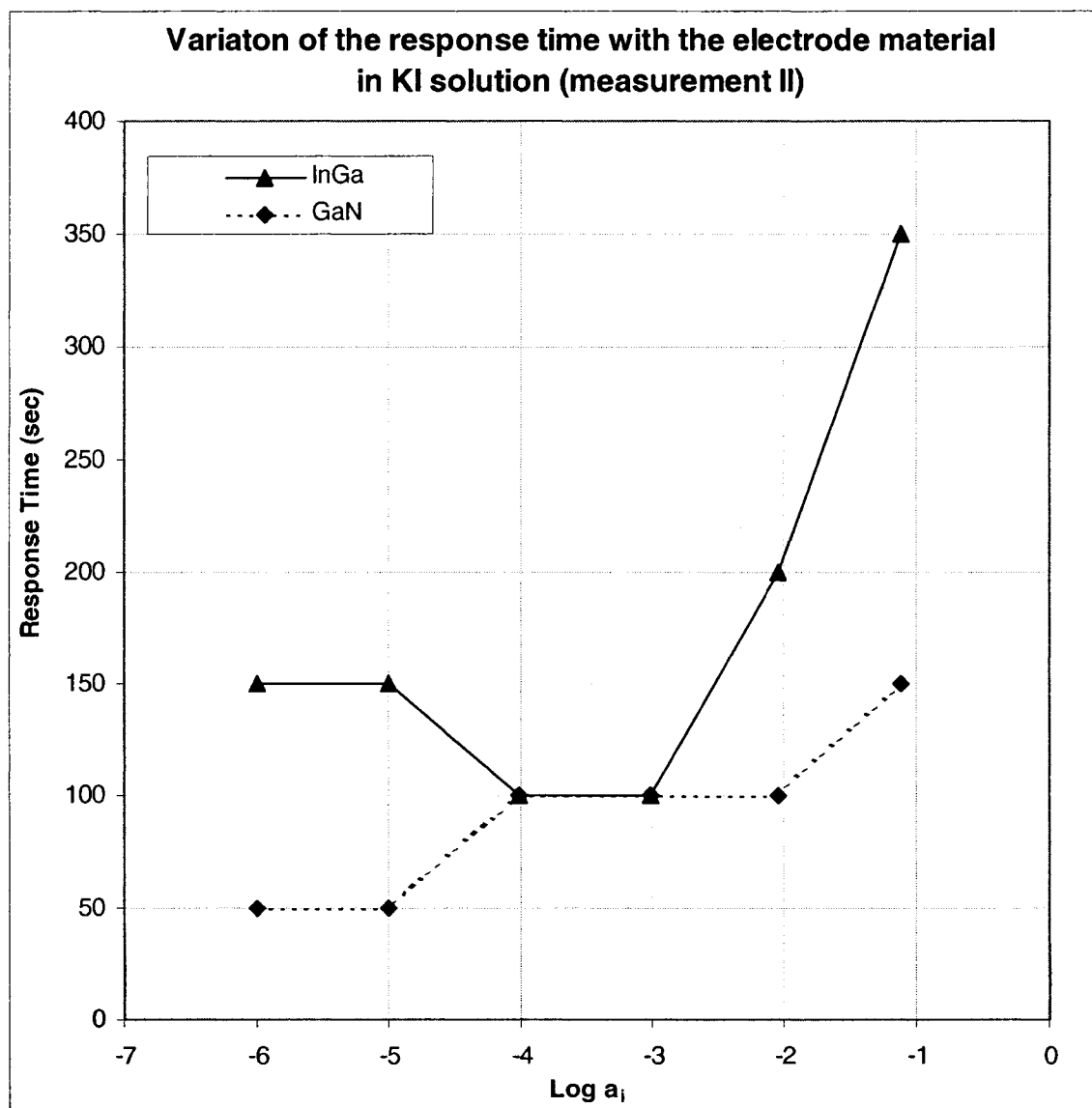
d) Measurement II in KBr solution



e) Measurement I in KI solution



e) Measurement II in KI solution



The data presented on Fig. III.4 show that in the tested three electrolyte solutions, the response time of the GaN sample electrode S1 is faster than the response time of InGaN sample electrode S3 during both series of measurements. This indicates that the electrochemical system attains equilibrium much faster with the GaN sample electrode S1 than with the InGaN sample electrode S3.

Because of limitations of the available electrochemical cell design, the observed response times were measured in unstirred solutions and reflect the time needed for the entire electrochemical system to attain equilibrium. At the end of each measurement, the semiconductor electrodes

Results & Discussion

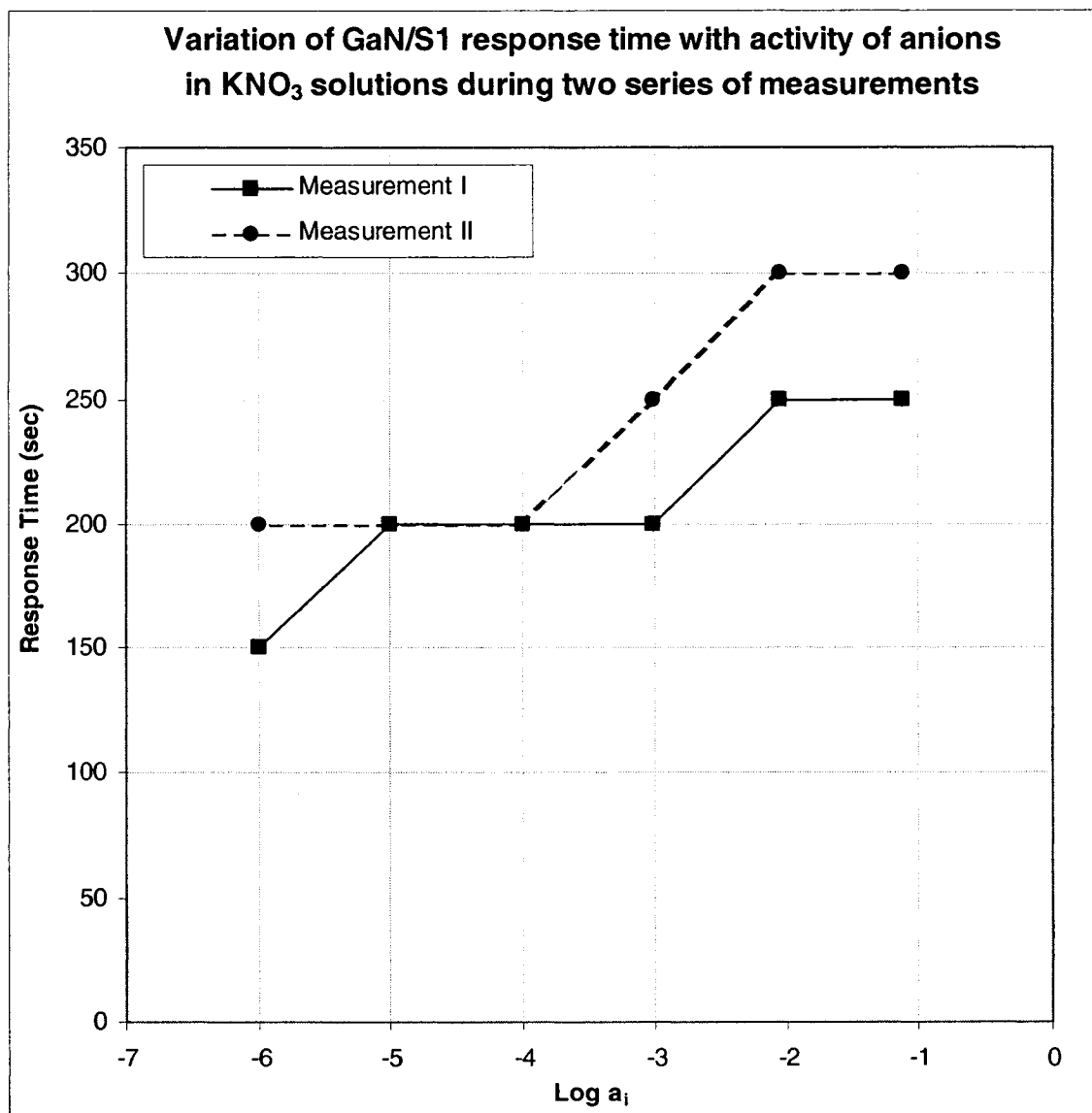
were disconnected from the measuring apparatus, removed from the solution, and carefully rinsed with nano pure water (NPW). Next, the electrodes were immersed into the new solution (with different concentration) and reconnected to the measuring apparatus, upon which the electrochemical system had to regain its equilibrium. This experimental method is believed to generally result in slower response times in comparison with the method in which the concentration change is produced by rapid addition of aliquots of concentrated solution of the desired ions (Bailey, 1980), but it was chosen because of the small size of the electrochemical cell, which did not allow to use the additions method. Bailey (1980) concludes that a response time of 10 minutes or less for an ISE utilized in a manual procedure is acceptable. Based on this conclusion, and considering the limitations of selected experimental method, the response times of GaN and InGaN electrodes, which are generally less than 12 minutes, can be considered acceptable.

III.2.2. Reproducibility of the Response Time Results

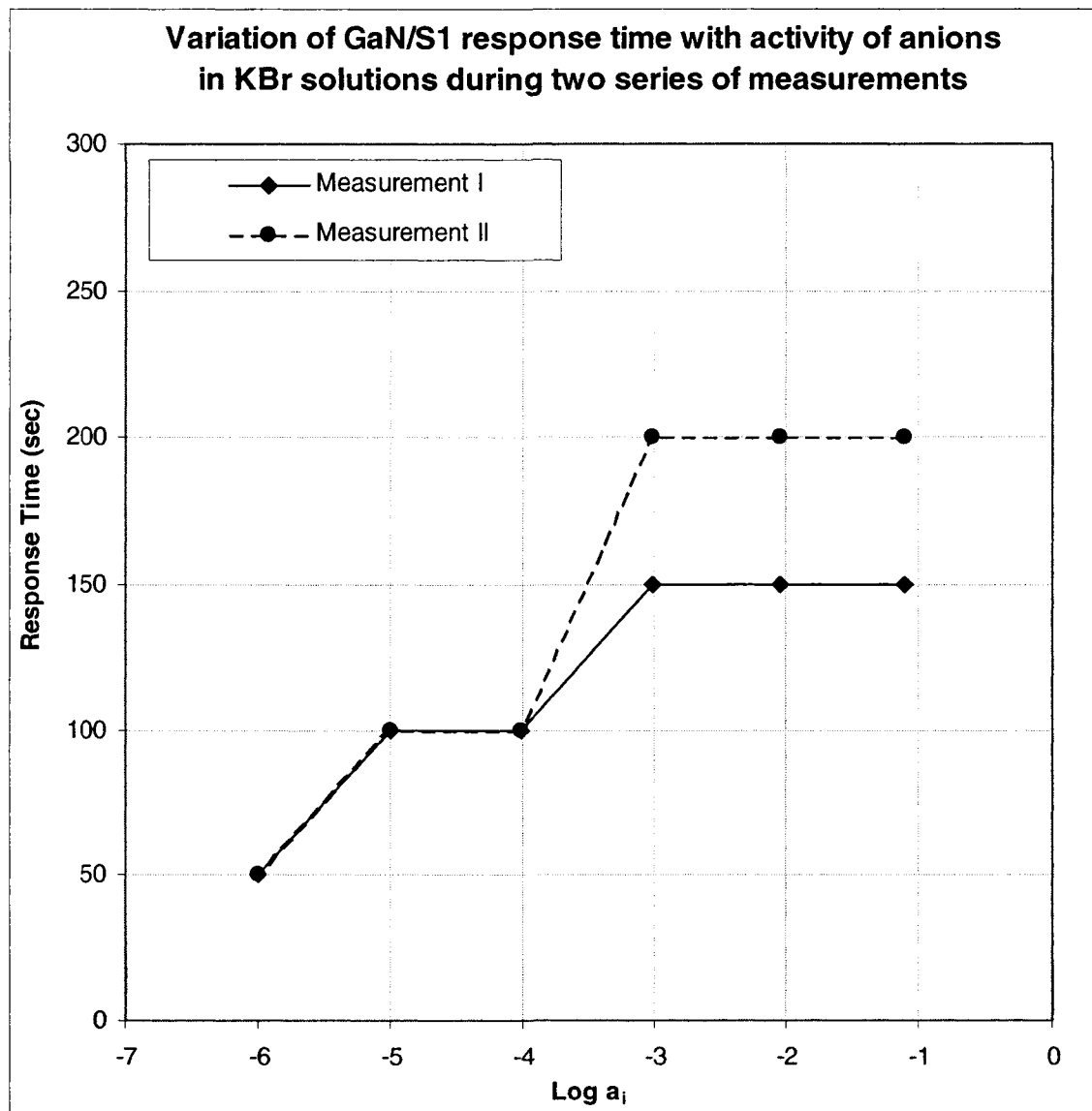
The plots, presented on Fig. III.5 and Fig. III.6, provide a graphical representation of the results obtained during the two series of measurements in the selected for detailed analysis of the response time results three solutions.

Fig. III.5 Reproducibility of response time results for GaN sample electrode S1 in KNO₃, KBr and KI solutions

a) GaN sample electrode S1 in KNO₃ solutions



b) GaN sample electrode S1 in KBr solutions



c) GaN sample electrode S1 in KI solutions

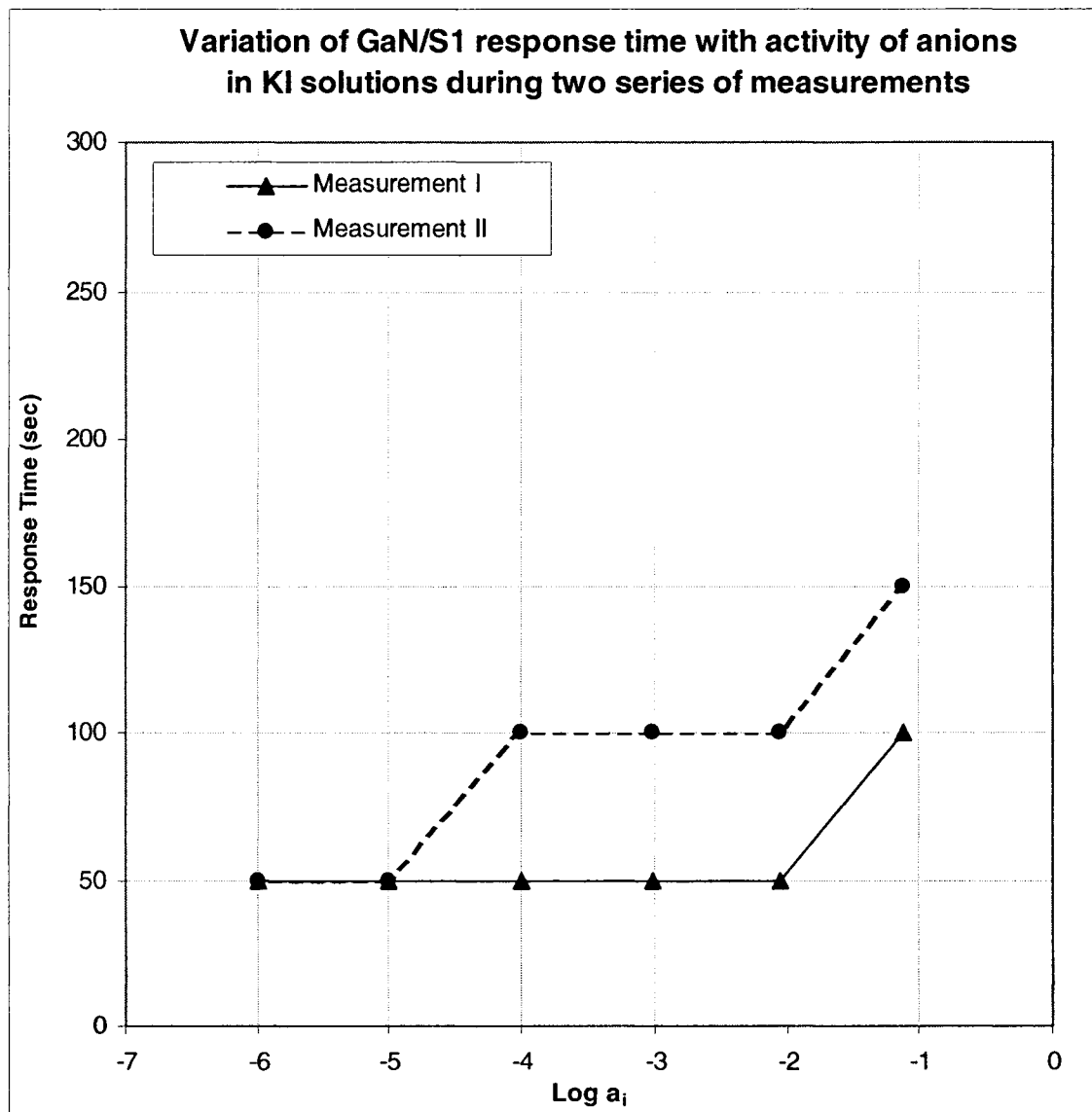
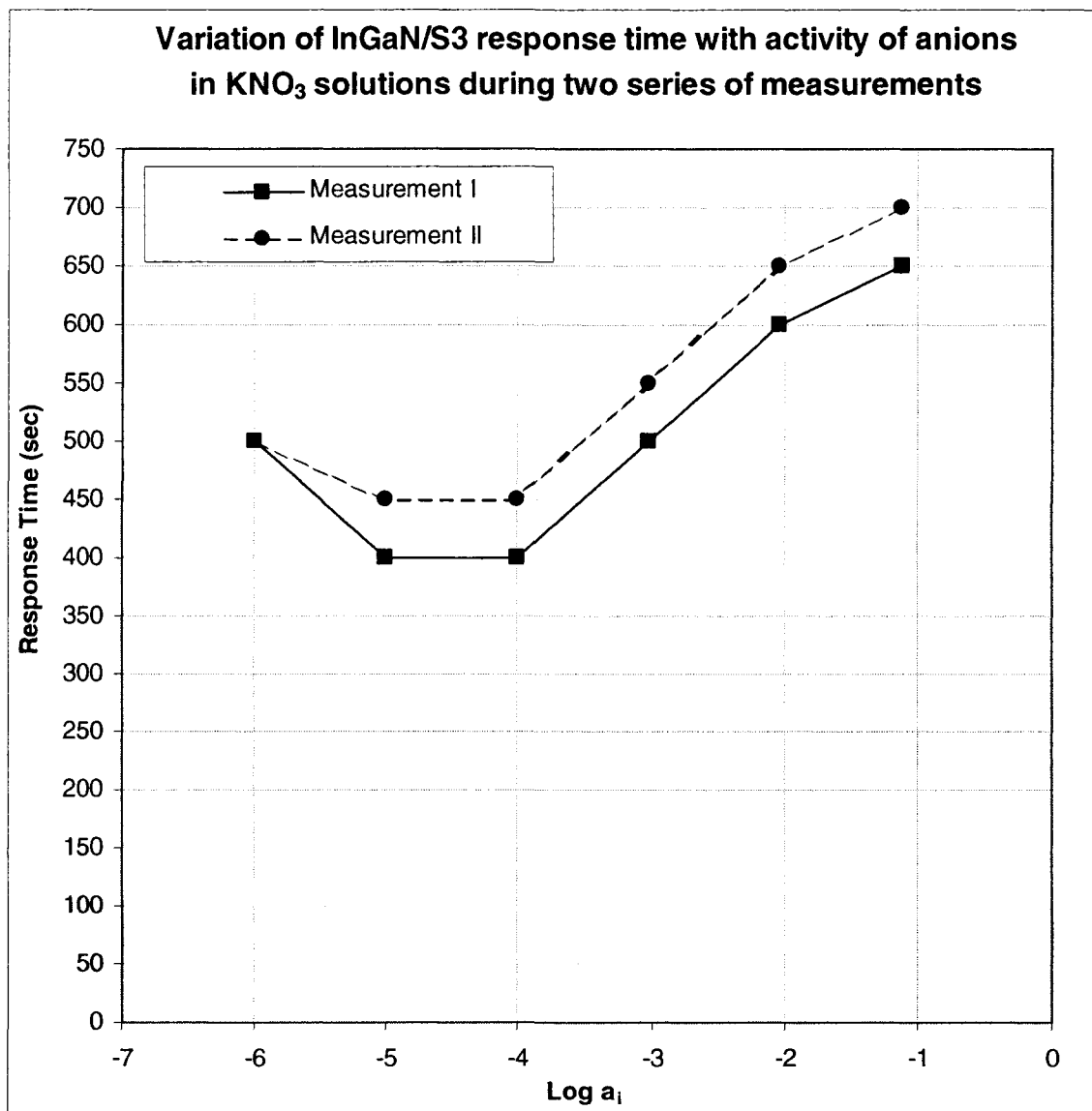
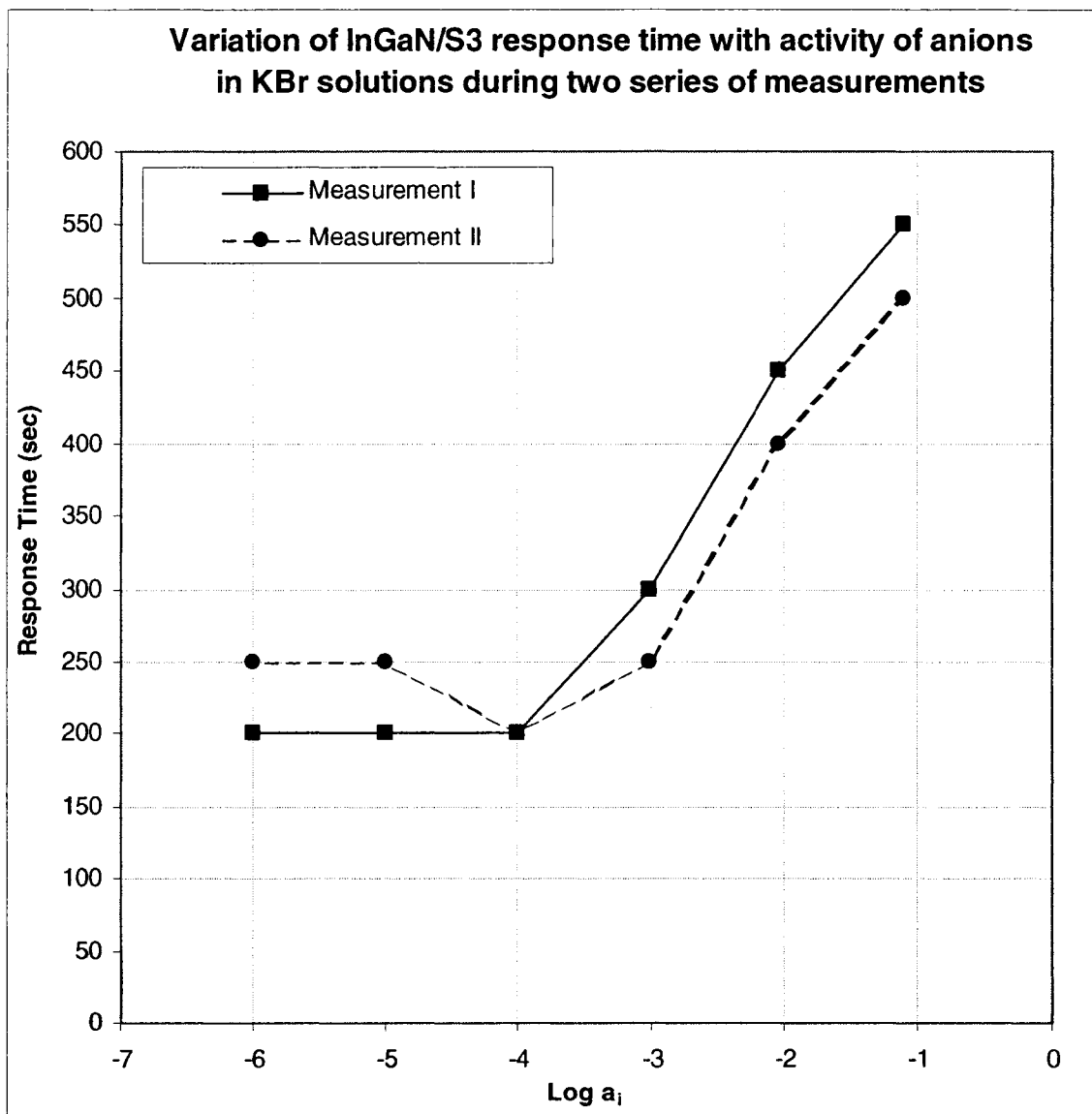


Fig. III.6 Reproducibility of response time results for InGaN sample electrode S3 in KNO₃, KBr and KI solutions

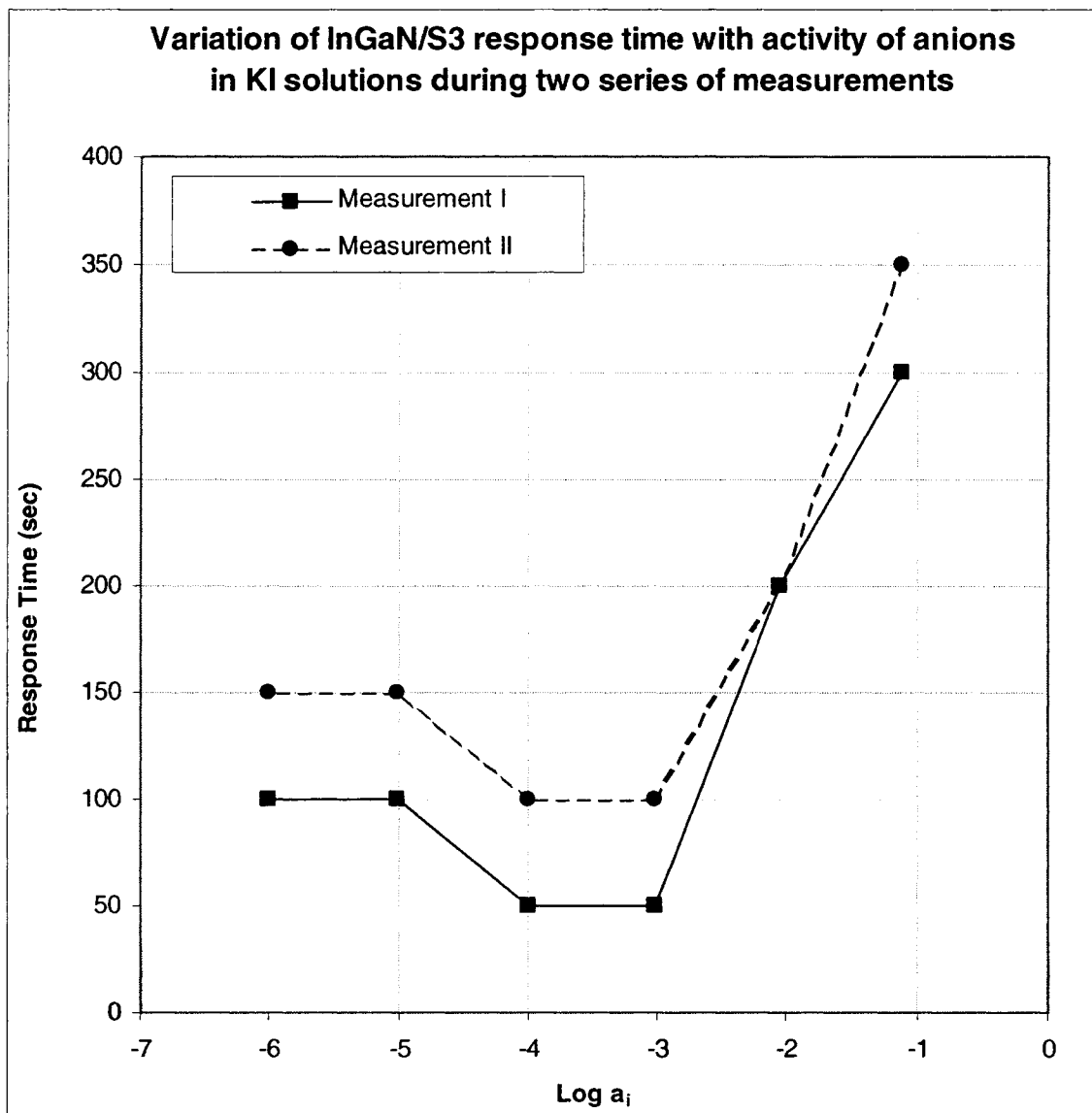
a) InGaN sample electrode S3 in KNO₃ solutions



b) InGaN sample electrode S3 in KBr solutions



c) InGaN sample electrode S3 in KI solutions



Figures III.5 and III.6 show that the response times for both GaN sample electrode S1 and InGaN sample electrode S3 during the two series of measurements differ by 50 seconds or less. The response time during the second series of measurements was either equal to or longer than the response time during the first series of measurements for a solution of a given electrolyte with a given concentration. This result can be attributed to one or more of the following factors:

Results & Discussion

- Some minor contamination of the electrodes sensing element as a result of the experiments performed between the two series of measurements (During the period between the measurements, both GaN and InGaN electrodes were used five days/week and 8 hours/day);
- Hysteresis effects caused by constantly removing and immersing the electrodes in solutions of different electrolytes. IUPAC (1994) explains that the systematic error of hysteresis is generally in the direction of the concentration of the solution in which the electrode was previously immersed. Matencio et al. (2003) analyzed the origins of the hysteresis effect at electrodes prepared with conducting polymers. They distinguished two types of hysteresis: a) dynamic hysteresis and b) stationary or thermodynamic hysteresis. The first type of hysteresis is associated with kinetics of redox reactions occurring at the electrode/electrolyte interface and is observed when a slow charge transfer reaction causes the redox system to depart from the thermodynamic equilibrium. This hysteresis is current dependent and is characteristic of irreversible redox systems. In contrast, the stationary hysteresis is not current dependent and is caused by an interaction between species in the solution and the electrode surface. According to Matencio et al, 2003 these interactions could be electrostatic or mechanical depending on the ions present in the solution and on the composition of the electrode material. In another study, Bousse et al. (1990) investigated the causes of hysteresis and drift for silicon nitride electrodes. They concluded that hysteresis effects are caused by the fact that some sites react slowly to changes, which can be due to some roughness or microscopic porosity of the electrode surface (Bousse et al., 1990). These researchers also reported that it took about 10 hours for their electrochemical system to equilibrate and eliminate the hysteresis effects. Based on the above two studies, the most probable cause of the hysteresis observed at the GaN and InGaN sample electrodes may be the variation in the kinetics of the adsorption and desorption processes leading to longer periods needed by the electrochemical system to attain equilibrium. Considering that the experiments in solutions with various concentrations were performed 20 minutes apart from each other, the electrochemical system may not have had sufficient time to equilibrate. In turn, this probably resulted in readings of OCP potentials slightly different from the equilibrium OCPs. Had the system been allowed sufficient time to attain equilibrium, the hysteresis effect might have been eliminated.

The initial investigation of the electrodes response showed that both the measured OCP and the response time are greatly affected if the surface of the electrodes' sensing element (semiconductor) was not cleaned before each experiment. The results from OCP measurements with the GaN sample electrode S1 and the InGaN sample electrode S3 in KNO₃ solutions before and after cleaning of the electrode surface are summarized in Table III.2. They demonstrate that the OCP for the GaN sample electrode S1 after cleaning is 3 to 10% higher than before cleaning. Similarly, the OCP for the InGaN sample electrode S3 after cleaning is 6 to 17% higher than before cleaning.

Table III.2 OC potentials measured with GaN/S1 and InGaN/S3 in KNO₃ solutions before and after cleaning

Electrode	Conc. (M)	Activity (M)	Log [a]	Measured OC potential (mV) vs SCE		Absolute Variation (mV)	Relative Variation (%)
				Not cleaned electrode	Cleaned electrode		
GaN/S1	1.00E-01	7.55E-02	-1.122	-612	-634	22	3
	1.00E-02	8.97E-03	-2.047	-566	-608	42	7
	1.00E-03	9.64E-04	-3.016	-541	-569	28	5
	1.00E-04	9.88E-05	-4.005	-463	-497	34	7
	1.00E-05	9.96E-06	-5.002	-454	-488	34	7
	1.00E-06	9.99E-07	-6.001	-427	-472	45	10
InGaN/S3	1.00E-01	7.55E-02	-1.122	-512	-561	49	9
	1.00E-02	8.97E-03	-2.047	-613	-654	41	6
	1.00E-03	9.64E-04	-3.016	-527	-599	72	12
	1.00E-04	9.88E-05	-4.005	-479	-527	48	9
	1.00E-05	9.96E-06	-5.002	-414	-445	31	7
	1.00E-06	9.99E-07	-6.001	-348	-421	73	17

Therefore, all sample electrodes were rinsed with NPW before each experiment and kept immersed in NPW when not in use.

III.3. Total Potentiometric Response

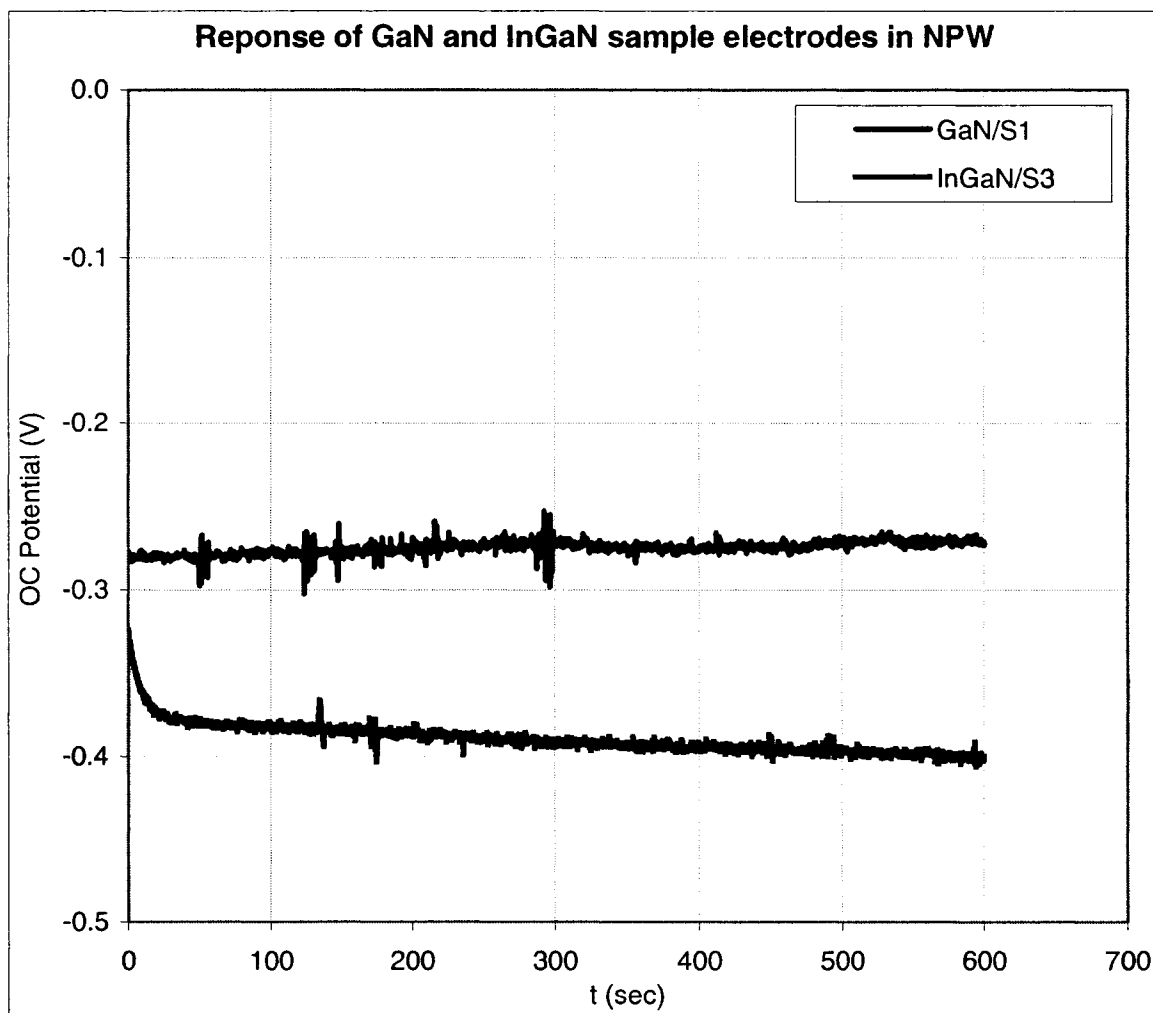
III.3.1. Baseline Measurements, i.e. Measuring the Sample Electrodes Response in NPW

The GaN and InGaN sample electrodes' response in NPW was investigated to obtain a baseline OCP against which to evaluate the overall potentiometric response of the electrodes to various anions. The OCP measurements in NPW (Fig. III.7) demonstrate that the OCP of GaN sample electrode, S1, remains almost constant with time (initial OCP is only 5mV different from the final equilibrium OCP). The fast response of GaN sample electrode S1 in NPW confirms that the electrochemical system attains equilibrium almost immediately after the electrode is immersed in NPW. Unlike S1, the OCP of the InGaN sample electrode S3 becomes more negative with time

Results & Discussion

(initial OCP is 76 mV higher than the final equilibrium OCP), which suggests that the time needed for the electrochemical system to attain equilibrium is much longer than for the GaN sample electrode S1. This conclusion is in agreement with the results from the response time measurements (see Section III.2.1), which also indicate faster response of for the GaN sample electrode S1 compared to the InGaN sample electrode S3.

Fig. III.7 Response of GaN sample electrode S1 and InGaN sample electrode S3 in NPW



The baseline values of the OCP for GaN sample electrode S1, and for InGaN sample electrode S3, are:

- $U_{NPW} = -271\text{mV}$ for S1, and
- $U_{NPW} = -419\text{mV}$ for S3.

III.3.2. Comparison Between the GaN and InGaN Sample Electrodes

The results obtained with the two GaN sample electrodes S1 and S2 were compared to obtain information about variations of OCP between two electrodes made with the same semiconductor material. Table III.3 contains the OCP values measured with both GaN sample electrodes S1 and S2 in various electrolyte solutions. The differences in measured OCP between the two GaN sample electrodes for a given electrolyte solution range between 3 and 9% and may be attributed to the heterogeneity of the GaN thin film across the wafer.

Table III.3 Variation of OCPs with solution for GaN sample electrodes S1 and S2

Solution		Measured OCP (mV) for S1 (GaN) vs SCE	Measured OCP (mV) for S2 (GaN) vs SCE	Absolute Variation between S1 and S2 (mV)	Relative Variation between S1 and S2 (%)
Conc.	Electrolyte				
0.1M	KF	-611	-640	29	5
0.1M	KNO ₃	-634	-597	37	6
0.1M	CH ₃ COOK	-479	-463	16	3
0.1M	KBr	-510	-555	45	9
0.1M	KI	-453	-467	14	3

Accordingly, the results from OCP measurements with the GaN sample electrode S1 and InGaN sample electrode S3 were compared to obtain information about the variation of measured potentials with the type of semiconductor material. The results from this comparison are presented in Table III.4. In most tested electrolytes, the variation between OCPs measured for the two semiconductor electrodes remains within 27%, depending on the activity of the anions and type of electrolyte and can be attributed to the different response of the investigated semiconductor materials. The only exception is the KF solution, in which the measured OCPs of the two electrodes are quite different at the lower concentrations (62% variation in 10⁻⁶M KF) and similar at the high concentrations (variation of only 1% in the 10⁻¹M KF). This is probably because the response time of the InGaN electrode is generally slower than the response time of the GaN electrode, and this effect is most pronounced in the solution containing anions with weak adsorption capacity (KF) at their lowest measured activity (10⁻⁶M). In this solution (10⁻⁶M KF), the OCP reading for the InGaN electrode was probably taken before the system had reached equilibrium, while the OCP reading for the GaN electrode was taken in an equilibrated system. Hence, in the KF solution the large difference between measured OC potentials of the two electrodes cannot be only attributed to the semiconductor material. As the activity of anions increases, the time needed for the electrochemical system to attain equilibrium becomes shorter, and the variation between measured OCPs with two electrodes becomes smaller.

Results & Discussion

The factors that influence the electrodes response are investigated in more detail in the following sections.

Table III.4 Variation of OCPs with activity of anions and type of electrolyte for GaN/S1 and InGaN/S3 electrodes

Salt	Conc. (M)	Activity (M)	Measured OC potential (mV) vs SCE		Absolute Variation between S1 and S3 (mV)	Relative Variation between S1 and S3 (%)
			S1 (GaN)	S3 (InGaN)		
KF	1.00E-01	7.62E-02	-611	-603	8	1
	1.00E-02	8.99E-03	-569	-463	106	23
	1.00E-03	9.64E-04	-560	-427	133	31
	1.00E-04	9.88E-05	-508	-366	142	39
	1.00E-05	9.96E-06	-471	-315	156	50
	1.00E-06	9.99E-07	-453	-280	173	62
KNO ₃	1.00E-01	7.55E-02	-634	-561	73	13
	1.00E-02	8.97E-03	-608	-654	46	7
	1.00E-03	9.64E-04	-569	-599	30	5
	1.00E-04	9.88E-05	-497	-527	30	6
	1.00E-05	9.96E-06	-488	-445	43	10
	1.00E-06	9.99E-07	-472	-421	51	12
KCl	1.00E-01	7.60E-02	-560	-597	37	6
	1.00E-02	8.98E-03	-534	-530	4	1
	1.00E-03	9.64E-04	-504	-492	12	2
	1.00E-04	9.88E-05	-488	-474	14	3
	1.00E-05	9.96E-06	-424	-420	4	1
	1.00E-06	9.99E-07	-427	-413	14	3
HOC ₆ H ₄ COONa	1.00E-01	7.51E-02	-518	-554	36	6
	1.00E-02	8.97E-03	-511	-542	31	6
	1.00E-03	9.64E-04	-497	-506	9	2
	1.00E-04	9.87E-05	-439	-387	52	13
	1.00E-05	9.94E-06	-392	-345	47	14
	1.00E-06	9.96E-07	-384	-348	36	10
KSCN	1.00E-01	7.81E-02	-541	-535	6	1
	1.00E-02	9.02E-03	-525	-529	4	1
	1.00E-03	9.65E-04	-510	-498	12	2
	1.00E-04	9.88E-05	-465	-423	42	10
	1.00E-05	9.96E-06	-407	-355	52	15
	1.00E-06	9.99E-07	-387	-398	11	3
CH ₃ COOK	1.00E-01	7.59E-02	-479	-455	24	5
	1.00E-02	8.98E-03	-492	-483	9	2
	1.00E-03	9.64E-04	-488	-478	10	2
	1.00E-04	9.86E-05	-477	-470	7	1
	1.00E-05	9.92E-06	-412	-365	47	13
	1.00E-06	9.93E-07	-414	-406	8	2
KClO ₄	1.00E-01	7.44E-02	-546	-608	62	10
	1.00E-02	8.95E-03	-526	-501	25	5
	1.00E-03	9.64E-04	-471	-382	89	23
	1.00E-04	9.88E-05	-438	-364	74	20
	1.00E-05	9.96E-06	-392	-315	77	24
	1.00E-06	9.99E-07	-378	-327	51	16
KBr	1.00E-01	7.81E-02	-510	-663	153	23
	1.00E-02	9.02E-03	-472	-586	114	19
	1.00E-03	9.65E-04	-440	-560	120	21
	1.00E-04	9.88E-05	-398	-512	114	22
	1.00E-05	9.96E-06	-360	-491	131	27
	1.00E-06	9.99E-07	-339	-467	128	27
KI	1.00E-01	7.64E-02	-453	-621	168	27
	1.00E-02	8.99E-03	-476	-575	99	17
	1.00E-03	9.65E-04	-483	-597	114	19
	1.00E-04	9.88E-05	-411	-511	100	20
	1.00E-05	9.96E-06	-391	-530	139	26
	1.00E-06	9.99E-07	-347	-452	105	23

III.3.3. Total Potentiometric Response

The total potentiometric response of the GaN and InGaN sample electrodes was calculated as the difference between the baseline OCP, where the concentration of the tested anions was 0M, and the OCPs measured in the solutions with the highest concentration of tested anions, i.e. 0.1M.

The total potentiometric responses of the GaN sample electrode S1 and the InGaN sample electrode S3 are presented in Table III.5.

Table III.5 Total Potentiometric Response of GaN (S1) and InGaN (S3) sample electrodes for several potassium and sodium salts

(Response in 0.1 M minus response to pure water)

Salt	Baseline OCP (mV) of S1 (GaN)	OCP (mV) of S1 (GaN) in 0.1M salt solutions	Total potentiometric response (mV) of S1 (GaN)	Baseline OCP (mV) of S3 (InGaN)	OCP (mV) of S3 (InGaN) in 0.1M salt solutions	Total potentiometric response (mV) of S3 (InGaN)
KF	-271	-611	-340	-419	-603	-184
KNO ₃	-271	-634	-363	-419	-561	-142
KCl	-271	-560	-289	-419	-597	-178
HOC ₆ H ₄ COONa	-271	-518	-247	-419	-554	-135
KSCN	-271	-541	-270	-419	-535	-116
CH ₃ COOK	-271	-479	-208	-419	-455	-36
KClO ₄	-271	-546	-275	-419	-608	-189
KBr	-271	-510	-239	-419	-663	-244
KI	-271	-453	-182	-419	-621	-202

The results in the Table III.5 show that the total potentiometric response for the GaN sample electrode S1 is generally higher than for the InGaN sample electrode S3. Hence, with the exception of Br⁻ and I⁻ anions, the sensitivity of the GaN sample electrode to anions is better than that of the InGaN sample electrode.

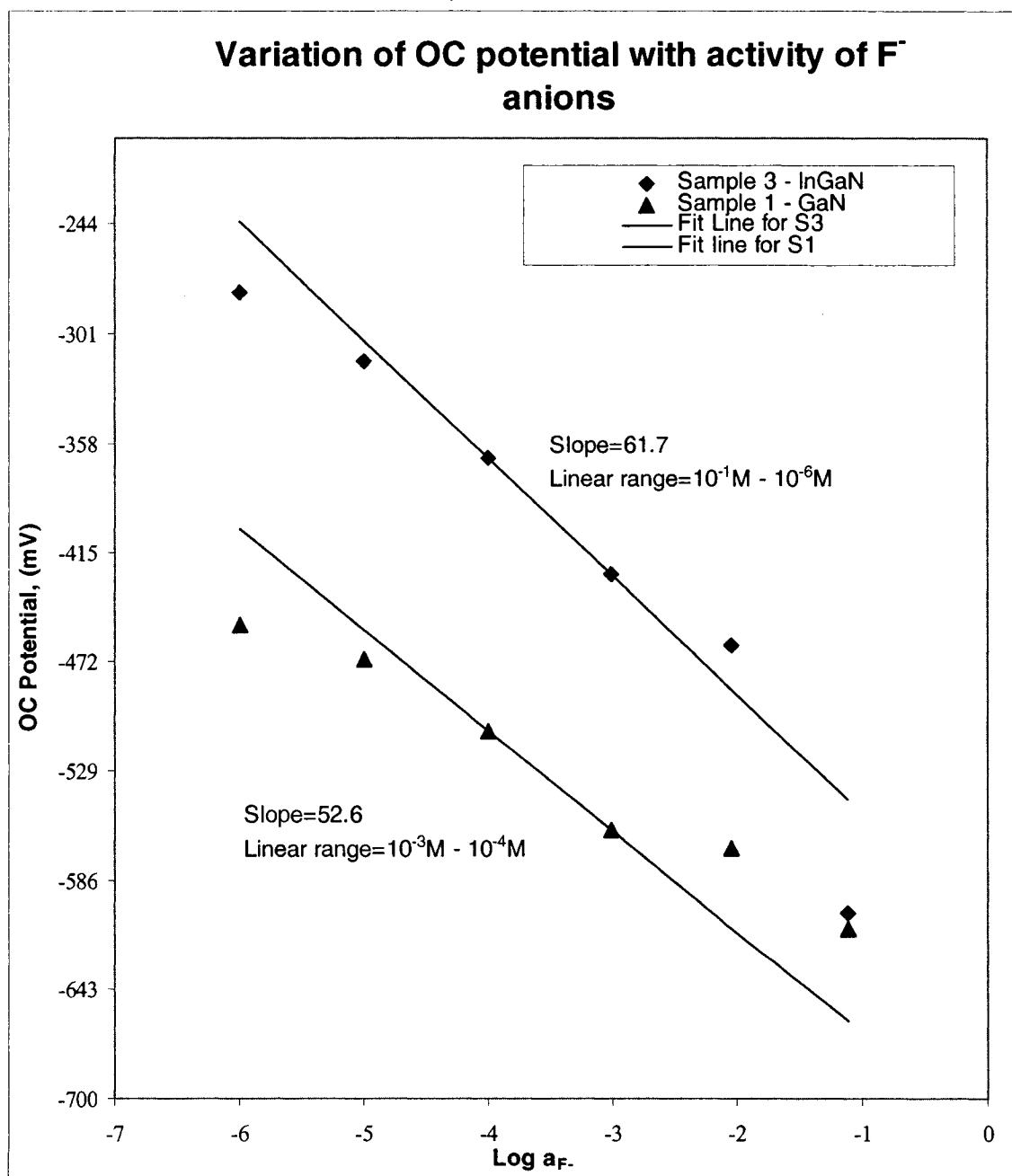
III.4. Construction of Calibration Curves

In this section, results pertaining to the electrodes response versus activity of anions in the solution will be presented. The objective of the next stage of the research was to construct a complete set of calibration curves for the GaN sample electrode S1 and for the InGaN sample electrode S3. Calibration curves were obtained for all nine test electrolytes: KF, KNO₃, KCl, HOC₆H₄COONa, KSCN, CH₃COOK, KClO₄, KBr and KI. In each electrolyte solution the variation of the OCP with time was constantly monitored with the Solartron potentiostat. When the variation of the OCP with time became less than or equal to 5mV/min, the value of the OCP was recorded and used in the construction of the calibration curves. The main source of experimental error with respect to the construction of the calibration curves comes from the risk

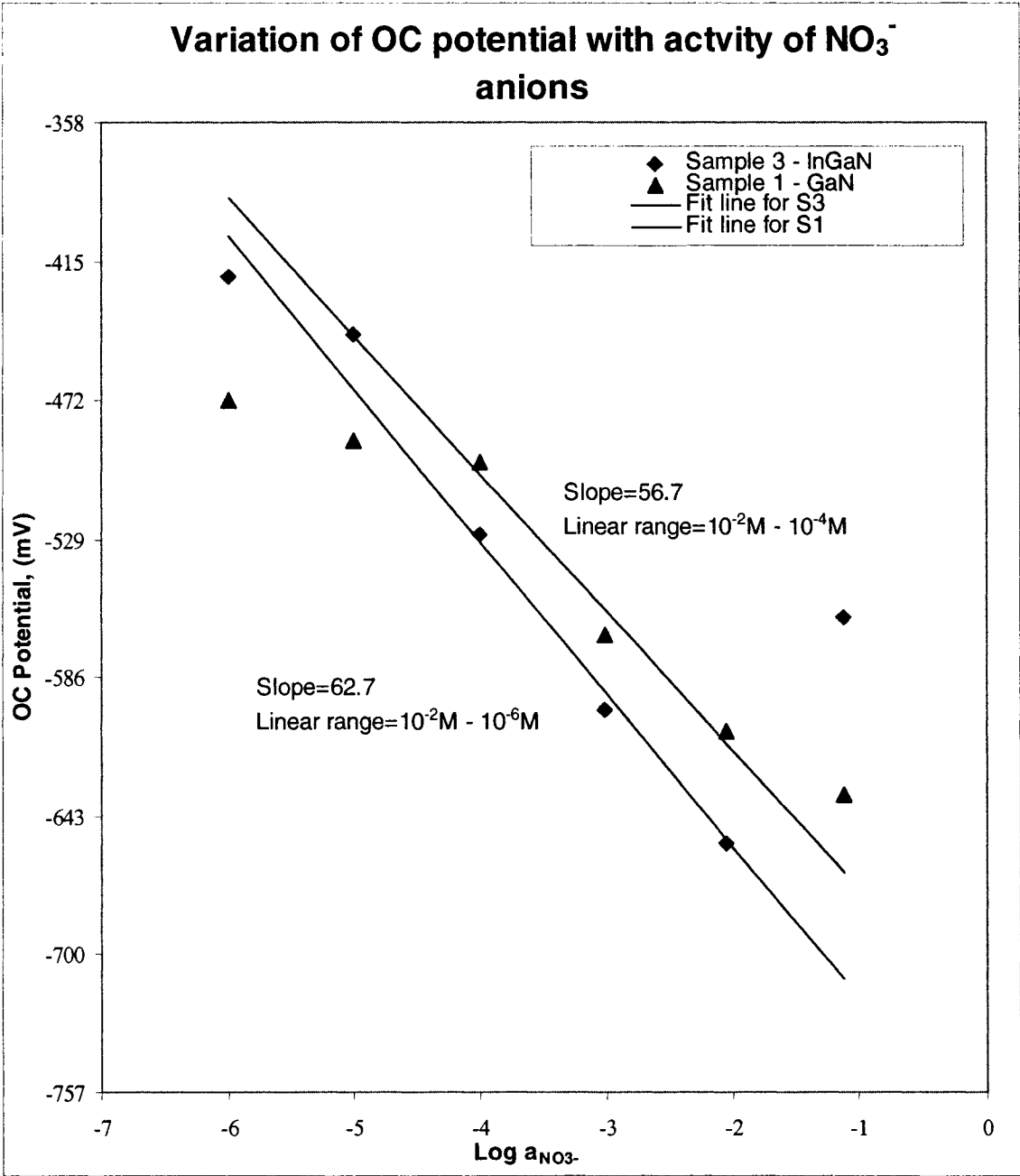
of using an OCP value that is somewhat different from the final steady state potential of the electrochemical system. As for the GaN and InGaN semiconductor electrodes the final steady state potential of the electrode in measured solutions is unknown there is no way to completely eliminate this error. The calibration curves for the GaN sample electrode S1 and for the InGaN sample electrode S3 in all test electrolytes are presented on Fig. III.8.

Fig. III.8 Calibration curves of the GaN sample electrode, S1, and the InGaN sample electrode, S3, in nine test electrolytes

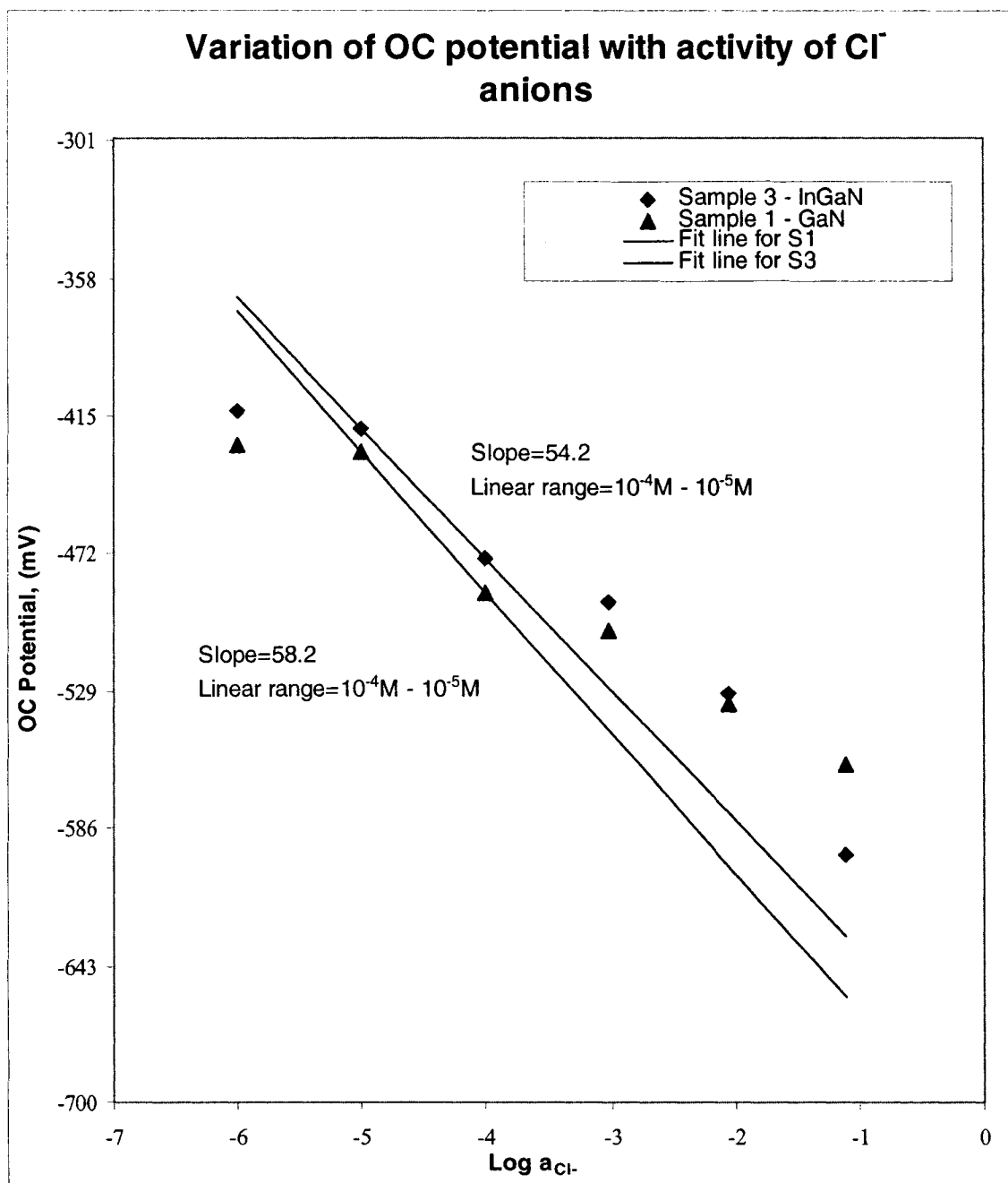
a) KF solutions



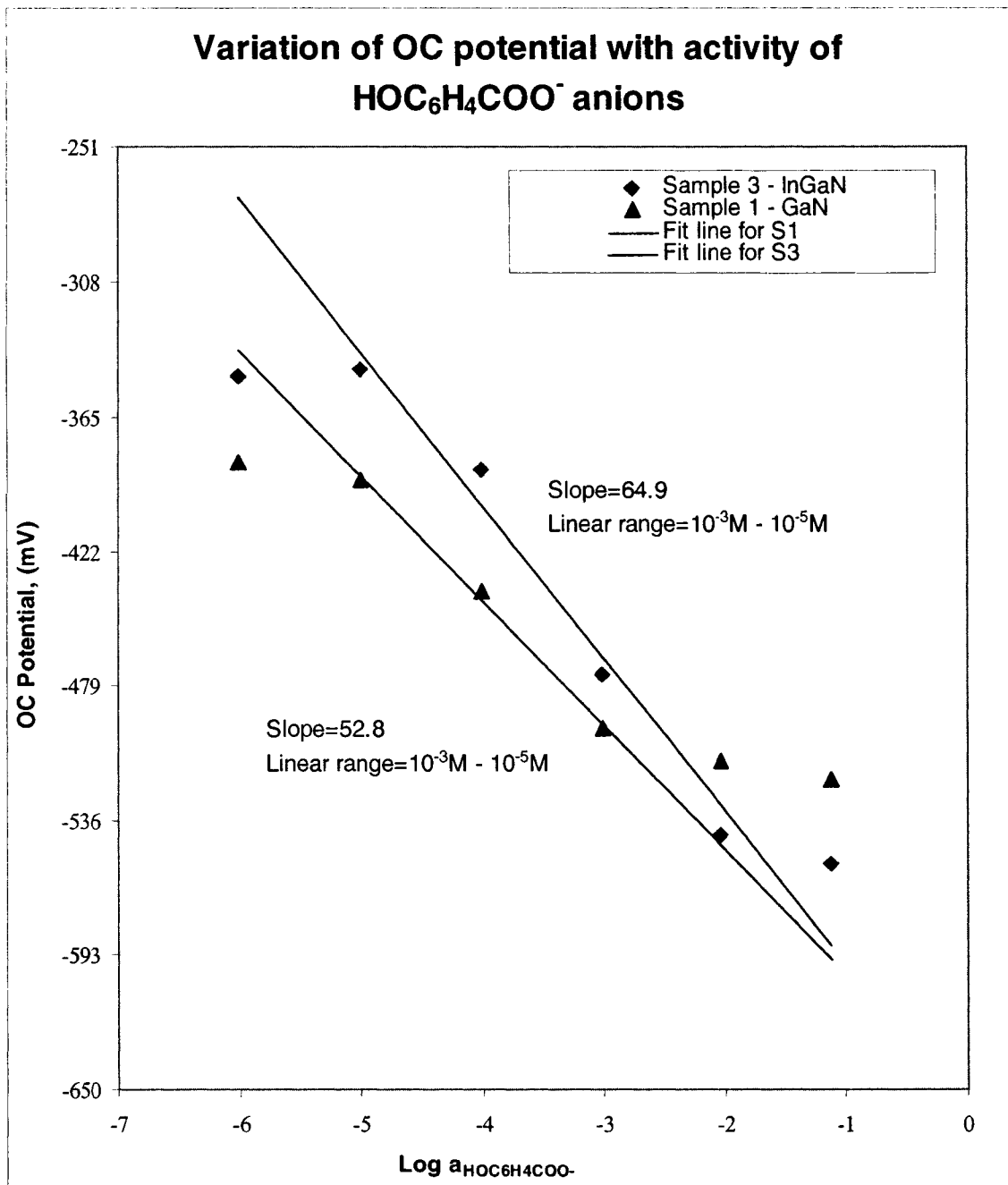
b) KNO₃ solutions



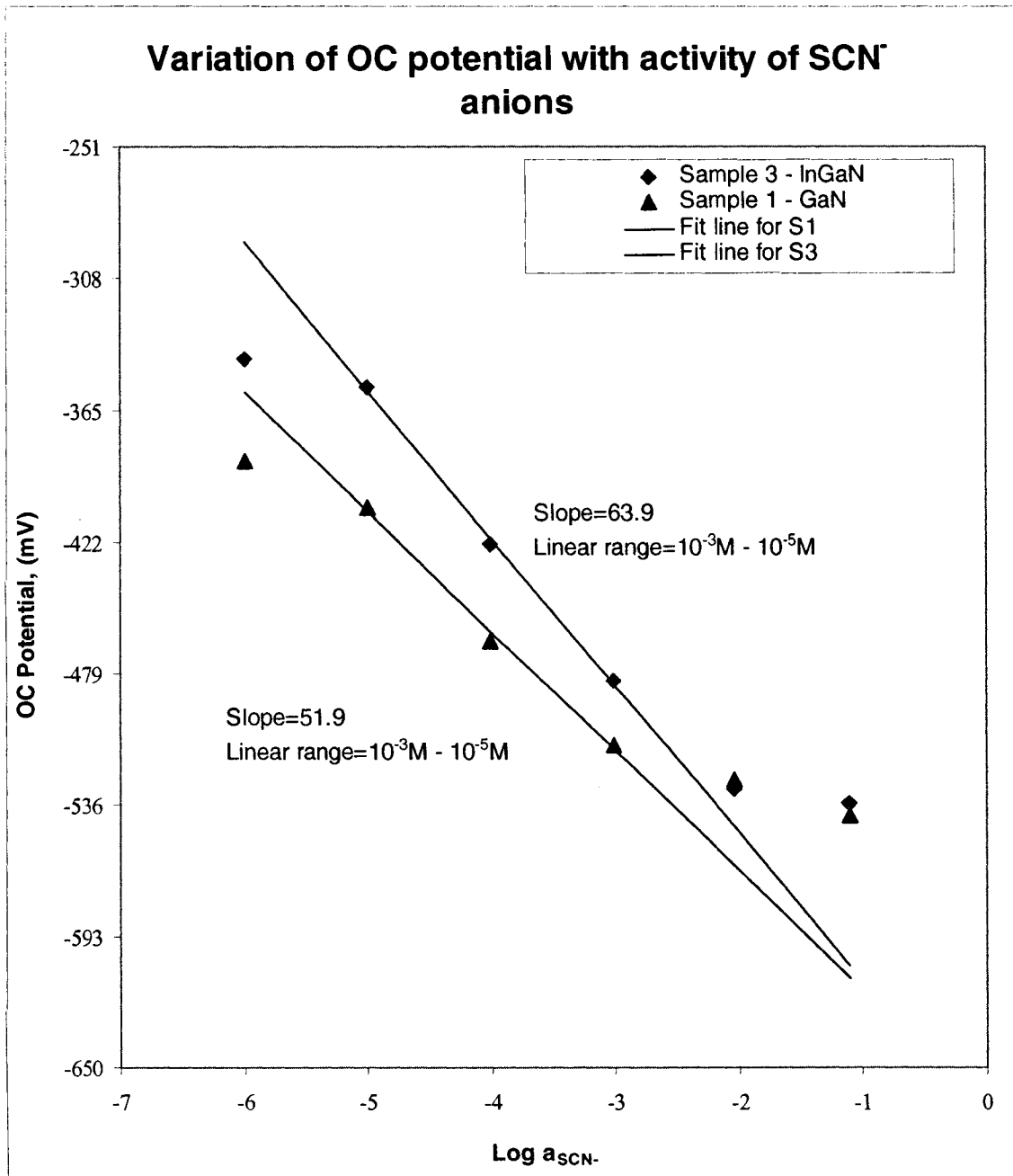
c) KCl solutions



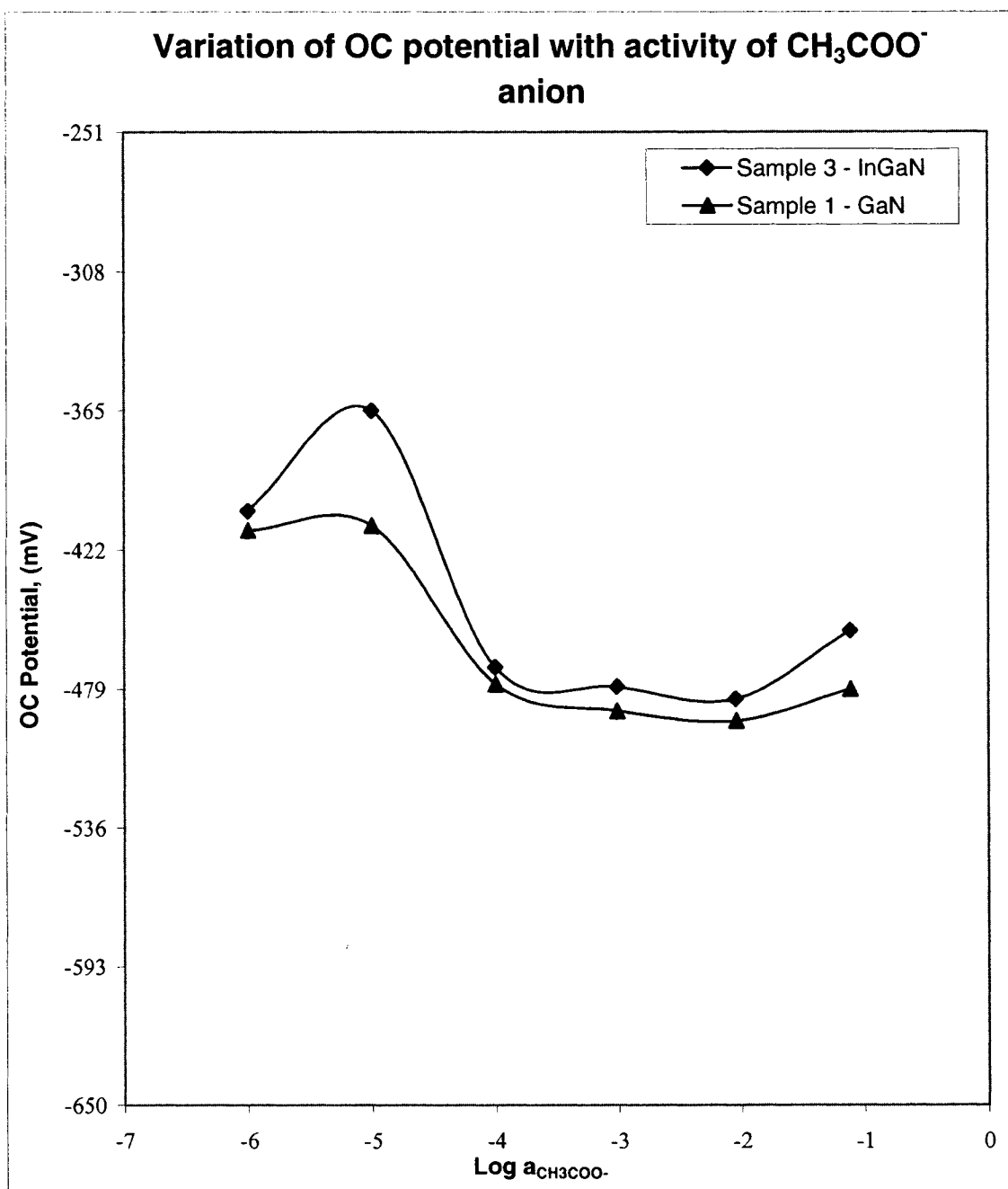
d) $\text{HOC}_6\text{H}_4\text{COONa}$ solutions



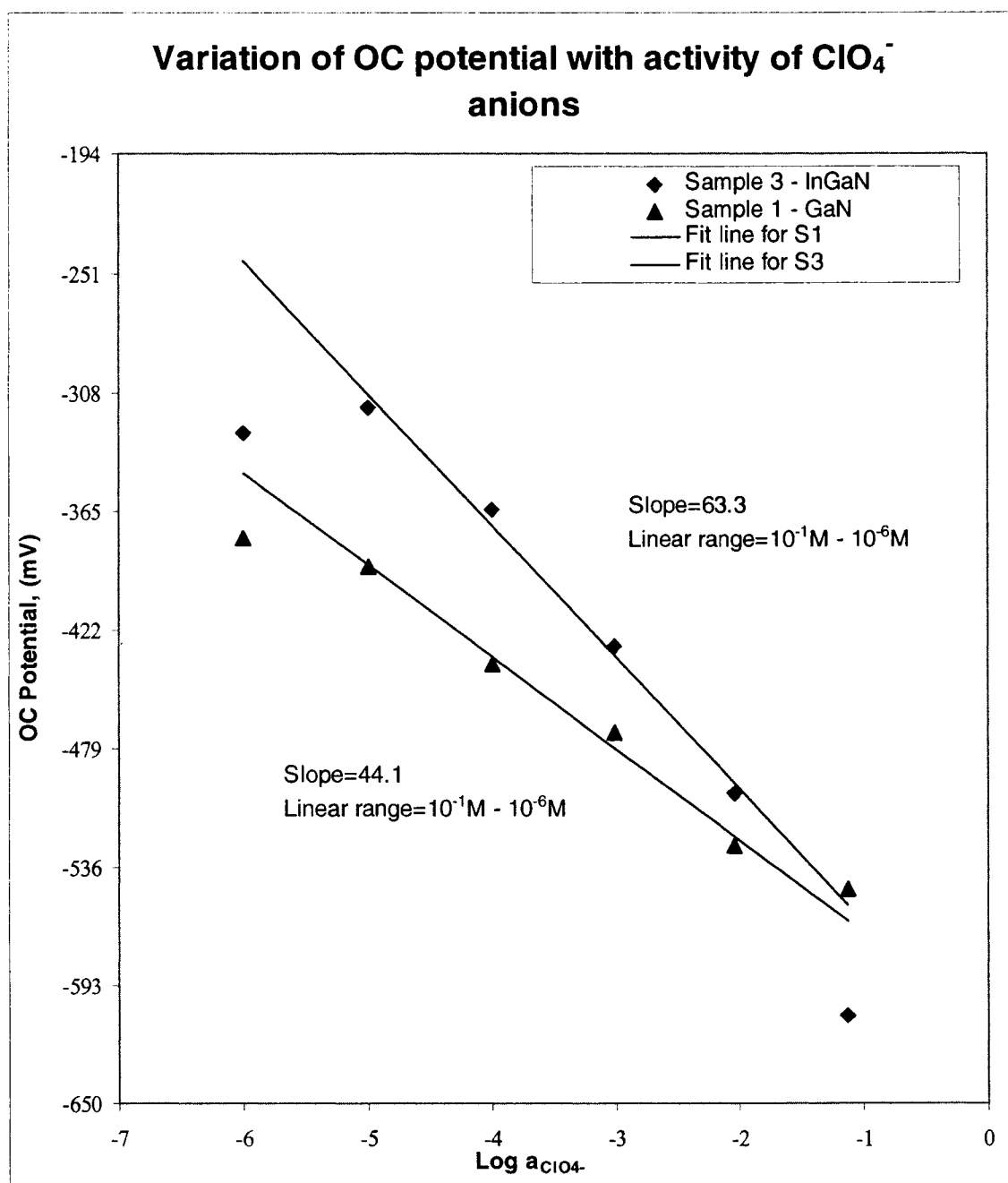
e) KSCN solutions



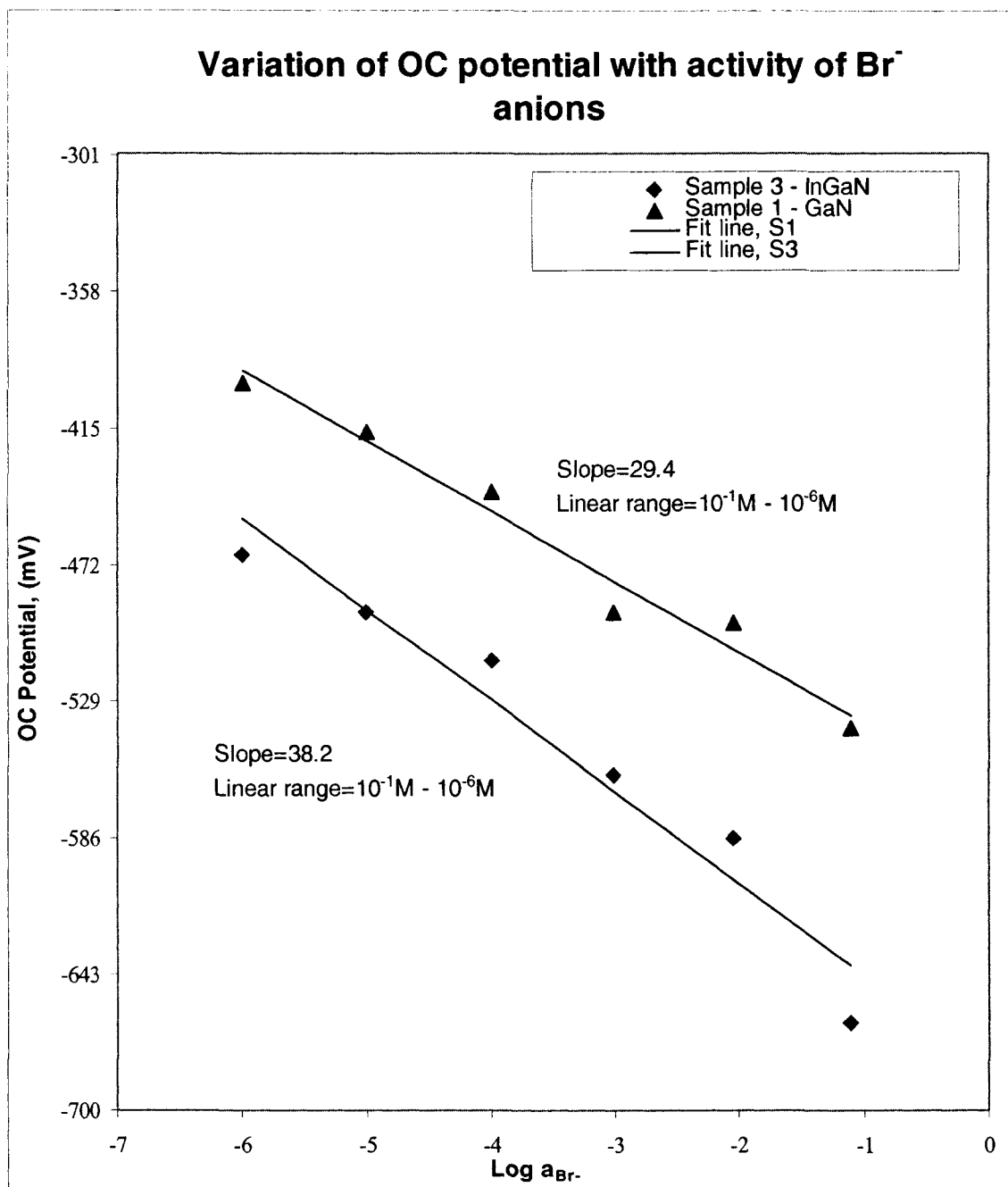
f) CH₃COOK solutions



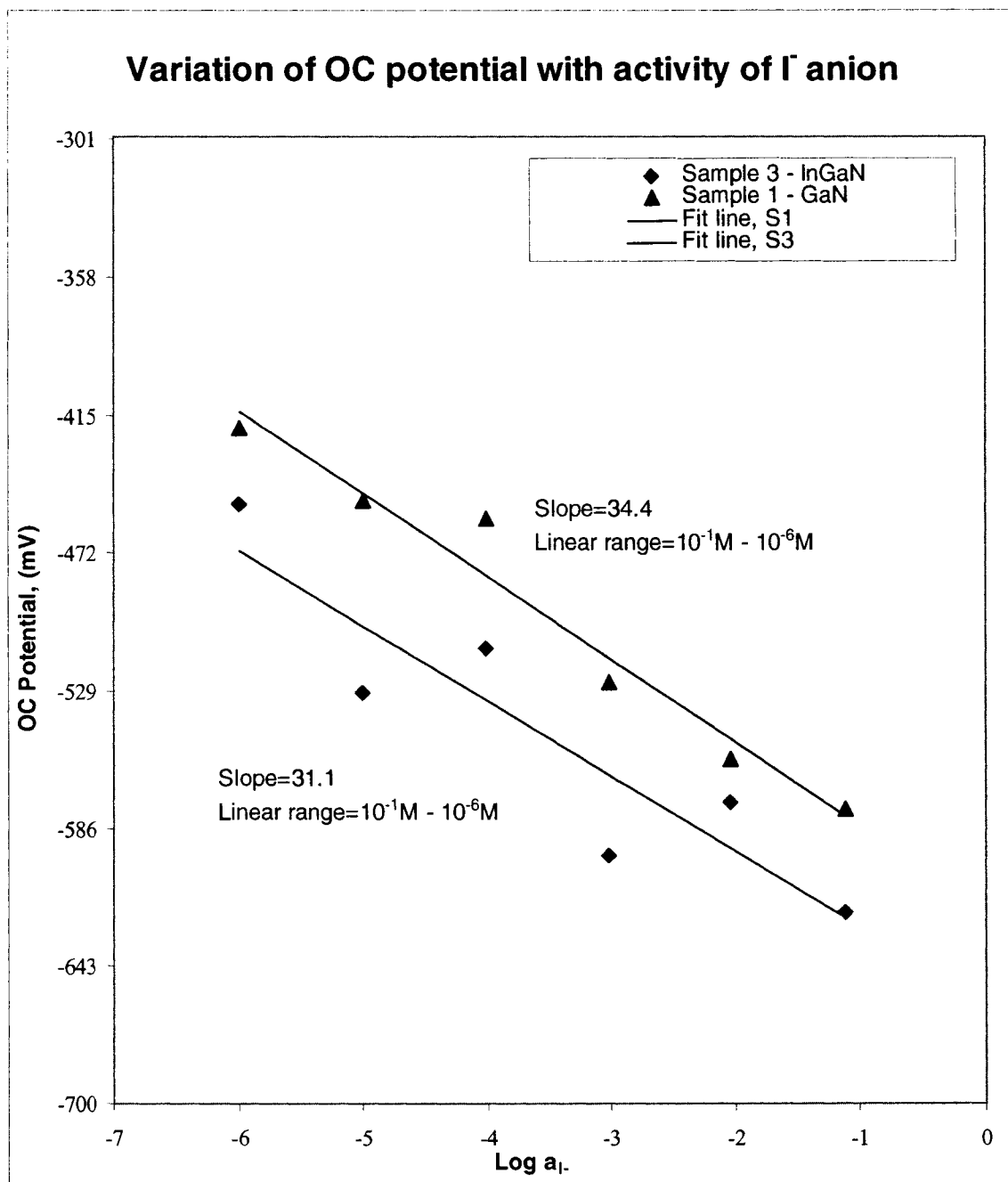
g) KClO_4 solutions



h) KBr solutions



i) KI solutions



For each calibration curve, a linear range of variation of OCP with activity of tested anions was defined. Next, the experimental data falling within the linear range were modeled by fitting a straight line using the method of least squares. The slope of the fit line and the correlation coefficient between the experimental data and the fit line were calculated. The slope of the straight line represents the change of the OCP (mV) per decade of activity change. The obtained

Results & Discussion

slopes were compared to the theoretical slope value for the linear range calculated using the Nikolsky-Eisenman equation (IUPAC, 1994) (See Equation 1.2 of Chapter I):

$$\text{Slope} = \frac{2.303RT}{Z_A F} = \frac{2.303 \times 8.314510 \times 294}{1 \times 96.485309} = 58.3 \text{ mV/decade} \quad (3.1)$$

where

R is the gas constant and is equal to $8.314510 \text{ J K}^{-1} \text{ mol}^{-1}$;

T is the absolute temperature (294 K);

F is the Faraday constant and is equal to $9.6485309 \times 10^4 \text{ C mol}^{-1}$;

Z_A is the charge of the measured anion

The calibration curves obtained for each test anion are discussed below:

- In **KF** solutions (Fig. III.8a), the linear region of the calibration curve for the GaN sample electrode S1 between activities 10^{-3}M and 10^{-4}M , while the linear region of the calibration curve for the InGaN sample electrode S3 extends over the entire range of measured activities ($10^{-1} - 10^{-6}\text{M}$). For the InGaN sample electrode S3, the calculated slope of 61.7mV/decade is very close to the theoretical prediction of 58.3mV/decade . The high correlation coefficient (0.97) between the experimental data and the best-fit line provides additional corroboration that the region of linearity was correctly defined. For the GaN sample electrode S1, however, the calculated slope of 52.6mV/decade is also relatively close to the theoretical value and the correlation coefficient is higher (0.99).
- In **KNO₃** solutions (Fig. III.8b), the linear region of the calibration curve for the GaN sample electrode S1 extends between activities of 10^{-2} and 10^{-4}M and the linear region of the calibration curve for the InGaN sample electrode S3 extends between activities of 10^{-2} and 10^{-6}M . For the InGaN sample electrode S3, the calculated slope of 62.7mV/decade is close to the theoretical value of 58.3mV/decade and the correlation coefficient between the experimental data and the best-fit line is very good (0.99). For the GaN sample electrode S1, the calculated slope of 56.7mV/decade is also close to the theoretical value and the correlation coefficient is good (0.97).
- In **KCl** solutions (Fig. III.8c), the linear region of the calibration curves for both GaN sample electrode S1 and InGaN sample electrode S3 extends between activities 10^{-4}M and 10^{-5}M .

Results & Discussion

For the InGaN sample electrode S3, the calculated slope of 54.2mV/decade is a bit lower than the theoretical prediction of 58.3mV/decade. The correlation coefficient between the experimental data and the best-fit line is good (0.97). For the GaN sample electrode S1, however, the calculated slope of 58.2mV/decade is equal to the theoretical prediction and the correlation coefficient is good (0.98).

- In **HOC₆H₄COONa** solutions (Fig. III.8d), the linear region of the calibration curves for both the InGaN sample electrode S3 and the GaN sample electrode S1 extends between activities 10^{-3} M and 10^{-5} M. For the InGaN sample electrode S3, the calculated slope of 64.9mV/decade is a bit higher than the theoretical prediction of 58.3mV/decade. The correlation coefficient between the experimental data and the best-fit line is good (0.98). For the GaN sample electrode S1, the calculated slope of 52.8mV/decade is also close to the theoretical prediction and the correlation coefficient is very good (0.998).
- In **KSCN** solutions (Fig. III.8e), the linear region of the calibration curves for both GaN sample electrode S1 and InGaN sample electrode S3 extends between activities 10^{-3} M and 10^{-5} M. For the InGaN sample electrode S3, the calculated slope of 63.9mV/decade is slightly higher than the theoretical prediction of 58.3mV/decade. The correlation coefficient between the experimental data and the best-fit line is very good (0.997). For the GaN sample electrode S1 the calculated slope of 51.9mV/decade is also close to the theoretical value and the correlation coefficient is very good (0.998).
- In **CH₃COOK** solutions (Fig. III.8f) no linear region can be defined for the calibration curves of both the GaN sample electrode S1 and the InGaN sample electrode S3. Hence, although the semiconductor electrodes can in theory selectively respond to variations in the activity of the CH₃COO⁻ anions, this response cannot be used for measuring sample solutions with unknown activity of these anions.
- In **KClO₄** solutions (Fig. III.8g), the linear region of the calibration curves for both GaN sample electrode S1 and InGaN sample electrode S3 extends over the entire range of measured activities (10^{-1} - 10^{-6} M). For the InGaN sample electrode S3, the calculated slope of 63.3mV/decade is slightly higher than the theoretical prediction of 58.3mV/decade. The

Results & Discussion

correlation coefficient between the experimental data and the best-fit line is good (0.95). For the GaN sample electrode S1, however, the calculated slope of 44.1mV/decade is much lower than the theoretical value, but the correlation coefficient is very good (0.99).

- In **KBr** solutions (Fig. III.8h), the linear region of the calibration curves for both GaN sample electrode S1 and InGaN sample electrode S3 extends over the entire range of measured activities (10^{-1} - 10^{-6} M). For the InGaN sample electrode S3, the calculated slope of 38.2mV/decade is much lower than the theoretical prediction of 58.3mV/decade. The correlation coefficient between the experimental data and the best-fit line is good (0.97). For the GaN sample electrode S1, the calculated slope of 29.4mV/decade is also much lower than the theoretical, but the correlation coefficient is good (0.99).
- In **KI** solutions (Fig. III.8i), the linear region of the calibration curves for both GaN sample electrode S1 and InGaN sample electrode S3 extends over the entire range of measured activities (10^{-1} - 10^{-6} M). For the InGaN sample electrode S3, the calculated slope of 31.1mV/decade is much lower than the theoretical prediction of 58.3mV/decade. The correlation coefficient between the experimental data and the best-fit line is 0.92. For the GaN sample electrode S1, the calculated slope of 34.4mV/decade is also much lower than the theoretical value. The correlation coefficient is 0.98.

A summary of the calibration curves evaluation is presented in Table III.6.

Table III.6 Summary of the Calibration Curves evaluation

Salt	GaN sample electrode, S1				InGaN sample electrode, S3			
	Linear Region		Slope	Correlation Coefficient	Linear Region		Slope	Correlation Coefficient
	From	To			From	To		
KF	10 ⁻¹ M	10 ⁻⁶ M	-33.1	0.9885	10 ⁻¹ M	10 ⁻⁶ M	-61.7	0.9673
KNO ₃	10 ⁻¹ M	10 ⁻⁶ M	-36.2	0.9706	10 ⁻² M	10 ⁻⁶ M	-62.7	0.9894
KCl	10 ⁻¹ M	10 ⁻⁵ M	-32.8	0.9751	10 ⁻¹ M	10 ⁻⁵ M	-42.1	0.9738
HOC ₆ H ₄ COONa	10 ⁻³ M	10 ⁻⁵ M	-52.8	0.9980	10 ⁻¹ M	10 ⁻⁵ M	-59.2	0.9585
KSCN	10 ⁻³ M	10 ⁻⁵ M	-51.9	0.9975	10 ⁻² M	10 ⁻⁵ M	-60.6	0.9879
CH ₃ COOK	NA	NA	-	-	NA	NA	-	-
KClO ₄	10 ⁻¹ M	10 ⁻⁶ M	-37.3	0.9899	10 ⁻¹ M	10 ⁻⁶ M	-57.6	0.9160
KBr	10 ⁻¹ M	10 ⁻⁶ M	-35.9	0.9966	10 ⁻¹ M	10 ⁻⁶ M	-38.2	0.9726
KI	10 ⁻² M	10 ⁻⁶ M	-35.4	0.9591	10 ⁻¹ M	10 ⁻⁶ M	-31.1	0.9167

The results of the GaN electrode calibration measurements have been compared with the results reported by Chaniotakis et al. (2004), who performed similar calibration experiments with GaN electrodes. The slopes of the GaN electrode calibration curves calculated from the graphs presented in the paper by Chaniotakis et al. (2004) vary between 39.2 and 69.5mV/decade, and the regions of linearity extend between 10⁻² and 10⁻⁵M in KF, KCl, KNO₃, KSCN and KClO₄ solutions. Thus, the slopes of the GaN sample electrode S1 are very similar to the results reported by Chaniotakis et al. (2004). Table III.6, shows that the slopes of the GaN sample electrode S1 and the InGaN sample electrode S3 calibration curves are also close to the theoretical value of 58.3mV/decade in most of the investigated electrolyte solutions, as expected from the Nikolsky-Eisenman equation. Exceptions occur for the GaN sample electrode S1 in KClO₄, KBr and KI electrolytes and for the InGaN sample electrode S3 in KBr and KI electrolytes. In these electrolytes, the electrodes response is not consistent and does not follow the expected S-shape variation of OCP with activity of anions, which is typical for the other solutions. This effect may be caused by a strong interaction between species in the solution and the electrode material, causing significant deviation from the Nerstian behaviour observed in the other electrolytes. It is also apparent that, while the slopes of calibration curves for the GaN sample electrode S1 are consistent with the ones obtained by Chaniotakis et al. (2004), the regions of linearity in the present study are more variable and in some cases narrower than in

Results & Discussion

Chaniotakis et al. (2004) . The shorter regions of linearity for the GaN sample electrode S1 may be due to:

- Non-homogeneity of the electrode sensing element. Both the GaN sample electrode S1 and the InGaN sample electrode S3 utilized in the current project have a mixed polarity surface, while Chaniotakis et al. (2004) claim that their GaN electrodes have a homogeneous Ga-face surface.
- Contamination of the electrode's sensing element. Chaniotakis et al. (2004) emphasised that the surface of the GaN electrode should remain clean down to atomic level to achieve the optimum sensitivity of the electrode to tested anions, but they did not describe the cleaning method utilized in their research. The cleaning procedure used in the current project involved rinsing the electrodes with NPW before each measurement and keeping them immersed in NPW when not in use. However, this might not have been sufficient to ensure a completely clean electrode surface before each experiment.

Table III.7 compares the OCP values measured for the GaN sample electrode S1 in electrolytes of various concentrations with the OCP values reported by Chaniotakis et al. (2004). The experiments described in Chaniotakis et al (2004) were performed versus an Ag/AgCl reference electrode, while the experiments in the current project were performed versus a SCE. Thus, for the purpose of accurate comparison, the OCPs reported by Chaniotakis et al. (2004) have been adjusted to SCE potentials by subtracting 14mV from their reported values. Fig. III.9 shows plots of OCPs measured for the GaN sample electrode S1 versus the adjusted OCPs reported by Chaniotakis et al. (2004).

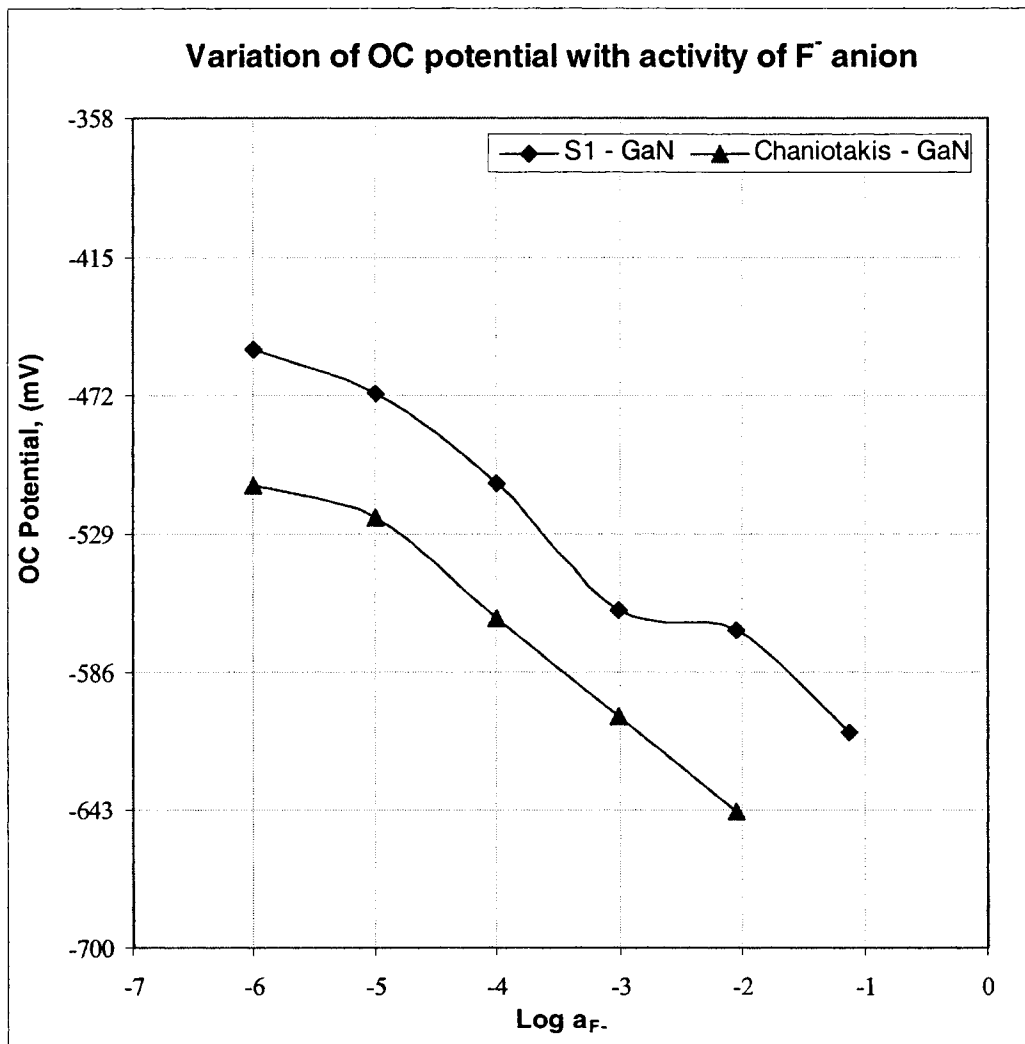
Results & Discussion

Table III.7 Variation of OC potential with concentration

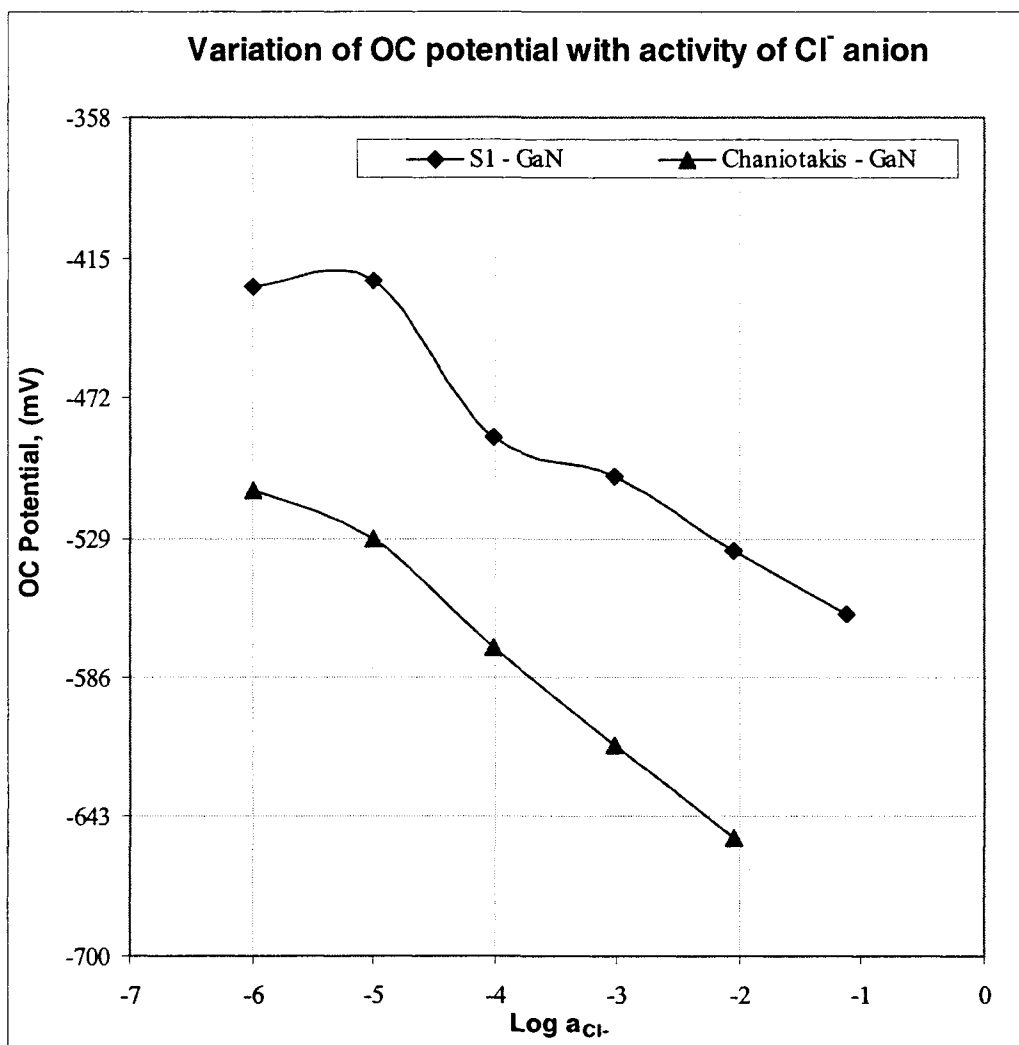
Salt	Conc. (M)	Activity (M)	Log [a]	Measured OC potential (mV)			Absolute Variation between S1 and Chaniotakis et al (mV)	Relative Variation between S1 and Chaniotakis et al (%)
				S1 (GaN) vs SCE	Chaniotakis et al (GaN) vs SCE	Chaniotakis et al (GaN) vs Ag/AgCl		
KF	1.00E-01	7.62E-02	-1	-611				
	1.00E-02	8.99E-03	-2	-569	-644	-630	75	12
	1.00E-03	9.64E-04	-3	-560	-604	-590	44	7
	1.00E-04	9.88E-05	-4	-508	-564	-550	56	10
	1.00E-05	9.96E-06	-5	-471	-522	-508	51	10
	1.00E-06	9.99E-07	-6	-453	-509	-495	56	11
KNO ₃	1.00E-01	7.55E-02	-1	-634				
	1.00E-02	8.97E-03	-2	-608	-689	-675	81	12
	1.00E-03	9.64E-04	-3	-569	-644	-630	75	12
	1.00E-04	9.88E-05	-4	-497	-592	-578	95	16
	1.00E-05	9.96E-06	-5	-488	-531	-517	43	8
	1.00E-06	9.99E-07	-6	-472	-509	-495	37	7
KCl	1.00E-01	7.60E-02	-1	-560				
	1.00E-02	8.98E-03	-2	-534	-652	-638	118	18
	1.00E-03	9.64E-04	-3	-504	-614	-600	110	18
	1.00E-04	9.88E-05	-4	-488	-574	-560	86	15
	1.00E-05	9.96E-06	-5	-424	-529	-515	105	20
	1.00E-06	9.99E-07	-6	-427	-509	-495	82	16
KSCN	1.00E-01	7.81E-02	-1	-541				
	1.00E-02	9.02E-03	-2	-525	-734	-720	209	28
	1.00E-03	9.65E-04	-3	-510	-659	-645	149	23
	1.00E-04	9.88E-05	-4	-465	-589	-575	124	21
	1.00E-05	9.96E-06	-5	-407	-529	-515	122	23
	1.00E-06	9.99E-07	-6	-387	-509	-495	122	24
KClO ₄	1.00E-01	7.44E-02	-1	-546				
	1.00E-02	8.95E-03	-2	-526	-594	-580	68	11
	1.00E-03	9.64E-04	-3	-471	-546	-532	75	14
	1.00E-04	9.88E-05	-4	-438	-514	-500	76	15
	1.00E-05	9.96E-06	-5	-392	-476	-462	84	18
	1.00E-06	9.99E-07	-6	-378	-454	-440	76	17

Fig. III.9 Comparison between measured OCPs for GaN sample electrode S1 and adjusted OCPs reported by Chaniotakis et al. (2004)

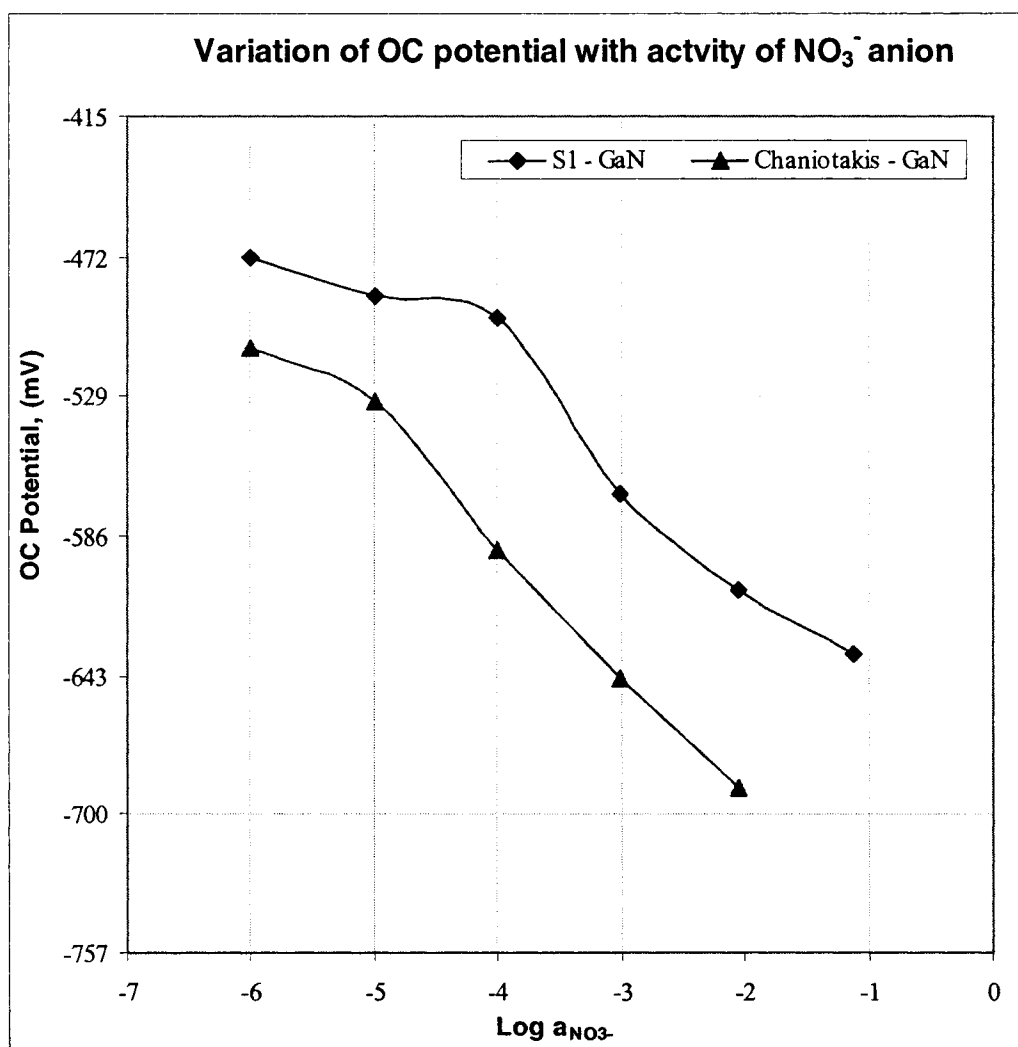
a) KF solutions



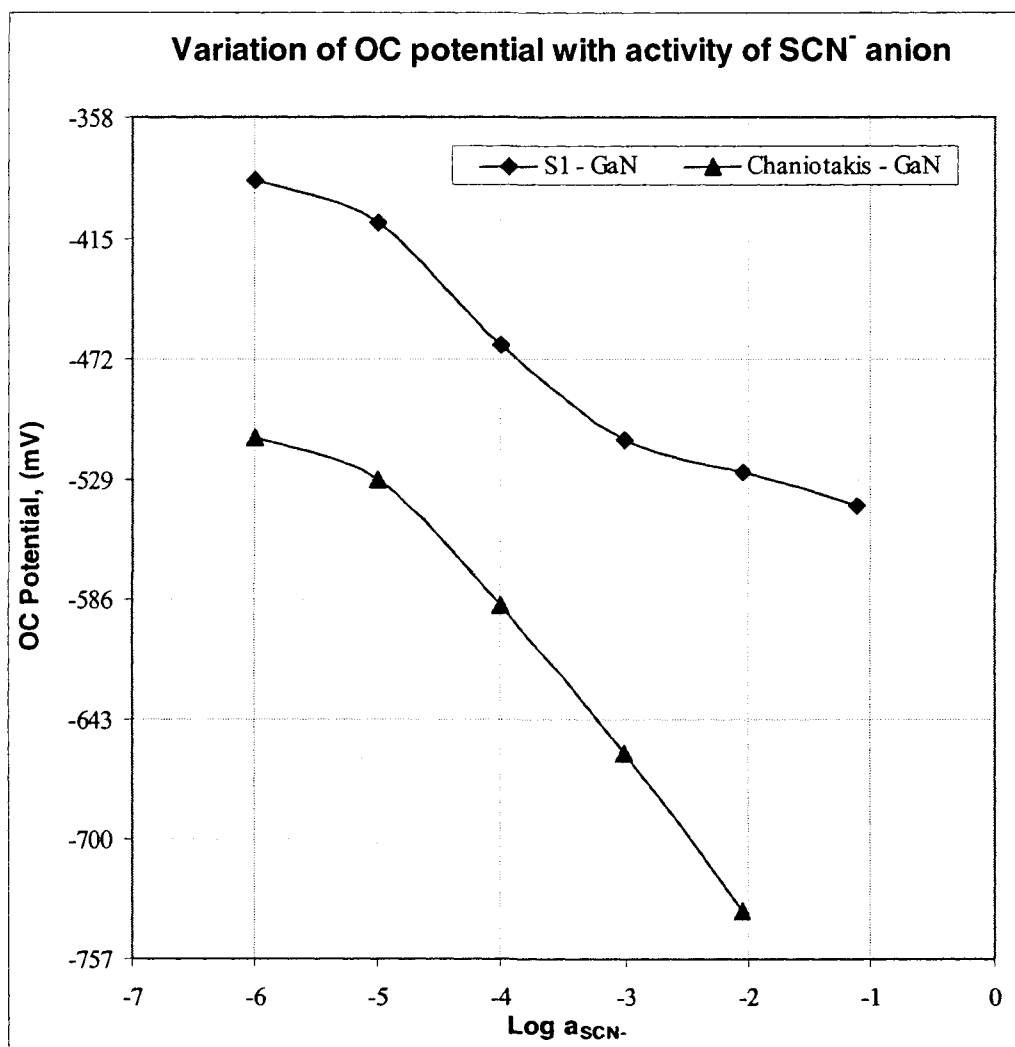
b) KCl solutions

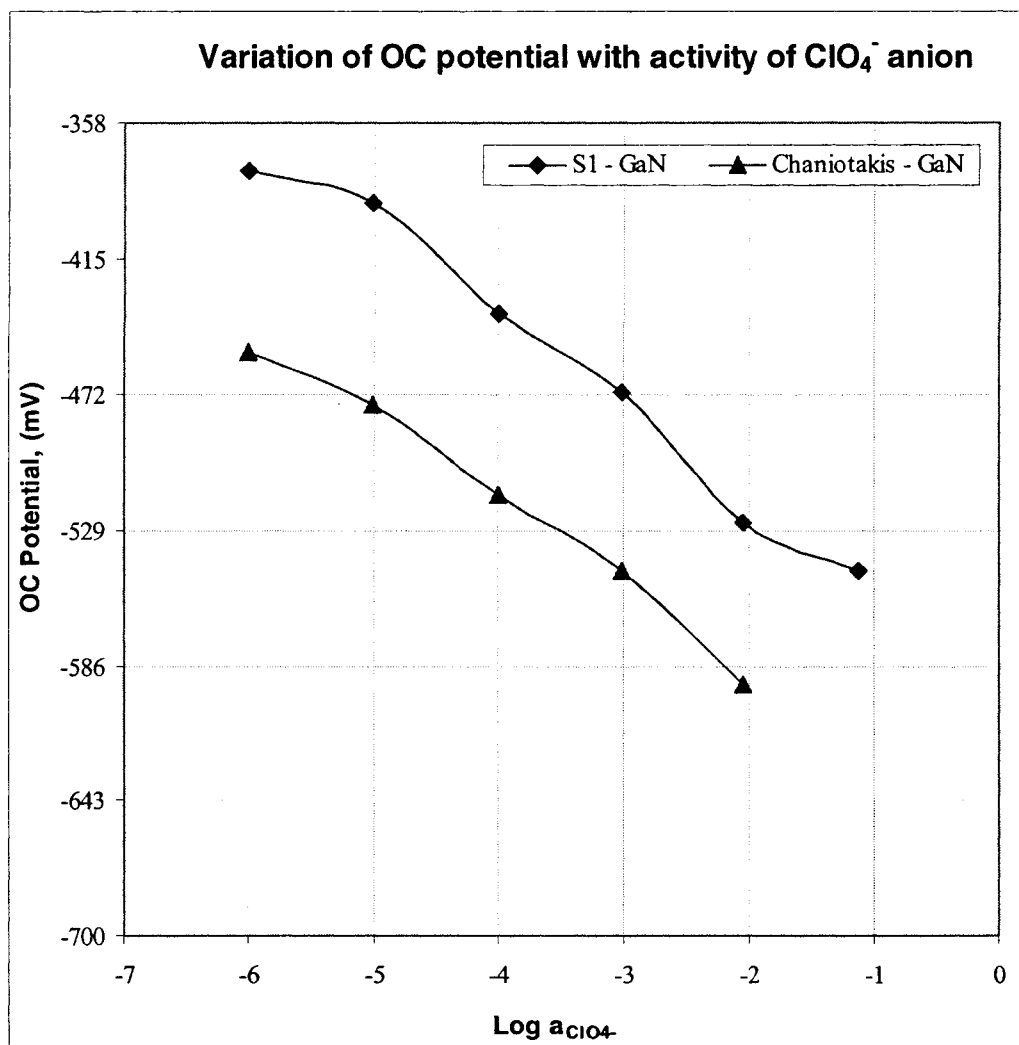


c) KNO_3 solutions



d) KSCN solutions



e) KClO_4 solutions

The plots presented on Fig. III.9 demonstrate that the measured OCPs for GaN sample electrode S1 follow the same pattern of variation with anion activity as the OCPs for the GaN electrodes tested by Chaniotakis et al. There are differences ranging from 44 to 209mV in actual OC potential values between the two studies, which represent a relative percentage of variation between 7% and 28%. Such differences can be attributed to the mixed polarity of the GaN thin film, utilized for the fabrication of GaN electrodes in the project.

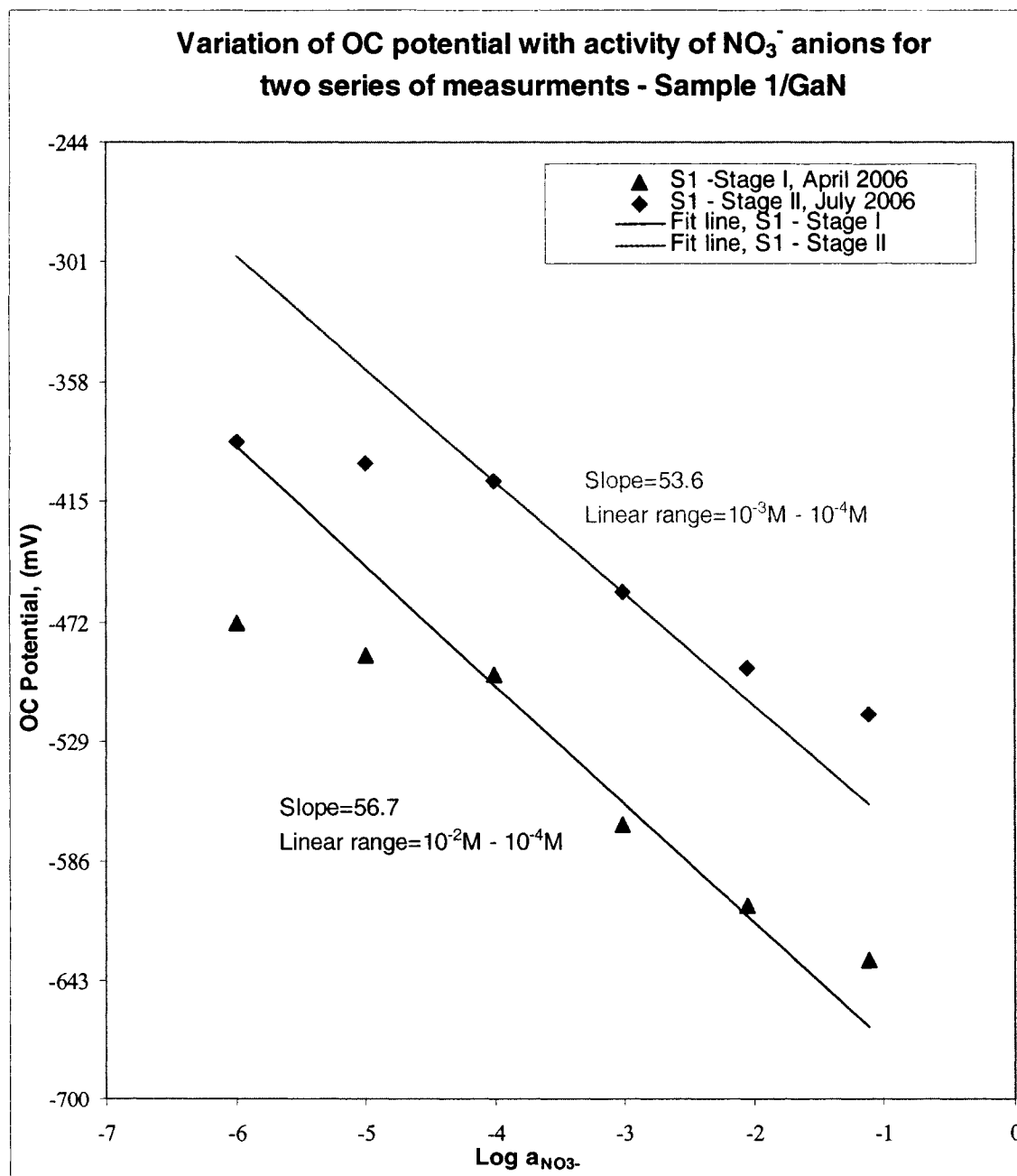
III.5. Reproducibility of Results

The reproducibility of OCP measurements was investigated by repeatedly measuring the OCP potentials of both GaN sample electrode S1 and InGaN sample electrode S3 in KNO_3 , KBr and

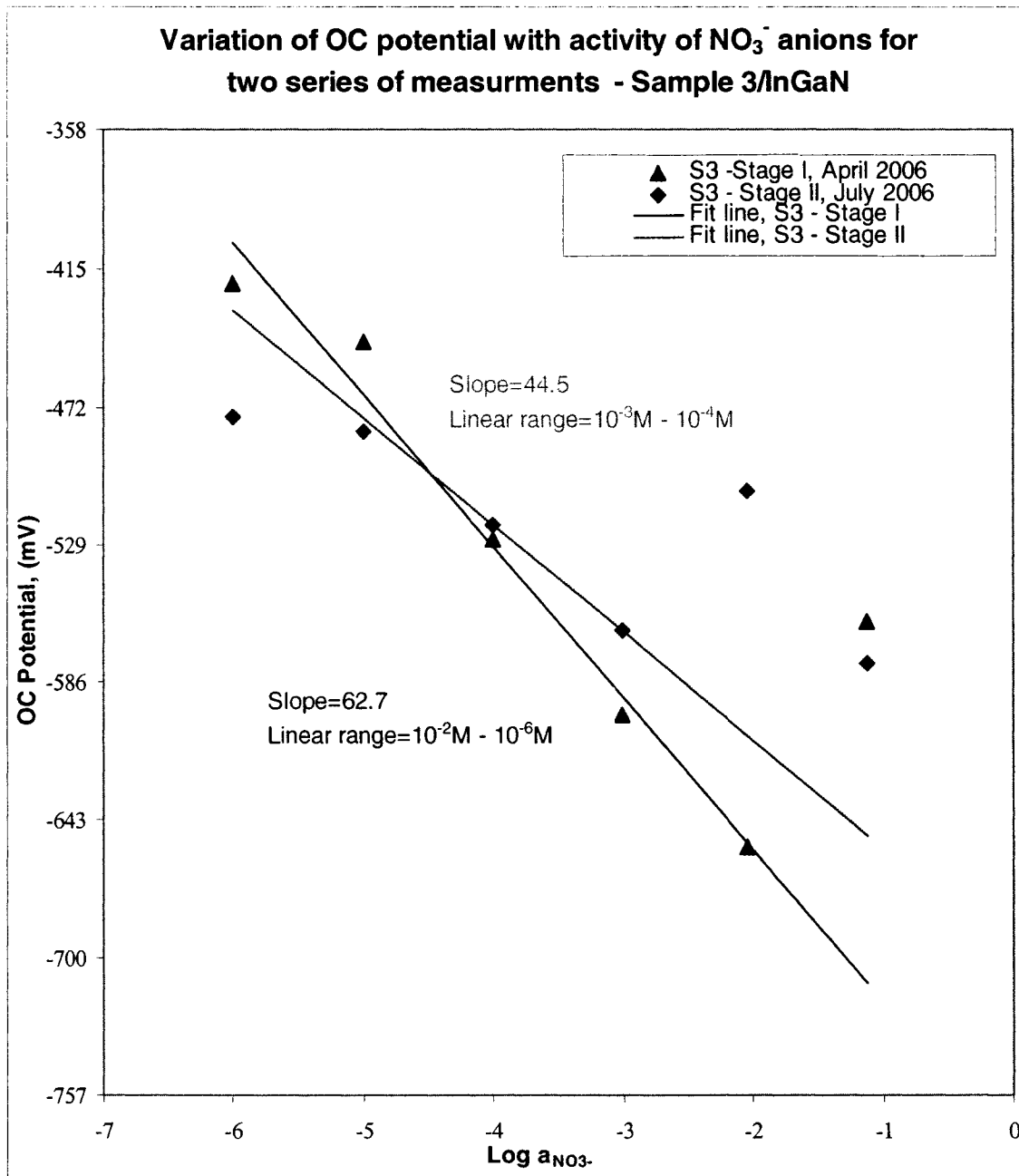
Results & Discussion

KI solutions with concentrations ranging from 10^{-6}M to 10^{-1}M over a period of three months. The results of these measurements are presented on Fig. III.10.

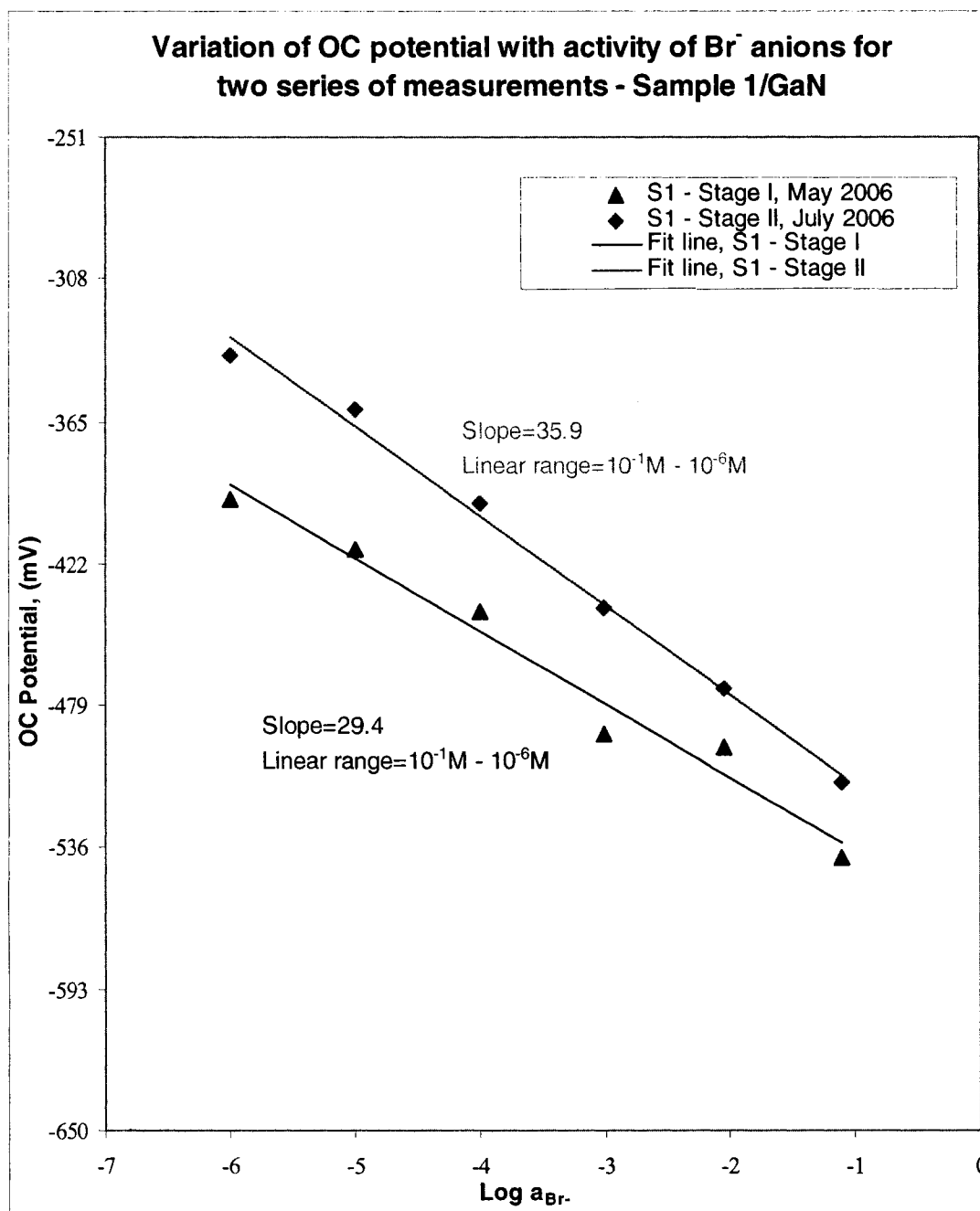
Fig. III.10 Reproducibility of OCP measurements in various salt solutions
a) GaN/ S1 in KNO_3 solutions



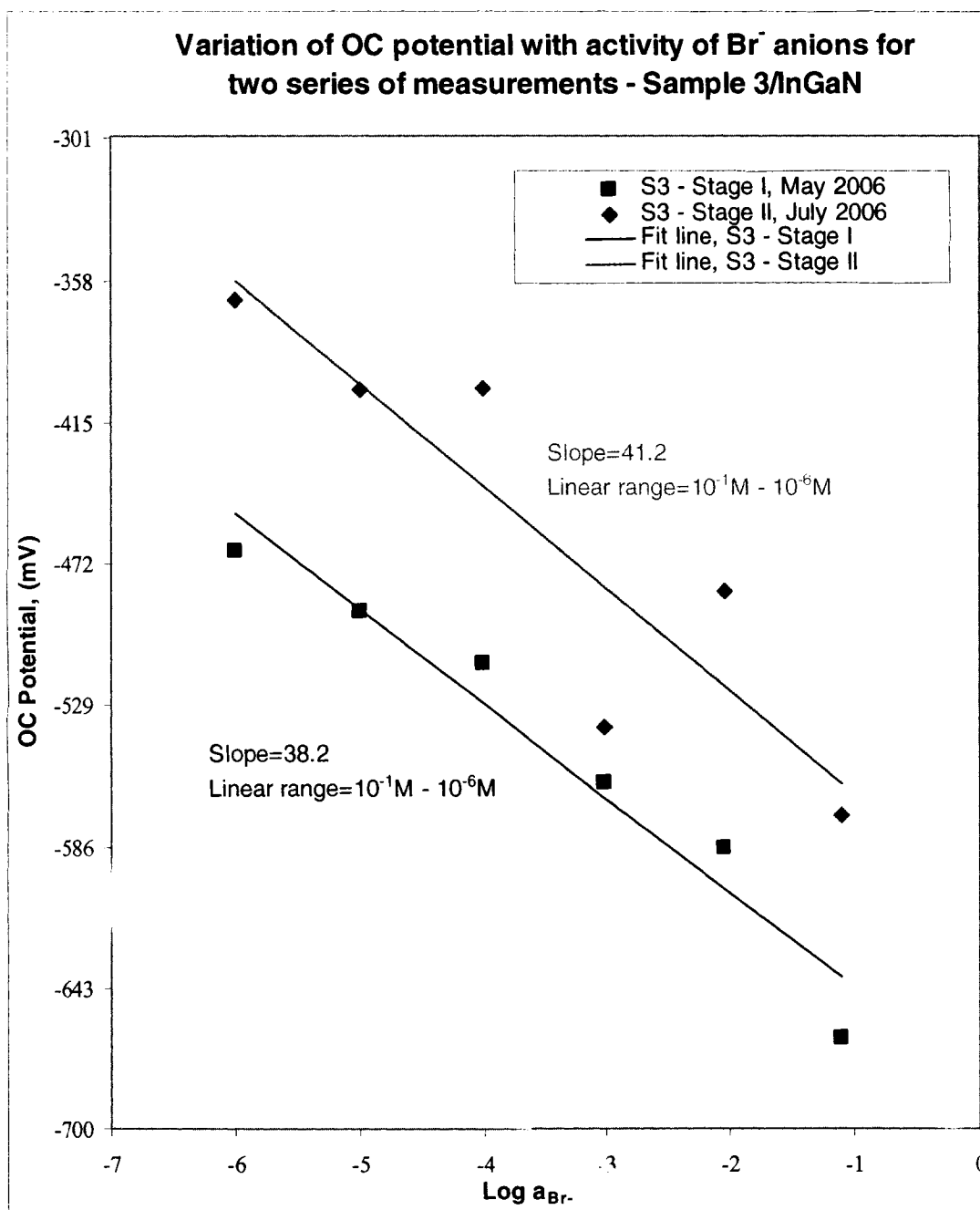
b) InGaN/ S3 in KNO₃ solutions



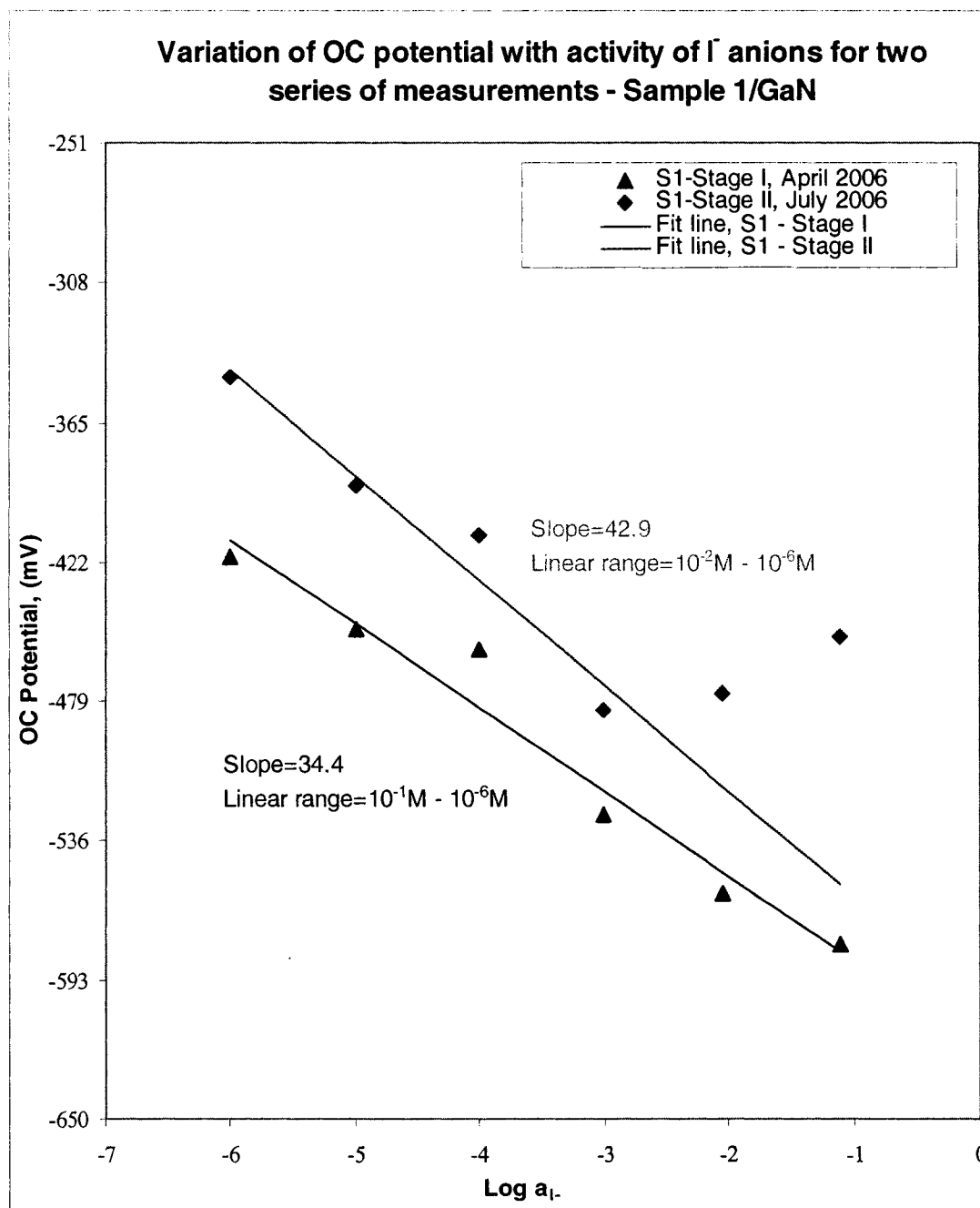
c) GaN/ S1 in KBr solutions



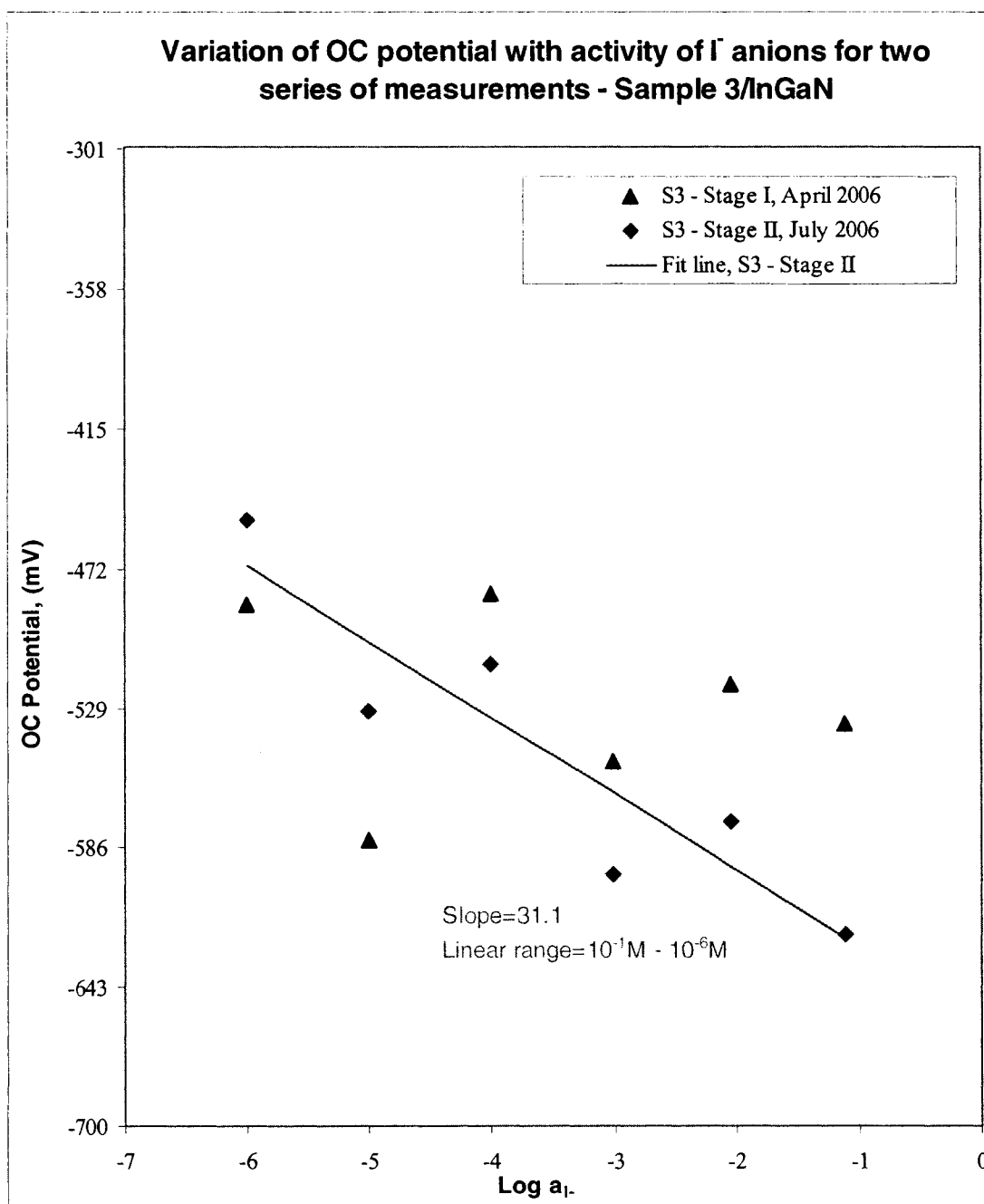
d) InGaN/ S3 in KBr solutions



e) GaN/ S1 in KI solutions



f) InGaN/ S3 in KI solutions



In KNO_3 solutions of different concentrations (Fig. III.10a and b), the results from the multiple OCP measurements over time show the following:

- For GaN sample electrode S1 (Fig. III.10a):
 - The slope of the electrode response curve during the two series of measurements remained almost constant (56.7mV/decade during first series of measurements versus

Results & Discussion

53.6mV/decade during the second series of measurements) and close to the theoretical value of 58.3mV/decade.

- The actual value of the measured OCPs in millivolts drifts downwards by an average value of 102mV.
- For the InGaN sample electrode S3 (Fig. III.10b):
 - The slope of the electrode response curve dropped down from 62.7mV/decade during the first series of measurements to 44.5mV/decade during the second series of measurements. The linear region narrowed down from 4 decades of activities to one decade of activities.

In **KBr** solutions with different concentrations (Fig. III.10c and d), the results from the multiple OCP measurements over time show the following:

- For GaN sample electrode S1 (Fig. III.10c):
 - The slope of the electrode response curve during the two series of measurements remains almost constant (29.4mV/decade during first series of measurements versus 35.9mV/decade during the second series of measurements) but still lower than the theoretical value of 58.3mV/decade.
 - The actual value of the OCP in millivolts drifts downwards by an average value of about 43mV.
- For the InGaN sample electrode S3 (Fig. III.10d):
 - The slope of the electrode response curve during the two series of measurements remains almost constant (38.2mV/decade during first series of measurements versus 41.2mV/decade during the second series of measurements) but lower than the theoretical value of 58.3mV/decade.
 - The actual value of the measured OCPs in millivolts drifts downwards by an average value of 86mV.

Results & Discussion

In **KI** solutions with different concentrations (Fig. III.10e and f), the results from the multiple OCP measurements over time show the following:

- For GaN sample electrode S1 (Fig. III.10e):
 - The slope of the electrode response curve during the two series of measurements remains similar (34.4mV/decade during first series of measurements versus 42.9mV/decade during the second series of measurements) but lower than the theoretical value of 58.3mV/decade.
 - The actual value of the measured OCPs in millivolts drifts downwards by an average value of 60mV.
- For the InGaN sample electrode S3 (Fig. III.10f):
 - The electrode response during both series of measurement is inconsistent and lacks the S-shape typical of ion selective electrodes. No acceptable straight line fit of the experimental data is possible for the first series of measurements and consequently, no linear range or slope of the electrode response curve can be determined. For the second series of measurements a straight-line fitting is possible, but the overall electrode potential drift cannot be evaluated.

In summary, the GaN sample electrode S1 exhibits a general electrode drift downwards from more negative to less negative values over time. This drift reaches a maximum value of approximately 102mV for KNO₃ solutions. Taking into account that the time between the two series of measurements was about 2 months (60days), this produces a maximum average electrode drift of 1.7mV per day. Given that the average drift values of commercial ISEs is about 1mV/day (NICO 2000 Ltd., 2005), it can be concluded that, under the described experimental conditions, the electrode drift is within acceptable limits. The possible causes of electrode drift are as follows:

- Hysteresis effects caused by constantly removing and immersing the sample electrodes in different solutions. These effects were enhanced by the fact that in between the two series of measurements in KNO₃ solutions, the electrodes were used to measure OCPs in solutions containing anions with stronger adsorption potential (i.e., KI and KBr).

- The GaN sample electrode, S1 was subjected to a series of potentiostatic experiments, during which an external potential was imposed on the working electrode. This might have altered the surface composition of the sensing element and decreased its adsorption capacity.
- Although the SCE reference electrode has a stable potential over time, some of the observed drift may be attributed to other potential changes in other parts of the measuring system, i.e. variations in the liquid junction potentials or variations during re-equilibration of the electrochemical system.

The response of the InGaN sample electrode S3, however, demonstrates a lower reproducibility in the investigated three test solutions, which may be caused by the fact that the readings of the electrode's OCP in some solutions might have been taken before the electrochemical system has attained equilibrium.

III.6. Investigation of pH Response of the Sample Electrodes

The pH responses of the GaN sample electrode S1 and InGaN sample electrode S3 were investigated over the pH range between pH=1.34 and pH=12.80. The obtained results were compared with the results from Alifragis et al. (2005), whose OCP measurements were used in the comparison of the electrodes calibration curves (See I.4). Again, for the purpose of accurate comparison, the OCPs reported by Alifragis et al have been adjusted to SCE potentials by subtracting 14mV from the reported values. Additionally, the pH values at which the measurements were made were selected to be as close as possible to the values of pH at which Alifragis et al (2005) performed their measurements. The results of the pH response investigation for GaN sample electrode S1 and InGaN sample electrode S3 are presented on Fig. III.11. The same graph contains the adjusted pH response of GaN electrodes, reported by Alifragis et al. (2005).

Fig. III.11 Variation of OC potential with pH for GaN sample electrode S1, InGaN sample electrode S3 and GaN electrodes, utilized by Alifragis et al. (2005)

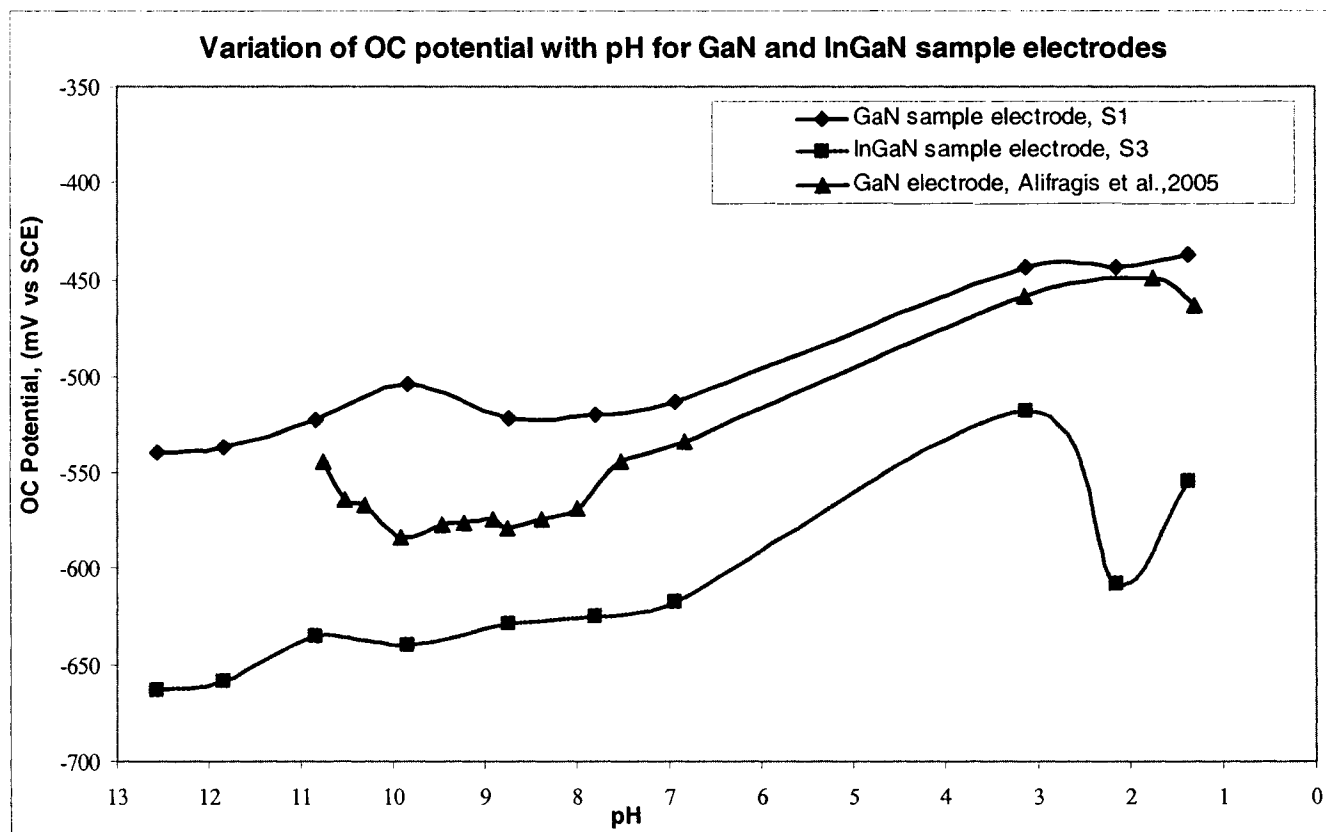


Fig. III.11 shows that for the GaN sample electrode S1 and for the InGaN sample electrode S3, the OCP becomes less negative with decreasing pH. This result is consistent with the pH response of GaN electrodes reported by Alifragis et al (2005), with the only difference being that the measured potentials for the GaN sample electrode S1 differ from the ones reported by Alifragis et al (2005) by 10mV to 60mV. Similarly to the calibration curves measurements, such a difference can be attributed to the variations in the surface polarity (Ga-face for Alifragis et al (2005) versus mixed surface polarity for the GaN sample electrode S1).

Over the pH range pH=12.80-3.13, the InGaN sample electrode S3 response follows similar pattern as the one described for the GaN sample electrode S1. The measured OCPs, though, are some 100mV more negative than those for GaN.

Alifragis et al. (2005) determined that the observed pH sensitivity of the GaN electrodes is due to the selective interaction of the positively charged GaN surface with the hydroxide ions from the

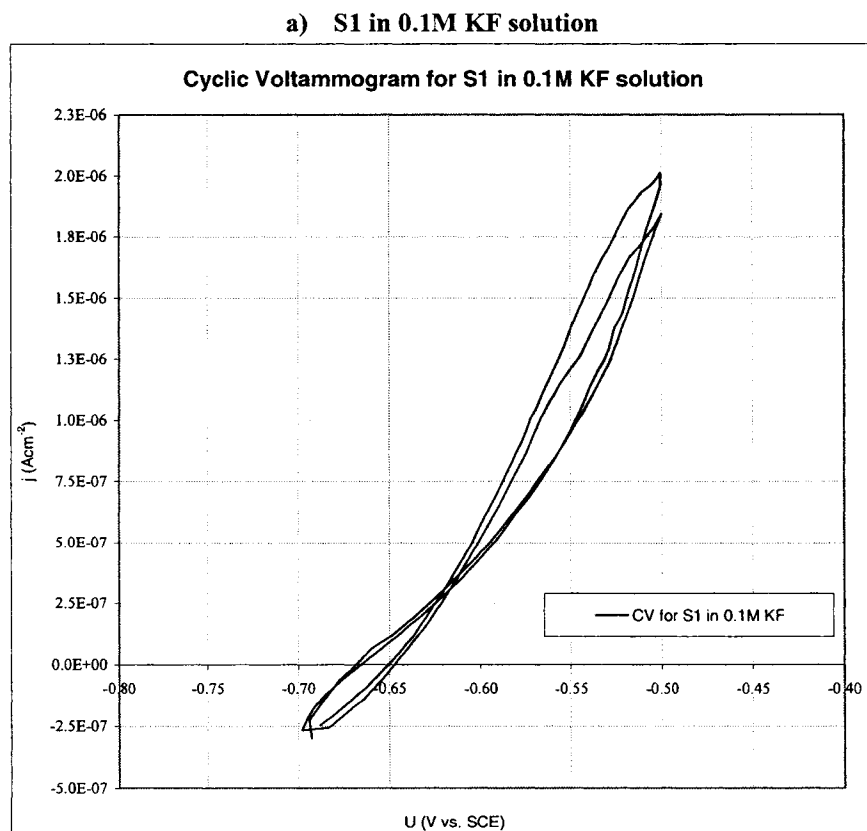
Results & Discussion

solution (Alifragis et al., 2005). At high pH values (pH=12.8-7.0), the activity of the OH⁻ anions is high, and all the available Ga or InGa bonds on the outer surface of the GaN and InGaN electrodes are presumably saturated, forming a N_{Ga}-OH or N_{In}-OH bonds. Within this pH range, the rate of OCP variation with pH is very small. At pH values in the range pH=7.0-3.0, the OH⁻ anions adsorbed on the surface of the semiconductor material begin to desorb, causing a shift of the measured OCP to less negative values. The rate of desorption increases with decreasing pH, thus leaving more adsorption sites on the surface of the GaN and InGaN electrodes unoccupied. At about pH=3.0, the desorption is complete and the electrode potential stabilizes again.

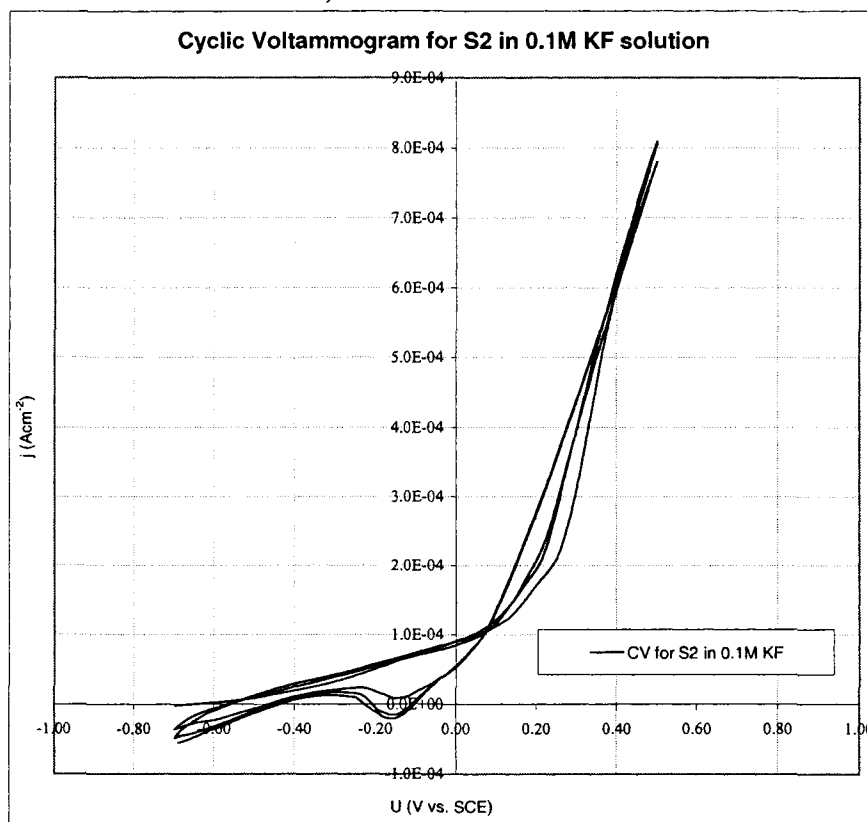
III.7. Cyclic Voltammetry

Cyclic Voltammetry (CV) experiments were performed with GaN sample electrodes S1 and S2 to obtain more information about the charge transfer reactions occurring at the semiconductor/electrolyte interface. Fig. III.12 presents the results of the CV experiments in various salt solutions.

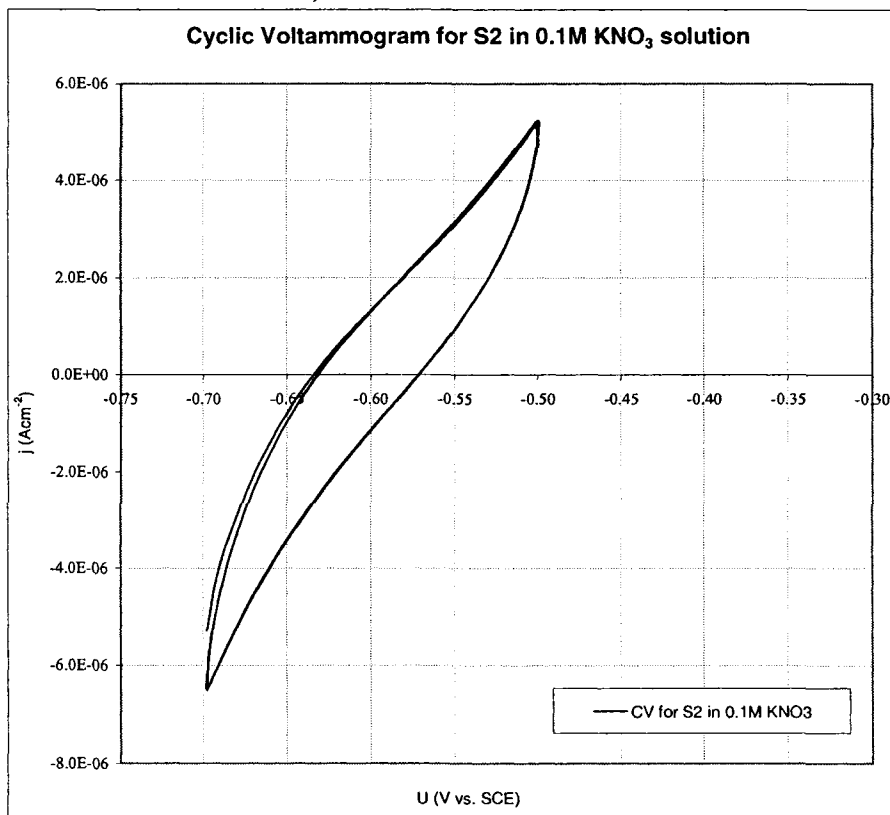
Fig. III.12 Cyclic Voltammograms for GaN sample electrodes in 0.1M salt solutions



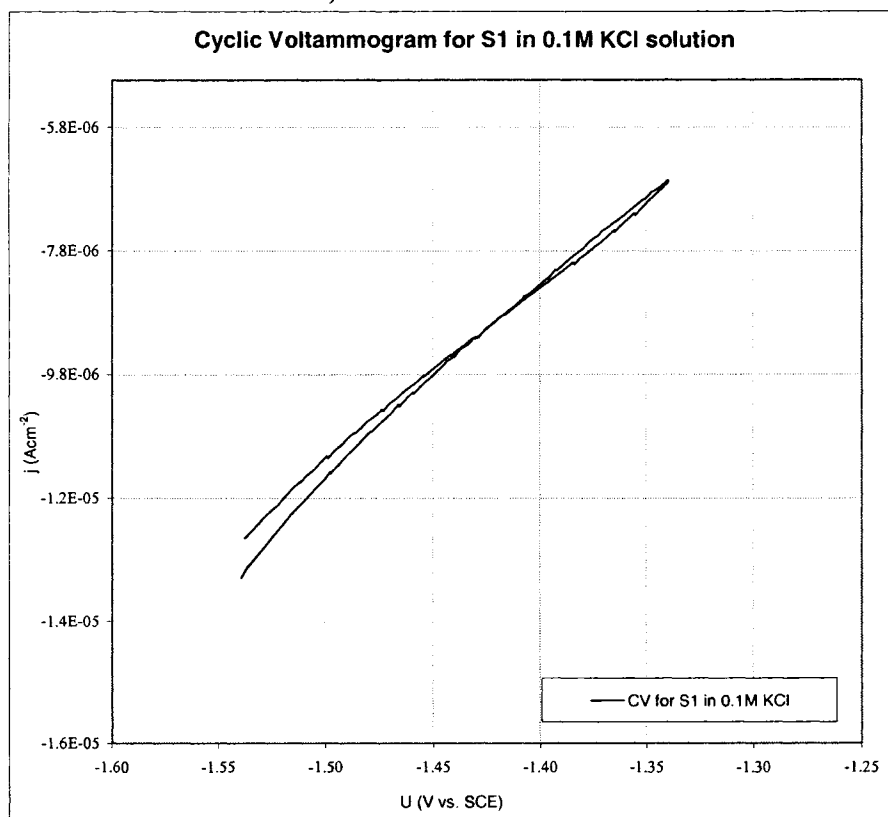
b) S2 in 0.1M KF solution



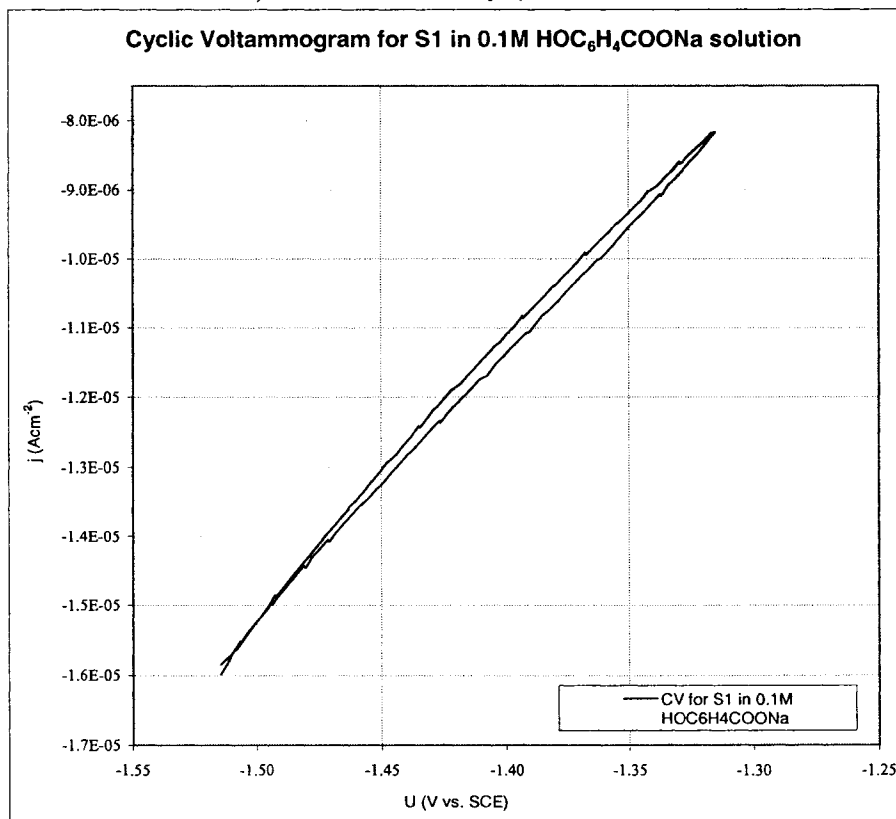
c) S2 in 0.1M KNO₃ solution



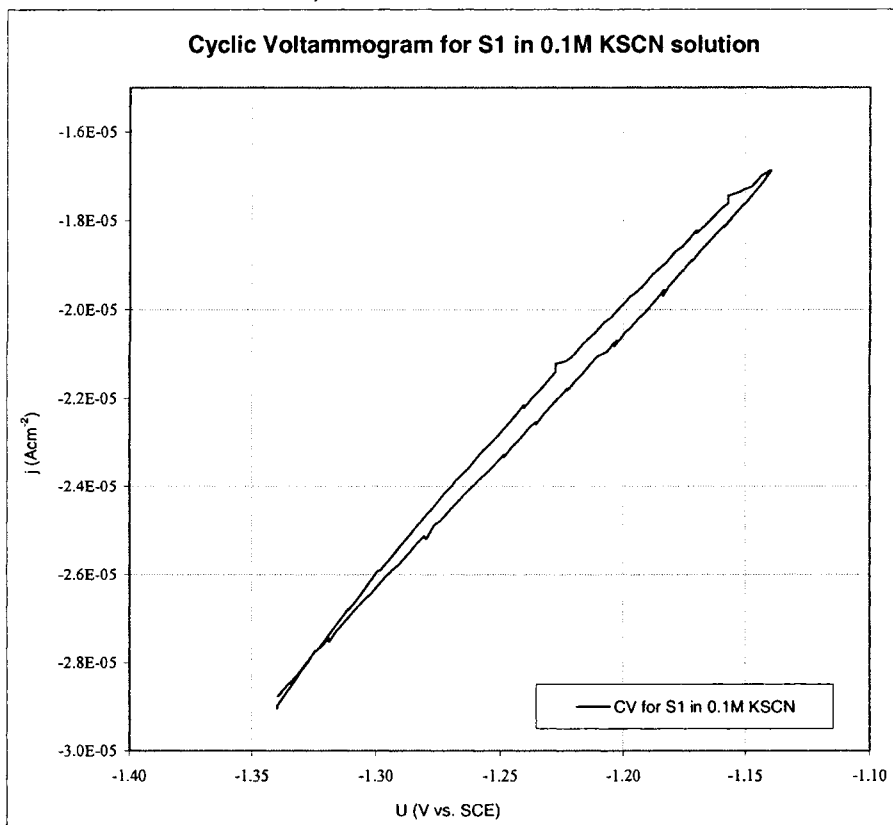
d) S1 in 0.1M KCl solution



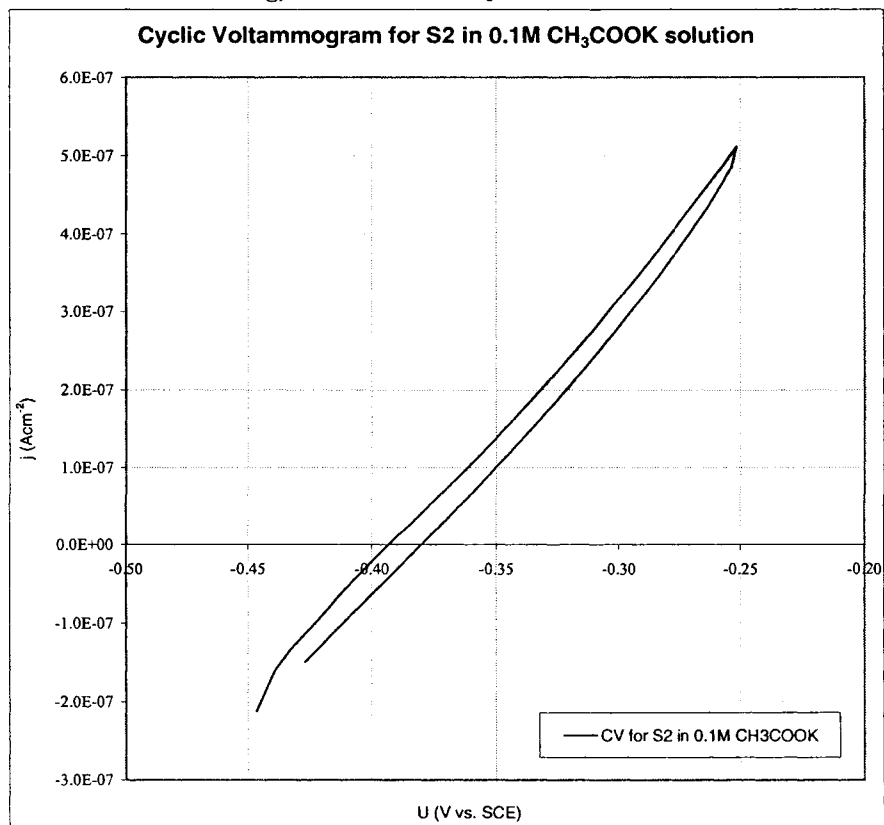
e) S1 in 0.1M $\text{HOC}_6\text{H}_4\text{COONa}$ solution



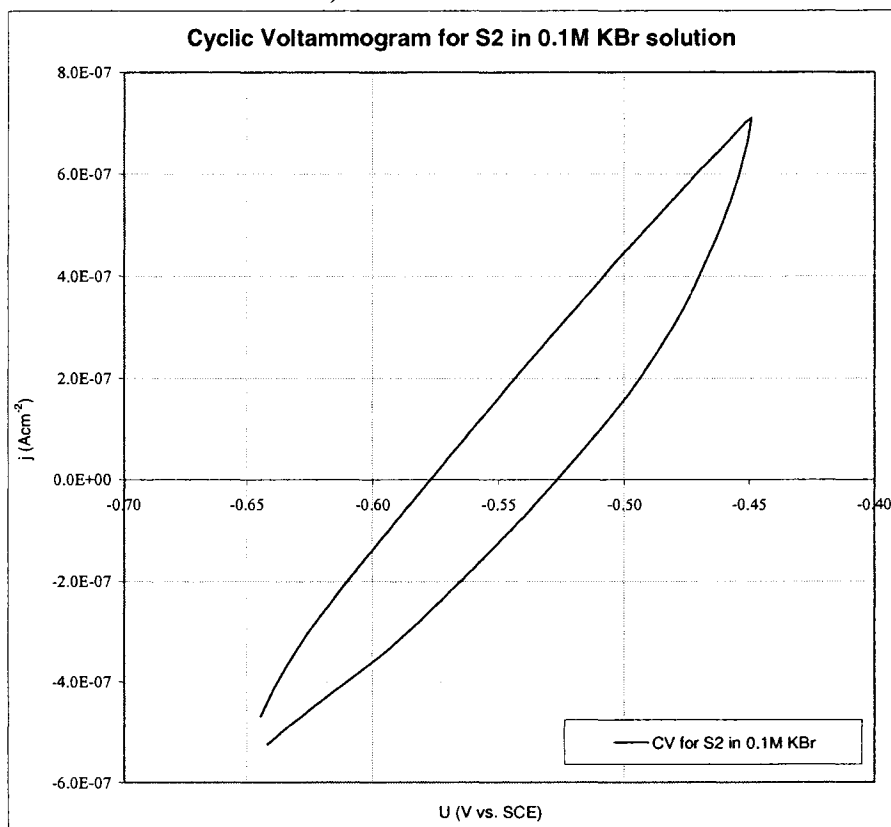
f) S1 in 0.1M KSCN solution



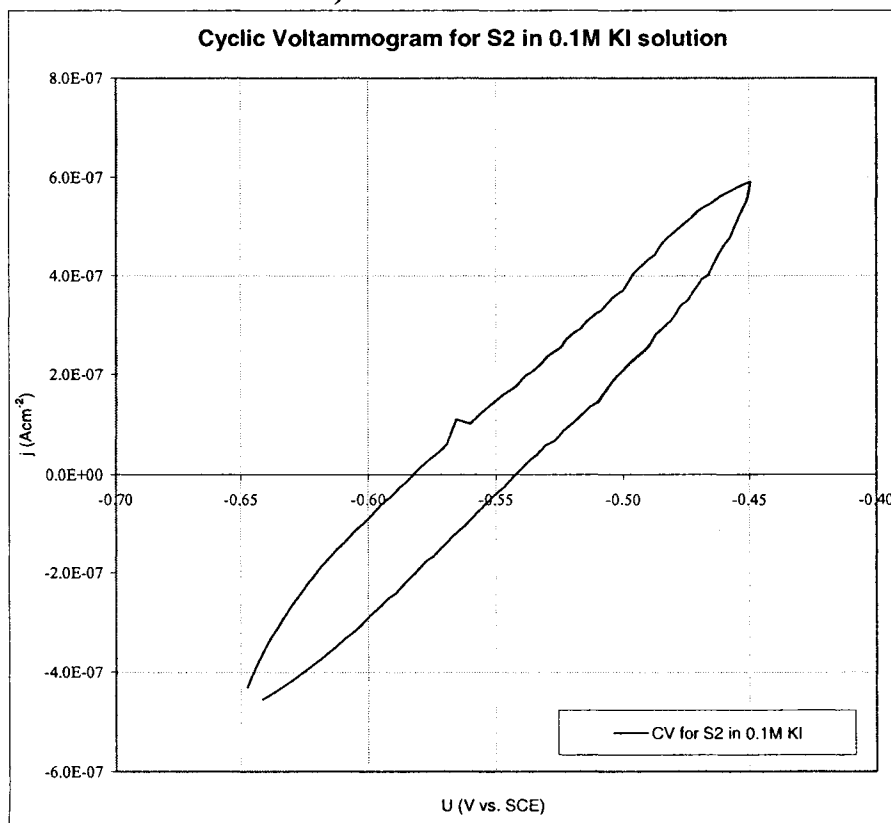
g) S2 in 0.1M CH_3COOK solution



h) S2 in 0.1M KBr solution



i) S2 in 0.1M KI solution



Results & Discussion

In the following discussion, the charge transfer reactions occurring at the semiconductor/electrolyte interface have been identified purely on the basis of the comparison between their standard reduction potentials and the band edge energy levels of the semiconductor (Fig. III.13) using the approach described below:

Consider the following two reactions:



The first reaction (Reaction 3.2) is a reduction reaction, and the second reaction (Reaction 3.3) is an oxidation reaction. The standard reduction potential of the reduction reaction can be found in tables of standard reduction potentials. The standard reduction potential of the oxidation reaction has the same absolute value as the standard reduction potential for the reduction reaction but opposite sign. If the standard reduction potential of the oxidation reaction for a given redox couple present in solution lies above the conduction band edge energy level of the semiconductor electrode, then the oxidation reaction is thermodynamically possible. In this scenario, the electron energy of the reducer species of the redox couple is higher than the energy of the electrons at the bottom states of the semiconductor conduction band and, hence, the transfer of electrons from the reducer species in solution to the conduction band of the semiconductor is favoured. This electron transfer will result in the oxidation of reducer species to the oxidant species according to the oxidation reaction 3.3. By contrast, when the standard reduction potential of the oxidation reaction lies below the conduction band edge energy level, no charge transfer between the semiconductor and the redox species in the solution can occur.

Following a similar logic, if the standard reduction potential of the reduction reaction lies below the conduction band edge energy level of the semiconductor electrode, then an electron transfer from the conduction band of the semiconductor to the oxidant species in solution will be thermodynamically favoured, and this electron transfer will result in the reduction of the oxidant species to the reducer species (Reaction 3.2).

In semiconductors, however, charge transfer can occur not only via exchange of electrons through the conduction band, but also via exchange of holes through the valence band. Whether charge transfer occurs through the conduction band or through the valence band depends on the

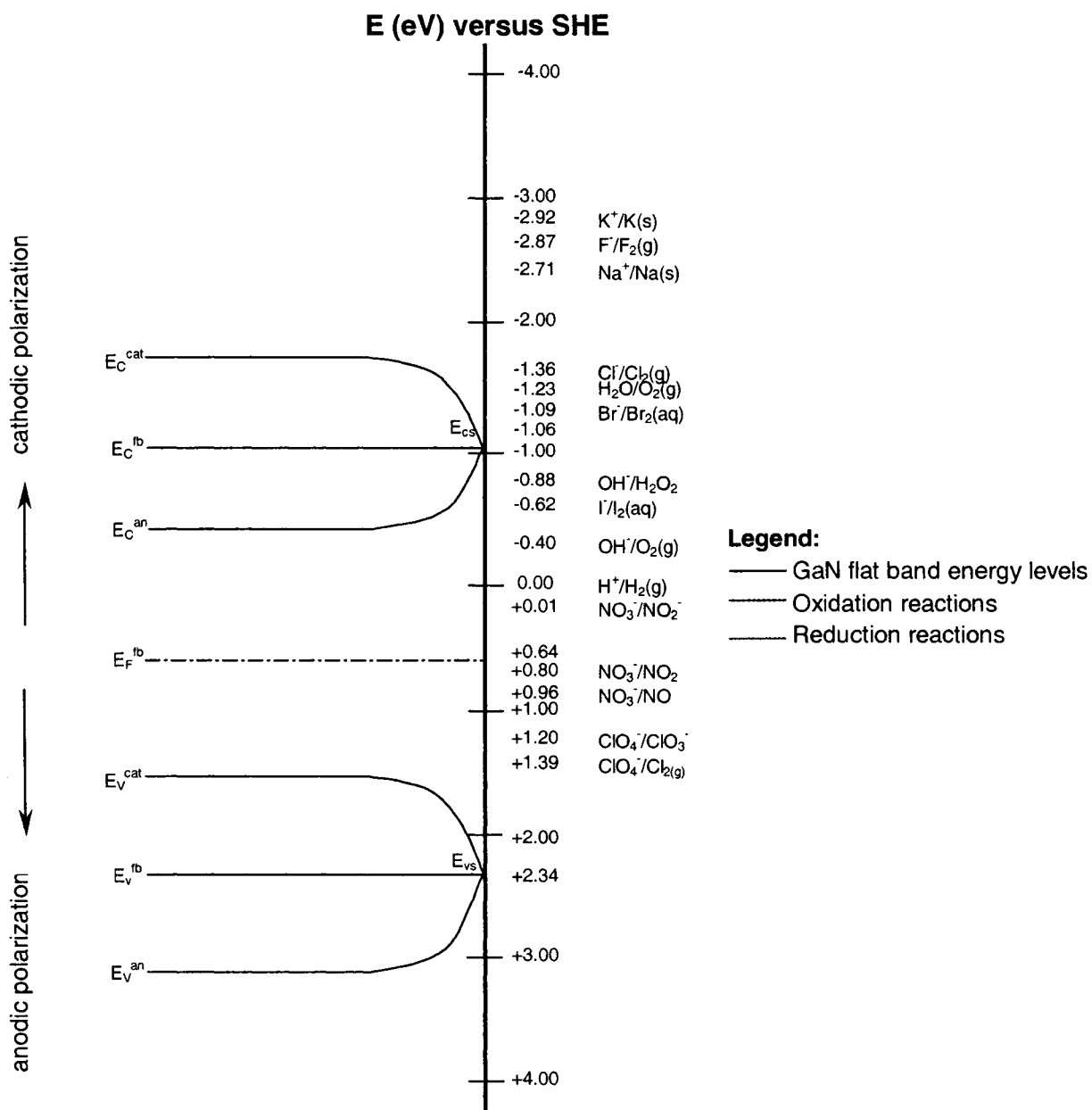
Results & Discussion

relative positions of the band edge energies of the semiconductor and the standard redox potentials of the redox couples in the solution. If the standard reduction potential of a given redox couple is closer to the conduction band than to the valence band, the charge transfer through the conduction band will be favoured. Similarly, if the standard reduction potential of a given redox couple is closer to the valence band than to the conduction band, charge transfer through the valence band will be favoured (Morrison, 1980). Fig. III.13 indicates that the standard reduction potentials for oxidation reactions involving the redox couples present in the tested solutions are closer to the conduction band. Hence, for these redox couples, charge transfer through the conduction band can be expected. The only exception is the oxidation of GaN, which has been identified from the literature review rather than by the approach described above.

Reduction reactions can occur through either the capture electrons from the conduction band or the injection of holes into the valence band. However, only the former mechanism has been considered in order to simplify the discussion.

Once both oxidation and reduction reactions have been identified, even though they are thermodynamically possible, other factors such as reaction kinetics and adsorption phenomena may influence their occurrence at the semiconductor/ electrolyte interface. Further studies will be required to determine which reactions are actually taking place in the electrochemical system, as well as the reaction rates of these reactions. Such study falls outside the scope of this research project.

Fig. III.13 Comparison of GaN band edge energies with energy levels of redox couples in tested solutions



1. In 0.1M **KF** solution (Fig. III.12a and b), the potential scan for the GaN sample electrode S1 was performed between potentials $U = -0.7V$ and $U = -0.5V$ versus SCE. For the GaN sample electrode S2, the potential scan was performed between $U = -0.7V$ and $U = +0.5V$ versus SCE. For the GaN sample electrode S1, a maximum cathodic current of $0.25\mu A$ flows under cathodic polarization (changing the potential of the semiconductor electrode to more negative potentials), and a maximum anodic current of $2\mu A$ flows under anodic polarization (changing the potential of the semiconductor electrode to more positive potentials). For the

GaN sample electrode S2, the cathodic current has a maximum of 50.0 μ A and the anodic current has a maximum of 800 μ A.

For the GaN sample electrode S1, the anodic current can be associated with one or more of the following oxidation reactions:

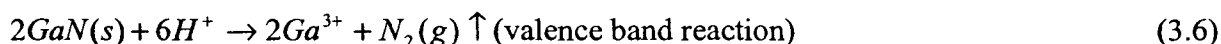
Oxidation of fluoride anions (conduction band reaction):



Oxidation of water (conduction band reaction):



For the GaN sample electrode S2, besides the oxidation reactions listed for S1 (Reactions 3.4 and 3.5), some minor oxidation (etching) of the GaN electrode surface might have occurred. This conclusion was made because the anodic polarization of GaN sample electrode S2 reached 0.5V vs SCE, and some researchers (Fujii and Ohkawa, 2006) have observed etching of the surface of GaN semiconductor electrodes at potentials close to this value. These observations were made under anodic polarization in acidic as well as basic solutions. According to Fujii and Ohkawa (2006), the dissolution of GaN occurs according to the following oxidation reaction:

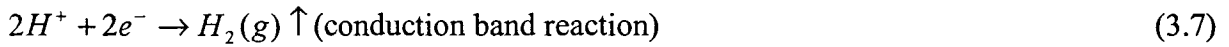


Because no standard reduction potential has been defined for the redox couple GaN/N₂(g), the occurrence of reaction 3.6 could not be predicted by comparison of its standard reduction potential to the positions of the band edge energies in the semiconductor electrode, unlike what was done for all other reactions.

The same group of researchers (Fujii and Ohkawa, 2006) showed that the current resulting from the anodic dissolution of the GaN represents only a small portion (less than 1%) of the total anodic current flowing through the electrochemical system. Therefore, the anodic current for the GaN sample electrode S2 is likely determined by one or more of the oxidation reactions listed for electrode S1 (Reactions 3.4 and 3.5).

Results & Discussion

The cathodic current for both GaN sample electrodes (S1 and S2) can be associated with hydrogen evolution according to the reduction reaction:



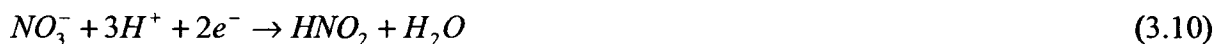
2. In 0.1M KNO_3 solution (Fig. III.12c), the potential scan for the GaN sample electrode S2 was performed between potentials $U = -0.7V$ and $U = -0.5V$ versus SCE. Experiments were not performed with the GaN sample electrode S1. For GaN sample electrode S2, a maximum cathodic current of $6.5\mu A$ flows under cathodic polarization and a maximum anodic current of $5.2\mu A$ flows under anodic polarization.

The anodic current can be associated with the oxidation of water (Reaction 3.5).

To ensure GaN chemical stability over the selected scan range, the potential scan for the GaN sample electrode S2 was limited to small overpotentials in comparison with the electrode's OCP. Under such conditions, the anodic current could be entirely attributed to the oxidation of water.

The cathodic current for GaN sample electrode S2 in KNO_3 solution can be attributed to one or more of the following reduction reactions:

- Hydrogen evolution according to reaction 3.7, and
- Reduction of nitrate according to one or more of the following reactions:



The cathodic current ($6.5\mu A$) for GaN sample electrode S2 in 0.1M KNO_3 solution is much smaller than the cathodic current for the same electrode at the same potential in 0.1M KF solution ($50.0\mu A$). This may be because the anodic scan to high positive potentials in 0.1M KF solution resulted in higher reaction rates of the oxidation reactions, thus producing higher concentration of reactants (oxidized species), which were reduced during the reverse scan.

Results & Discussion

On the contrary, the anodic scan for GaN sample electrode S2 in 0.1M KNO₃ solution was done within a very small range of negative potentials, resulting in lower reaction rates of the oxidation reactions (smaller anodic current). Thus, a lower concentration of reactants was reduced during the reverse scan, which in turn led to a smaller cathodic current in the 0.1M KNO₃ solution.

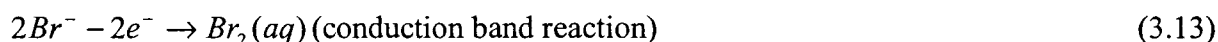
3. In 0.1M **KCl** solution (Fig. III.12d), the potential scan for the GaN sample electrode S1 was performed between potentials $U = -1.54\text{V}$ and $U = -1.34\text{V}$ versus SCE. Experiments were not performed with GaN sample electrode S2. Under such high cathodic polarization, the maximum cathodic current was $13.3\mu\text{A}$. Since GaN is expected to be stable over the scan range, this current can only be attributed to the hydrogen evolution reaction (Reaction 3.7).
4. In 0.1M **HOC₆H₄COONa** solution (Fig. III.12e), the potential scan for the GaN sample electrode S1 was performed between potentials $U = -1.52\text{V}$ and $U = -1.32\text{V}$ versus SCE. Experiments were not performed with GaN sample electrode S2. Similarly to the experiments in 0.1M KCl solution, a maximum cathodic current of $16.0\mu\text{A}$ was measured under such high cathodic polarization. Since GaN is expected to be stable over the scan range, this current can be attributed to hydrogen evolution (Reaction 3.7).
5. In 0.1M **KSCN** solution (Fig. III.12f), the potential scan for the GaN sample electrode S1 was performed between potentials $U = -1.34\text{V}$ and $U = -1.14\text{V}$ versus SCE. Experiments were not performed with GaN sample electrode S2. Similarly to the experiments in 0.1M KCl solution, under such high cathodic polarization, only a cathodic current having a maximum of $29.0\mu\text{A}$ is measured. Since GaN is expected to be stable over the scan range, the current can be attributed to the hydrogen evolution (Reaction 3.7)
6. In 0.1M **CH₃COOK** solution (Fig. III.12g), the potential scan for the GaN sample electrode S2 was performed between potentials $U = -0.45\text{V}$ and $U = -0.25\text{V}$ versus SCE. Experiments were not performed with GaN sample electrode S1. For GaN sample electrode S2, a maximum cathodic current of $0.21\mu\text{A}$ is measured under cathodic polarization and a maximum anodic current of $0.51\mu\text{A}$ is measured under anodic polarization. The anodic

current can be associated with the oxidation of water (Reaction 3.5), and the cathodic current can be attributed to hydrogen evolution (Reaction 3.7).

7. In 0.1M **KBr** solution (Fig. III.12h), the potential scan for the GaN sample electrode S2 was performed between potentials $U = -0.65V$ and $U = -0.45V$ versus SCE. Experiments were not performed with the GaN sample electrode S1. For GaN sample electrode S2, the maximum cathodic current was $0.53\mu A$ under cathodic polarization and the maximum anodic current was $0.7\mu A$ under anodic polarization.

The anodic current can be associated with one or more of the following oxidation reactions:

- Oxidation of water (Reaction 3.5).
- Oxidation of bromide anions:



The cathodic current for GaN sample electrode S2 in KBr and can be attributed to hydrogen evolution according to Reaction 3.7.

8. In 0.1M **KI** solution (Fig. III.12i), the potential scan for the GaN sample electrode S2 was performed between potentials $U = -0.65V$ and $U = -0.45V$ versus SCE. Experiments were not performed with the GaN sample electrode S1. For GaN sample electrode S2, the maximum cathodic current was $0.6\mu A$ under cathodic polarization and the maximum anodic current was $0.45\mu A$ under anodic polarization.

The anodic current can be associated with the oxidation of water (Reaction 3.5), and the cathodic current can be attributed to hydrogen evolution (Reaction 3.7).

III.8. Electrochemical Impedance Spectroscopy

Electrochemical Impedance Spectroscopy (EIS) measurements were carried out to investigate the structure of the electrical double layer at the semiconductor/electrolyte interface, the charge transfer processes in the semiconductor and electrolyte, as well as the parameters defining the limiting steps of the electrode processes. EIS measurements were carried out at bias DC potentials within 100mv of the OCP measured for the respective sample electrode and solution.

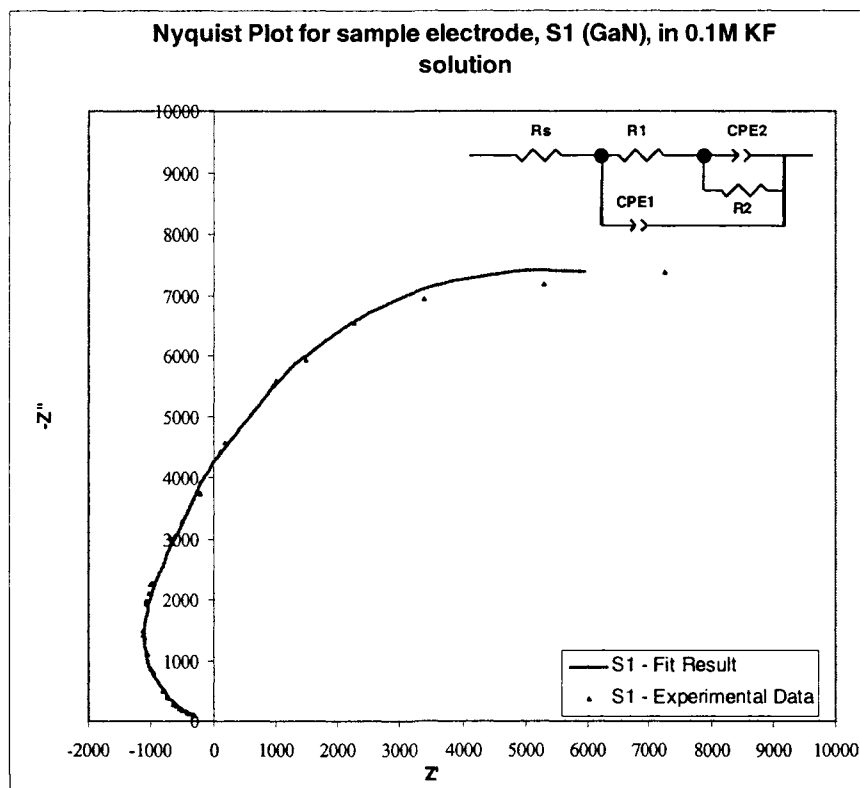
Results & Discussion

The significant scattering of the experimental data observed during the initial investigation of the GaN sample electrodes has been limited to the lower frequency range by adjusting the interval I (number of points per decade of frequencies) to $I = 100$ points/decade (compared to $I=15$ points/decade during the initial testing). This adjustment means that the frequency scan rate has been made slower, allowing the electrochemical system more time to equilibrate.

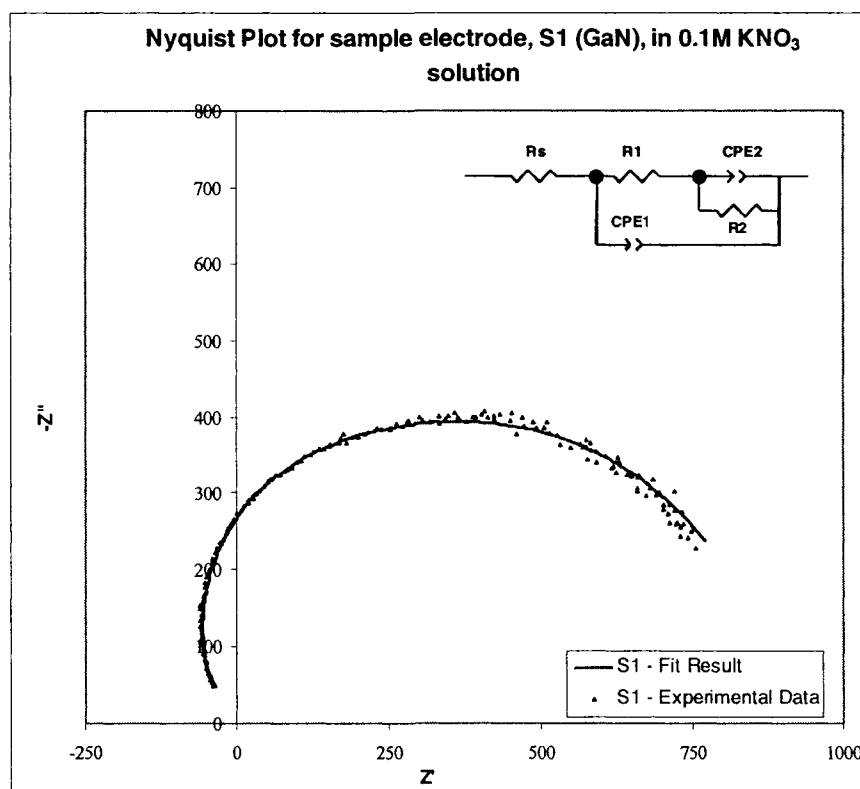
The EIS results obtained for the GaN sample electrode S1 and the InGaN sample electrode S3 in 10^{-1} M electrolyte solutions are presented as Nyquist Plots on Figures III.14 and III.15, respectively.

Fig. III.14 Nyquist Plots for GaN sample electrode S1 in 0.1M electrolyte solutions

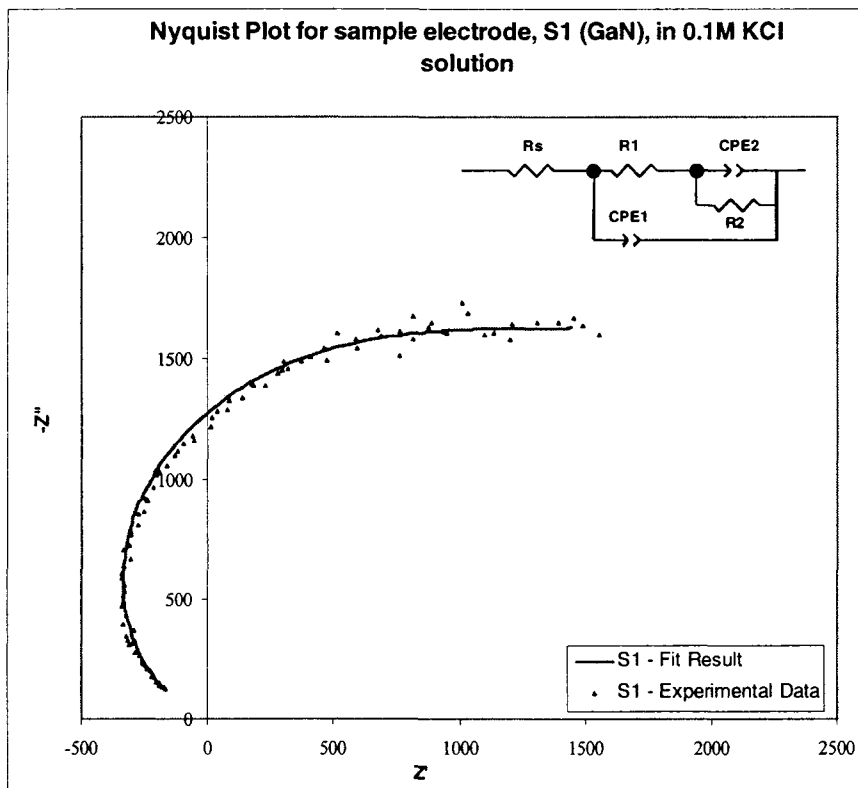
a) GaN sample electrode S1 in 0.1M KF solution



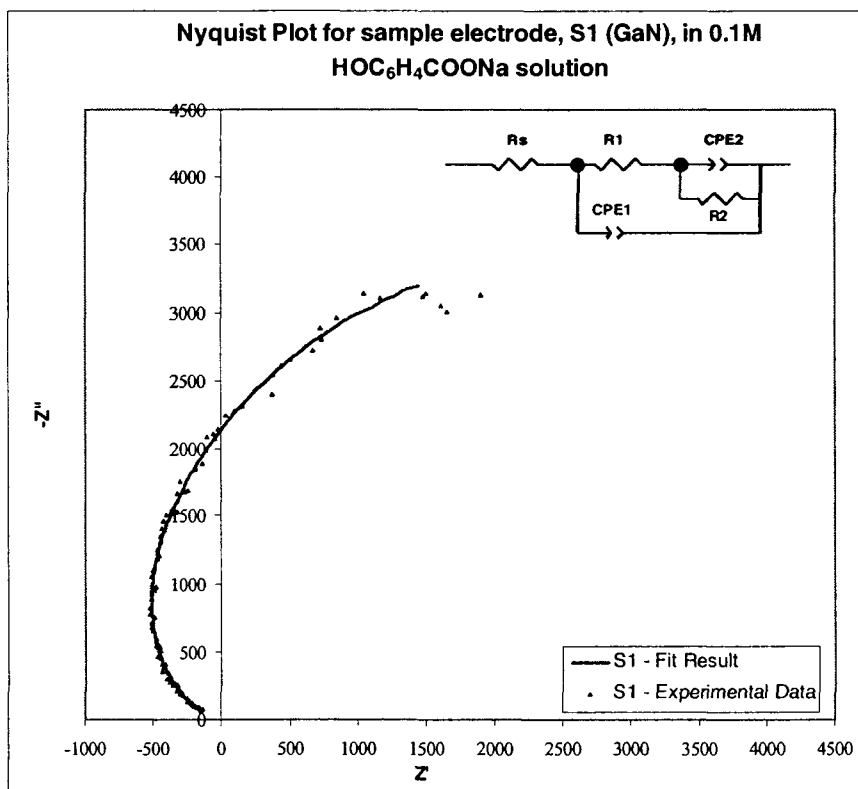
b) GaN sample electrode S1 in 0.1M KNO_3 solution



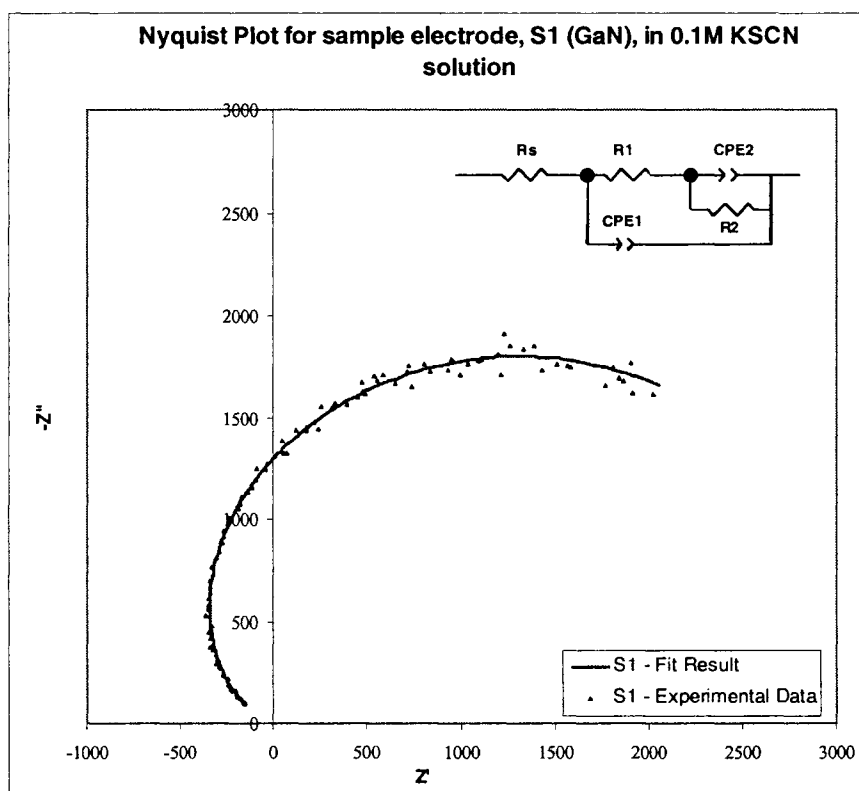
c) GaN sample electrode S1 in 0.1M KCl solution



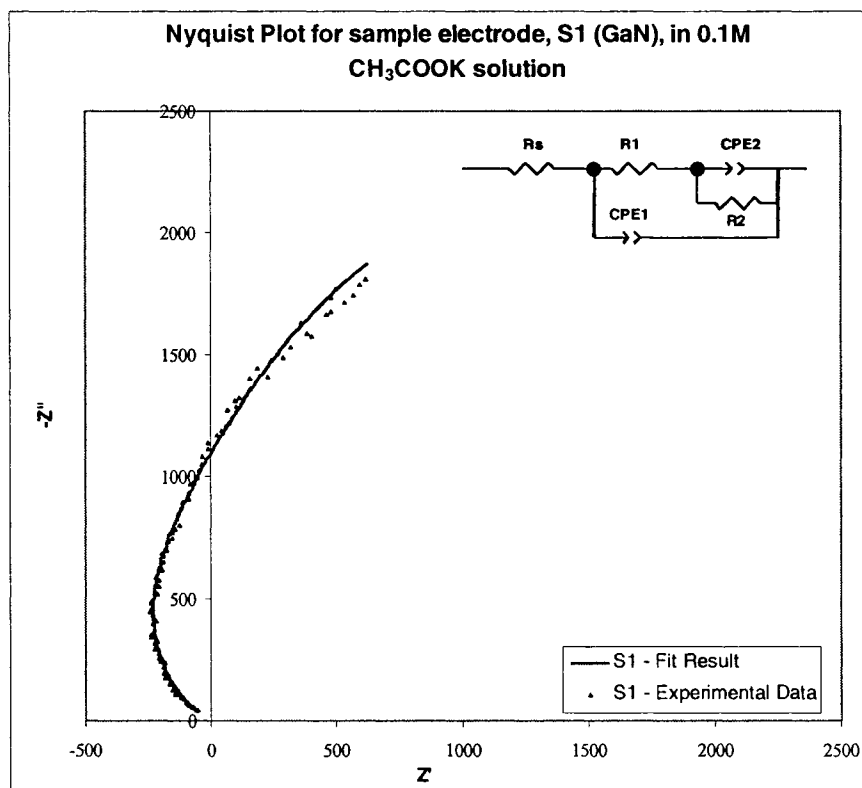
d) GaN sample electrode S1 in 0.1M HOC₆H₄COONa solution



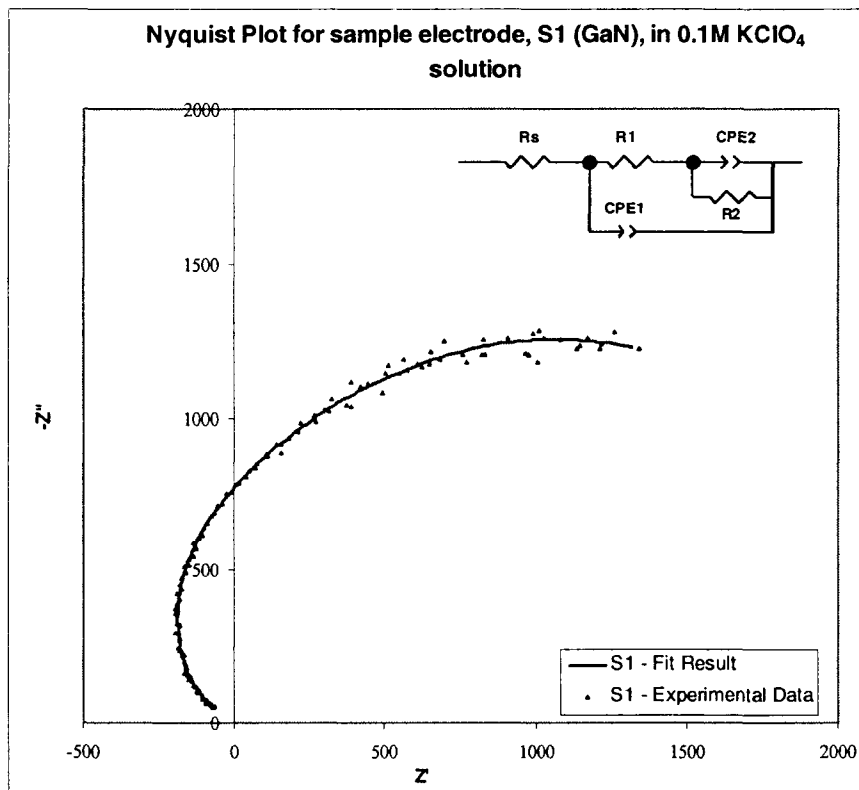
e) GaN sample electrode S1 in 0.1M KSCN solution



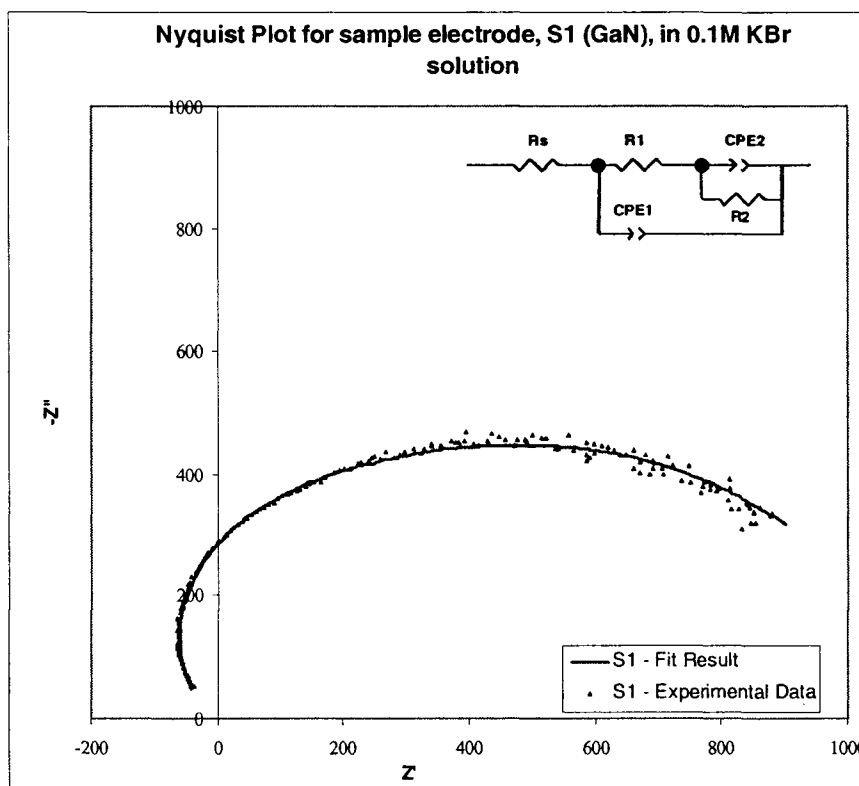
f) GaN sample electrode S1 in 0.1M CH₃COOK solution



g) GaN sample electrode S1 in 0.1M KClO₄ solution



h) GaN sample electrode S1 in 0.1M KBr solution



i) GaN sample electrode S1 in 0.1M KI solution

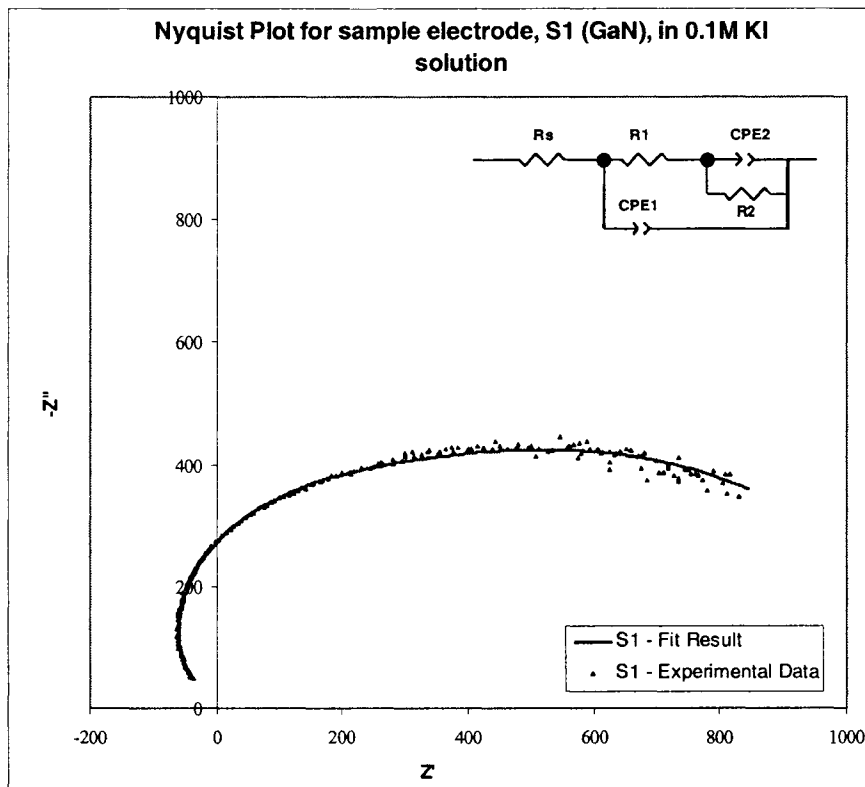
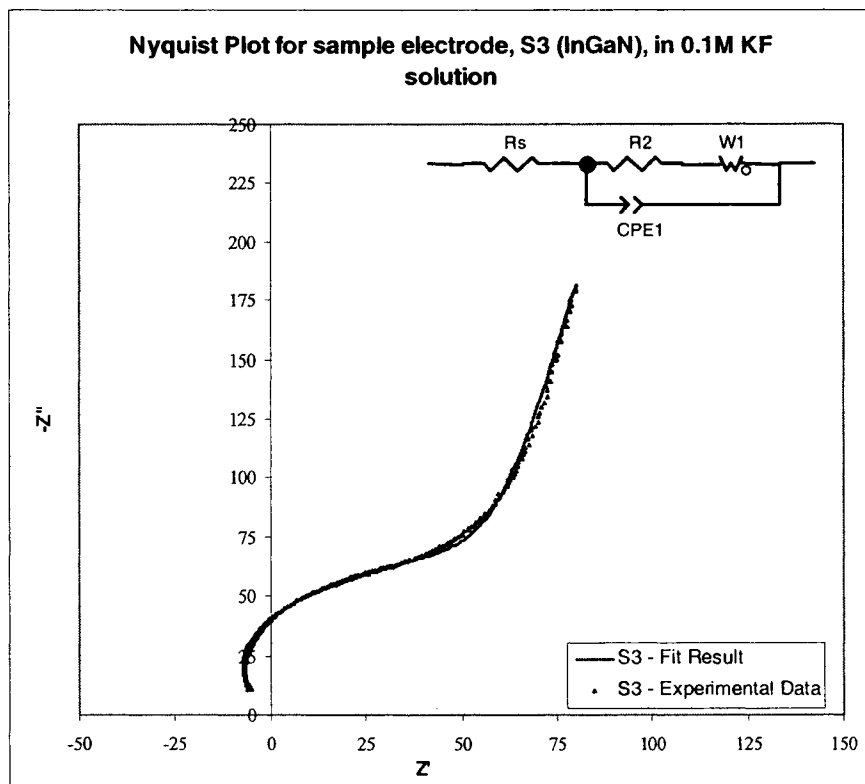
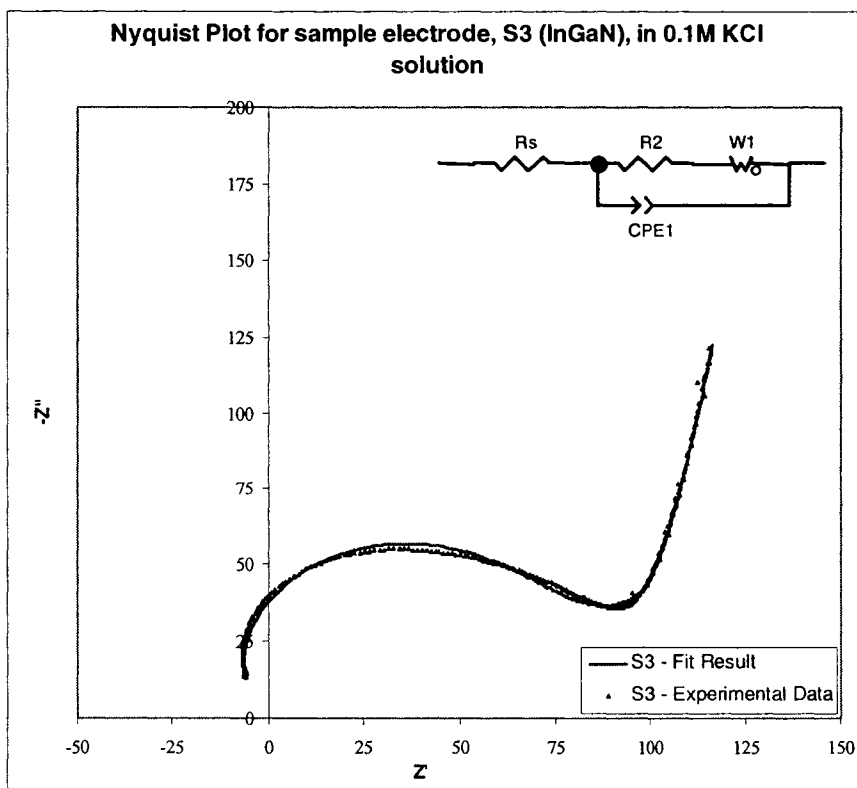
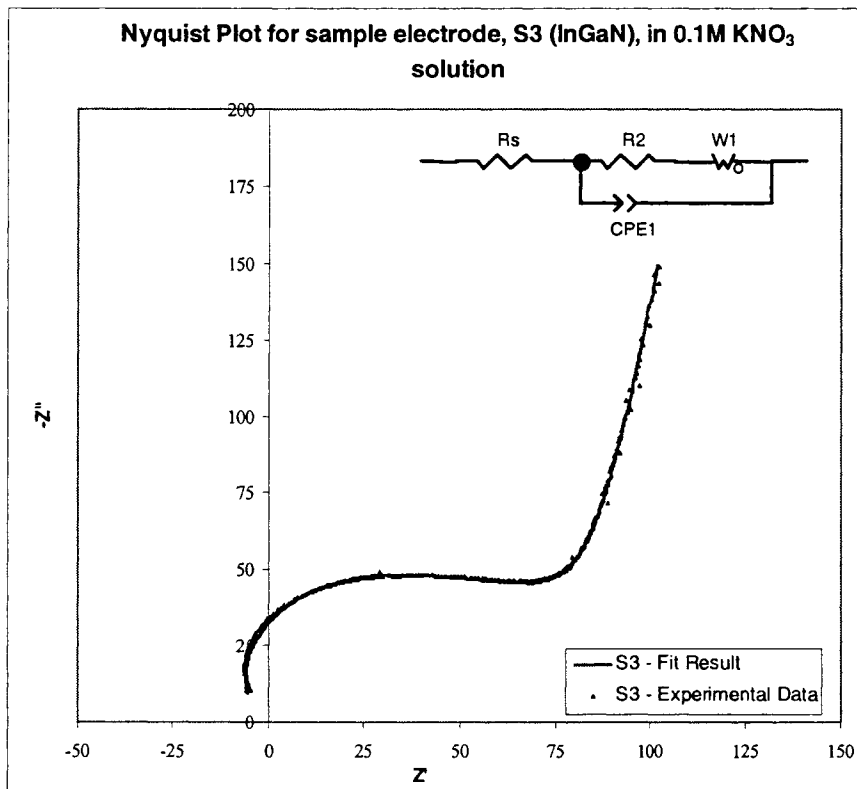


Fig. III.15 Nyquist Plots for InGaN sample electrode, S3 in 0.1M electrolyte solutions

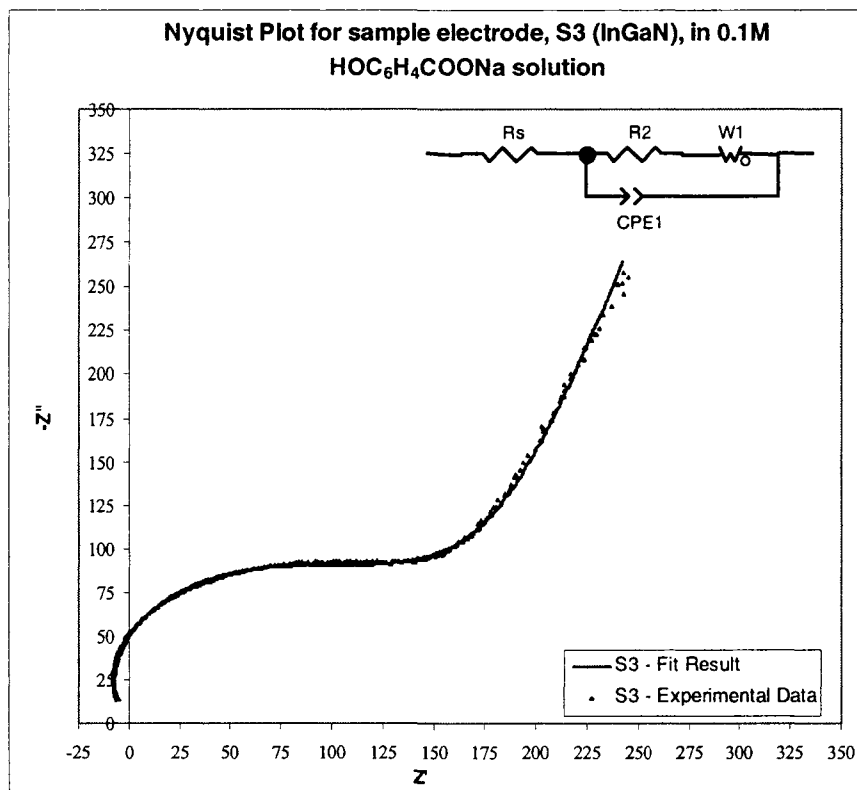
a) InGaN sample electrode S3 in 0.1M KF solution



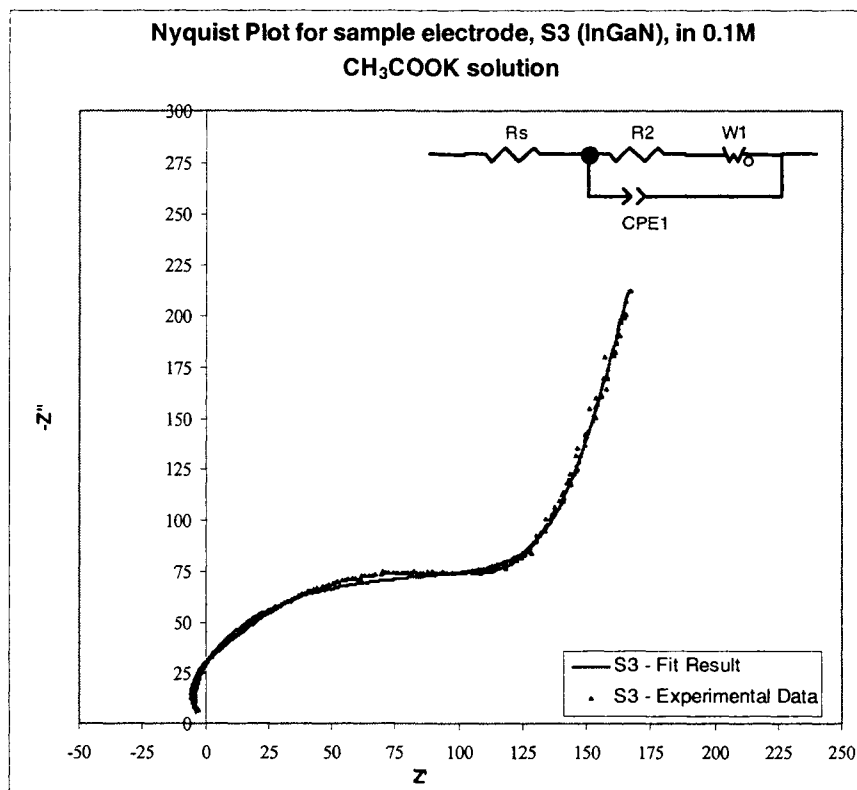
b) InGaN sample electrode S3 in 0.1M KNO₃ solution



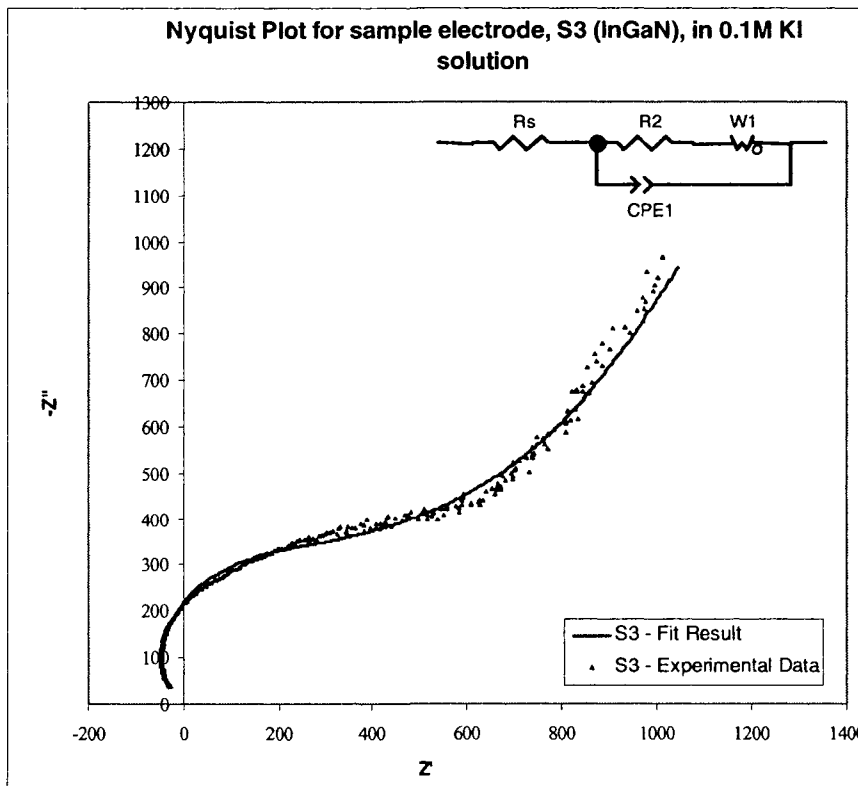
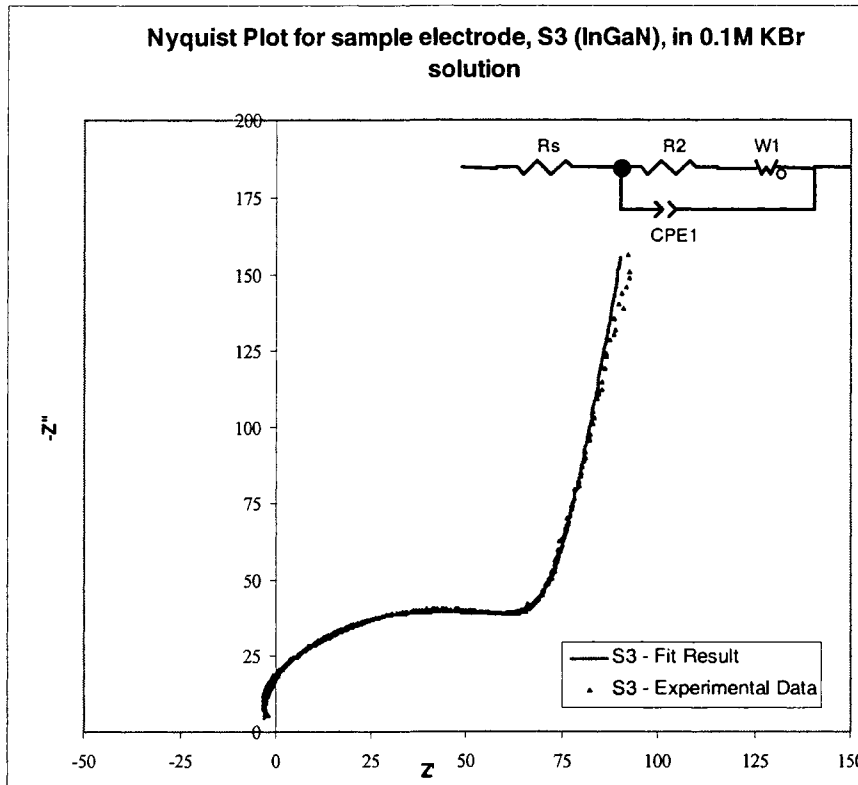
d) InGaN sample electrode S3 in 0.1M $\text{HOC}_6\text{H}_4\text{COONa}$ solution



f) InGaN sample electrode S3 in 0.1M CH₃COOK solution



h) InGaN sample electrode S3 in 0.1M KBr solution



Results & Discussion

To analyze the frequency dependencies of the real (Z') and imaginary (Z'') components of the complex impedance, the response of the cell has been modelled by an equivalent circuit, which has a response to the external perturbation identical to the response of the electrochemical cell. The equivalent circuit models for the GaN sample electrode S1 and for the InGaN sample electrode S3 are presented on Figures III.16 and III.17, respectively.

Fig. III.16 Equivalent Circuit Model for GaN sample electrode S1

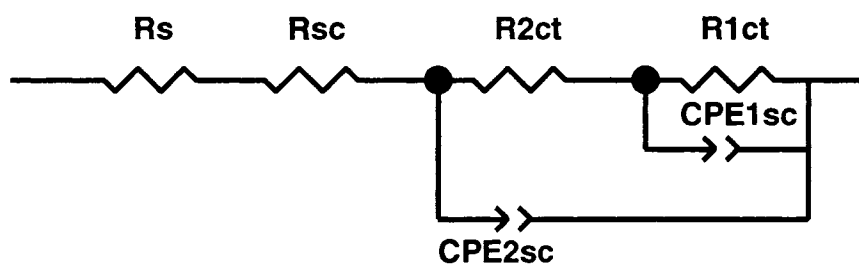
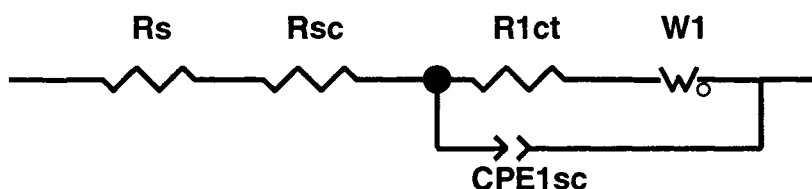
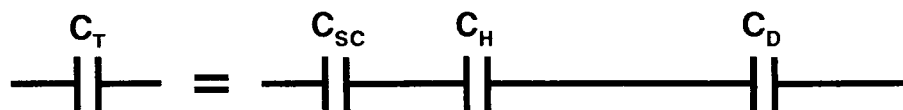


Fig. III.17 Equivalent Circuit Model for InGaN sample electrode S3



According to the description of the semiconductor/electrolyte interface provided in I.5.2, three ranges can be distinguished within the electrical double layer: the space charge layer of the semiconductor, the Helmholtz layer, and the diffuse or the Gouy layer. The total differential capacity of the semiconductor/electrolyte interface C_T can be represented by three capacitors connected in series, corresponding respectively to the capacitance of the space charge layer of the semiconductor C_{SC} , the capacitance of the Helmholtz layer C_H , and the capacitance of the diffuse or Gouy layer C_D (Fig. III.18).

Fig. III.18 Representation of the capacitance of the semiconductor/electrolyte interface



Results & Discussion

For 0.1M electrolyte solutions, the potential drop across the diffuse layer can be neglected, thus simplifying the analysis of the semiconductor/electrolyte interface (Memming, 2001). Hence, in these solutions the differential capacity of the semiconductor/electrolyte interface can be represented by two capacitors, C_{SC} and C_H , connected in series.

Practically, the main part of the potential drop across the semiconductor/electrolyte interface occurs across the space charge layer of the semiconductor (Memming, 2001), i.e. $C_{SC} \gg C_H$ and, as a result, the main contribution to the total interfacial capacitance comes from the capacitance of the space charge layer of the semiconductor. Thus, in the simplest model, the semiconductor/electrolyte interface can be represented by a charge transfer resistance R_{1ct} and a space charge capacity C_{sc} , connected in parallel. The charge transfer resistance R_{1ct} represents the resistance of the space charge layer of the semiconductor to the transfer of charge (electrons or holes) from the semiconductor to the solution.

The capacitors in real electrochemical systems, however, often do not behave ideally. Instead, they act as a Constant Phase Element (CPE) characterized by a phase shift between the perturbation signal and the resulting current different from $\pi/2$, contrary to the ideal capacitor for which the phase shift is always $\pi/2$. This is valid for the GaN and InGaN sample electrodes as well. Instead of behaving like an ideal capacitor, which would result in ideal semicircles appearing on all impedance diagrams at high frequencies, the space charge layer behaves non-ideally (the semicircles are depressed). Thus, the space charge was modeled by a constant phase element CPE_{1SC} in the equivalent circuit model (Fig. III.16 and Fig. III.17).

For the GaN sample electrode S1 (Fig. III.16), the behaviour of the space charge region is further complicated by the mixed polarity of the electrode (Ga-face and N-face regions). To account for this mixed polarity, a second constant phase element, CPE_{2SC} , has been added to the above described set of circuit elements, representing the capacitance of the regions with inversed polarity (N-face instead of Ga-phase) within the space charge layer. Accordingly, the charge transfer resistance across these regions has been represented by R_{2ct} . Given that the InGaN sample electrode S3 has fewer and much smaller regions with inversed polarity, such modification of the space charge layer capacitance is not necessary.

Results & Discussion

During a charge transfer process, electroactive species are consumed and produced at the electrode/electrolyte interface. This brings about gradients in the concentrations of these species near the interface, thus creating a driving force for mass transport by diffusion. The diffusion process should have an influence on the electrochemical impedance of the electrode reaction, as far as it is affected by a perturbation of the potential across the electrode/electrolyte interface (Hens and Gomes, 1997). Therefore, any mass transport limitations would introduce a Warburg impedance in the impedance of the electrochemical system. In the present research, it is suggested that the abundance of charge carriers in the InGaN semiconductor leads to higher rate of the charge transfer reactions at the semiconductor/electrolyte interface in InGaN in comparison with the GaN. As the surface of the sample electrodes is covered by a layer of specifically and non-specifically adsorbed anions, the electroactive species in the solution will have to diffuse under the influence of the formed concentration gradients through this layer in order to reach the surface of the electrode and participate in a charge transfer reaction (oxidation or reduction through exchange of electrons via the conduction band of the semiconductor). The experimental data corroborate this hypothesis, since a straight line, characteristic of the Warburg impedance, is clearly visible on the impedance spectra recorded for the InGaN sample electrode S3 in all investigated electrolyte solutions. The presence of a diffusion controlled process at the InGaN electrode/electrolyte surface is modeled by adding a Warburg element to the equivalent circuit model for InGaN (Fig. III.17).

In modern three-electrode electrochemical cells, the potentiostat compensates for the solution resistance between the counter and the reference electrodes. However, the solution resistance between the reference electrode (SCE) and the working electrode (semiconductor) remains uncompensated and should be accounted for in the electrical circuit model of the electrochemical system. Therefore, another resistance R_s , representing the solution resistance, should be added to the equivalent circuit models for both GaN sample electrode S1 (Fig. III.16) and for the InGaN sample electrode S3 (Fig. III.17). The resistance of the semiconductor itself, R_{sc} , should also be included into the electrical circuit model (Fig. III.16 and Fig. III.17).

For both investigated sample electrodes, GaN sample electrode S1 and InGaN sample electrode S3, the Nyquist plots obtained for all 0.1M electrolyte solutions show that two ranges of frequencies can be distinguished within the impedance spectra:

Results & Discussion

- The appearance of a depressed semicircle at the high frequency range (300kHz – 10kHz) of the impedance spectra, obtained for both sample electrodes – GaN sample electrode S1 and InGaN sample electrode S3 - confirms that at high frequencies the impedance of the electrochemical cell is dominated by the space charge layer of the semiconductor electrode.
- A large scattering of experimental data is observed for the GaN sample electrode S1 at low frequencies (10kHz – 100Hz) and for all electrolytes, which impedes the analysis of the full impedance spectra for this electrode. By contrast, the impedance diagrams for the InGaN sample electrode S3 are much clearer and can be analyzed.
- At low frequencies, the shape of the impedance diagrams obtained for the InGaN sample electrode S3 suggests that the impedance is no longer dominated by the semiconductor electrode properties and that the electrochemical reactions occurring at the semiconductor/electrolyte interface should also be taken into account. Within this frequency range, the impedance spectra indicate the presence of a diffusion-controlled process at the semiconductor/electrolyte interface.

Similar shapes of the impedance diagrams were obtained by other researchers who performed EIS measurements with semiconductor electrodes (Aroutiounian et al., 2000 and 2006; Ramesham and Rose, 1997; Hens and Gomes, 1997). Aroutiounian et al. (2000 and 2006) also suggested that the main contribution to the impedance at high frequencies ($>10^3$ Hz) is the space charge layer of the semiconductor, while at low frequencies ($<10^3$ Hz) a slow diffusion process dominates the impedance spectra. The equivalent circuit model that they developed to fit their experimental data contains the same main elements as the equivalent circuit models proposed in the present study. These elements represent the series-connected resistances of the bulk of the semiconductor and the electrolyte, the capacitance of the space-charge layer connected in parallel with the charge transfer resistance across the space charge layer, and the Warburg impedance modelling the diffusion-controlled processes at the interface.

As the response of the proposed equivalent circuit to potential perturbations was identical (or very similar) to the response of the electrochemical system, it was concluded that the circuit model correctly represents the structure of the semiconductor/ electrolyte interface. The

Results & Discussion

parameters of the equivalent circuit elements for the GaN sample electrode S1 and for the InGaN sample electrode S3 are presented in Tables III.8 and III.9, respectively.

Table III.8 Equivalent Circuit Parameters for S1 (GaN) in 0.1M electrolyte solutions

Salt	Potential (mV)	Rs (Ωcm^2)	Rsc (Ωcm^2)	R1ct (Ωcm^2)	CPE1sc-T (Fcm^{-2})	CPE1sc-P	R2ct (Ωcm^2)	CPE2sc-T (Fcm^{-2})	CPE2sc-P
KF	-611	55.21	-1390.24	249.00	6.7610E-10	0.9998	14754.00	6.8550E-11	0.9998
KNO ₃	-512	56.18	-96.95	200.38	3.7610E-11	0.9999	1040.00	4.0923E-08	0.8398
KCl	-560	55.33	-735.78	120.67	4.27E-09	0.9098	4000.07	6.76E-11	0.9999
HOC ₆ H ₄ COONa	-518	52.71	-948.12	286.08	1.65E-09	0.9998	7729.66	5.76E-11	0.9980
KSCN	-541	42.93	-737.56	213.02	1.4800E-09	0.9998	3600.45	3.9610E-11	0.9980
CH ₃ COOK	-479	55.16	-554.82	210.17	4.2420E-09	0.9998	4410.43	7.1610E-11	0.9980
KClO ₄	-546	59.23	-524.47	215.67	3.3660E-09	0.9998	2500.61	2.7610E-11	0.9980
KBr	-540	25.82	-395.87	218.67	5.8747E-08	0.8098	1250.54	2.7610E-11	0.9999
KI	-453	48.57	-398.51	210.09	6.2022E-08	0.8098	1200.04	2.7610E-11	0.9999

Table III.9 Equivalent Circuit Parameters for S3 (InGaN) in 0.1M electrolyte solutions

Salt	Potential (mV)	Rs (Ωcm^2)	Rsc (Ωcm^2)	R1ct (Ωcm^2)	CPE1sc-T (Fcm^{-2})	CPE1sc-P	W1-R (Ωcm^2)	W1-T (Fcm^{-2})	W1-P
KF	-579	59.20	-70.74	105.10	3.6745E-08	0.9900	51.56	5.0942E-06	0.4671
KNO ₃	-601	57.27	-69.56	78.76	3.6745E-08	0.9900	61.05	3.4310E-05	0.4424
KCl	-597	54.97	-71.35	96.37	2.5016E-08	0.9935	46.36	5.1706E-05	0.4279
HOC ₆ H ₄ COONa	-554	53.89	-70.9	144.10	2.9565E-08	0.9935	96.47	3.8924E-05	0.3703
KSCN	-535	53.39	-71.01	84.77	2.9637E-08	0.9970	105.90	1.3300E-04	0.4560
CH ₃ COOK	-455	62.49	-69.45	104.20	7.8912E-08	0.9995	123.30	1.4366E-04	0.4243
KClO ₄	-608	62.54	-71.64	76.89	7.2235E-08	0.9910	50.40	7.4877E-05	0.4277
KBr	-663	65.79	-70.13	63.18	1.0598E-07	0.9999	50.52	8.3543E-05	0.4449
KI	-621	10.13	-70.91	590.20	7.6310E-09	0.9999	261.60	1.6968E-05	0.3393

In the ZView2 impedance analysis software, a Constant Phase Element is defined by two parameters, CPE-T and CPE-P, and its impedance is calculated according to the equation:

$$Z_{CPE} = 1/[CPE - T(j * \omega)^{CPE - P}] \quad (3.14)$$

where:

CPE-T is the capacitance of the Capacitor (F) (See CPE1sc-T and CPE2sc-T in Table III.8 and CPE1sc-T in Table III.9)

CPE-P is an exponent, which equals 1 for a capacitor (See CPE1sc-P and CPE2sc-P in Table III.8 and CPE1sc-P in Table III.9)

Results & Discussion

ω is the radial frequency, (rad)

j is the imaginary number (square root of -1).

If CPE-P equals 1, then the equation is identical to that of a capacitor. In fact, a capacitor is actually a constant phase element - one with a constant phase angle of 90 degrees. If CPE-P equals 0.5, a 45 degree line is produced on the Nyquist plot.

In the ZView2, a finite length Warburg Impedance is defined by three parameters, W_o-R , W_o-T , and W_o-P . Its impedance is calculated according to the equation:

$$Z_w = W_o - R * \text{ctnh}([j * W_o - T * \omega]^{W_o - P}) / (j * W_o - T * \omega)^{W_o - P} \quad (3.15)$$

where:

W_o-P is an exponent with a value between 0 and 1 (See $W1-P$ in Table III.9);

$W_o-T = \delta^2 / D$ (See $W1-T$ in Table III.9)

D is the effective diffusion coefficient of the redox species ($\text{m}^2 \text{s}^{-1}$);

δ is the effective thickness of the diffusion layer (m);

W_o-R is the diffusion resistance (Ω) (See $W1-R$ in Table III.9);

ω is the radial frequency (rad);

j is the imaginary number.

The values of the parameters of the equivalent circuit for the GaN sample electrode S1 show that the capacitance of the GaN semiconductor space charge layer (CPE1sc-T, Table III.8) varies between $3.76\text{E-}11$ and $6.20\text{E-}08 \text{ F.cm}^{-2}$. For the InGaN sample electrode S3, the capacitance of the space charge layer (CPE1sc-T, Table III.9) is slightly higher than for the GaN sample electrode S1 and varies between $7.63\text{E-}09$ and $1.06\text{E-}07 \text{ F.cm}^{-2}$. This is probably because the thickness of the space charge layer formed within the GaN semiconductor electrode is expected to be greater than the thickness of the space charge layer formed within the InGaN electrode due to the higher concentration of charge carriers (electrons and holes) in the semiconductor with the lower band gap, i.e. in the InGaN. The obtained results for the capacitance of the space charge layers in both investigated materials were compared with the values found in the literature for other semiconductor electrodes. Aroutiounian et al. (2000) performed EIS experiments with iron oxide semiconductors doped with titanium and found that the capacitance of the space charge layer of the iron oxide semiconductor electrodes varies between $9.16\text{E-}07$ and $9.54\text{E-}07 \text{ F.cm}^{-2}$. These values are close to the results obtained in the current study. In another study,

Results & Discussion

Aroutiounian et al. (2006) experimented with iron oxide semiconductors doped with Sn^{4+} and Nb^{5+} . The results of their EIS experiments produced values of the space charge layer capacitance between $3.12\text{E-}08$ and $7.04\text{E-}08 \text{ F.cm}^{-2}$, which are even closer to the values obtained in the current research for GaN and InGaN semiconductor electrodes.

The cation adsorption on the surface regions with inversed polarity (N-face) at the surface of the GaN sample electrode S1 is expected to be weaker due to the overall positive polarization charge of the electrode surface. This suggestion is corroborated by the values obtained for the capacitance of these regions (CPE2sc-T, Table III.8), which are lower than the capacitance of the Ga-face regions in most investigated electrolyte solutions. Additionally, for the capacitors, representing the regions with inversed polarity, the values of the exponential factor CPE2sc-P are very close to unity, suggesting that these capacitors approximate the behaviour of an ideal capacitor. The same behaviour is observed for the capacitors representing the Ga-face regions in KF, KNO_3 , $\text{HOC}_6\text{H}_4\text{COONa}$, KSCN, CH_3COOK and KClO_4 solutions.

The charge transfer resistance across the space charge layer R1 varies between 120.7 and 286.1 Ωcm^2 for the GaN sample electrode S1 (Table III.8) and between 63.2 and 590.2 Ωcm^2 for the InGaN sample electrode S3 (Table III.9). These values are consistent with the ones obtained by Aroutiounian et al. (2006), who found that the charge transfer resistance in 5N NaOH solutions and iron oxide electrodes ranges from 310 to 11060 Ωcm^2 .

The values of the solution resistance R_s range between 25.8 and 59.2 Ωcm^2 for the GaN sample electrode S1 (Table III.8) and between 10.1 and 65.8 Ωcm^2 for the InGaN sample electrode S3 (Table III.9). They are in the same order of magnitude as the ones reported in the literature for other semiconductor electrodes. Aroutiounian et al. (2000) performed experiments with iron oxide electrodes in 1M H_2SO_4 solutions and obtained values of the solution resistance around 37-42 Ωcm^2 . Ramesham and Rose (1997) carried out corrosion studies of boron-doped diamond film electrodes in 0.5M NaCl solutions and determined the solution resistance to be between 148 and 152 Ωcm^2 .

Ramesham and Rose (1997) also calculated the resistance of the semiconductor films (boron-doped diamond) as being equal to 873-1195 Ωcm^2 . Such resistance is very similar to the

Results & Discussion

resistance R_{sc} of the GaN thin film electrode S1 (Table III.8), which absolute values vary between 97 and 1390 Ωcm^2 . Because of the lower band gap energy of the InGaN semiconductor (1eV) in comparison with the band gap energy of the GaN semiconductor (3.4eV), under the same excitation conditions (ambient light and room temperature), the number of charge carriers (electrons and holes) in the InGaN is expected to be much greater than the number of charge carriers in the GaN. This would result in significantly greater electrical conductivity and respectively lower resistance to passage of current of the InGaN sample electrode S3 in comparison with the GaN sample electrode S1. The values obtained by the EIS study of the electrodes are consistent with the above suggestion and show that the resistance of the InGaN semiconductor electrode S3 varies between 69 and 71.6 Ωcm^2 (Table III.9), which is 1.3 to 19 times lower than the resistance R_{sc} of the GaN semiconductor electrode S1 (Table III.8).

The charge transfer resistance R_{ct} across the space charge layer of the semiconductor electrodes is also expected to be larger in the GaN semiconductor than in the InGaN due to greater abundance of charge carriers and the smaller length of the space charge layer in the InGaN. Within the GaN film, the negative charges of the anions, adsorbed on the positively charged Ga-face surface cause accumulation of holes on the semiconductor side to counter these charges and to preserve the electrical neutrality of the interface. The large concentration of holes in the space charge layer of the Ga-face regions inhibits the electron transfer across the space charge layer formed in the regions with inversed polarity (N-face) as the electrons would recombine with the holes. Because the space charge layers in the two regions with opposite polarity (Ga-face and N-face) do not have distinct boundaries and interpenetrate each other, within the space charge layer in N-face regions only few electrons would reach the surface of the electrode. This model is supported by the experimental data showing that the charge transfer resistance R_{2ct} (Table III.8) in the N-face regions is 6 to 59 times larger than the charge transfer resistance R_{1ct} (Table III.8) in the Ga-face regions.

III.9. Potentiostatic Experiments

The objective of this set of experiments was to investigate the behaviour of the GaN semiconductor material under strong cathodic polarisation (potential of the electrode is changed to more negative values). The first experiment involved polarization of the GaN sample

Results & Discussion

electrode S2 in the cathodic region by setting the potential of the working electrode at $U = -1.1\text{V}$ vs. SCE for a period of 500s. For the second experiment, the potential of the WE (GaN sample electrode S2) was set at $U = -1.2\text{V}$ vs. SCE for another period of 500s. The second experiment was repeated with the GaN sample electrode S1. The resulting current through the electrochemical cell was recorded during both experiments and readings of OCPs were taken before and after each potentiostatic experiment.

Initially, the potentiostatic experiments for the GaN sample electrode S2 produced a steady state cathodic current in the μA range accompanied with current oscillations (Fig. III.20), which was interpreted as an indication of the existence of cracks in the electrode's epoxy glue coverage. After the deposition of an additional layer of epoxy glue on the electrode (leaving only the surface of the sensing element exposed), the steady state current cathodic at the same potential went down to the nA range (Fig. III.21). The potentiostatic experiments for the GaN sample electrode S1 produced steady state cathodic current in the nA range (Fig. III.19).

Fig. III.19 Variation of current density with time for GaN sample electrode S1 in 0.1M KCl solution at cathodic polarization

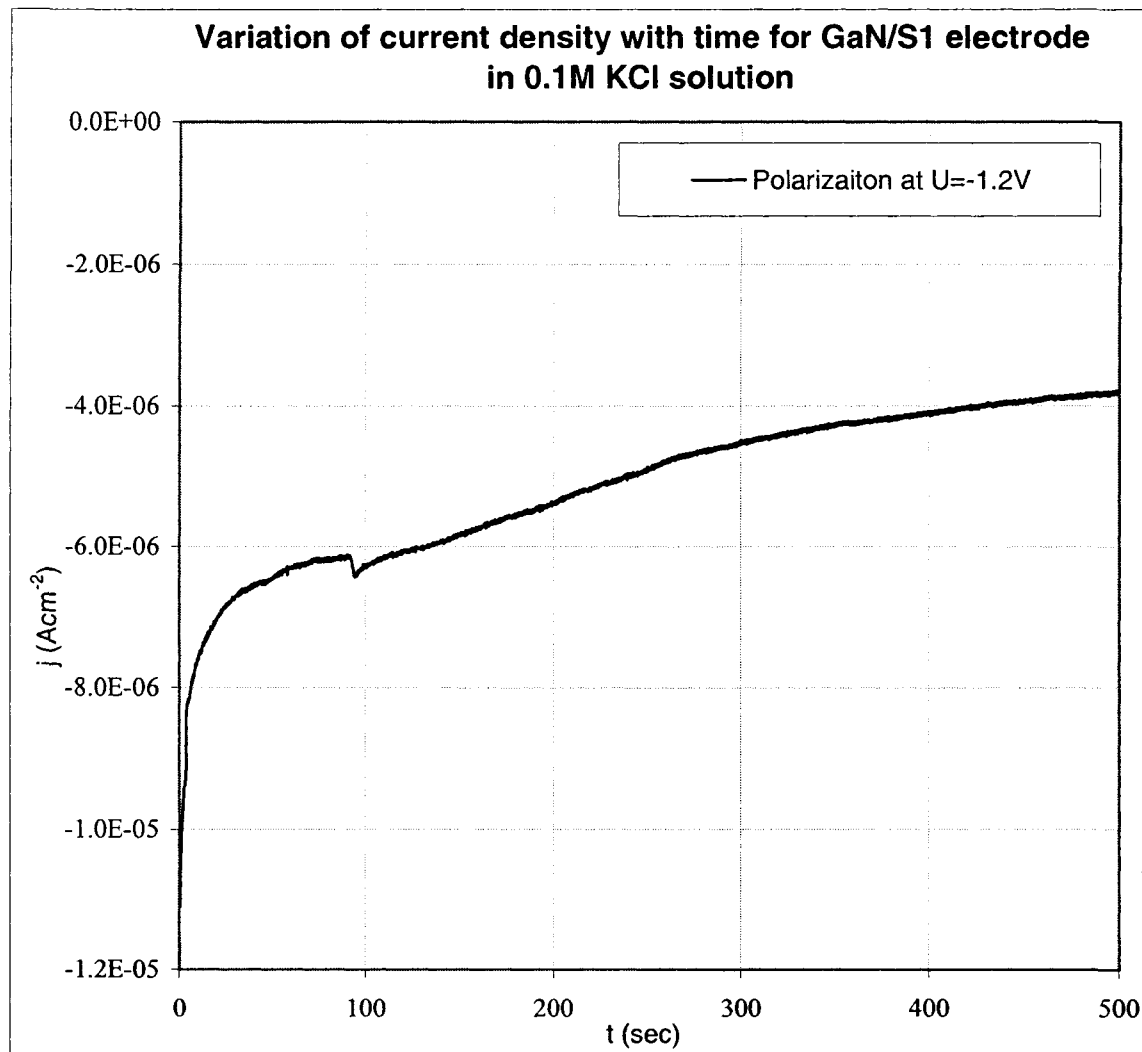


Fig. III.20 Current oscillations for GaN sample electrode S2 at cathodic polarization in 0.1M KCl solution

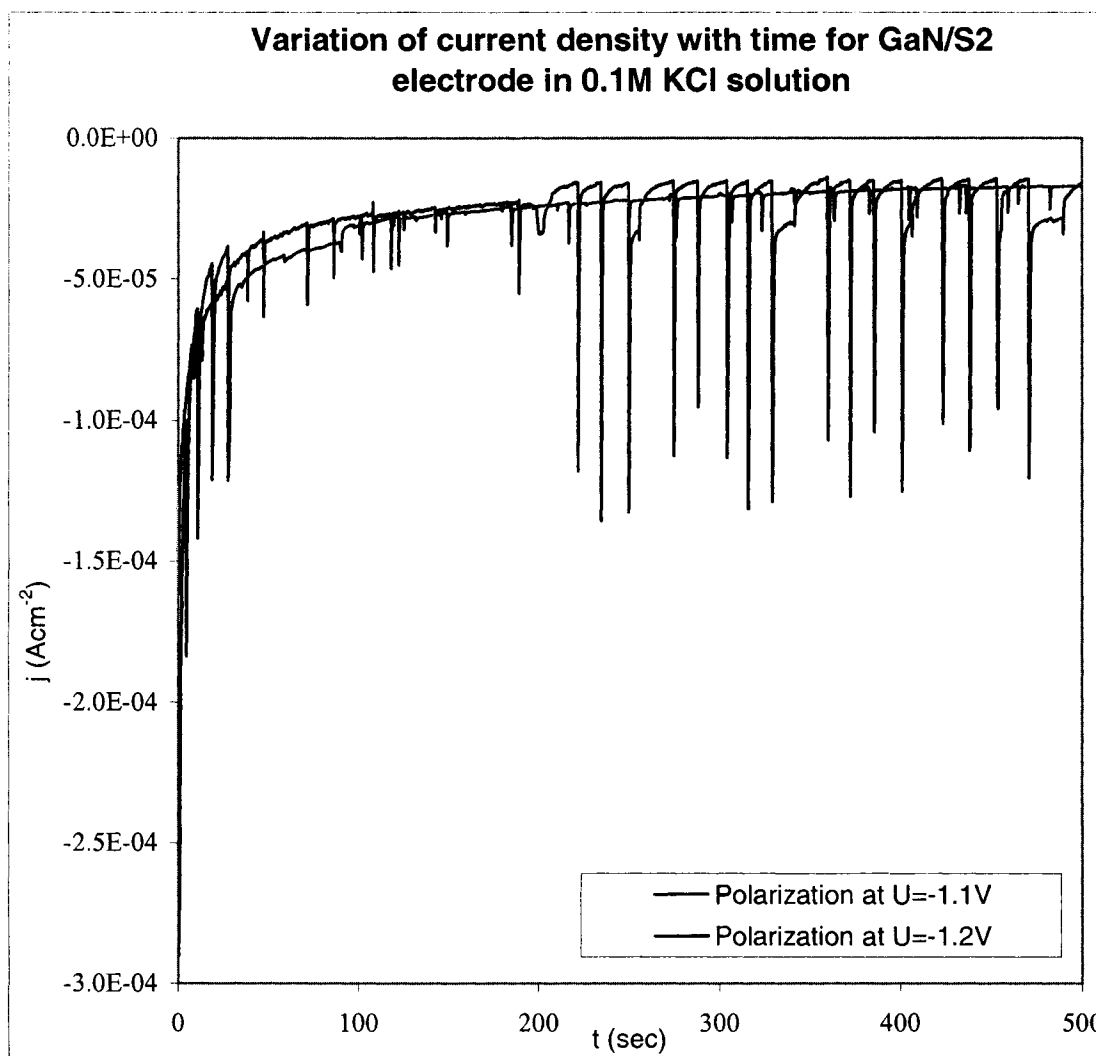
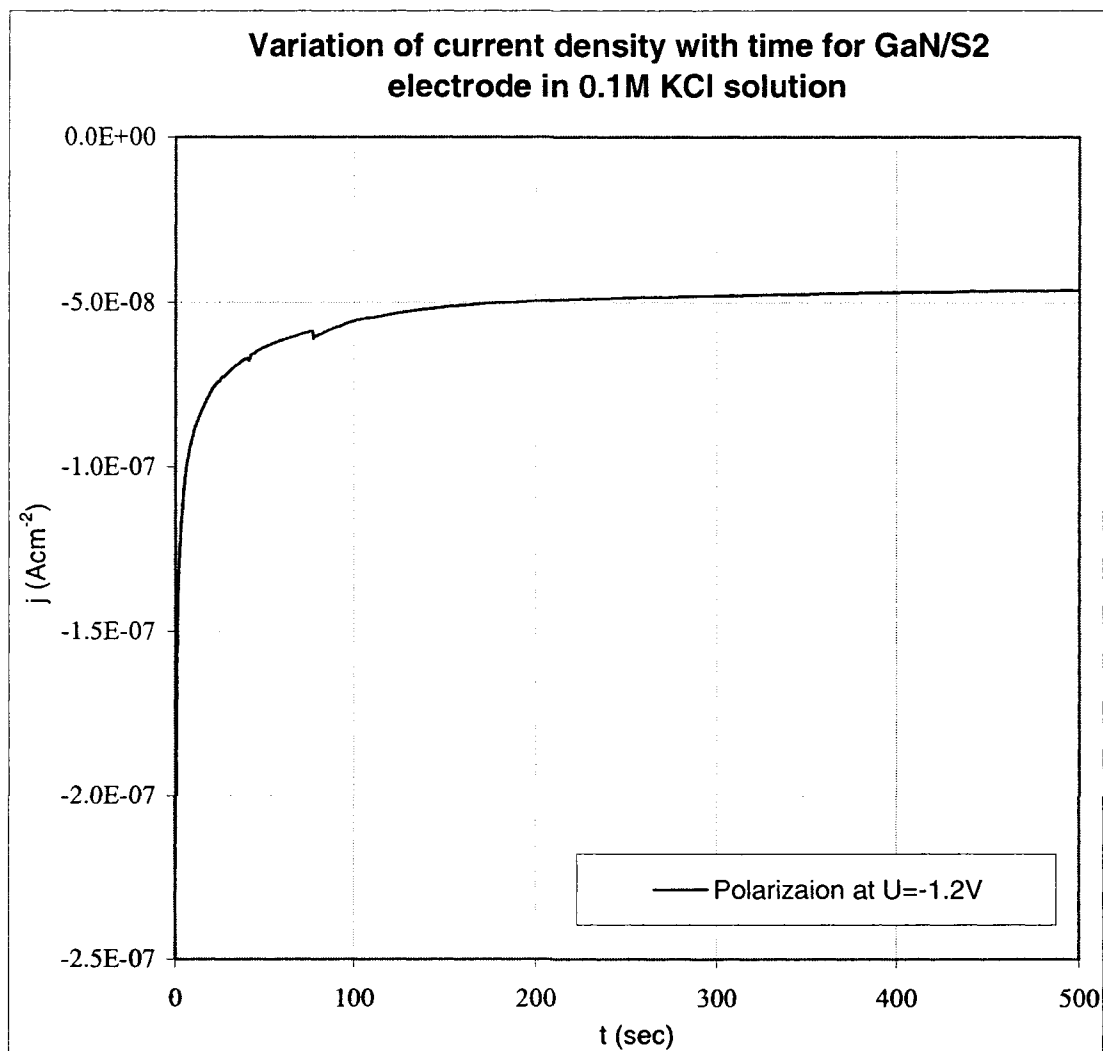


Fig. III.21 Variation of current with time for GaN sample electrode S2 in 0.1M KCl solution at cathodic polarization after deposition of additional layer of epoxy glue



For both GaN sample electrodes S1 and S2 the cathodic current can be attributed to the hydrogen evolution reaction (Reaction 3.7).

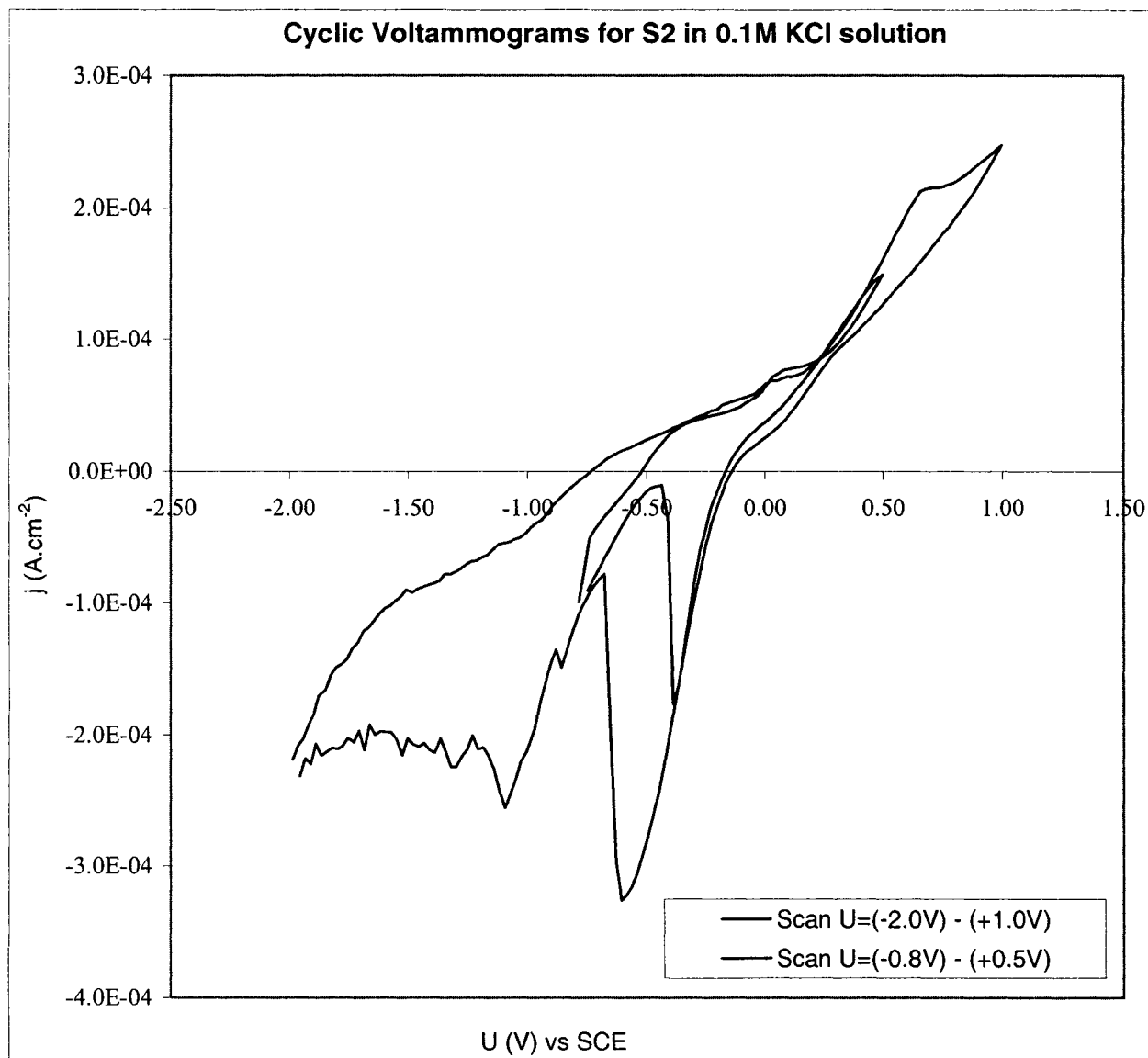
III.10. Range Tests

The range tests involved polarization of GaN sample electrode S2 to high positive and high negative potentials in 0.1M KCl solution to investigate the etching processes of the GaN semiconductor material. According to Chazalviel et al (2000), metallic gallium is unstable at potentials more positive than $U = -0.8V$ vs SCE in acidic solutions. Therefore, if the potential of the GaN working electrode is set to values more positive than $U = -0.8V$ vs SCE, the GaN surface is expected to start etching, altering the properties of the semiconductor electrode. To induce

Results & Discussion

surface etching, the GaN sample electrode S2 was subjected to two subsequent scans with increasing end potential values. The first scan was performed between potentials $U = -0.8\text{V}$ and $U = +0.5\text{V}$ versus SCE. During the second scan, the polarization of the electrode was done between potentials $U = -2.0\text{V}$ and $U = +1.0\text{V}$ versus SCE. The obtained cyclic voltammograms during the two scans are presented on Fig. III.22.

Fig. III.22 Cyclic voltammograms for GaN sample electrode S2 for two scans with increasing end potentials



The shape of both cyclic voltammograms suggests that an anodic current in the μA range flows through the working semiconductor electrode during the forwards scans (to more positive potentials), and a cathodic current in the μA range flows during the reverse scans (to more negative potentials). Similar cyclic voltammograms have been recorded by Huygens et al (2000)

for n-GaN in KCl solution. According to their study, the anodic current during the forward scans may be associated with the following oxidation reactions:

- Formation of chlorine gas (conduction band reaction):



- Oxidation of water (See I.7, Reaction 3.5)
- Etching of the GaN semiconductor electrode (See III.7, Reaction 3.6)

The cathodic current during the second scan is characterized by two distinct peaks. The first peak occurs approximately at a potential $U = -0.6V$ vs SCE, and the second peak occurs at a potential $U = -1.1V$ vs SCE. Only the first peak is visible on the cyclic voltammogram recorded for the first scan, and it occurs at a potential $U = -0.4V$ vs SCE. The first peak of the cathodic current observed during both scans is most probably associated with the hydrogen evolution reaction (See I.7, Reaction 3.7). The second peak may be due to the reduction of the chlorine gas formed during the forward scan according to the reduction reaction:



Cyclic voltammetry is a technique that can provide information for the type of the electrochemical reactions (oxidation or reduction) occurring at the semiconductor/electrolyte interface, but cannot define the specific reactions. Therefore, one of the objectives of the surface studies described in the next chapter was to provide additional insights about the reactions that actually took place in the electrochemical system during the range tests.

III.11. Surface Study of GaN and InGaN Sample Electrodes

SEM-EDS surface studies of the GaN and InGaN unused sample materials and the of the used GaN sample electrode S2 were carried out to determine:

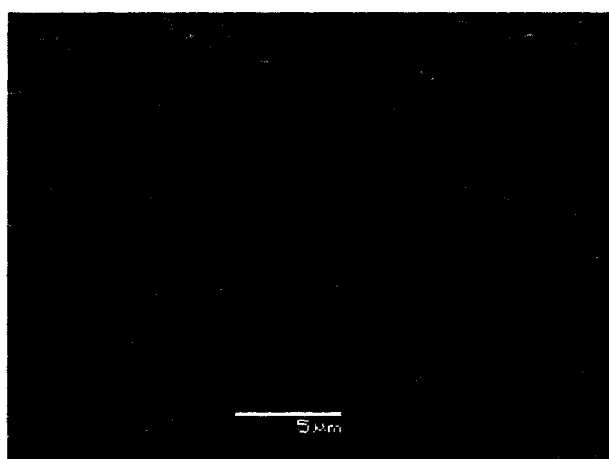
- The morphology and surface polarity of the GaN and InGaN thin films; and
- Whether and how the surface of the GaN sample electrode S2 had been altered as a result of the performed range tests (see Chapter III.10).

Results & Discussion

To improve the quality of the SEM images, the surface of the GaN and InGaN samples was coated with an atomic layer of gold. The results of the surface study were complemented by EDS elemental analysis. The SEM images (secondary electron mode) obtained for the GaN and InGaN unused samples are presented on Fig. III.23. Fig. III.24 presents images of different regions of GaN sample electrode S2 after performing the range tests, described in the previous chapter.

Fig. III.23 SEM images of GaN and InGaN unused sample materials

a) GaN thin film



b) InGaN thin film

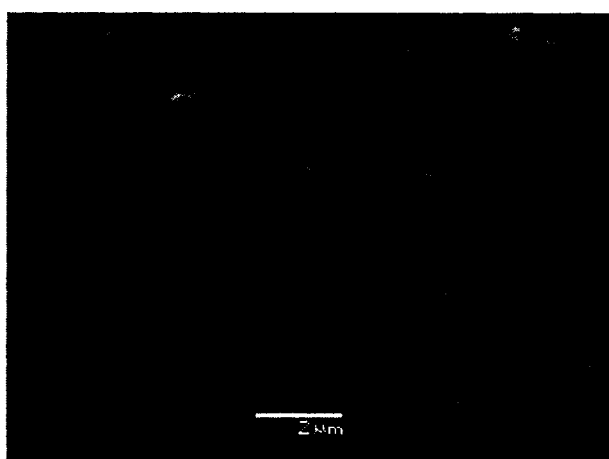


Fig. III.24 SEM images of GaN sample electrode, S2 after experiments

a)



b)



The SEM image of GaN unused sample material (Fig. III.23a) shows that the surface of the GaN film is quite smooth. The observed polarity, however, is mixed as initially assumed, i.e. there are Ga-face regions (dark background) and N-face regions (lighter hexagonal structures). The polarity of the observed structures has been defined on the basis of the study by Hellman (1998),

Results & Discussion

which found that the hexagonal faceting is a characteristic of N-face GaN material. Similar GaN images have been presented by Piquette et al. (1999), who defined the mixed polarity of the GaN samples the same way as above. According to Piquette et al. (1999), a mixed polarity surface can be formed due to the different growth rates of G-faces and N-faces of the GaN crystal. Unlike the GaN, the InGaN samples show better-defined surface polarity with less N-face regions.

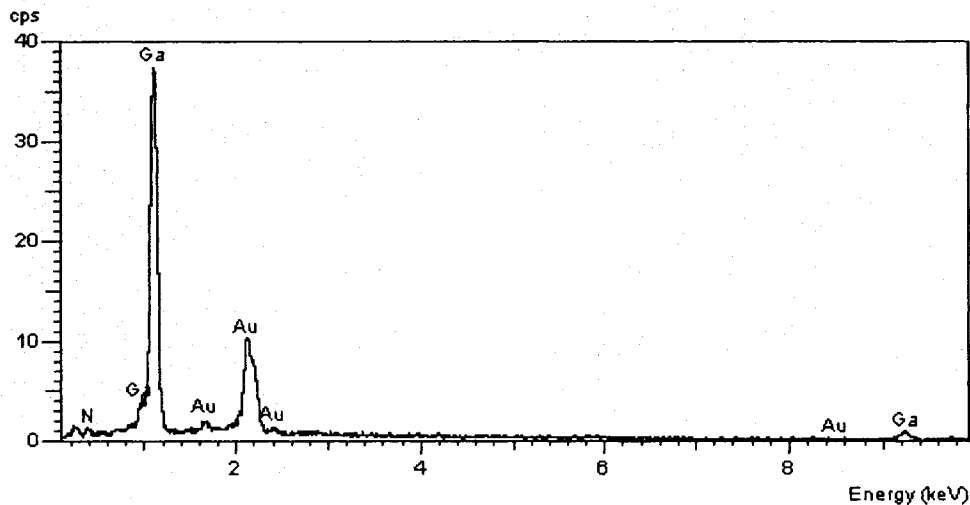
SEM images of the GaN unused material show that, although Ga-face regions are dominant, the N-face regions occupy a substantial part of the surface. This observation corroborates the results of the calibration and impedance measurements with the GaN sample electrodes, which were consistent with a mixed polarity surface.

The SEM image of the GaN sample electrode S2 after the range tests indicates a significant alteration of the surface and confirms the assumption, made during these tests, that the surface of the GaN electrode would be etched under high anodic polarization.

The results from the EDS study of the GaN and InGaN unused sample materials are presented on Fig. III.25. Fig. III.26 presents the results from the EDS study of different regions of GaN sample electrode S2 after the performed range tests.

Fig. III.25 EDS results for GaN and InGaN unused sample materials

a) GaN before experiments



b) InGaN before experiments

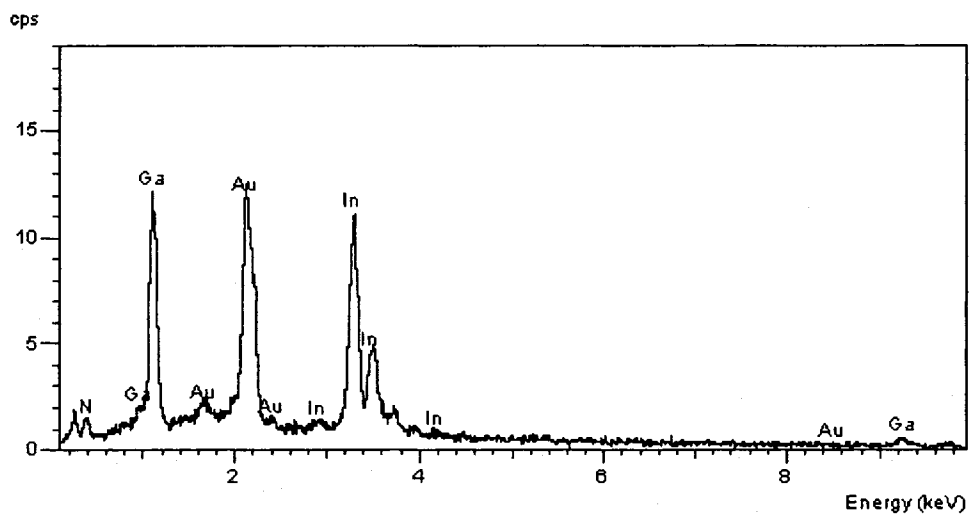
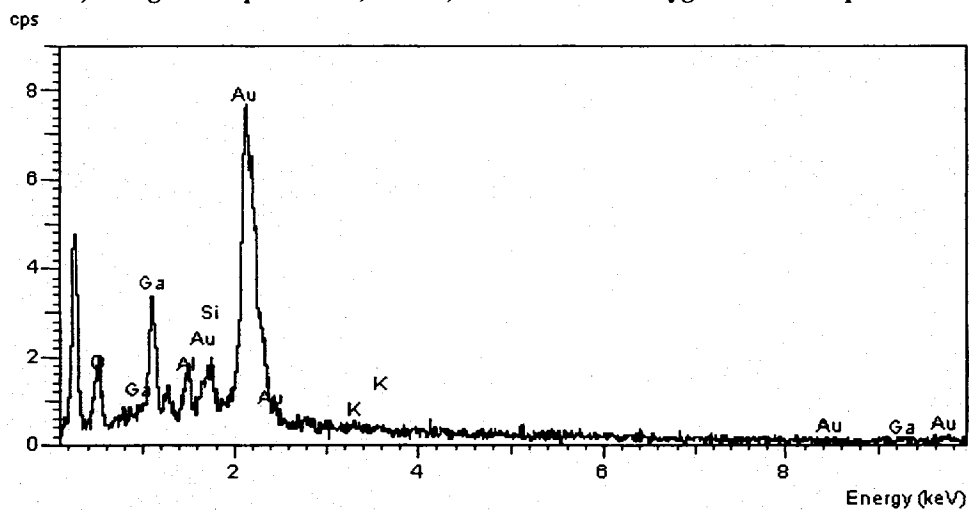
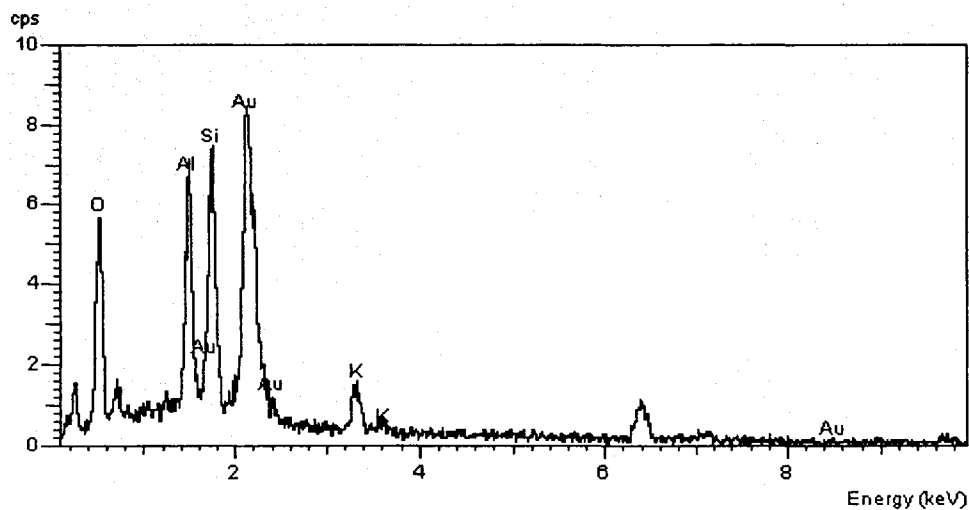


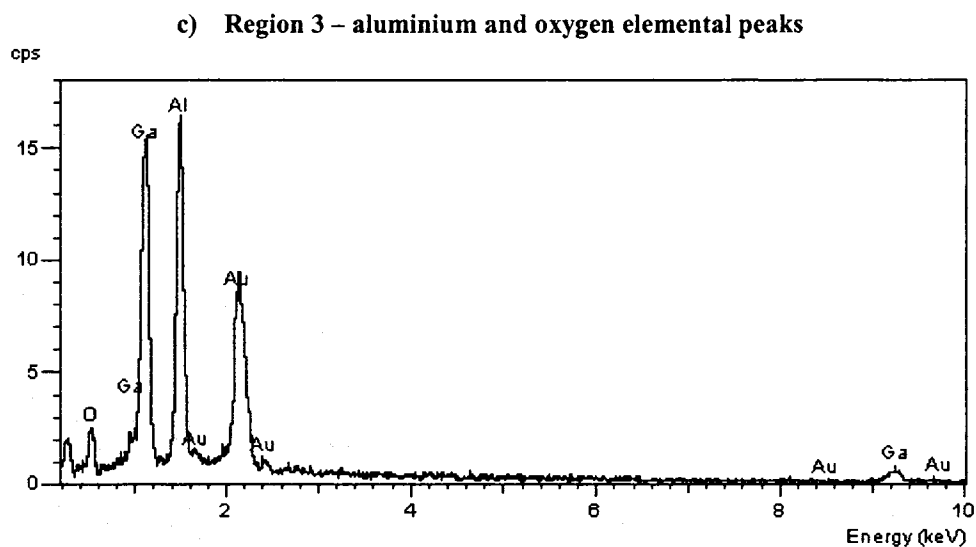
Fig. III.26 EDS results for different regions of GaN sample electrode, S2 after experiments

a) Region 1 – potassium, silicon, aluminium and oxygen elemental peaks



b) Region 2 – potassium, silicon, aluminium and oxygen elemental peaks





The EDS elemental analysis shows that before the experiments, the surface of the GaN sample contained only Ga and N atoms (Fig. III.25a). However, after the experiments, the GaN sample electrode S2 shows strong O and Al elemental peaks on EDS diagrams for one sample region (Fig. III.26c) and additional Si and K elemental peaks in two other regions (Fig. III.26a and b). This indicates substantial alteration of the surface of the GaN sample electrode S2 as a result of performed range tests. This alteration may have proceeded as follows:

- The presence of an Al and O elemental peaks is an evidence of deep etching of the surface down to the sapphire substrate (Al_2O_3);
- The presence of a Si elemental peak is probably caused by unintentional doping of the GaN sample during the GaN growth process. Although any doping of the GaN semiconductor material would potentially cause changes in the electrode behaviour, the Si is only present in EDS diagrams of the GaN sample electrode S2 after the range tests i.e. close to the sapphire substrate. No Si is observed on the EDS diagram of the unused GaN sample and therefore, we can assume that the Si doping effect occurs deep in the GaN film and not at the surface and this, cause none or negligible effect on the behaviour of the GaN sample electrode S2.
- The presence of a K suggests that during the range tests in 0.1M KCl electrolyte, the K^+ cations in the solution have been adsorbed on the electrode surface.

IV. SUMMARY AND CONCLUSIONS

This chapter provides a summary of the main results obtained from the study of GaN and InGaN semiconductor electrodes and outlines the conclusions derived from these results. It also provides some recommendations for future research on the use of GaN and InGaN semiconductors as materials for the preparation of ion selective electrodes.

IV.1. Summary of Research Results and Conclusions

Conclusions regarding each portion of the research are presented below, including response time of the GaN and InGaN semiconductor electrodes, sensitivity to various anions and to pH variations, response range and slope of electrodes, reproducibility of results, cyclic voltammetry (CV) and electrochemical impedance spectroscopy (EIS) experiments, potentiostatic experiments and range tests, and, finally, surface studies and elemental analysis.

IV.1.1. Response Time

The GaN and InGaN semiconductor electrodes demonstrate relatively fast response times ranging from 50 to 700 s, depending on the electrolyte, electrode material, and activity of anions in solution. For both GaN and InGaN electrodes, the dependence of response time on electrolyte follows the order of adsorption capacity of the anions, i.e., the response time is faster for anions with strong adsorption capacity and slower for anions with weak adsorption capacity. In the investigated electrolyte solutions, the response time is faster for GaN sample electrodes than for the InGaN sample electrode. The variation of the electrode response time versus anion activity in the electrolyte solutions is not consistent and hence no pattern of variation could be established.

The reproducibility of response time measurements is good: the variation in response time between two series of measurements, performed two months apart from each other, in the same electrolyte is 50s or less. The response time of electrodes during the second series of measurements is consistently slower than during the first series, which may be attributable to contamination of the electrode semiconductor sensing element or to a hysteresis effect caused by using the electrodes in various electrolyte solutions. The impact of these factors on the response time can be minimized if an adequate procedure for cleaning the electrode surface before each measurement is employed.

IV.1.2. Total Potentiometric Response

OCP measurements with the GaN and the InGaN electrodes in KF, KNO₃, KCl, HOC₆H₄COONa, KSCN, CH₃COOK and KClO₄ electrolyte solutions show that the total potentiometric response of the GaN electrode is higher than the one of the InGaN electrode. The only exception occurs in the KBr and KI solutions, in which the response of the InGaN electrode is higher than the response of the GaN electrode. Hence, with the exception of Br⁻ and I⁻ anions, the sensitivity of the GaN electrode to anions is better than that of the InGaN electrode.

IV.1.3. Calibration Curves (Response Range and Slope)

In most electrolyte solutions, the slope of both the GaN and InGaN electrodes varies between 52 and 65mV/decade of activity change. These slopes are close to the theoretical value of 58.3mV/decade calculated from the Nikolsky-Eisenman equation and compare favourably with previous results for GaN electrodes reported in the literature (Chaniotakis et al. 2004). However, large deviations from the theoretical slope value occur for the GaN electrode in KClO₄, KBr and KI electrolytes and for the InGaN electrode in KBr and KI electrolytes. In these solutions, the slope of the electrodes is lower than the theoretical value (between 29 and 44mV/decade of activity change). This may be attributed to strong interaction between species in solution and the electrode material.

The linearity regions for the GaN and InGaN electrodes are found to be relatively narrow. In CH₃COOK solutions no linear region exists at all. In some other electrolytes (e.g., GaN electrode in KF, KNO₃, and KCl; InGaN electrode in KCl and KSCN), the linearity region encompasses only one or two decades of activity change. Such linear regions are narrower than the reported in the literature for GaN electrodes in the same test solutions (Chaniotakis et al, 2004). These narrow linear regions may be due to the mixed polarity of the sensing elements of the electrodes and/or to contamination of the electrode surface. In other solutions (KClO₄, KBr and KI), however, the regions of linearity are larger and extend over the entire range of measured activities (five decades of activity change between 10⁻¹ and 10⁻⁶M). In these solutions, the GaN electrode linear regions compare favourably with the linear regions of four decades of activity change, reported by Chaniotakis et al. (2004).

IV.1.4. Reproducibility

During a sequence of measurements, the GaN electrode shows a drift of the OCP from more negative to less negative values over time. This drift is most probably caused by either a change in the surface composition of the electrode sensing element and/or by potential changes in other parts of the measuring system. The average drift value of 1.7mV per day compares favourably with the drift values of commercially available ISEs (NICO 2000 Ltd., 2005).

The InGaN sample electrode exhibits a low reproducibility of measured electrode potential that may be caused by taking the OCP readings in some solutions before the system has attained equilibrium.

IV.1.5. pH Response

Both the GaN and InGaN electrodes demonstrate good pH response. A linear variation of measured OCP with respect to pH is observed in the pH range between 7.5 and 3. The pH sensitivity of the semiconductor electrodes can be attributed to the selective interaction between the positively charged surface of the sensing element and the hydroxide anions in the solution, which results in a decrease of OCP with decreasing pH.

IV.1.6. CV Results

The reactions occurring at the semiconductor/electrolyte interface have been identified by comparing the positions of the valence and conduction band edges of the semiconductor electrode with the standard potentials of the redox couples present in the electrolyte solutions. Further investigation accounting for other factors such as reaction kinetics and adsorption phenomena will be needed to determine whether a particular reaction is taking place or not.

IV.1.7. EIS study

The EIS study shows that the space charge layer of the semiconductor dominates the impedance of the electrochemical system at high frequencies. The large scattering of results observed at low frequencies for the GaN electrode impedes the analysis of the impedance spectra for this electrode. The shape of the impedance curve for the InGaN electrode at low frequencies (below approximately 10kHz) suggests that the impedance of the electrochemical system is dominated

Summary and Conclusions

by the slow diffusion of electroactive species across the layer of adsorbed ions present at the surface of the electrode. The equivalent circuit model proposed in this study can effectively fit the EIS experimental data.

IV.1.8. Potentiostatic Experiments

The potentiostatic experiments with the GaN electrode show that, under cathodic polarization, a cathodic current flows through the electrochemical cell, which is most probably due to the hydrogen evolution reaction.

IV.1.9. Range Tests

The range tests were carried out to investigate the etching process of the GaN semiconductor as well as the behaviour of the GaN electrode under strong cathodic and anodic polarizations. The anodic current that flows under anodic polarization suggests that the oxidation reactions taking place at the semiconductor/electrolyte interface are most probably the formation of chlorine gas, the oxidation of water, and the oxidative etching of GaN. The cathodic current could be attributed to the reduction of chlorine gas, formed during the anodic scan, to chloride anions.

IV.1.10. Surface Studies and Elemental Analysis

The SEM studies suggest that both GaN and InGaN samples have mixed a polarity surface, which exposes both the Ga-face (or InGa-face) and the N-face of the semiconductor crystal. The EDS elemental analysis confirmed that the surface of one of the GaN electrodes had been etched during the range tests.

IV.2. Overall Conclusions

Overall, this work has shown that GaN and InGaN electrodes are sensitive to all the tested anions and have a good pH response. Additionally, the experimental results demonstrated that under open circuit conditions the surface of the electrodes remains mechanically intact and chemically stable in all electrolyte solutions. This suggests that electrodes constructed of GaN and InGaN would have good stability and excellent lifetime. As such, GaN and InGaN semiconductors could be employed to fabricate ion selective electrodes that are both durable and easy to use. The surface polarity of the semiconductor crystal may have a major impact on the overall

Summary and Conclusions

performance of the electrodes and, in particular, on the reproducibility of results and on the slope and linear range of the calibration curves.

Attempts to describe the electrochemical reactions occurring at the semiconductor/electrolyte interface were partially successful as potential charge transfer reactions were identified but no definite knowledge was obtained about the reactions that actually occur in the electrochemical system. Thus, some recommendations for further research are made below.

IV.3.Recommendations for Further Research

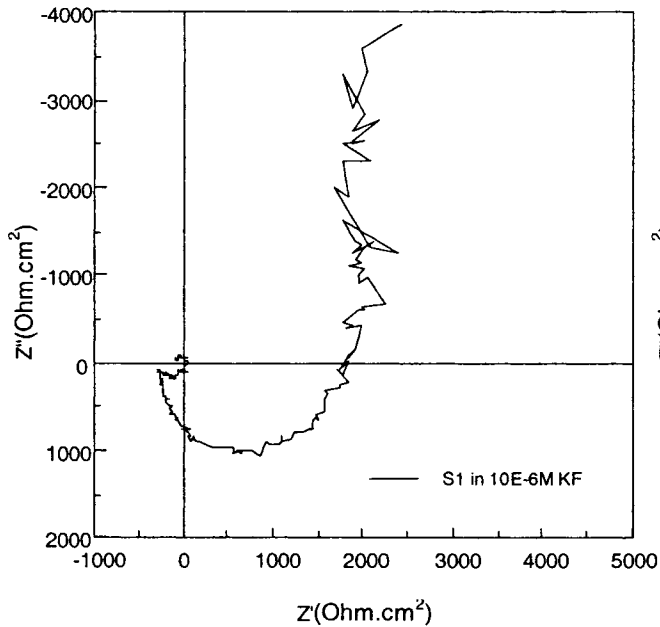
The main recommendation is to investigate the effect of surface polarity on the response of the electrode by repeating all the calibration experiments using GaN and InGaN samples with homogeneous Ga-face or InGa-face surfaces. A study to identify the electrochemical reactions occurring in the electrochemical system would provide additional insights on the processes occurring at the semiconductor/electrolyte interface and would complement the work commenced in this thesis. Although the range tests and the subsequent surface studies confirmed that the GaN electrode could be etched under certain experimental conditions, it would be useful to define the exact potential at which the etching begins, as it is directly related to the electrode chemical stability.

All the above recommendations only pertain to the evaluation of GaN and InGaN semiconductors as ion selective electrodes. Once their potential is confirmed, the research should be expanded to take into account factors such as the availability of high quality semiconductor crystals, cost, mechanical design, and maintenance of the electrodes to determine whether GaN and InGaN can ultimately be used for the fabrication of commercial ion selective electrodes.

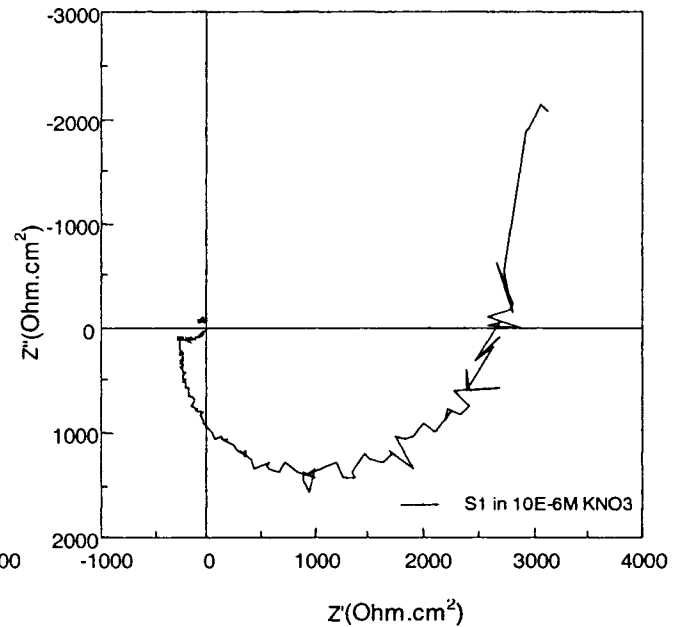
V. APPENDIX A

Nyquist Plots for GaN sample electrode S1 and InGaN sample electrode S3 in electrolyte solutions with concentrations from 10^{-6}M to 10^{-2}M

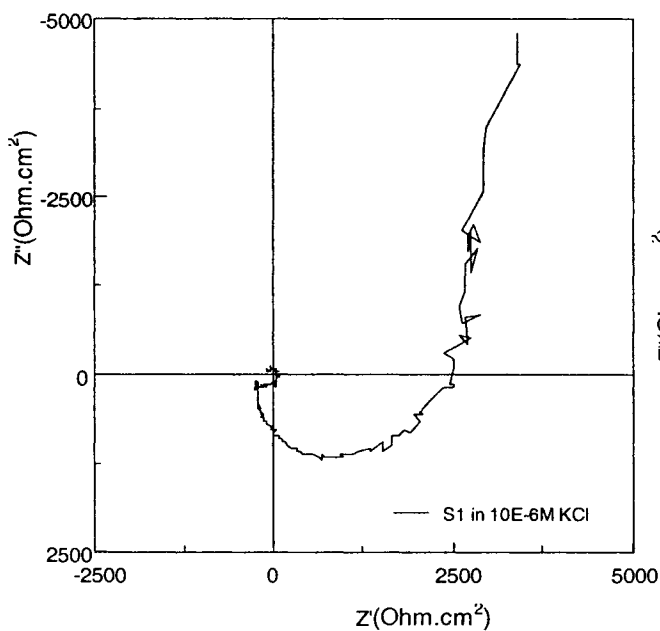
1) GaN/S1 in 10^{-6}M KF solution



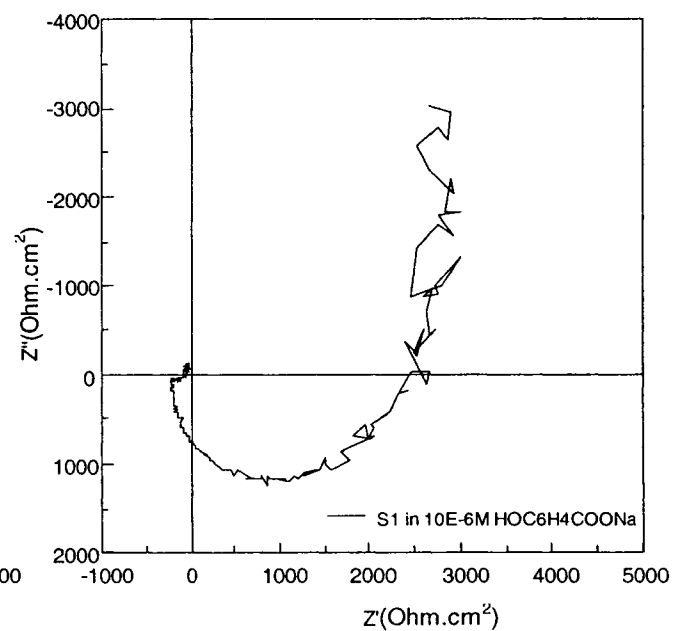
2) GaN/S1 in 10^{-6}M KNO₃ solution



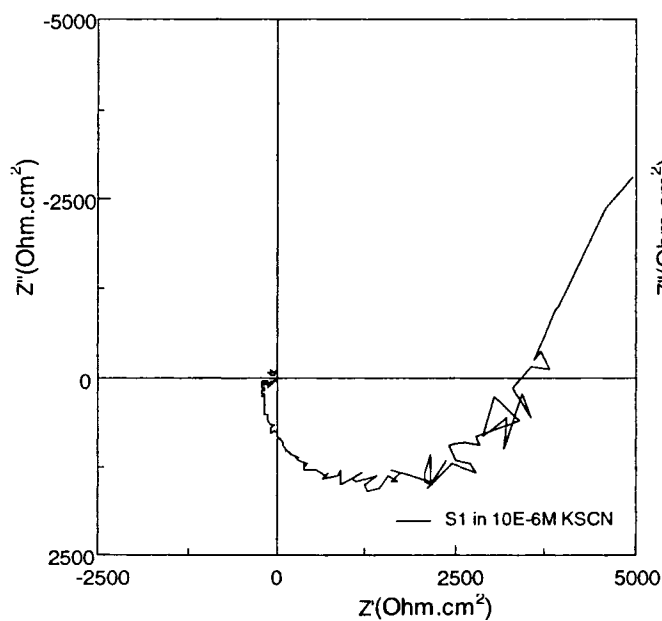
3) GaN/S1 in 10^{-6}M KCl solution



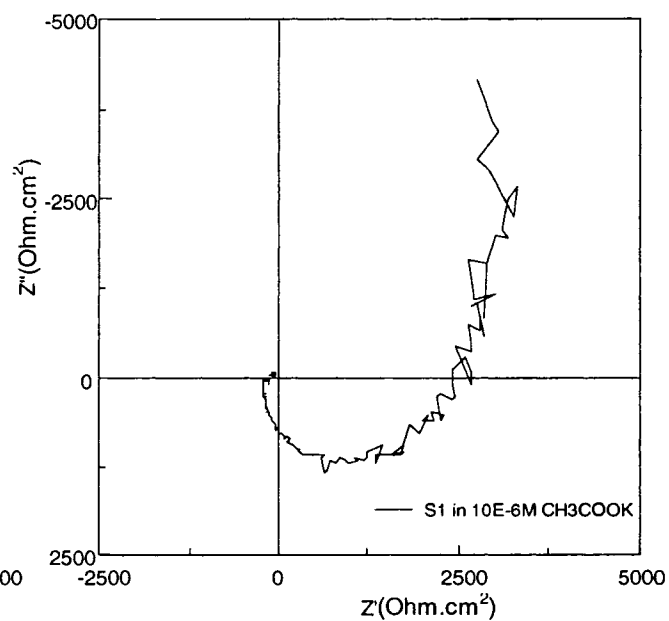
4) GaN/S1 in 10^{-6}M HOC₆H₄COONa solution



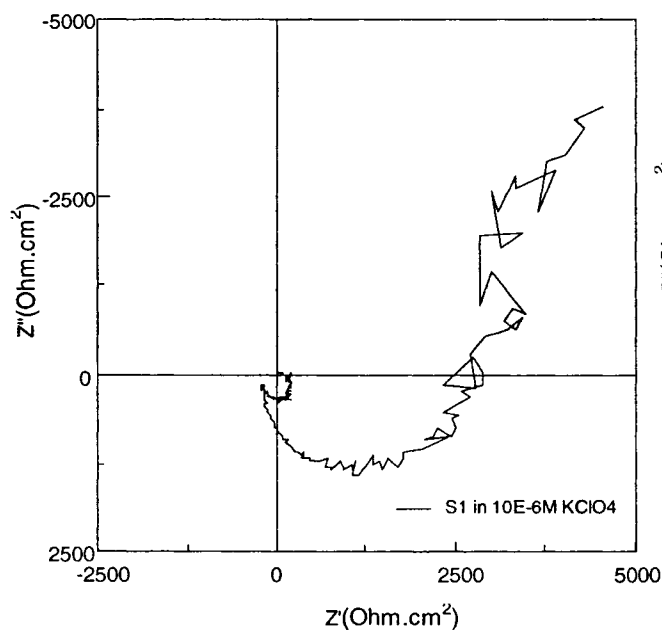
5) GaN/S1 in 10^{-6} M KSCN solution



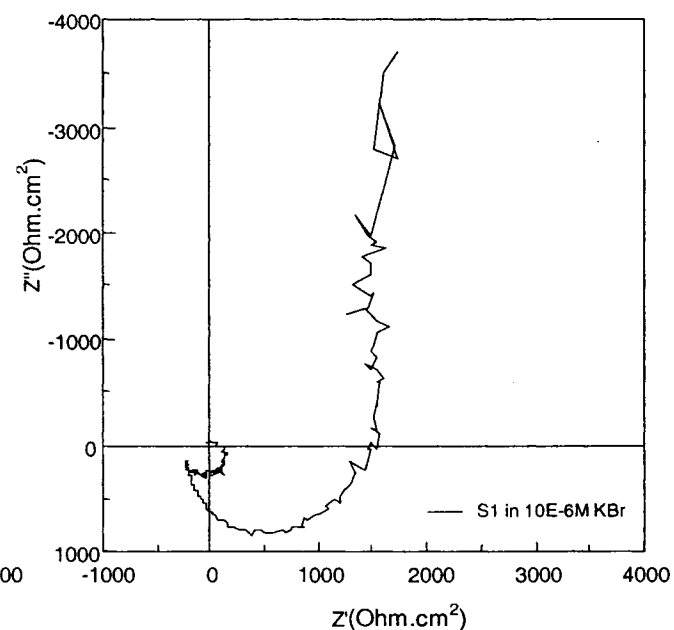
6) GaN/S1 in 10^{-6} M CH_3COO solution



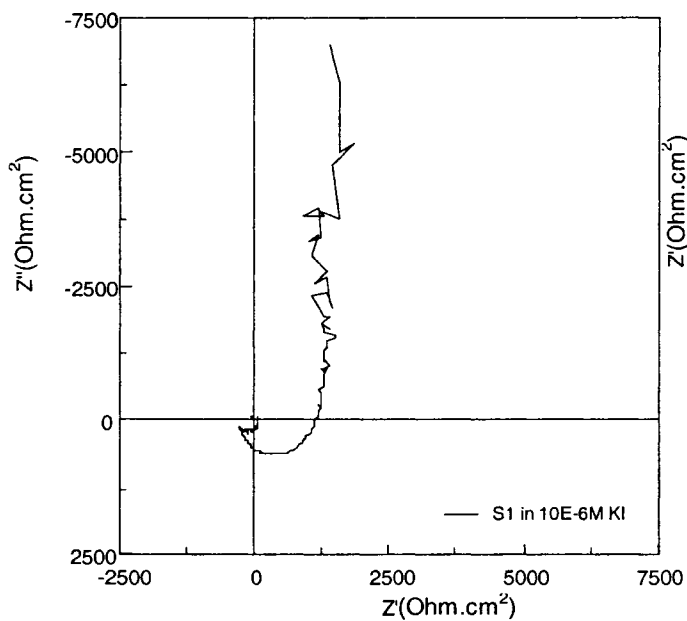
7) GaN/S1 in 10^{-6} M KClO_4 solution



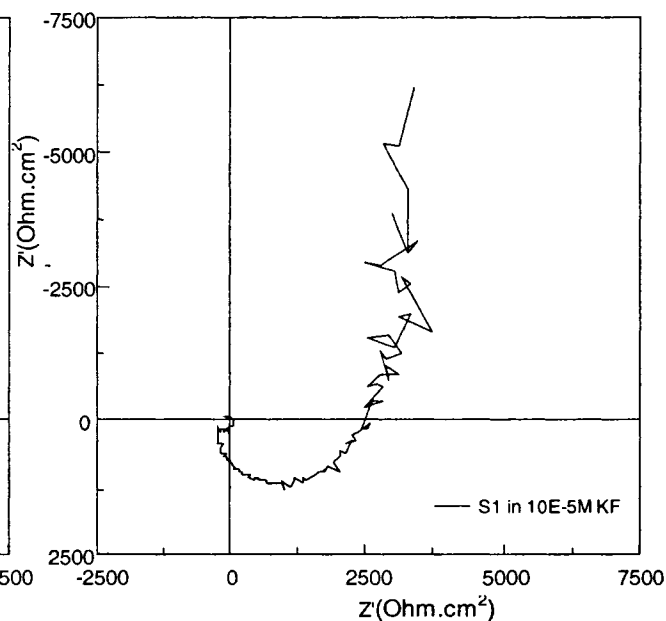
8) GaN/S1 in 10^{-6} M KBr solution



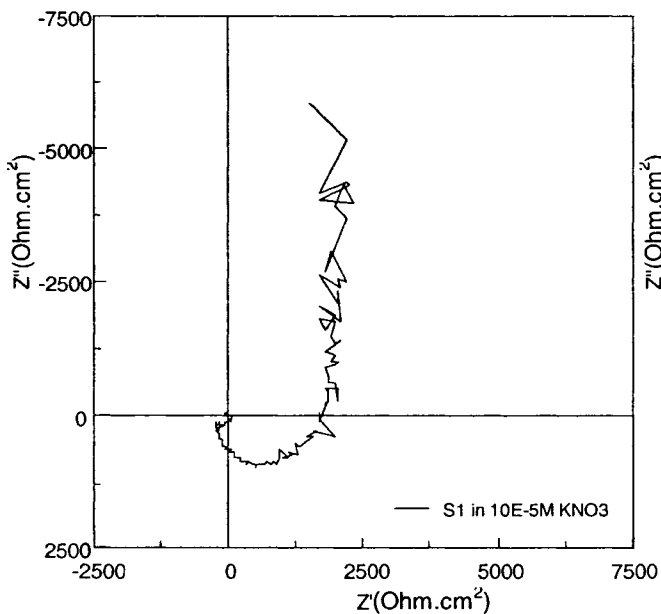
9) GaN/S1 in 10^{-6} M KI solution



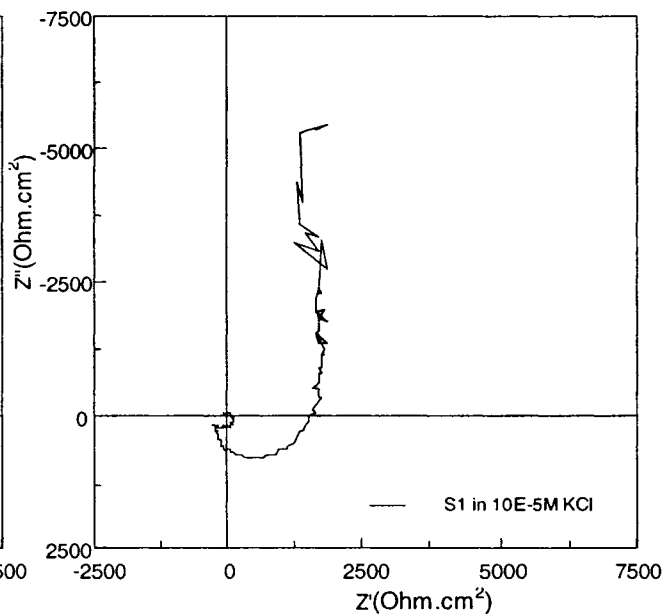
10) GaN/S1 in 10^{-5} M KF solution



11) GaN/S1 in 10^{-5} M KNO₃ solution

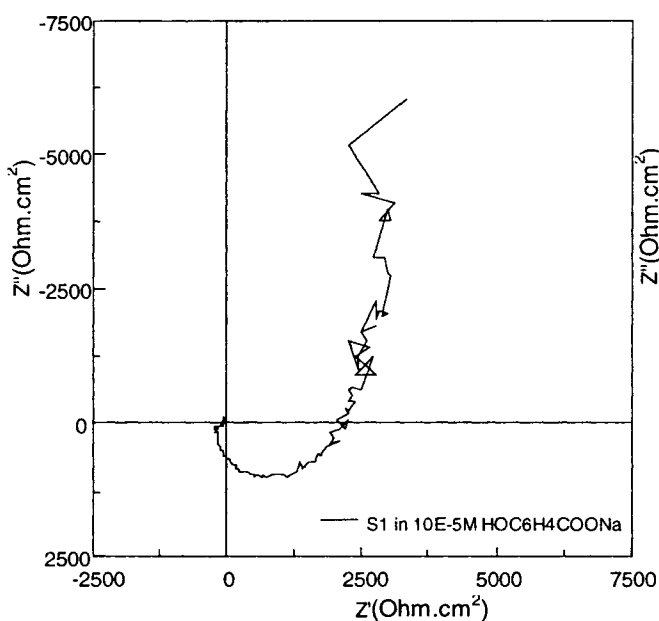


12) GaN/S1 in 10^{-5} M KCl solution

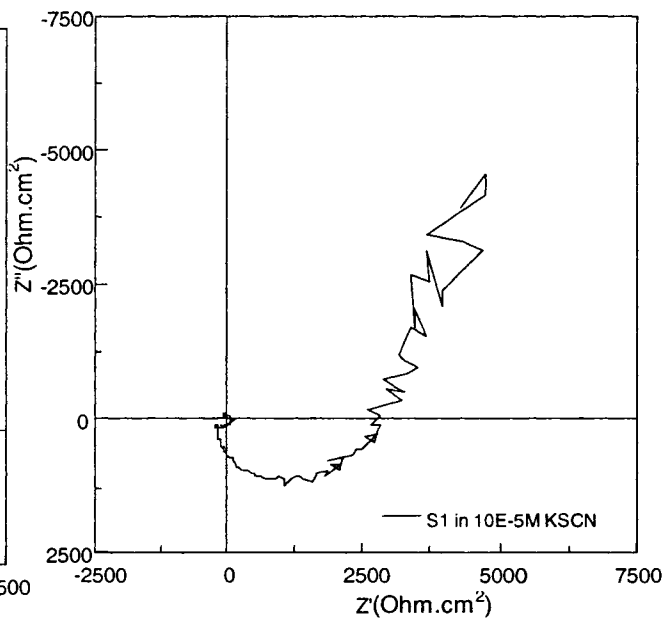


Appendix A

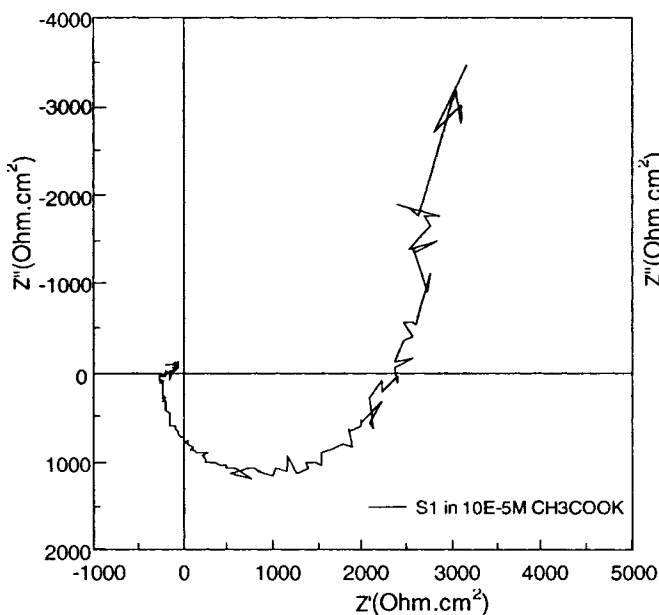
13) GaN/S1 in 10^{-5} M $\text{HOC}_6\text{H}_4\text{COONa}$ solution



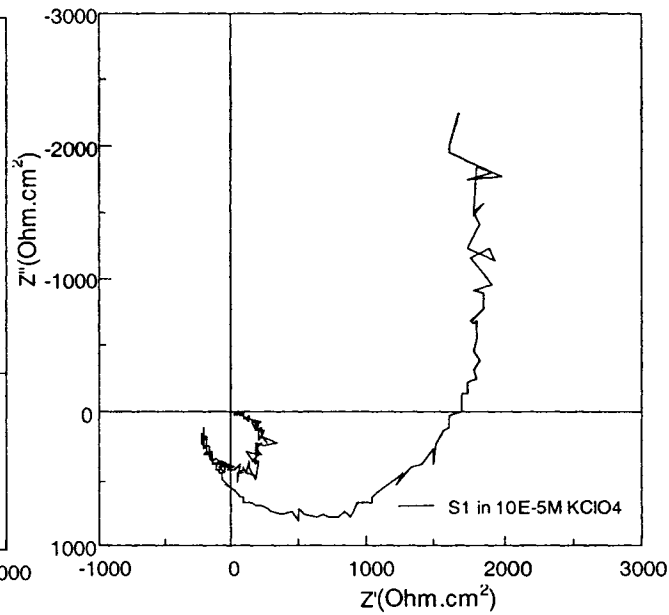
14) GaN/S1 in 10^{-5} M KSCN solution



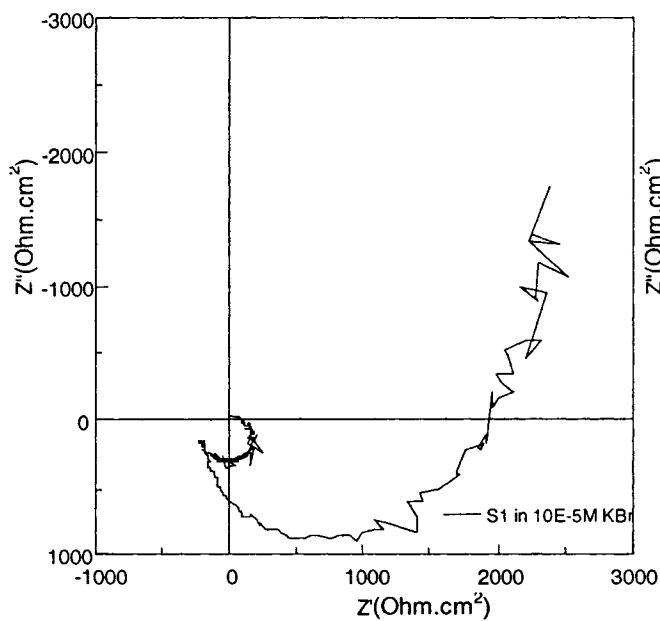
15) GaN/S1 in 10^{-5} M CH_3COOK solution



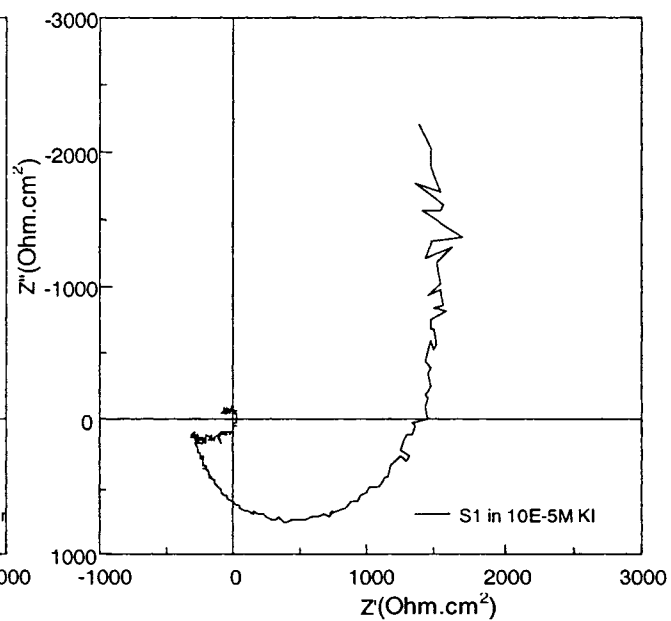
16) GaN/S1 in 10^{-5} M KClO_4 solution



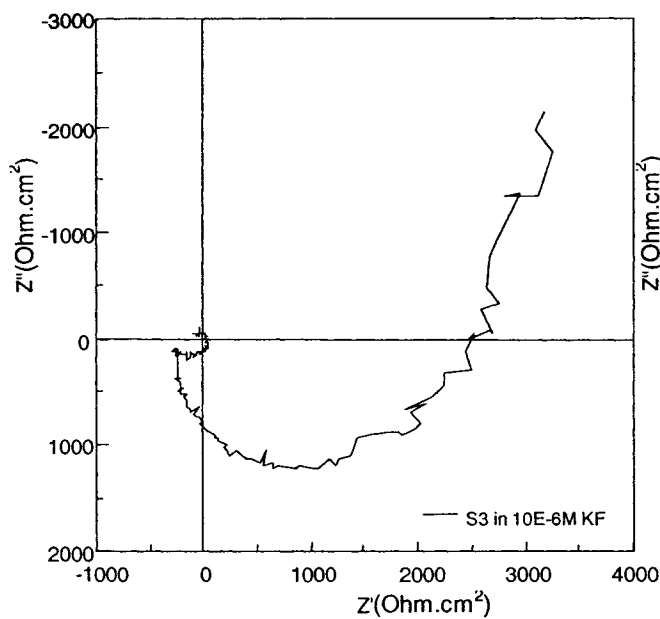
17) GaN/S1 in 10^{-5} M KBr solution



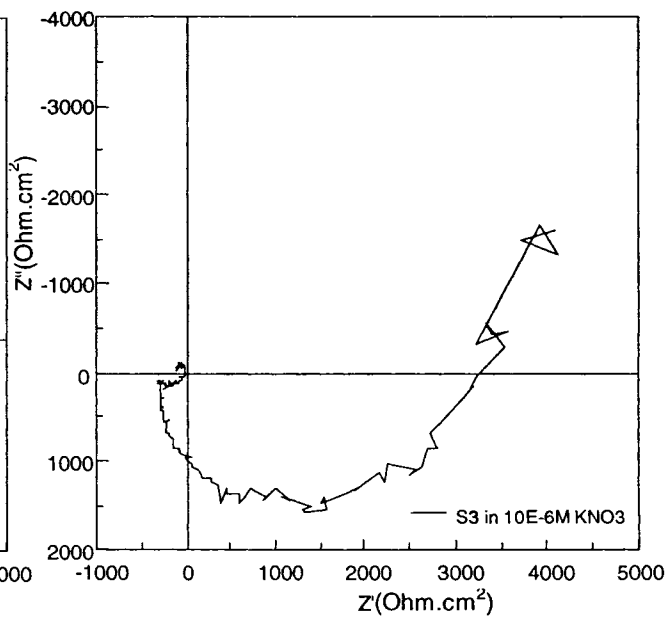
18) GaN/S1 in 10^{-5} M KI solution



19) InGaN/S3 in 10^{-6} M KF solution

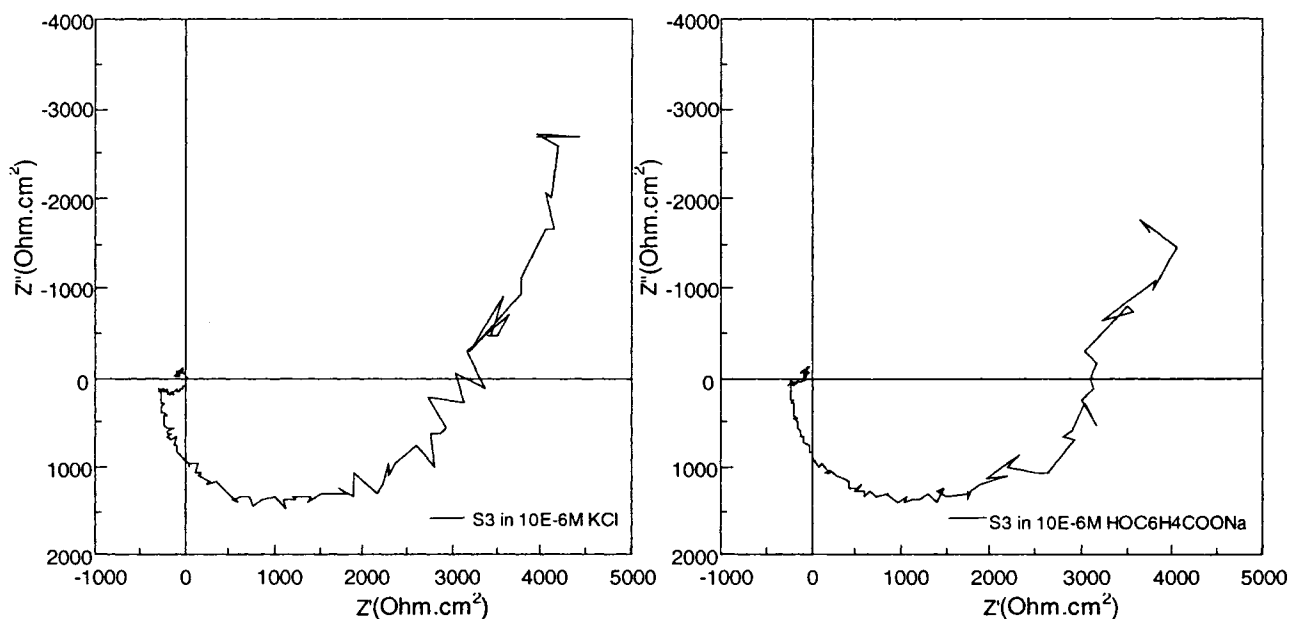


20) InGaN/S3 in 10^{-6} M KNO₃ solution

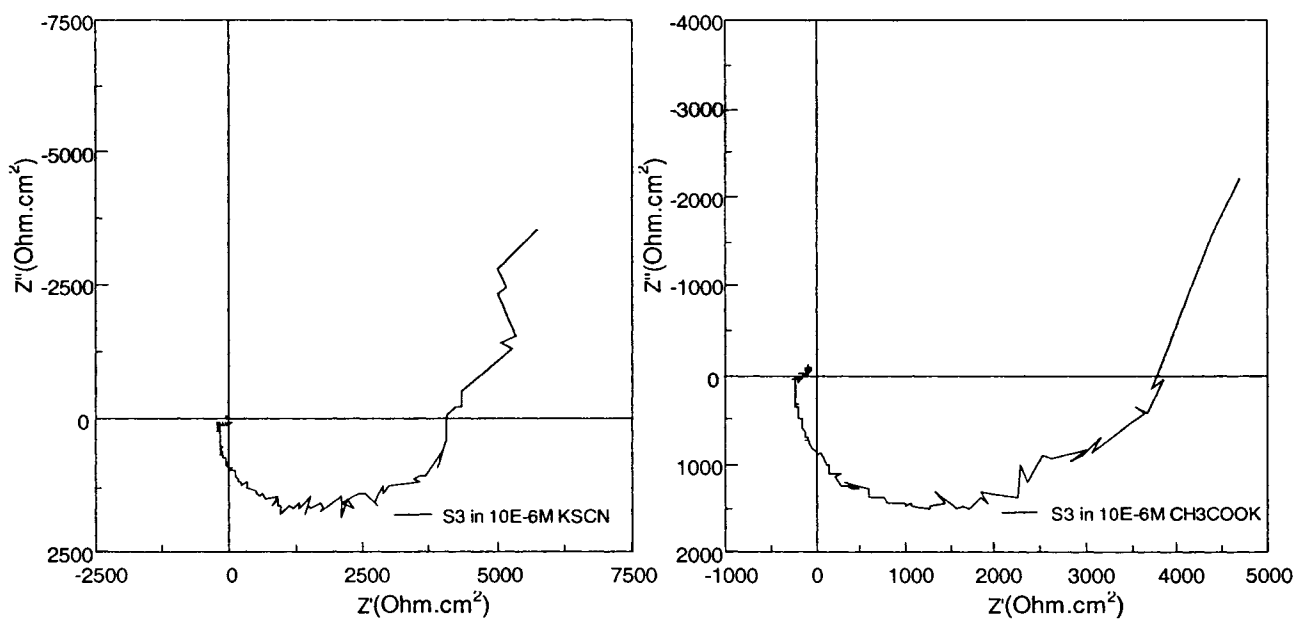


Appendix A

21) InGaN/S3 in 10^{-6} M KCl solution 22) InGaN/S3 in 10^{-6} M HOC₆H₄COONa solution

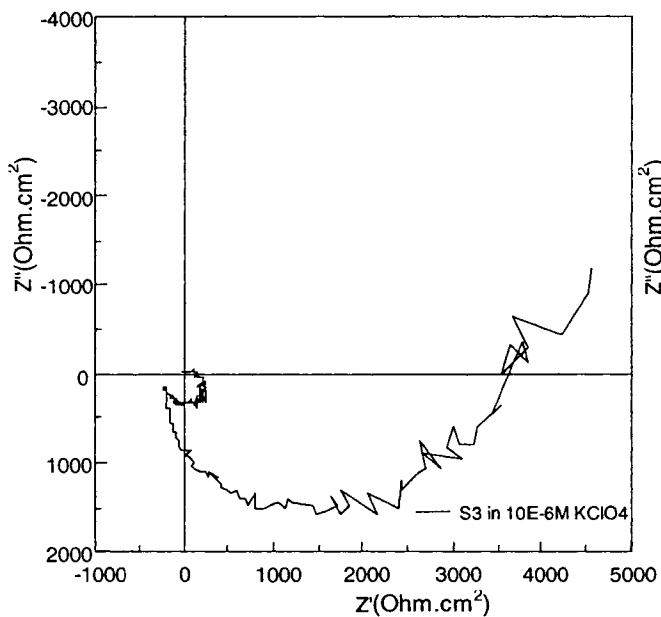


23) InGaN/S3 in 10^{-6} M KSCN solution 24) InGaN/S3 in 10^{-6} M CH₃COOK solution

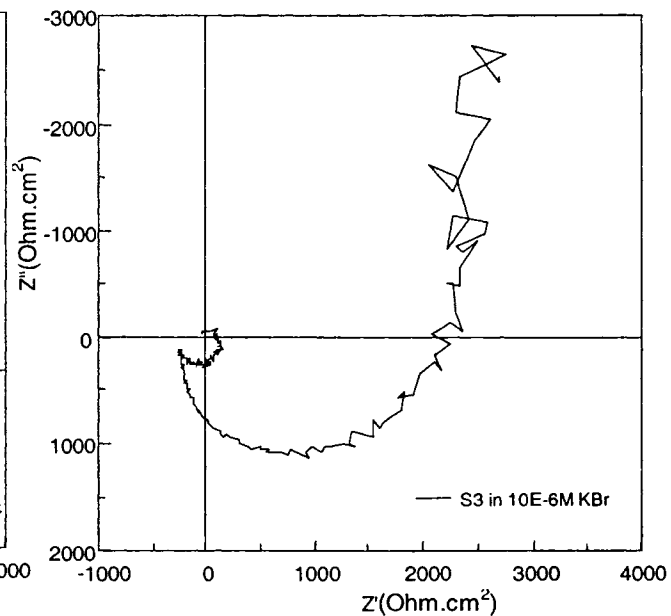


Appendix A

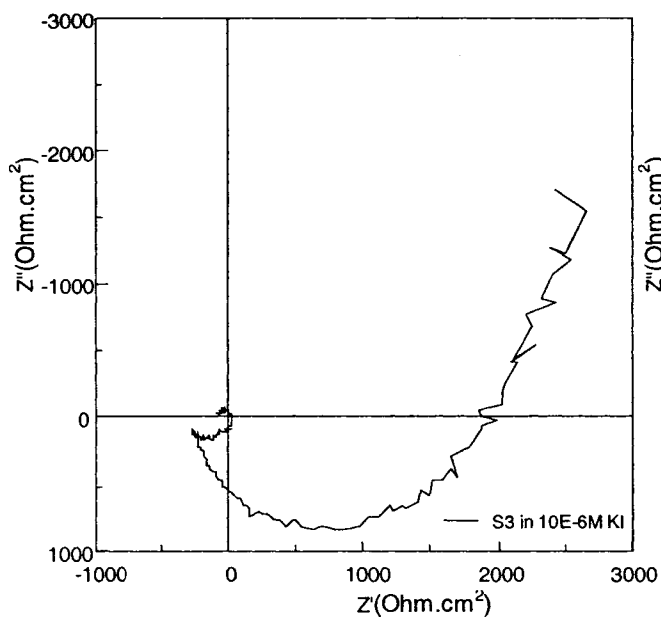
25) InGaN/S3 in 10^{-6} M KClO₄ solution



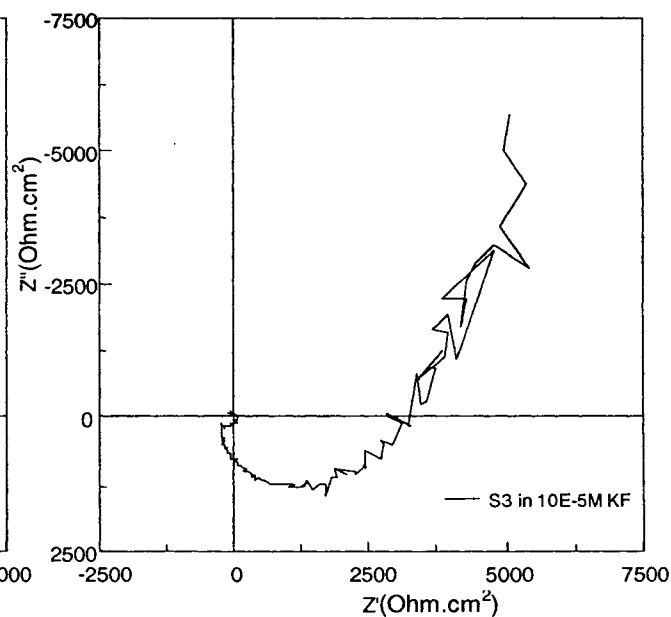
26) InGaN/S3 in 10^{-6} M KBr solution



27) InGaN/S3 in 10^{-6} M KI solution

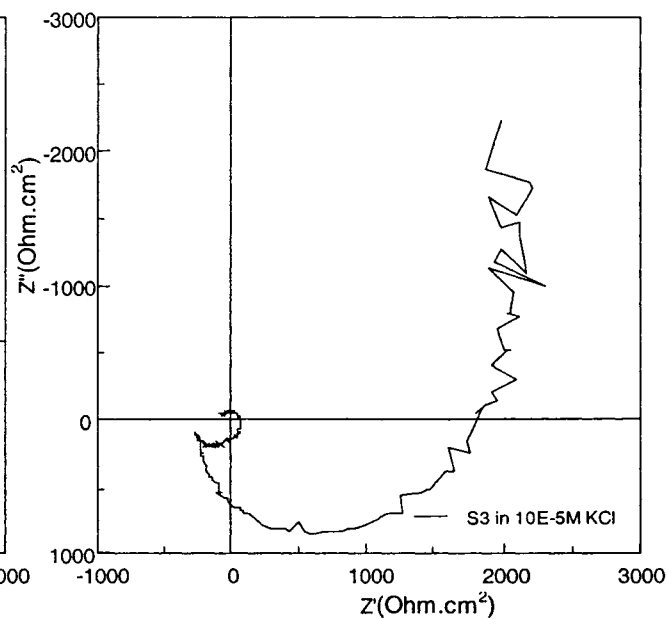
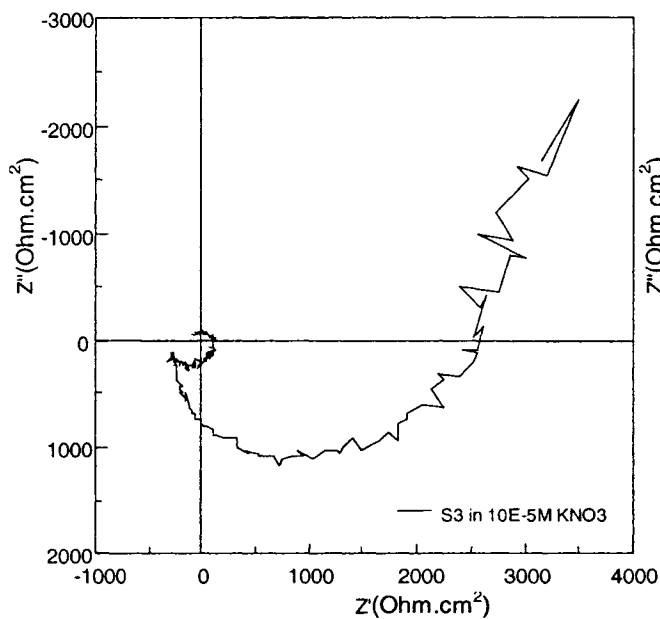


28) InGaN/S3 in 10^{-5} M KF solution



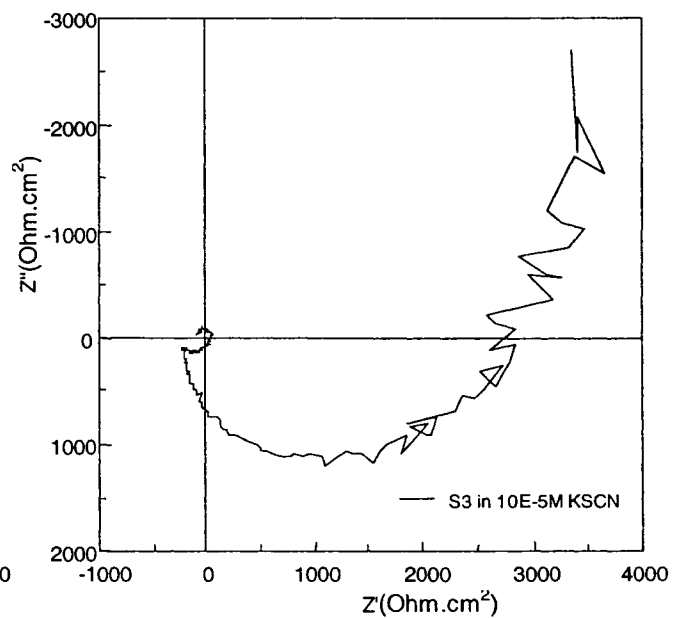
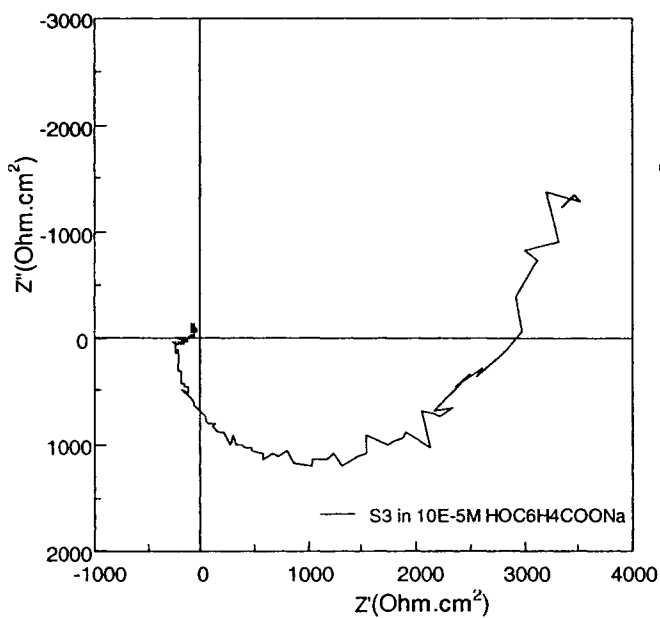
29) InGaN/S3 in 10^{-5} M KNO_3 solution

30) InGaN/S3 in 10^{-5} M KCl solution



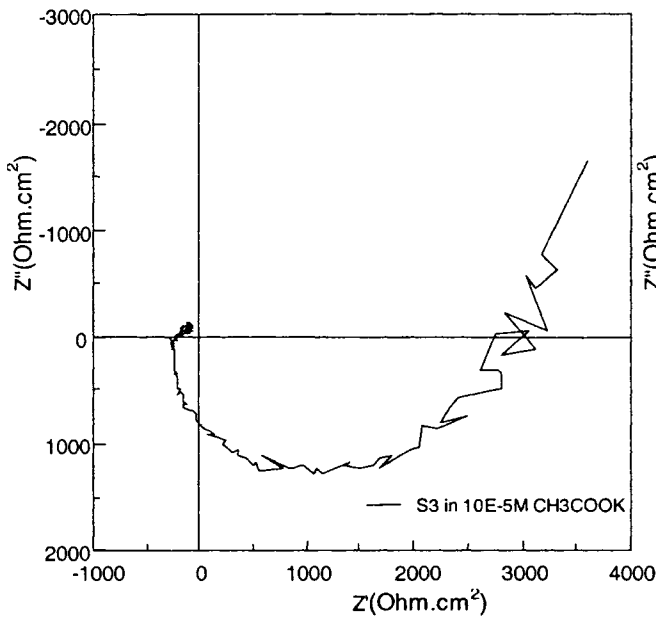
31) InGaN/S3 in 10^{-5} M $\text{HOC}_6\text{H}_4\text{COONa}$ solution

32) InGaN/S3 in 10^{-5} M KSCN solution

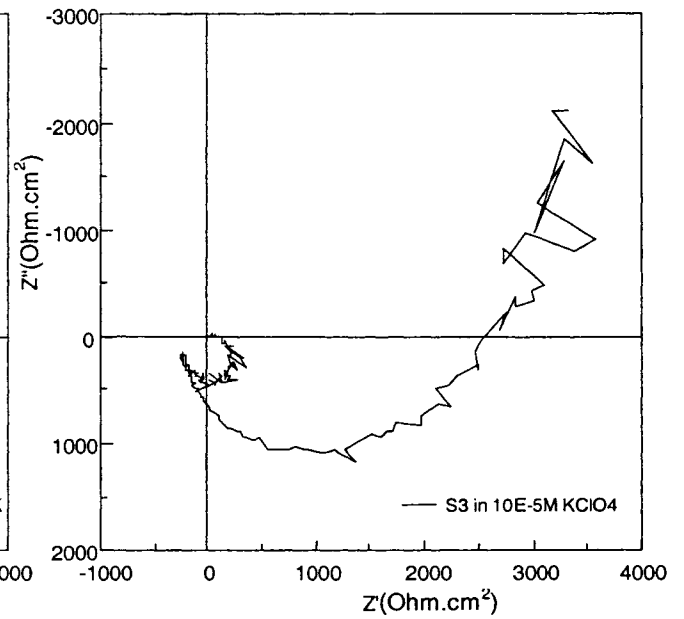


Appendix A

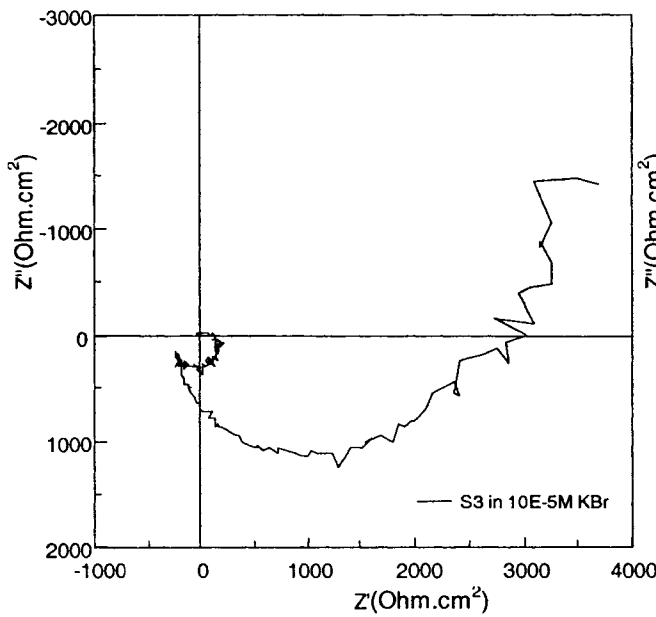
33) InGaN/S3 in 10^{-5} M CH_3COOK solution



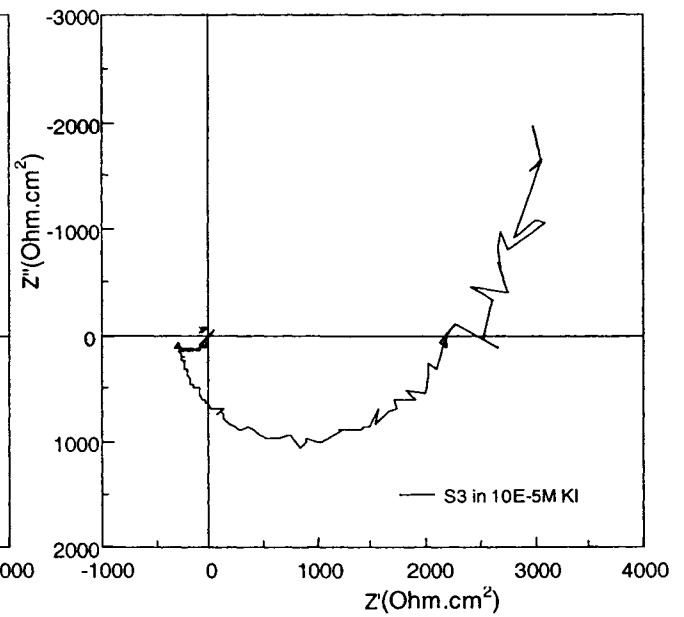
34) InGaN/S3 in 10^{-5} M KClO_4 solution



35) InGaN/S3 in 10^{-5} M KBr solution



36) InGaN/S3 in 10^{-5} M KI solution



VI. REFERENCES

1. Alexandrov D., “*Electronic structure and properties of nitride semiconductor compound alloys*”, Journal of Optoelectronics and Advanced Materials, 2005, Vol. 7 (1), pgs. 51-58.
2. Alexandrov D., Butcher S., Tansley T., “*Electron band structure and optical properties of InN and related alloys*”, Physica status solidi. A - Applications and Material Science, 2006, Vol. 203 (1), pgs. 25 -34.
3. Alifragis Y., Konstantinidis G., Georgakilas A., Chaniotakis N.; “*Anion Selective Potentiometric Sensor Based on Gallium Nitride Crystalline Membrane*”; Electroanalysis, 2005, Vol. 17 (5-6), pgs.527-531.
4. Analytical Technology, Inc, “*Continuous, on-line monitoring for optimal fluoride levels*”, available at: http://www.analyticaltechnology.com/Product_Lit_PDF/L-A15-82.pdf, accessed: November, 2006.
5. Aroutiounian V., Arakelyan V., Shahnazaryan G., Stepanyan G., Khachaturyan E., Turner J., “*Investigations of the structure of the iron oxide semiconductor-electrolyte interface*”, C.R. Chimie, 2006, Vol. 9, pgs. 325–331.
6. Aroutiounian V., Arakelyan V., Shahnazaryan G., Stepanyan G., Turner J., Kocha S., “*Investigations of the Fe_{1.99}Ti_{0.01}O₃–electrolyte interface*”, Electrochimica Acta, 2000, Vol. 45, pgs. 1999–2005.
7. Bailey P., “*Analysis with Ion-Selective Electrodes*”, Second edition, Heyden & Son Ltd, Spectrum House, Philadelphia, USA, 1980.
8. Bansal A., Turner J., “*Suppression of band edge migration at the p-GaInP₂/H₂O interface under illumination via catalysis*”, Journal of Physical Chemistry B, 2000, Vol. 104 (28), pgs. 6591-6598.
9. Beach J., Collins R., Turner J., “*Band-Edge Potentials of n-Type and p-Type GaN*”, Journal of the Electrochemical Society, 2003, Vol. 150 (7), pgs. A899 – A904.
10. Bourgeois W., Romain A., Nicolasb J., Stuetz R.; “*The use of sensor arrays for environmental monitoring: interests and limitations*”; Journal of Environmental Monitoring, 2003, Vol. 5, pgs. 852-860.
11. Bousse L., Hafeman D., Tran N., “*Time-dependence of the Chemical Response of Silicon Nitride Surfaces*”, Sensors and Actuators B1, 1990, Vol. 1, pgs. 361-367.
12. Callister, Jr., W., “*Materials Science and Engineering – An Introduction*”, Fourth Edition, John Wiley & Sons, Inc, Toronto, Canada, 1997.
13. Chaniotakis N., Alifragis Y., Georgakilas A., Konstantinidis G., “*GaN-based anion selective sensor: Probing the origin of the induced electrochemical potential*”; Applied Physics Letters, 2005, Vol. 86, Art. No. 164103.

References

14. Chaniotakis N., Alifragis Y., Konstantinidis G., Georgakilas A., "*Gallium Nitride-based potentiometric Anion Sensor*"; Analytical Chemistry, 2004, Vol. 76, pgs.5552-5556.
15. Chazalviel J., Belaidi A., Safi M., Maroun F., Erne B., Ozanam F., "*In situ semiconductor surface characterization: a comparative infrared study of Si, Ge and GaAs*", Electrochimica Acta, 2000, Vol. 45, pgs. 3205-3211.
16. Covington A., "*Ion Selective Electrode Methodology. Volume 1*", CRC Press. Boca Raton, FL, 1979.
17. Fujii K., Kusakabe K., Ohkawa K., "*Photoelectrochemical properties of InGaN for H₂ generation from aqueous water*", 2005, Japanese Journal of Applied Physics, Vol. 44 (10), pgs. 7433-7435.
18. Fujii K., Ohkawa K., "*Bias-Assisted H₂ Gas Generation in HCl and KOH Solutions Using n-Type GaN Photoelectrode*", Journal of the Electrochemical Society, 2006, Vol. 153 (3), pgs. A468 – A471.
19. Hellman E., "*The Polarity of GaN: a Critical Review*", MRS Internet Journal of Nitride Semiconductor Research, 1998, Vol. 3, article 11.
20. Hens Z., Gomes W., "*On the Diffusion Impedance at Semiconductor Electrodes*", Journal of Physical Chemistry B, 1997, Vol. 101, pgs. 5814-5821.
21. International Union of Pure and Applied Chemistry, Analytical Chemistry Division, Commission on Electroanalytical Chemistry; "*Recommendations for nomenclature of Ion-Selective Electrodes*"; Journal of Pure and Applied Chemistry, 1994, Vol. 66, No. 12, pgs. 2527-2536.
22. Kim C., Lee J., Lee Y., Cho N., Kim D., Kang W., "*Hydrogen sensing characteristics of Pd-SiC Schottky diode operating at high temperature*", Journal of Electronic Materials, 1999, Vol. 28 (3), pgs. 202-205.
23. Kobayashi N., Narumi T., Morita R., "*Hydrogen Evolution from p-GaN Cathode in Water under UV Light Irradiation*", Japanese Journal of Applied Physics, 2005, Vol. 44 (24), pgs. L784 – L786.
24. Lynde S., "*Environmental Sampling and Monitoring Primer*", available at: <http://ewr.cee.vt.edu/environmental/teach/sprimer/ise/ise.html>, accessed: May, 2005.
25. Matencio T., Pernaut J., Vieil E., "*Analysis of Hysteresis Phenomenon as Observed from Voltammetric Data of Conducting Polymers - Part I*", Journal of Brazilian Chemical Society, 2003, Vol. 14 (1), pgs. 90-96.
26. Materials Evaluation and Engineering, Inc., "*Handbook of Analytical Methods*", available at: <http://www.mee-inc.com/eds.html>, accessed: May, 2006,

References

27. Memming R., "*Semiconductor Electrochemistry*", First edition, Wiley-VCH Verlag GmbH, Weinheim, Federal Republic of Germany, 2001.
28. Miller E., Yu E., "*Influence of the dipole interaction energy on clustering in $In_xGa_{1-x}N$ alloys*", Applied Physics Letters, 2001, Vol. 78 (16), pgs. 2303-2305.
29. Morrison R., "*Electrochemistry at Semiconductor and Oxidized Metal Electrodes*", First edition, Plenum Press, New York, N.Y.10013, 1980.
30. NICO 2000 Ltd., "*Beginners Guide to ISE Measurement - Chapter 10: Methods of Analysis*", available at: <http://www.nico2000.net/Book/Guide11.html>; accessed: May, 2005.
31. NICO 2000 Ltd., "*Beginners Guide to ISE Measurement - Chapter 2: Introduction to Ion Selective Electrodes*"; available at: <http://www.nico2000.net/Book/Guide3.html>; accessed: May, 2005.
32. NICO 2000 Ltd., "*Beginners Guide to ISE Measurement - Chapter 3: Basic Theory of ISE Measurements*"; available at: <http://www.nico2000.net/Book/Guide4.html>; accessed: May, 2005.
33. NICO 2000 Ltd., "*Beginners Guide to ISE Measurement - Chapter 4: Types of Ion Selective Electrodes*"; available at: <http://www.nico2000.net/Book/Guide5.html>; accessed: May, 2005.
34. NICO 2000 Ltd., "*Beginners Guide to ISE Measurement - Chapter 5: Reference Electrodes*"; available at: <http://www.nico2000.net/Book/Guide6.html>; accessed: May, 2005.
35. NICO 2000 Ltd., "*Beginners Guide to ISE Measurement - Chapter 6: Problems with ISE Measurements*"; available at: <http://www.nico2000.net/Book/Guide7.html>; accessed: May, 2005.
36. NICO 2000 Ltd., "*Beginners Guide to ISE Measurement - Chapter 7: Calibration Theory*", available at: <http://www.nico2000.net/Book/Guide8.html>; accessed: May, 2005.
37. Orion Research Inc., "*Ion Selective Electrodes*", available at: <http://www.orionres.com>, accessed: May, 2005.
38. Ottow S., "*Basics of Semiconductor Electrochemistry*", available at: <http://www.tf.uni-kiel.de/matwis/amat/poren/ecintro.html>, accessed: August, 2006.
39. Piquette E., Bridger P., Bandic Z., McGill T., "*Morphology, polarity, and lateral molecular beam epitaxy growth of GaN on sapphire*", Journal of Vacuum Science & Technology B, 1999, Vol. 17 (3), pgs. 1241-1245.
40. Ponce F.A., "*Defects and Interfaces in GaN Epitaxy*", MRS Bulletin, 1997, Vol. 22, pgs. 51.
41. Ragoisha G., "*Potentiodynamic Electrochemical Impedance Spectroscopy*", 2004, Physico-Chemical Research Institute, Belarusian State University, available at: <http://www.abc.chemistry.bsu.by/vi/>, accessed: July 2005.

References

42. Ramesham R., Rose M., “*Corrosion Studies of CVD Diamond Coated Molybdenum, Evaluation of Equivalent Circuit and the Effect of Pinholes in Diamond Film on Cyclic Voltammetric Behavior*”, Corrosion Science, 1997, Vol. 39 (10-11), pgs. 2019-2033.
43. Rieger P., “*Electrochemistry*”, Second edition, Chapman & Hall, Inc., New York, USA, 1994.
44. Rinaldi F., “*Basics of Molecular Beam Epitaxy (MBE)*”, Annual Report, Optoelectronics Department, University of Ulm, 2002. available at: http://www-opto.e-technik.uni-ulm.de/forschung/jahresbericht/2002/ar2002_fr.pdf; accessed: July, 2005.
45. Takayama T., Yuri M., Itoh K., Harris, Jr., J., “*Theoretical predictions of unstable two-phase regions in wurtzite group-III-nitride-based ternary and quaternary material systems using modified valence force field model*”, Journal of Applied Physics, 2001, Vol. 90 (5), pgs. 2358-2369.
46. Thomas J., Moody G., Ryan T., Fleet B., Whitfield M., Garbett K., Craggs A., “*Ion selective electrodes*”, Proceedings of the Analytical Division of the Chemical Society, 1975, Vol. 12 (2), pgs. 48-64.
47. Toth K., “*The significance of selective sensors in chemical analysis*”; Magyar Kemiai Folyoirat, 1999, Vol. 105 (5), pgs.173-199.